NEW APPROACHES IN FORENSIC ANALYTICAL CHEMISTRY

EDITED BY: Alberto Salomone, Grzegorz Zadora and Paolo Oliveri
PUBLISHED IN: Frontiers in Chemistry

frontiers Research Topics

frontiers

ISSN 1664-8714
ISBN 978-2-88966-487-0
DOI 10.3389/978-2-88966-487-0

About Frontiers

Frontiers is more than just an open-access publisher of scholarly articles: it is a pioneering approach to the world of academia, radically improving the way scholarly research is managed. The grand vision of Frontiers is a world where all people have an equal opportunity to seek, share and generate knowledge. Frontiers provides immediate and permanent online open access to all its publications, but this alone is not enough to realize our grand goals.

Frontiers Journal Series

The Frontiers Journal Series is a multi-tier and interdisciplinary set of open-access, online journals, promising a paradigm shift from the current review, selection and dissemination processes in academic publishing. All Frontiers journals are driven by researchers for researchers; therefore, they constitute a service to the scholarly community. At the same time, the Frontiers Journal Series operates on a revolutionary invention, the tiered publishing system, initially addressing specific communities of scholars, and gradually climbing up to broader public understanding, thus serving the interests of the lay society, too.

Dedication to Quality

Each Frontiers article is a landmark of the highest quality, thanks to genuinely collaborative interactions between authors and review editors, who include some of the world's best academicians. Research must be certified by peers before entering a stream of knowledge that may eventually reach the public - and shape society; therefore, Frontiers only applies the most rigorous and unbiased reviews.
Frontiers revolutionizes research publishing by freely delivering the most outstanding research, evaluated with no bias from both the academic and social point of view. By applying the most advanced information technologies, Frontiers is catapulting scholarly publishing into a new generation.

What are Frontiers Research Topics?

Frontiers Research Topics are very popular trademarks of the Frontiers Journals Series: they are collections of at least ten articles, all centered on a particular subject. With their unique mix of varied contributions from Original Research to Review Articles, Frontiers Research Topics unify the most influential researchers, the latest key findings and historical advances in a hot research area! Find out more on how to host your own Frontiers Research Topic or contribute to one as an author by contacting the Frontiers Editorial Office: frontiersin.org/about/contact

NEW APPROACHES IN FORENSIC ANALYTICAL CHEMISTRY

Topic Editors:
Alberto Salomone, University of Turin, Italy
Grzegorz Zadora, University of Silesia of Katowice, Poland
Paolo Oliveri, University of Genoa, Italy

Citation: Salomone, A., Zadora, G., Oliveri, P., eds. (2021). New Approaches in Forensic Analytical Chemistry. Lausanne: Frontiers Media SA.
doi: 10.3389/978-2-88966-487-0

Table of Contents

frontiers in Chemistry

EDITORIAL
published: 12 January 2021
doi: 10.3389/fchem.2020.638460

Editorial: New Approaches in Forensic Analytical Chemistry

Alberto Salomone[1]*, *Paolo Oliveri*[2] *and Grzegorz Zadora*[3]

[1] Department of Chemistry, University of Turin, Turin, Italy, [2] Department of Pharmacy, University of Genoa, Genoa, Italy, [3] Forensic Chemistry Research Group, University of Silesia in Katowice, Katowice, Poland

Keywords: NPS, likelihood ratio, forensic science, forensic chemistry, scientific evidence

Editorial on the Research Topic

New Approaches in Forensic Analytical Chemistry

Some place their faith in forensic science to the degree that they are under the impression that it is absolute, infallible and unassailable. In truth it is a manmade construct, dependent on manmade machinery, man-calibrated accuracy, man-led action under manmade protocols and analyzed by man – an altogether human construct (American Academy of Forensic Sciences cited in Pyrek, 2007).

People have always strived to discover and understand the world, and the scientific quest to provide explanations fuels technological progress. This drive has fuelled forensic chemistry, where information is obtained through the examination of various evidential materials to assist the justice system piece together stories of the past. Concurrently, the validity and reliability of the information provided by forensic experts, its ability to discriminate between the standpoints of defense and prosecution, is being questioned and challenged as never before (Pyrek, 2007; Fraser and Williams, 2009). Even though analytical methods have substantially changed over time, from highly subjective assessments of information-poor data to chromatographic and spectroscopic signals, which morph into knowledge thanks to the achievements of chemometrics and statistics, forensic chemistry still is—and always will be—prone to error. The above-cited observation of the *American Academy of Forensic Sciences* is an explicit reminder of the fact that forensic science—even if increasingly enhanced with powerful computational methods—is largely a "human construct," especially at the culmination of the examination process, which involves the interpretation and communication of findings. As a consequence, questioning the scientificity of forensics is inevitable and, thus, it is imperative to turn the focus onto the credibility of the examination process. This means that, prior to the implementation of any new forensic technique, specific steps must be taken to objectively demonstrate that the proposed methodology is suitable for its intended use (ENFSI, 2014). In other words, each of the newly developed methods has to be validated.

The role of forensic chemists is not limited solely to manufacturing valid analytical techniques and their products (physicochemical data). Many self-proclaimed forensic authors overlook the fact that these data need to be realized, as properly performed expertise also involves the interpretation and communication findings to assist fact finders (e.g., judges or prosecutors), who often lack any form of chemical knowledge or technological understanding of employed methods, in their decision making. According to the standards acknowledged among the forensic community (Zadora et al., 2014; ENFSI, 2015; Aitken et al., 2018), the communication of results should be expressed in a probabilistic manner. Any categorical conclusions are not allowed—unless the compared samples present completely different physicochemical profiles, or the results of the so-called jigsaw fitting procedure are considered—as 100% certainty can never be guaranteed. Consequently, perceiving results as categorical, and neglecting at the same time the "fuzziness of boundaries," may lead to forensic misconduct. With that in mind, frontier research in the field of forensic chemistry should also focus on the implementation of generally accepted measures

OPEN ACCESS

Edited and reviewed by:
Ashok Mulchandani, University of California, Riverside, United States

***Correspondence:**
Alberto Salomone
alberto.salomone@unito.it

Specialty section:
This article was submitted to Analytical Chemistry, a section of the journal Frontiers in Chemistry

Received: *06 December 2020*
Accepted: *14 December 2020*
Published: *12 January 2021*

Citation:
Salomone A, Oliveri P and Zadora G (2021) Editorial: New Approaches in Forensic Analytical Chemistry. Front. Chem. 8:638460. doi: 10.3389/fchem.2020.638460

for assessing the weight of the evidence—the likelihood ratio approach—to aid the evaluation of evidence.

The articles collected in this Research Topic explore a broad range of issues that underpin the establishment of any sound analytical approach in forensic chemistry, starting from basic research, through to the development and validation of analytical tools, and the evaluation and communication of findings. When dealing with biological samples, particularly urine, extensive knowledge of the metabolic fate of substances is crucial for developing comprehensive screening procedures. Wagmann et al. studied *in vitro* approaches to investigate the metabolism of several new psychoactive substances (NPS), thus underlining the potential of zebrafish larvae as a tool for elucidating the toxicokinetics of NPS, especially when human studies are not feasible due to ethical concerns. In turn, Putz et al. performed a comprehensive *in vivo* metabolism study focused on trenbolone, a synthetic anabolic-androgenic steroid, which is misused for performance enhancement in sports. Using Hydrogen Isotope Ratio Mass Spectrometry and Liquid Chromatography/High Accuracy/High Resolution Mass Spectrometry, the authors identified new potential metabolites. A further investigation will be put in place to verify or falsify the true added value of the identified trenbolone metabolites for routine doping controls.

Given the reputation of forensic science, which has been significantly tarnished in recent years due to some infamous forensic pathologies (Trager, 2018), the challenge today is to make certain that the evidence is tested with credible analytical methods. The development of such tools is also the subject of several articles in this Research Topic. A study by Jendrzejewska addressed the authentication of popular dietary supplements containing magnesium and calcium. An X-ray structural analysis, more precisely, the comparison between diffraction lines in the recorded and reference diffraction images, provided a method for distinguishing counterfeit preparations from authentic products. Malejko et al. demonstrated that the ICP-MS method is suitable for the determination of Cd and Tl in different developmental stages of the blowfly, which—according to the authors—could be used as an alternative material for the detection of the trace element content present in the body at the time of death.

The group of NPS compounds, which are designed to mimic the activity of already existing illegal recreational drugs, receive a considerable amount of scientific interest. The continued emergence of NPS poses a number of analytical challenges for forensic laboratories. The importance of this issue is reflected in the number of NPS-directed papers submitted to this Research Topic. For example, a study authored by Calò et al. developed and validated a bioanalytical method for oral fluid analysis, using high-performance liquid chromatography coupled with mass spectrometry with minimal sample pretreatment, while Salerno et al. analyzed real "street" samples seized by law enforcement by coupling gas-chromatography to Fourier Transform Infrared Spectroscopy. Both methods proved effective for the unequivocal identification of NPS. To facilitate the work of law enforcement agencies, Bulska et al. presented a cooperative study toward the synthesis and characterization of selected NPS. The proposed non-routine analytical protocol combined X-ray diffraction with methods of chromatographic separation followed by the identification of synthesized products using mass spectrometry. Vincenti et al. reported on the successful application of molecular networking (MN) for the identification of new and unexpected fentanyl analogs within the Global Natural Product Search (GNPS), based on untargeted LC–HRMS data. The chemical structures of the compounds identified were then confirmed by NMR analysis.

Finally, Biosa et al. shed light on the interpretation of analytical data in the forensic context, with special consideration given to the likelihood ratio approach, which is now considered the most suitable framework for determining the value of forensic evidence (Zadora et al., 2014; ENFSI, 2015; Aitken et al., 2018). This particular study introduced a two-class classification strategy based on penalized logistic regression with a calculation of likelihood ratios. The method was applied to classify chronic alcohol drinkers using alcohol biomarker data. A versatile open-source and free-of-charge data processing app[1], based on the R environment, was also presented.

AUTHOR CONTRIBUTIONS

AS, PO, and GZ: manuscript draft and revision. All authors contributed to the article and approved the submitted version.

[1]https://dianagiurghita.shinyapps.io/ForensicClassification/ (accessed December 6, 2020).

REFERENCES

Aitken, C., Nordgaard, A., Taroni, F., and Biedermann, A. (2018). Commentary: likelihood ratio as weight of forensic evidence: a closer look. *Front. Genet.* 9:224. doi: 10.3389/fgene.2018.00224

ENFSI (2014). *Guidelines for the Single Laboratory Validation of Instrumental and Human Based Methods in Forensic Science*. Available online at: http://enfsi.eu/wp-content/uploads/2017/06/Guidance-QCC-VAL-002.pdf (accessed December 18, 2020).

ENFSI (2015). *Guideline for Evaluative Reporting in Forensic Science*. Available online at: http://enfsi.eu/wp-content/uploads/2016/09/m1_guideline.pdf (accessed December 18, 2020).

Fraser, J., and Williams, R. (2009). "The contemporary landscape of forensic science," in *Handbook of Forensic Science*, eds J. Fraser and R. Williams (Portland, OR: Willan Publishing), 1–20.

Pyrek, K. M. (2007). *Forensic Science Under Siege*. Amsterdam: Elsevier Press.

Trager, R. (2018). *Forensics in Crisis*. Chemistry World. Available online at: https://www.chemistryworld.com/features/forensics-in-crisis/3009117.article (accessed December 18, 2020).

Zadora, G., Martyna, A., Ramos, D., and Aitken, C. (2014). *Statistical Analysis in Forensic Science: Evidential Values of Multivariate Physicochemical Data*. Chichester: Wiley.

Conflict of Interest: The authors declare that the research was conducted in the absence of any commercial or financial relationships that could be construed as a potential conflict of interest.

frontiers in Chemistry

ORIGINAL RESEARCH
published: 20 May 2020
doi: 10.3389/fchem.2020.00435

Identification of Trenbolone Metabolites Using Hydrogen Isotope Ratio Mass Spectrometry and Liquid Chromatography/High Accuracy/High Resolution Mass Spectrometry for Doping Control Analysis

*Marlen Putz, Thomas Piper and Mario Thevis**

Center for Preventive Doping Research, Institute of Biochemistry, German Sport University Cologne, Cologne, Germany

OPEN ACCESS

Edited by:
Alberto Salomone, University of Turin, Italy

Reviewed by:
Benjamin L. Oyler, Vaccine Research Center (NIAID), United States
Roberta Risoluti, Sapienza University of Rome, Italy

***Correspondence:**
Mario Thevis
thevis@dshs-koeln.de

Specialty section:
This article was submitted to Analytical Chemistry, a section of the journal Frontiers in Chemistry

Received: *28 February 2020*
Accepted: *27 April 2020*
Published: *20 May 2020*

Citation:
Putz M, Piper T and Thevis M (2020) Identification of Trenbolone Metabolites Using Hydrogen Isotope Ratio Mass Spectrometry and Liquid Chromatography/High Accuracy/High Resolution Mass Spectrometry for Doping Control Analysis. Front. Chem. 8:435. doi: 10.3389/fchem.2020.00435

Trenbolone is a synthetic anabolic-androgenic steroid, which has been misused for performance enhancement in sports. The detection of trenbolone doping in routine sports drug testing programs is complex as methods utilizing gas chromatography/mass spectrometry are complicated by unspecific derivatization products and artifacts, and liquid chromatography/mass spectrometry-based assays have shown to allow for comparably high limits-of-detection only. The number of previously reported metabolites in human urine is limited, and most analytical methods rely on targeting epitrenbolone, trenbolone glucuronide, and epitrenbolone glucuronide. In order to probe for the presence of additional trenbolone metabolites and to re-investigate the metabolism, an elimination study was conducted. One single dose of 10 mg of 5-fold deuterated trenbolone was administered to a healthy male volunteer and urine samples were collected for 30 days. For sample processing, published protocols were combined considering unconjugated, glucuronic acid-, sulfo- and alkaline-labile conjugated steroid metabolites. The sample preparation strategy consisted of solid-phase extractions, liquid-liquid extractions, metabolite de-conjugation, HPLC fractionation, and derivatization. Analytical methods included gas chromatography/thermal conversion/hydrogen isotope ratio mass spectrometry combined with single quadrupole mass spectrometry as well as liquid chromatography/high accuracy/high resolution mass spectrometry of the hydrolyzed and non-hydrolyzed samples. Twenty deuterium-labeled metabolites were identified including glucuronic acid-, sulfo- and potential cysteine-conjugates, and characterized by parallel reaction monitoring experiments yielding corresponding product ion mass spectra. Main metabolites were attributed to trenbolone-diol and potential trenbolone-diketone derivatives excreted as glucuronic acid and sulfo-conjugated analytes with detection windows of 5, respectively 6 days.

Further characterization was conducted with pseudo MS^3 experiments of the intact conjugates and by comparison of resulting product ion mass spectra with reference material.

Keywords: gas chromatography thermal conversion isotope ratio mass spectrometry (GC-TC-IRMS), liquid chromatography high resolution mass spectrometry (LC-HRMS), human metabolism, steroids, phase-II conjugates, pseudo MS^3 product ion mass spectra, sports drug testing, *in vivo* metabolism

INTRODUCTION

Trenbolone (Tren) belongs to the class of synthetic anabolic-androgenic steroids (AAS) and is structurally characterized by a 4,9,11-triene-3-one structure composing a highly conjugated π-electron system (**Figure 1**). The significant anabolic properties of Tren resulting in increased muscle size and strength have generated an incentive for illicit applications including doping and livestock breeding. In sports, the use of trenbolone has been prohibited by the World Anti-Doping Agency (WADA) at all times, categorized under S1 1. (anabolic androgenic steroids) in the Prohibited List (WADA, 2020). According to WADA's annual statistics, anabolic agents are the most frequently misused substance group in sports with a total of 1,823 adverse analytical findings (AAFs) in 2018. Within this group, Tren occurrences account for 6% (WADA, 2019). The statistics however can only reflect cases of detectable Tren and does not conclusively address the question whether Tren is less favored by users of AAS or if available detection strategies do not offer the required analytical retrospectivity.

For that reason the objective of this project was to re-investigate the metabolism of Tren in order to probe for metabolic products potentially supporting the extension of the detection window. The number of previously reported Tren metabolites is scarce, and for doping control purpose the analysis focuses at present on the main human urinary metabolites epitrenbolone (EpiTREN), epitrenbolone glucuronide (EpiTREN Glu), and trenbolone glucuronide (TREN Glu) (De Boer et al., 1991; Schänzer, 1996). Regarding the detection windows, two data sets have been published spanning from approximately 3 days (Spranger and Metzler, 1991) to 32 days (Sobolevsky and Rodchenkov, 2015). Besides glucuronides, sulfates (Rzeppa et al., 2015), and cysteine conjugates (Sobolevsky and Rodchenkov, 2015) of Tren and Epitren were reported.

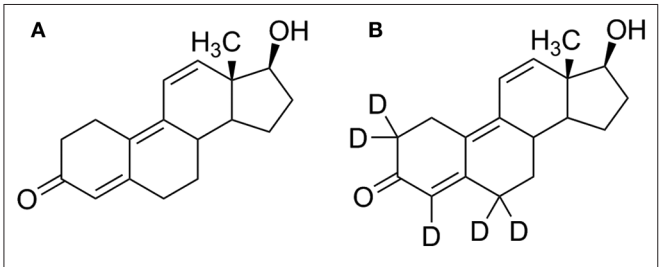

FIGURE 1 | Structure formulae of **(A)** trenbolone and **(B)** d_5-trenbolone used for the excretion study.

Cysteine conjugates are produced by phase-II metabolism, where the tripeptide glutathione is covalently bound via the sulfur atom by glutathione transferase and, subsequently, glutamate and glycine are eliminated. In general, cysteine conjugates are hydrolyzed employing alkaline conditions (Blair, 2006; Fabregat et al., 2010, 2011, 2013; Pozo et al., 2010), but the cysteine conjugate of trenbolone described by Sobolevsky and Rodchenkov (2015). was found to be stable during alkaline hydrolysis and was analyzed by high performance liquid chromatography electrospray ionization tandem mass spectrometry (HPLC-ESI-MS/MS) as in-source fragment in ESI negative mode and as intact conjugate in ESI positive mode (Sobolevsky and Rodchenkov, 2015). During *in-vitro* studies, several monohydroxylated metabolites, and trenbolone-diketone were generated (Metzler and Pfeiffer, 2001; Kuuranne et al., 2008).

Nowadays, LC-MS-based methods are commonly used for the analysis of Tren and its metabolites (Thevis et al., 2005a, 2009; Tudela et al., 2015) as GC-MS-based methods were found to be of limited utility due to derivatization artifacts and low thermal stability of the target analytes (De Boer et al., 1991; Ayotte et al., 1996; Casademont et al., 1996; Marques et al., 2007; Brun et al., 2011).

For systematic metabolism studies, a method for metabolite identification using hydrogen isotope ratio mass spectrometry was developed and successfully applied for the first time in 2013 (Thevis et al., 2013). The fundamental principle is analogous to metabolism studies using radioactively labeled compounds (Sano et al., 1976). The compounds can be detected selectively because of their isotopic labeling by measuring the radioactivity in case of tritium or ^{14}C labeled compounds or by measuring the hydrogen isotope ratios in case of deuterium labeled compounds.

Hydrogen isotope ratios are determined by gas chromatography/thermal conversion/isotope ratio mass spectrometry (GC-TC-IRMS). The organic compounds are converted under reducing conditions to CO and N_2 as well as molecular hydrogen (H_2), respectively the deuterated isotopologe HD. After ionization, detection is accomplished using m/z 2 for H_2^+ and m/z 3 for HD^+ by Faraday cups with different amplification factors (factor 1000 difference). Since the natural hydrogen abundance amounts on average to 99.985% for H and 0.015% for D (Dunn and Carter, 2018), comparable signals for H_2^+ and HD^+ are obtained for samples at natural abundance, while deuterated compounds lead to a significant increase of signals at m/z 3. Compounds resulting in diagnostic HD^+ signals are subsequently comprehensively characterized by gas chromatography/electron ionization/high accuracy/high resolution mass spectrometry (GC-EI-HRMS). This concept has

been proven in several studies (Thevis et al., 2013; Piper et al., 2016a,b, 2018, 2019).

Within this project, liquid chromatography/electrospray ionization/high accuracy/high resolution mass spectrometry (LC-ESI-HRMS) was applied for further characterization of trenbolone and its metabolites after GC-TC-IRMS analysis. Twenty metabolites were identified with a detectability of up to 6 days. Four metabolites exhibiting the longest detection windows were characterized by parallel reaction monitoring (PRM) experiments and comparison to reference material.

MATERIALS AND METHODS

Chemicals and Steroids

Trenbolone reference material and the internal standard 2,2,4,6,6-d_5-trenbolone were purchased from Toronto Research chemicals (Toronto, Canada), and epitrenbolone from the National Measurement Institute (Sydney, Australia). Steroid reference material for HPLC separation including ETIO (etiocholanolone), A (androsterone), T (testosterone), and PD (pregnanediol) was supplied by Sigma-Aldrich, and 11 K (11-ketoetiocholanolone), 5a (5α-androstanediol), and 5b (5β-androstanediol) were obtained from Steraloids (Newport, RI). Chromabond C18 solid-phase extraction (SPE) cartridges (500 mg, 6 mL) were purchased from Macherey & Nagel (Düren, Germany) and β-glucuronidase from Escherichia coli (140 U/mL) from Roche Diagnostics (Mannheim, Germany). Ultrapure water was prepared by a Barnstead™ GenPure™ xCAD Plus system (Thermo, Germany). All reagents and solvents were of analytical grade. Acetonitrile (ACN), formic acid (FA), methanol (MeOH), tert-butyl methyl ether (TBME), cyclohexane, pyridine, sodium hydroxide (NaOH), sulfuric acid (H_2SO_4), glacial acetic acid, and potassium tri-sec-butylborohydride (1 M in THF) were provided by Merck (Darmstadt, Germany). Acetic anhydride was supplied by Sigma Aldrich (Taufkirchen, Germany) and tetrahydrofuran (THF) by VWR (Darmstadt, Germany). *N*-methyl-*N*-trimethylsilyltrifluoroacetamide (MSTFA) was purchased from Chemische Fabrik Karl Bucher (Waldstetten, Germany).

Excretion Study

An excretion study was conducted in order to re-investigate the trenbolone metabolism. Following written informed consent, 10 mg of 5-fold deuterated trenbolone (**Figure 1**) dissolved in ultra-pure water/EtOH (80:20, *v*/*v*) was orally administered to one healthy male volunteer (43 years, 84 kg) who declared not to have used any medication or nutritional supplements during this study and for a wash-out period of at minimum 3 month (any compounds), respectively 6 month (deuterated compounds) before the study. Three blank samples were collected pre-administration, and post administration samples were collected for up to 30 days. During the first 48 h after trenbolone intake, every urine was collected. From day three until day five, two to three urine samples per day were collected, and afterwards only the first morning urine was sampled until the end of the study. The administration study was approved by the Ethics Committee of the National Institute of Sports of Romania (Bucharest, Romania, #2283, 2016).

Analysis of Hydrolyzed Steroids

Sample Preparation

An extensive sample preparation was required in order to reach adequate purity and undecomposed volatility of the metabolites for GC-TC-IMRS analysis. Urine samples were prepared according to established protocols for isotope ratio analysis of steroids. Here, every sample is separated into four main fractions: unconjugated steroids, glucuronic acid conjugates (Piper et al., 2008), sulfo-conjugates (Piper et al., 2010), and cysteine conjugates (Fabregat et al., 2010, 2011, 2013; Pozo et al., 2010). Subsequently, the fractions of glucuronides and sulfates are further divided by HPLC into seven sub-fractions (Thevis et al., 2013). Sample preparation and analysis is summarized in **Figure 2**.

For each sample, a volume of 20 mL urine was required. First, two C-18 SPE cartridges per sample were pre-conditioned with 2 mL of MeOH and subsequently washed with 2 mL of water. Then, every sample was split and 10 mL of urine were applied to each cartridge, which was subsequently washed with 2 mL of water, and finally eluted with 2 mL of MeOH. Both eluates of each sample were combined and evaporated to dryness under a gentle stream of compressed air at 50°C. Following evaporation, samples were reconstituted with 1 mL of an aqueous 0.2 M sodium phosphate buffer at pH 7, and a liquid-liquid-extraction (LLE) step with 5 mL of TBME was performed. Therefore, the mixture was shaken for 5 min and subsequently centrifuged for 5 min at 600 g before separating both layers. The organic layer yielded the fraction of the unconjugated steroids (fraction f; free).

The remaining aqueous layer was incubated with 100 µL of β-glucuronidase at 50°C for 1 h. To terminate hydrolysis, 500 µL of an aqueous 20% potassium carbonate buffer (pH 10) were added. In order to extract the liberated steroids, a second LLE step with TBME was performed and the resulting organic layer contained the former glucuronic acid conjugates (fraction Gluc). Then, the pH of the aqueous layer was adjusted to 5 with glacial acetic acid, and purified by SPE as described above. After evaporation, samples were incubated with 2.5 mL of EtOAc/MeOH (70/30, *v*/*v*) and 1 mL of EtOAc/H_2SO_4 (100 mL/200 ng, *v*/*w*) at 50°C for 1 h. Subsequently, 0.5 mL of methanolic NaOH (1 M) were added, the mixture was evaporated as described above, and reconstituted with 5 mL of water. A third LLE with TBME was conducted to extract the formerly sulfo-conjugated steroids (fraction Sulf). This was followed by alkalization of the aqueous layer with 300 µL of 6 M KOH and an incubation step at 60°C for 15 min. Finally, alkaline-labile steroids comprising potential cysteine conjugates were extracted by the last LLE (fraction Cys).

The four resulting TBME extracts per sample were evaporated to dryness and the fractions of glucuronides and sulfates further purified by HPLC. For that purpose, samples were reconstituted in 100 µL ACN/H_2O (50/50, *v*:*v*), and the entire volume was injected into an Agilent 1100 HPLC-UV system (Waldbronn, Germany) equipped with a X Bridge Shield RP18 column (4.6 × 250 mm) with 5 µm particle size (Waters, Eschborn, Germany). UV signals were acquired at 195 and 360 nm. Gradient elution

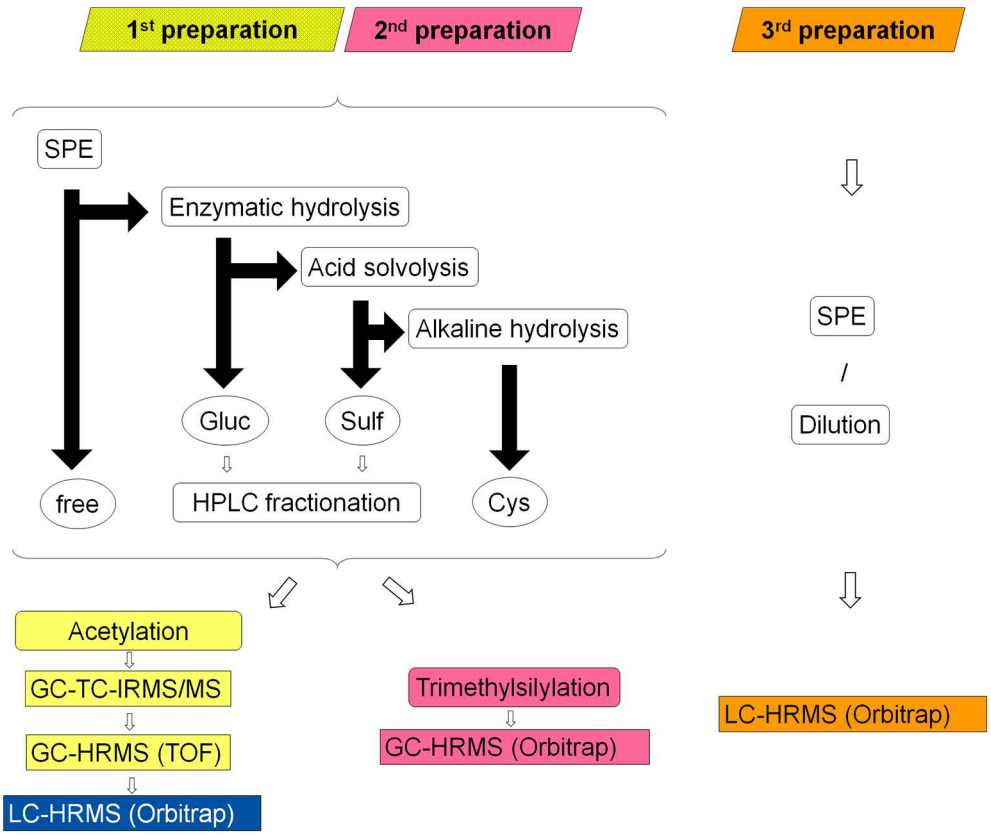

FIGURE 2 | Schematic overview of the three different sample preparations colored in yellow/blue (1st), pink (2nd) and orange (3rd); rounded corner boxes indicate sample processing steps, circles indicate former conjugation forms of the liberated steroids (free = unconjugated steroids, Gluc = glucuronides, Sulf = sulfates, Cys = cysteine conjugates), black arrows represent the sample separation by LLE: horizontal arrow represent processing of the aqueous layer and vertical arrows of the organic layer, rectangular boxes indicate the applied analytical systems.

was conducted as follows with a flow rate of 1 mL/min: Starting at 20% ACN/80% water, the gradient increased to 100% ACN within 25 min, was held for 10 min, and re-equilibrated for 5 min. With support of a Foxy R1 automatic fraction collector (Axel Semrau, Sprockhövel, Germany), the following HPLC sub-fractions were produced using the retention time markers shown in brackets. I: 3.00–10.00 min, II: 10.01–13.50 min (Tren, Epitren), III: 13.51–14.80 min (T), IV: 14.81–17.00 min (EpiT, DHEA, 5b, 5a, ETIO), V: 17.01–19.50 min (PD), VI: 19.51–24.50, and VII 24.51–33.00 min (16 EN).

The eluted HPLC sub-fractions were evaporated to dryness. Derivatization of all fractions derived from HPLC clean-up, as well as the fractions containing the cysteine adducts and free steroids was performed in accordance with the applied chromatographic system as described below.

Derivatization Techniques

Acetylation

For acetylation, samples were reconstituted in 75 µL of pyridine and 75 µL of acetic anhydride and derivatized for 1 h at 70°C. Subsequently, the derivatization mixture was evaporated. Samples were subjected to GC-TC-IRMS/MS (section GC-TC-IRMS/MS Setup), GC-EI-HRMS (QTOF) (section GC-EI-HRMS (QTOF) Setup) and LC-ESI-HRMS (section LC-ESI-HRMS (LC Orbitrap) Setup) analysis.

Trimethylsilylation

For trimethylsilylation, samples were reconstituted in 80 µL of MSTFA:NH_4:ethanethiol (1000:2:3, *v:w:v*), incubated at 60°C for 45 min (Mareck et al., 2004, 2008), and measured as described in section GC-EI-HRMS (Orbitrap) Setup.

Instrument Methods

GC-TC-IRMS/MS setup

After evaporation of the derivatization mixture, the acetylated samples were reconstituted in an appropriate volume of cyclohexane (typically 20 µL) for GC-TC-IRMS/MS analysis. Analysis was performed on a Delta V Plus IRMS coupled via a GC Isolink CNH for thermal conversion at 1,450°C with a ceramic reduction reactor and ConFlow IV to a Trace 1310 GC (Thermo, Bremen, Germany). Chromatographic separation was accomplished on a DB-17 MS column (30 m × 0.25 mm) with a film thickness of 0.25 mm. The temperature gradient was as follows: The temperature remained constant at 100°C for

1.5 min and increased with 40°C/min to 240°C and subsequently with 5°C/min to 320°C with a hold time of 2 min. Samples were injected in splitless mode at 300°C with an injection volume of 5 μL. A single taper inlet liner (900 μL volume, 4 mm inner diameter, 6.47 mm outer diameter, 78.5 mm length) with glass wool from Agilent (part number: 5190-2293) was used. After passing the GC column, the flow was split by a ratio of approximately 1:10 to an ISQ single quadrupole mass spectrometer (Thermo, Bremen, Germany). Data acquisition and processing was accomplished using Isodat 3.0 and Xcalibur 2.2 software (Thermo, Bremen, Germany).

GC-EI-HRMS (QTOF) setup

Following GC-TC-IRMS/MS analysis, the acetylated samples were diluted to a final volume of 200 μL cyclohexane and subjected to GC-EI-HRMS measurements on an Agilent 7200 QTOF system hyphenated to an Agilent 7890A gas chromatograph (Santa Clara, CA). The chromatography setup was equivalent to GC-TC-IRMS/MS described above (section GC-TC-IRMS/MS Setup), including the same analytical column and the same temperature program. The injection volume was reduced to 4 μL. Data were acquired within a range of *m*/*z* 50–800 with an acquisition rate of 5 spectra/s and evaluated with MassHunter software (version B.06, Agilent). Mass calibration was performed before and during each analytical batch.

GC-EI-HRMS (Orbitrap) setup

The trimethylsilylated samples were injected (2 μL injection volume) into a Q Exactive GC Orbitrap (Thermo, Bremen, Germany). Due to the different derivatization technique, the system was operated with modified chromatographic conditions adapted from routine protocols (Thevis et al., 2011). The GC was equipped with a HP-Ultra 1 column (17 m × 0.2 mm) of 0.11 mm film thickness. The temperature program started at 180°C and raised with 3°C/min to 240°C and with 40°C/min to 320°C, where it remained constant for 2 min. Samples were injected in split mode with a split flow of 5 mL/min. The mass range for full MS experiments was *m*/*z* 50–700 and a resolution of 60,000 FWHM was applied. Data were evaluated with Xcalibur software.

LC-ESI-HRMS (LC Orbitrap) setup

For LC-ESI-HRMS measurements, the acetylated samples were evaporated and reconstituted with 100 μL of ACN/H_2O (50:50, *v*/*v*) acidified with 0.1% FA. A Vanquish UHPLC (Thermo, Bremen, Germany) equipped with a Poroshell 120 EC-C8 (2.7 μm, 3 × 50 mm) (Agilent, Santa Clara, CA) was hyphenated to a Q Exactive HF-X (Thermo, Bremen, Germany). ACN and ultrapure water both containing 0.1% FA were employed as solvents, and the flow rate was set to 400 μL/min. A volume of 5 μL was injected per sample. The LC gradient run was as follows: Starting at 40% ACN, it was increased to 99% within 9 min, and hold for further 3 min until re-equilibration, yielding a total analysis time of 15 min. MS experiments comprised a full scan (*m*/*z* 200–800), AIF (all ions fragmentation), and PRM in positive ionization mode at a resolution of 60,000 FWHM. For PRM experiments, the isolation window was set to *m*/*z* 0.4 and in the higher-energy collisional dissociation (HCD) cell, collision energies of 20, 30, 35 or 40 eV were applied. For pseudo MS^3 experiments, the source induced dissociation (SID) energy was set to 20 eV.

Analysis of Conjugated Steroids

For the analysis of intact conjugated steroids, samples were diluted 1:1 with ultrapure water. In order to perform PRM experiments, selected samples were 5-fold pre-concentrated by SPE as described in section 2.3.1, and reconstituted in 50 μL 10% aqueous ACN. The setup for the LC-ESI-HRMS (Orbitrap) system was similar to the settings described in chapter LC-ESI-HRMS (LC Orbitrap) Setup, but employing a modified gradient. Starting at 1% ACN (containing 0.1% FA), the gradient increased to 40% ACN within 9 min, to 99% until 10.9 min, and to 1% until 11 min. The system was re-equilibrated for 3 min. Full MS, AIF, and PRM experiments were conducted and ESI with positive polarity was applied. In selected experiments, also negative ionization was used, which is explicitly indicated in the corresponding data sets.

Synthesis of Trenbolone-diol

Trenbolone-diol was synthesized by reduction of Tren under argon atmosphere. To 10 mg of Tren dissolved in 10 mL of anhydrous THF, 100 μL of potassium tri-sec-butylborohydride (1 M in THF) were added under constant stirring. After 15 min, the reaction was stopped with 10 mL of ultrapure water, and subsequently, a LLE with 20 mL of TBME was performed. An aliquot of the yielded products was acetylated as described in section Acetylation.

RESULTS AND DISCUSSION

Metabolite Identification With GC-TC-IRMS

The use of GC-TC-IRMS allows for comprehensive metabolite studies, particularly when investigating biotransformation products of deuterated compounds.

A significant increase of the ratio *m*/*z* 3 to *m*/*z* 2 indicates the presence metabolites of the administered substance, in this case trenbolone. Exemplary GC-TC-IRMS chromatograms of both a pre- and post-administration sample are displayed in **Figure 3**. The upper part (A) shows the chromatogram of the fraction containing the hydrolyzed glucuronides (fraction Gluc) of a pre-administration sample with deuterium levels at natural abundance. By contrast, the lower chromatogram (B) shows a sample collected 45 h following drug administration-, and several peaks of deuterated molecules corresponding to metabolites of Tren are visible. In the inset, details of the metabolites eluting at retention times between 1108 and 1110 s are shown.

Trenbolone Metabolites Identified by LC-ESI-HRMS

Selected HPLC fractions exhibiting signals of deuterated compounds of considerable abundance were additionally analyzed by LC-ESI-HRMS(/MS). For metabolite identification, mass-to-charge-ratios were computed by *in silico* prediction and their presence or absence was assessed in the post-administration samples. Promising metabolites, their corresponding HPLC

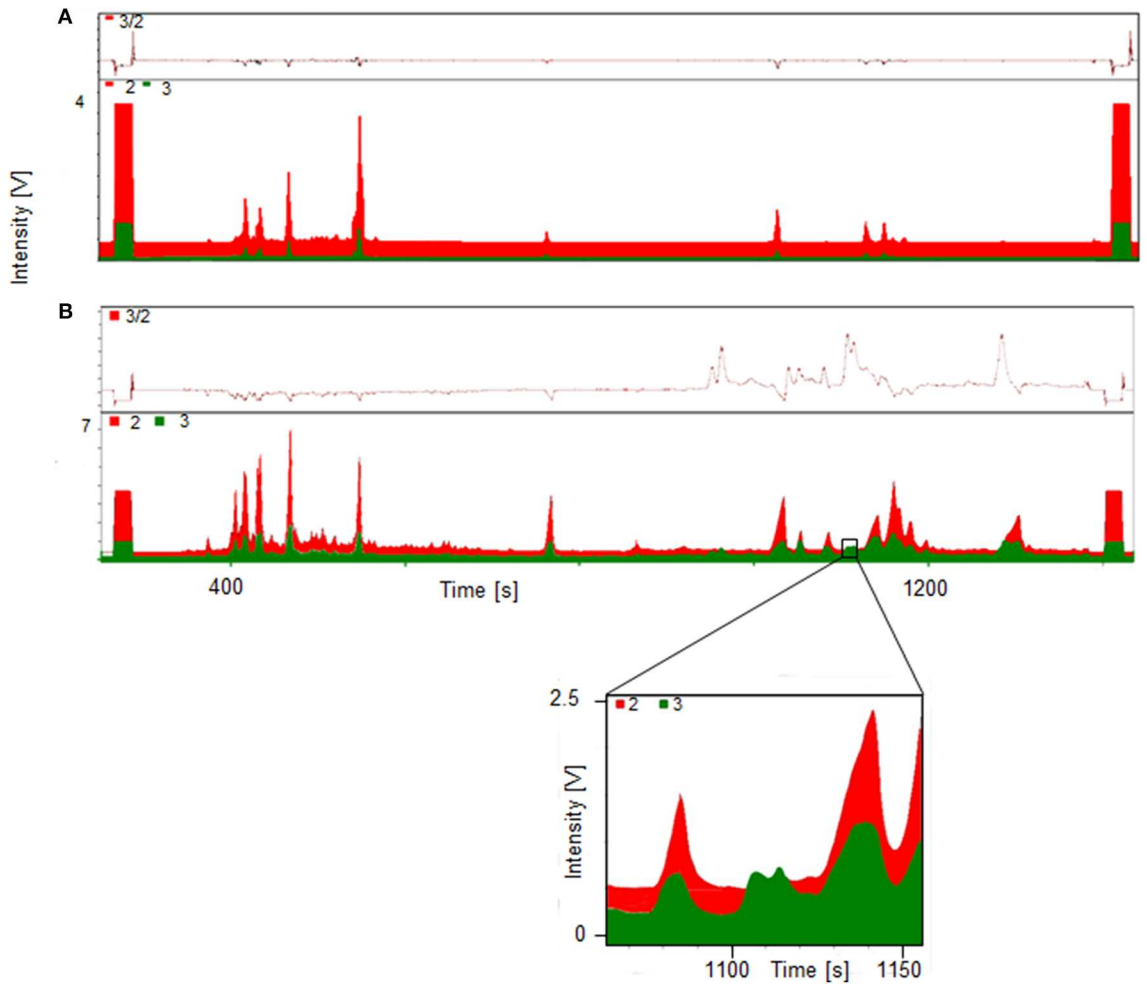

FIGURE 3 | GC-TC-IRMS chromatograms of HPLC fraction II Gluc of a pre- **(A)** and 45 h post- **(B)** administration sample collected following ingestion of 10 mg of d_5-TREN.

(sub-)fractions, retention times for LC-ESI-HRMS, exact masses, calculated elemental compositions, excretion forms, and detection windows are summarized in **Table 1**. Obtained elemental compositions were calculated within a maximum permitted mass error of ±4 ppm. Metabolites were determined in HPLC sub-fractions I, II, IV, and V. The number sequence corresponds to increasing retention times and decreasing polarity of the metabolites after hydrolysis, but before acetylation.

Altogether, a total of 20 phase-II metabolites of relevant traceability was identified. Almost all metabolites were found to be eliminated as differently conjugated products including the well-characterized glucuronic acid and sulfate conjugates, as well as alkaline-labile phase-II metabolites. De-conjugation under alkaline conditions is less established for human metabolism, but has already been assessed in preventive doping research to generate cysteine conjugates (Fabregat et al., 2010, 2013; Pozo et al., 2010; Gomez et al., 2014). Especially for Tren, cysteine conjugates are supposed to be of relevance (Sobolevsky and Rodchenkov, 2015).

Presumed phase-I reactions comprised hydroxylation, dehydrogenation, dehydration, and reduction of a keto to a hydroxyl moiety or *vice versa*. Most metabolites were identified as the 4-fold deuterated isomers of the metabolites although 5-fold deuterated Tren was administered. This suggests that a metabolic conversion occurs predominantly within the steroidal A or B ring. The 5-fold deuterated isomers of the well-known glucuronic acid-conjugated metabolites Tren (metabolite 4) and EpiTren (metabolite 3) were confirmed in the respective Gluc fraction and were unambiguously identified by retention time and product ion mass spectra in comparison to reference material.

For sports drug testing, especially long term metabolites with extended detection windows are of great interest. Within this study, metabolites 7, 8, 9, and 11 were found to have detection times between 118 h (5 days) and 142 h (6 days). Extracted ion chromatograms (EIC) displaying metabolite 9_Gluc in pre- and post-administration samples are depicted in **Figure 4**. The hydrolyzed metabolites 7 (excreted as glucuronide) and

TABLE 1 | Deuterated TREN metabolites and diagnostic product ions (CE = 20 and CE = 30 eV) after hydrolysis of phase-II metabolites, HPLC fractionation and acetylation identified by LC-ESI-HRMS.

#	HPLC fraction	Retention time HFX [min]	Exact mass [*m/z*]	Elemental composition	Error [ppm]	Excretion form[a]	Detection window [h]	Diagnostic production [*m/z*]	Elemental composition	Error [ppm]	Diagnostic production [*m/z*]	Elemental composition	Error [ppm]	Diagnostic production [*m/z*]	Elemental composition	Error [ppm]	Diagnostic production [*m/z*]	Elemental composition	Error [ppm]
1	I	4.39	301.2095	$C_{20}H_{21}D_4O_2^+$	−1.7	1_Sulf	45	259.2000	$C_{18}H_{19}D_4O^+$	2.1	241.1890	$C_{18}H_{17}D_4^+$	0.5						
						1_Cys	45												
2	I	5.25	301.2091	$C_{20}H_{21}D_4O_2^+$	−3.0	2_Sulf	45	259.1999	$C_{18}H_{19}D_4O^+$	1.7	241.1890	$C_{18}H_{17}D_4^+$	0.5						
						2_Cys	118												
3	II	3.33	318.2112	$C_{20}H_{20}D_5O_3^+$	−0.0	3_Gluc	21	276.2003	$C_{18}H_{18}D_5O_2^+$	−1.2	258.1896	$C_{18}H_{16}D_5O^+$	−1.8						
4	II	3.68	318.2112	$C_{20}H_{20}D_5O_3^+$		4_Gluc	45	276.2004	$C_{18}H_{18}D_5O_2^+$	−0.9	258.1897	$C_{18}H_{16}D_5O^+$	−1.5						
5	II	3.47	373.1944	$C_{22}H_{21}D_4O_5^+$	−1.0	5_Gluc	94	331.1837	$C_{20}H_{19}D_4O_4^+$	−1.8	313.1731	$C_{20}H_{17}D_4O_3^+$	−2.0	289.1731	$C_{18}H_{17}D_4O_3^+$	−1.8	271.1625	$C_{18}H_{15}D_4O_2^+$	−1.7
						5_Sulf	70												
6	II	3.56	313.1731	$C_{20}H_{17}D_4O_3^+$	−1.7	6_Gluc	94	271.1628	$C_{18}H_{15}D_4O_2^+$	−0.1	253.1523	$C_{18}H_{13}D_4O^+$	−0.8	227.1366	$C_{16}H_{11}D_4O^+$	−1.1			
						6_Sulf	70												
7	II	4.95	357.1995	$C_{22}H_{21}D_4O_4^+$	−1.0	7_Gluc	118	315.1888	$C_{20}H_{19}D_4O_3^+$	−1.5	297.1783	$C_{20}H_{17}D_4O_2^+$	−1.4	273.1784	$C_{18}H_{17}D_4O_2^+$	−1.2	255.1676	$C_{18}H_{15}D_4O^+$	−2.2
8	II	5.03	357.1996	$C_{22}H_{21}D_4O_4^+$	−0.7	8_Sulf	118	315.1888	$C_{20}H_{19}D_4O_3^+$	−1.5	297.1784	$C_{20}H_{17}D_4O_2^+$	−1.1	273.178	$C_{18}H_{17}D_4O_2^+$	−2.6	255.1678	$C_{18}H_{15}D_4O^+$	−1.4
						8_Cys	45												
9	IV	1.87	273.1787	$C_{18}H_{17}D_4O_2^+$	−0.1	9_Gluc	142												
						9_Sulf	94												
10	IV	3.35	313.1736	$C_{20}H_{17}D_4O_3^+$	−0.1	10_Sulf	94	271.1631	$C_{18}H_{15}D_4O_2^+$	0.1	253.1528	$C_{18}H_{13}D_4O^+$	1.2	227.1370	$C_{16}H_{11}D_4O^+$	0.7			
						10_Cys	45												
11	V	1.58	313.1736	$C_{20}H_{17}D_4O_3^+$	−0.1	11_Sulf	45	271.1635	$C_{18}H_{15}D_4O_2^+$	0.1	253.153	$C_{18}H_{13}D_4O^+$	2.0	227.1374	$C_{16}H_{11}D_4O^+$	2.4			
12	-	2.55	273.1788	$C_{18}H_{17}D_4O_2^+$	0.3	12_Cys	70	255.1685	$C_{18}H_{15}D_4O^+$	1.4	229.1531	$C_{16}H_{13}D_4O^+$	2.6						
13	-	4.83	359.2152	$C_{22}H_{23}D_4O_4^+$	−0.8	13_Cys	118	317.2054	$C_{20}H_{21}D_4O_3^+$	1.2	299.1946	$C_{20}H_{19}D_4O_2^+$	0.8	257.1840	$C_{18}H_{17}D_4O^+$	0.8	239.1737	$C_{18}H_{15}D_4^+$	1.9

[a] *De-conjugation under alkaline conditions expecting potential cysteine conjugates.*

8 (excreted as sulfate) are considered as isomers due to their identical elemental composition and their minor difference in retention time. Since metabolite 7/8 and metabolite 9 are excreted in two conjugation forms, in particular as glucuronides and sulfates, they were chosen for further characterization (see section Production Ion Mass Spectra).

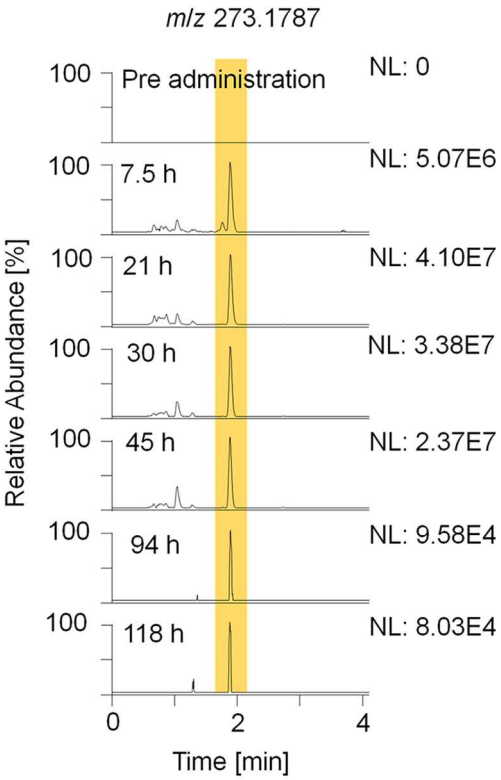

FIGURE 4 | EIC of *m/z* 273.1787 (± 5 ppm) representing metabolite 9_Gluc after hydrolysis and acetylation analyzed by LC-HRMS in +ESI full MS mode.

Metabolite Characterization

Product Ion Mass Spectra

Besides accurate mass measurements verifying the deuterium content, all identified metabolites were characterized by product ion mass spectra (MS^2) obtained from PRM experiments. Analysis was performed in ESI positive mode, as it was found to produce more characteristic product ion mass spectra compared to those obtained following negative ionization (Rzeppa et al., 2015). Collision induced dissociation (CID) was accomplished at different collision energies ranging from 20 to 40 eV.

The PRM mass spectrum of metabolite 9_G after hydrolysis and acetylation is illustrated in **Figure 5** as an example, the diagnostic product ions, elemental compositions, and mass errors of the other metabolites are listed in **Table 1**. From the elemental composition and the MS/MS-experiments, metabolite structures were postulated. Metabolite 5 is tentatively assigned to a hydroxyl-metabolite of Tren, which was substantiated by the 2-fold loss of an acetyl moiety [neutral loss of *m/z* 42 (Ac) and *m/z* 60 (AcOH)]. For this metabolite, the generation of a fourth double bond by oxidation of a tertiary carbon atom is additionally required.

The metabolites 7 and 8 are tentatively assigned to derivatives of Tren that result from the reduction of the 3-oxo functionality of the anabolic steroid as supported by the characteristic and repeatedly occurring losses of acetyl moieties. Further, the presence of two additional double bonds (of unknown position) is postulated.

The elemental composition of metabolite 9 indicates a potential metabolic conversion to trenbolone-diketone. The metabolite was not derivatized by pyridine/acetic anhydride,

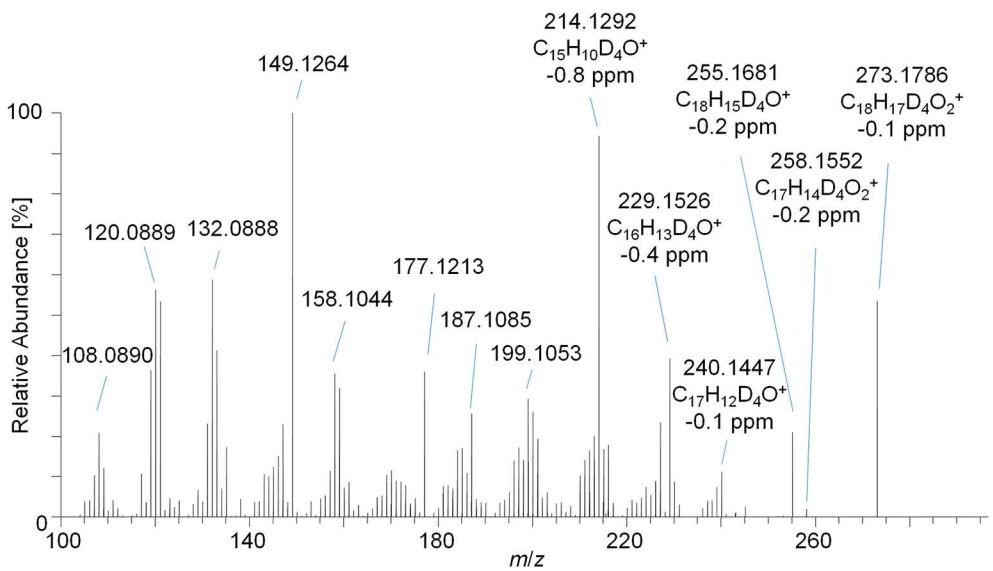

FIGURE 5 | PRM mass spectrum of *m/z* 273.1787 at 35 eV representing metabolite 9_Gluc after hydrolysis and acetylation analyzed by LC-HRMS.

which corroborates the absence of hydroxyl functions. In accordance with the current state of knowledge, free hydroxyl groups are acetylated under the applied conditions, but -oxo functions are not affected; however, failed derivatization due to steric hindrance cannot be excluded (Piper et al., 2008).

The detection of trenbolone-diketone, also known as 17-keto-trenbolone or trendione, was already reported in 1991 (Spranger and Metzler, 1991) for *in vivo* samples, and the compound could be generated *in vitro* by the same group by using human liver microsomes (Metzler and Pfeiffer, 2001).

Noteworthy, an additional abundant signal of *m/z* 97.0652 corresponding to C_6H_9O as elemental composition (±4.2 ppm) was observed in the PRM spectra. Since trenbolone-diketone is deuterated in the A- and B-ring, the signal has to be derived from the steroidal C- or D-ring. Structural elucidation of the equivalent diagnostic ion has been accomplished for androst-4-en-3-one-based steroids, but this structure cannot be immediately transferred to the herein investigated molecule as it was shown to originate from the steroidal A-ring (Thevis et al., 2012).

Synthesis of Trenbolone-diol

For the metabolites 7_Gluc and 8_Sulf, which were proposed to represent trenbolone-diol derivatives, further in-depth studies were conducted. In order to obtain a reference mass spectrum of trenbolone-diol, an in-house synthesis was accomplished by reducing Tren with potassium tri-sec butylborohydride. Two isomers of trenbolone-diol were successfully synthesized and PRM spectra of the free and acetylated forms were acquired. Remarkably, also 1-fold and 2-fold dehydrogenated trenbolone-diol derivatives were obtained as byproducts in two isomeric forms despite the employed reducing conditions. The 2-fold dehydrogenated trenbolone-diol derivative was found to be analog to the predicted metabolite 7/8 after hydrolysis. In **Figure 6**, the EIC of the synthesized 2-fold dehydrogenated trenbolone-diol derivative (A) is compared to the metabolites identified in the post-administration urine samples (B). The retention times (4.85 and 4.95 min) of the synthesized products are in accordance with the postulated metabolites. Both synthesized isomers were present in the glucuronide and the sulfate fraction. While the metabolite at 4.95 min is the most prominent isomer eliminated as glucuronide, the sulfated analog with the longest detection window at 5.03 min was not synthesized. The potential cysteine conjugates are less valuable due to their short detection window.

Product ion mass spectra of the acetylated 2-fold dehydrogenated trenbolone-diol derivative isomer at 4.95 min and the acetylated metabolite 7_Gluc after hydrolysis are in good agreement as demonstrated in **Figure 7**. The observed mass shift of four Da is caused by the 4-fold deuteration of the metabolite. The PRM mass spectra of the three hydrolyzed metabolites were highly comparable in all excretion forms. As a consequence, they are assumed to be different isomeric forms of the 2-fold dehydrogenated trenbolone-diol derivative. Isomers can be attributed to both stereo centers at C3 and C17, as well as various positions of the additional double bonds.

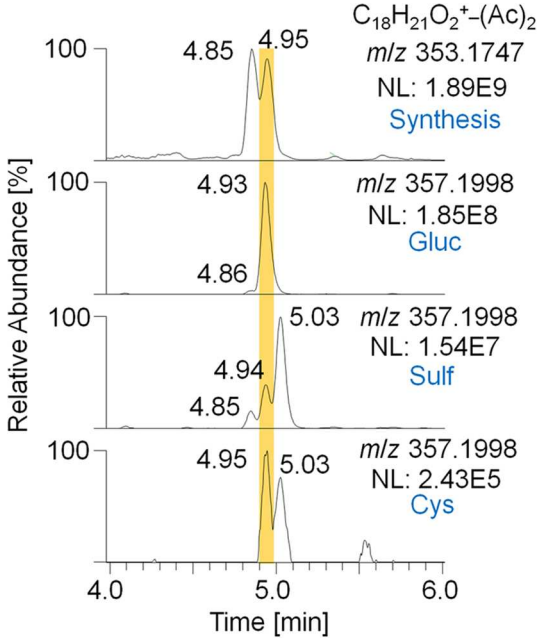

FIGURE 6 | EIC of *m/z* 353.1747 (± 5 ppm) representing the 2-fold dehydrogenated trenbolone-diol derivatives obtained by in-house synthesis and *m/z* 357.1998 (± 5 ppm) representing the deuterated metabolites 7/8 eliminated as glucuronide, sulfate, and cysteine conjugate after hydrolysis and acetylation analyzed by LC-HRMS in +ESI full MS mode.

Phase-II Conjugates

The sample preparation comprising SPE, LLE, hydrolysis, HPLC fractionation, and derivatization is very elaborate and may be accompanied by analyte losses and/or the formation of artifacts during derivatization (Piper et al., 2019). Moreover, the herein employed approach of analyzing acetylated steroids by LC-ESI-HRMS is certainly unconventional.

In sports drug testing, the implementation of new analytes/metabolites into existing methods is of great importance to enable a specific and sensitive detection of the target molecules as well as adequate detection windows. Currently, three different methods are routinely used for the analysis of doping control samples, where an implementation of novel Tren metabolites appears feasible: (a) measurement of analytes hydrolyzed and derivatized as TMS derivatives with GC-EI-MS/MS, (b) measurement of hydrolyzed, but not acetylated analytes, (c) measurement of intact phase-II metabolites with LC-ESI-HRMS. Since the ionization efficacy of steroid diols with low proton affinity such as metabolites 7/8 by ESI is usually limited, the existing LC-ESI-HRMS approach was not considered as the preferred option. When using LC-ESI-HRMS, it is generally advisable to measure the intact phase-II conjugates, which also results in a reduced workload (Gomez et al., 2014).

In order to investigate the new metabolites regarding their applicability to doping control routine testing, the intact phase-II metabolites were analyzed by LC-ESI-HRMS. For the potential

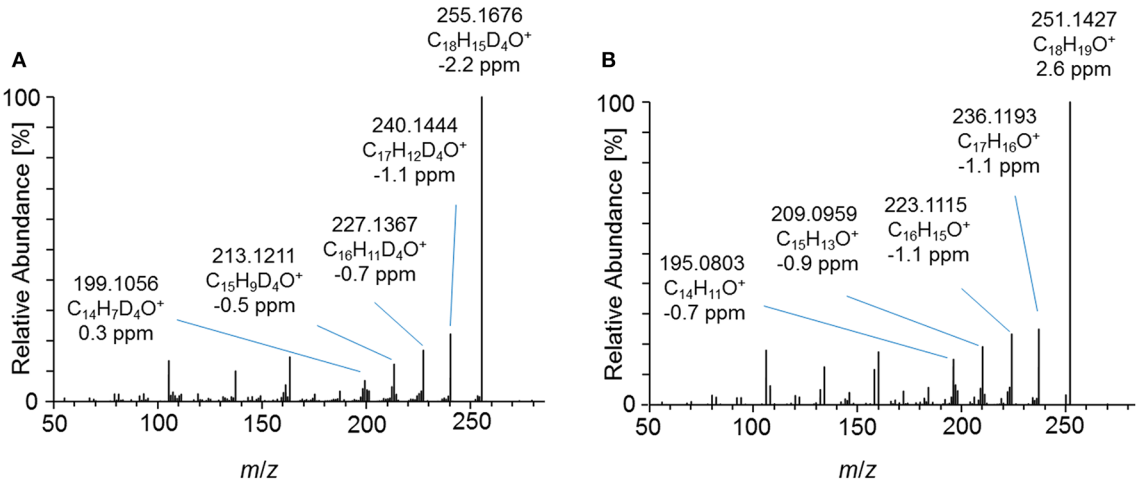

FIGURE 7 | PRM mass spectrum of **(A)** *m/z* 357.1995 at 40 eV representing the deuterated metabolite 7_Gluc after hydrolysis and acetylation and **(B)** *m/z* 353.1747 at 40 eV representing the synthesized 2-fold dehydrogenated trenbolone-diol derivatives at 4.95 min by LC-ESI-HRMS.

Tren-diol derivatives (metabolite 7_Gluc), a peak corresponding to the singly glucuronidated metabolite was identified. The pseudo MS^3 mass spectra of the intact glucuronide and the acetylated and hydrolyzed metabolite are compared in **Figure 8**. Both product ion mass spectra derived from *m/z* 273.1787 are in good agreement. Observed variations in the relative intensities are potentially caused by differences in the energetic status of both molecules resulting from the in-source dissociation process.

Comparison to Reference Material

As outlined in above, the characterization of metabolite 9 yielded a potential diketone derivative of trenbolone. A commercially available reference standard of trenbolone-diketone, 4,9,11-estratriene-3,17-dione, was analyzed by LC-ESI-HRMS. The pseudo MS^3 spectrum of the sulfated diketone metabolite in urine and the product ion mass spectrum of the reference standard are displayed in **Figure 9**. Again, the mass shift of four Da is caused by the 4-fold deuteration of the metabolite. The good agreement of both product ion mass spectra supports the assignment of metabolite 9_Sulf to a potential diketone derivative. It is noticeable that phase-II conjugation appears to occur via keto-/enol-tautomerism as described earlier also for androstenedione (Tajic and Kovacic, 1968; Goodall and James, 1979, 1981).

Determination of Detection Windows for Published Long-Term Metabolites

State-of-the-art routine doping control methods are primarily based on epitrenbolone, trenbolone glucuronide and epitrenbolone glucuronide (De Boer et al., 1991; Schänzer, 1996; Brun et al., 2011). In addition, trenbolone sulfate and the trenbolone cysteine adduct have been published (Rzeppa et al., 2015; Sobolevsky and Rodchenkov, 2015). While no detection windows for the sulfate conjugate have been described yet, limited data sets are available for the glucuronide conjugate. An early Tren metabolism study used radioactive labeling and investigated the urinary excretion. Spranger and Metzler detected 54% of the radioactivity within 26 h and 63% within 72 h post Tren administration, indicating a fast elimination (Spranger and Metzler, 1991). A publication from the former Russian anti-doping laboratory published the traceability of trenbolone administrations of 32 days when employing epitrenbolone glucuronide as target analyte; similarly the trenbolone cysteine adduct was detected for 32 days. The deuterated analogs of the described metabolites were also detected in this elimination study as illustrated in **Figure 10** by means of respective EIC.

Epitrenbolone was detectable for 45 h and Tren for 21 h after oral administration of 10 mg of trenbolone. For the sulfate conjugate, three potential isomers were identified, two of which are obviously induced by epimerization at position 17. The third one remained unclear but might be attributed to a conjugate directed to position 3. This can be derived from the occurrence of the above described assumed conjugation of the diketone derivatives metabolite 9_Gluc and 9_Sulf, which appear to be conjugated via a steroidal keto group. All three isomers were detectable for 45 h following administration. The Tren cysteine conjugate was observed for 45 h on *m/z* 276.2006 referring to the steroid structure which is generated by in source dissociation. The intact phase-II metabolite at *m/z* 397.2204 was also visible, but for **Figure 10**, the mass-to-charge ratio of the variant with the longest detectability was chosen.

The results generated in this study corroborate the primary data of Spranger and Metzler, where Tren was identified as substance with a fast elimination. Inter-individual variations in the metabolism of the volunteers of the different studies are a conceivable explanation for deviating results, but investigation of a larger population appear necessary and warranted to further substantiate the observations.

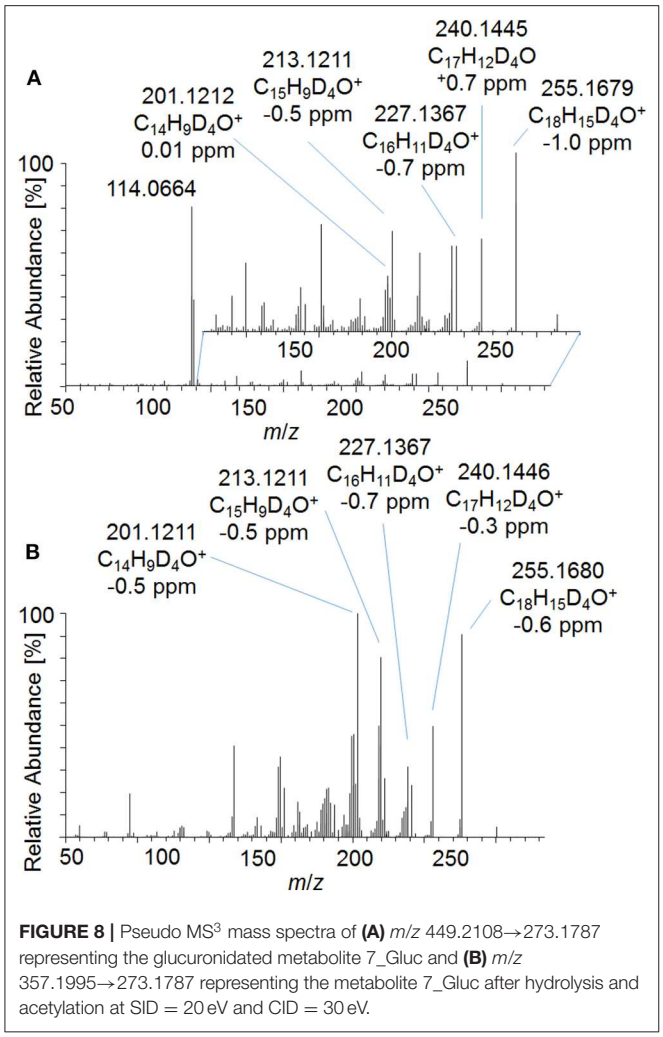

FIGURE 8 | Pseudo MS^3 mass spectra of **(A)** *m/z* 449.2108→273.1787 representing the glucuronidated metabolite 7_Gluc and **(B)** *m/z* 357.1995→273.1787 representing the metabolite 7_Gluc after hydrolysis and acetylation at SID = 20 eV and CID = 30 eV.

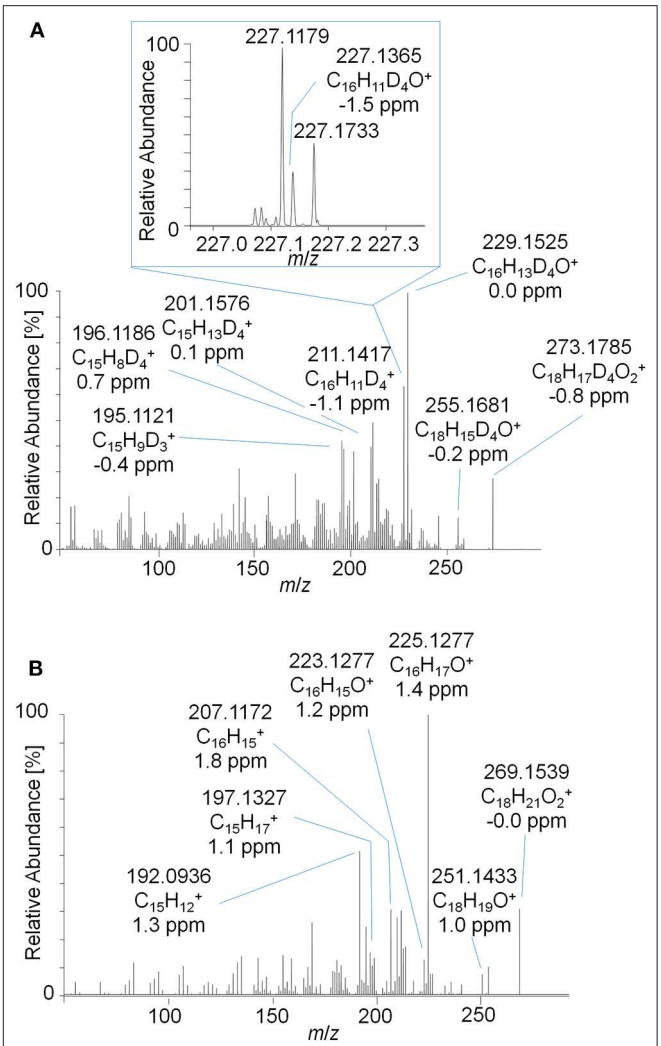

FIGURE 9 | (A) Pseudo MS^3 mass spectrum of *m/z* 353.1355→273.1787 at SID = 20 eV and CID = 30 eV representing the sulfated metabolite 9_Sulf and **(B)** PRM mass spectrum of *m/z* 269.1536 at 30 eV representing trenbolone-diketone reference material.

Limitations of Combining Data Obtained From GC-TC-IRMS/MS, LC-ESI-HRMS, and GC-EI-HRMS

In previous publications, GC-TC-IRMS/MS has been successfully employed in support of steroidal metabolite identification, especially when combined with GC-EI-HRMS (Thevis et al., 2013; Piper et al., 2016a,b, 2018, 2019).

This concept was adapted to this study, and referring to **Figure 3**, two metabolites were identified by using the conventional approach. The first peak at 1108 s was identified as the glucuronic acid conjugate of the well-characterized metabolite EpiTren by comparing the retention time and mass spectrum to reference material. The metabolite at 1110 s was formerly unknown and further characterized by GC-EI-HRMS (TOF) analysis. The resulting mass spectrum is shown in **Figure 11**. Under consideration of the different ionization and dissociation mechanisms, this mass spectrum was found to correspond to that of the deuterated 2-fold dehydrogenated trenbolone-diole derivative characterized by LC-ESI-HRMS (**Figure 7**).

Unfortunately, the described approach could not be applied to all metabolites. The quality of analytical data generated by the GC-TOF system suffered from an intense fragmentation, which led to a reduced abundance or absence of the molecular ion, complicating structural elucidation of new metabolites (Thevis et al., 2013; Piper et al., 2016a,b, 2018, 2019).

Therefore, a GC Orbitrap system with an alternative ion source design favoring higher abundances of ions with larger *m/z* values was used, and the measured TMS derivatives further exhibited a reduced in-source fragmentation compared to acetates (Piper et al., 2018, 2019). In addition, trimethylsilylation of steroidal analytes is routinely used, thus offering a platform for implementing potential new target analytes into sports drug testing methods. However, the analysis of TMS derivatives

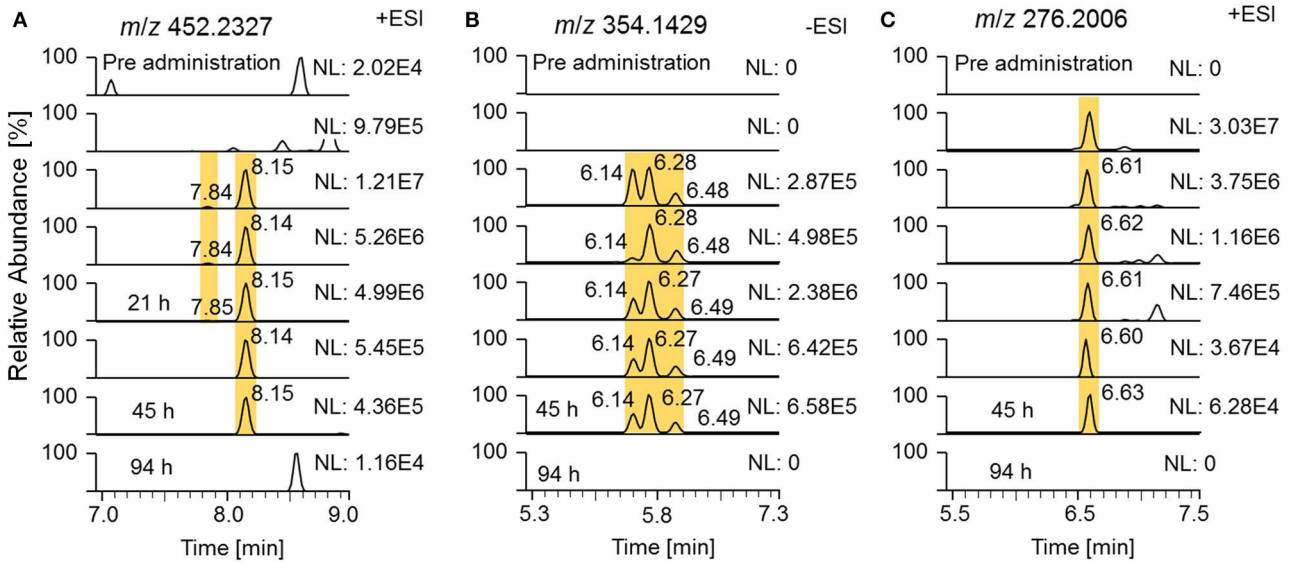

FIGURE 10 | EIC of **(A)** *m/z* 452.2327 (± 5 ppm) representing deuterated trenbolone glucuronide, **(B)** *m/z* 354.1429 representing deuterated trenbolone sulfate, and **(C)** *m/z* 276.2006 representing deuterated trenbolone cysteine adduct by LC-HRMS.

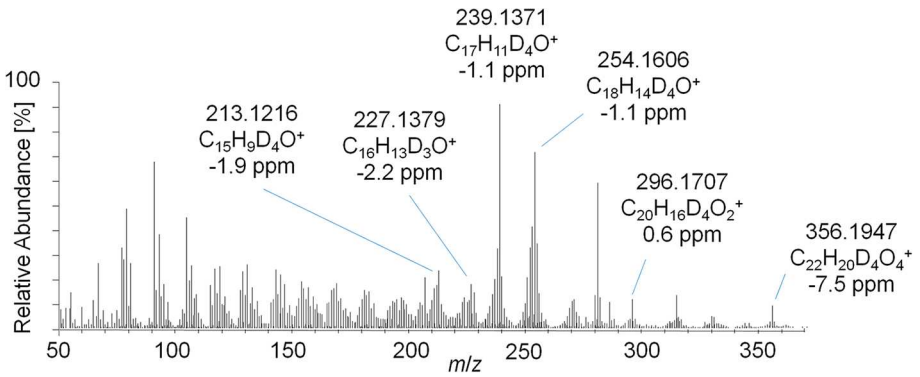

FIGURE 11 | GC-EI-HRMS full MS mass spectra of trenbolone-diol metabolites excreted as glucuronides (7_Gluc).

with the GC Orbitrap remained challenging as the analysis of reference material of trenbolone, epitrenbolone and d_5-trenbolone introduced as TMS-derivatives resulted in a variety of signals presumably caused by derivatization and thermal degradation artifacts. Consequently, no unreported metabolites could be identified. For the TMS derivatives of trenbolone and epitrenbolone, a signal at *m/z* 414.2405 representing the molecular ion is expected. Moreover, peaks at *m/z* 412.2248 and *m/z* 410.2092 have been reported, which belong to products eliminating two or four hydrogens (De Boer et al., 1991; Ayotte et al., 1996). As shown in **Figure 12**, several additional peaks of unknown origin were observed in the reference material, which suggested a significantly limited utility of this setup for identifying additional metabolites in urine.

It has to be taken into account that the herein investigated molecule possesses poor gas chromatographic properties, and the highly conjugated 4,9,11-triene-3-one structure results in derivatization artifacts with low thermal stability. Other structurally related molecules such as the designer steroid tetrahydrogestrione are not detectable in urine as TMS-derivatives as well, and remained hidden until its first identification as performance-enhancing drug in 2003 by means of LC-MS/MS (Catlin et al., 2004; Thevis et al., 2005a). In other words, Tren has a documented history of challenging analytics as corroborated by a variety of assessed derivatization techniques (De Boer et al., 1991; Ayotte et al., 1996; Casademont et al., 1996; Marques et al., 2007; Brun et al., 2011; Parker et al., 2012).

LC-ESI-MS was found to be suitable for the quantification of Tren (Thevis et al., 2005a,b, 2009) in the past, and common routine doping control procedures nowadays utilize LC-ESI-MS/MS for analytes of this and related structure. As a consequence, also here a LC-ESI-HRMS system was used to overcome the limitations regarding the mass resolution and the presence of the molecular ion. Furthermore, a derivatization

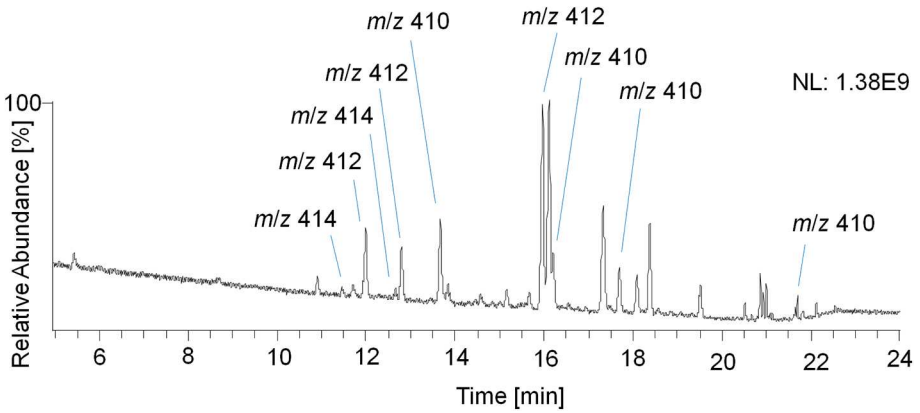

FIGURE 12 | GC-EI-HRMS full MS chromatogram of epitrenbolone reference material as TMS-derivatives.

by acetylation improved the proton affinity for ESI positive ionization mode, and especially the ionization of the trenbolone-diol derivatives metabolite was found to be strongly increased.

The advantage of the untargeted GC-TC-IRMS approach is unfortunately not as pronounced as in previous studies as aligning LC and GC chromatograms and (presumed) molecular ions for target analyte characterization is difficult.

CONCLUSION

In order to enhance the retrospectivity and sensitivity of analytical approaches targeting trenbolone misuse in sport, a comprehensive *in vivo* metabolism study was performed. An approach utilizing stable isotope-labeled substrates facilitating the investigation of biotransformations by GC-TC-IRMS was employed. While the strategy proved straightforward in earlier studies, trenbolone and its metabolic products presented comparably challenging target analytes due to their limited compatibility with gas chromatography. Nevertheless, by employing miscellaneous techniques of derivatization and chromatography, a total of 20 metabolites excreted as glucuronides, sulfates and potential cysteine conjugates were identified. Four metabolites, tentatively attributed to trenbolone-diketone and a 2-fold dehydrogenation product of trenbolone-diol, eliminated both as glucuronide and sulfate, were found to complement the existing urinary trenbolone metabolic pattern, offering detection windows of 6, respectively 5 days. Further characterization of these metabolites was conducted by pseudo-MS^3 experiments and comparison to commercially available or in-house synthesized reference material. To verify or falsify the true added value of the herein identified trenbolone metabolites for routine doping controls, those samples that return suspicious or even adverse analytical findings for trenbolone using established approaches will be further investigated regarding the new potential target analytes. If a positive contribution will be observed, future studies to confirm tentatively assigned structures e.g., by nuclear magnetic resonance analysis after upscaling of the synthesis and an administration study of unlabeled trenbolone could be warranted. Moreover, it might be of interest to administer other doses of trenbolone and to investigate a larger population for examination of inter-individual variations.

DATA AVAILABILITY STATEMENT

The datasets generated for this study are available on request to the corresponding author.

ETHICS STATEMENT

The administration study involving a human participant was approved by the Ethics Committee of the National Institute of Sports of Romania (Bucharest, Romania, #2283, 2016) according to the declaration of Helsinki. Informed consent was obtained from the volunteer.

AUTHOR CONTRIBUTIONS

MT and TP conceived conception and study design, contributed to data interpretation and discussion, and revised and edited the manuscript. MP conducted the sample preparation, measurements, data evaluation, and wrote the draft of the manuscript.

FUNDING

This project was financially supported by the Manfred-Donike Institute for Dope Analysis (Cologne, Germany) and the World Anti-Doping Agency (grant #17A31MT).

ACKNOWLEDGMENTS

The authors like to acknowledge the contribution of Dr. Andreas Thomas, Dr. Josef Dib, and the Romanian Doping Control Laboratory for analytical and administrative support.

REFERENCES

Ayotte, C., Goudreault, D., and Charlebois, A. (1996). Testing for natural and synthetic anabolic agents in human urine. *J. Chromatogr. B* 687, 3–25. doi: 10.1016/S0378-4347(96)00032-1

Blair, I. A. (2006). Endogenous glutathione adducts. *Curr. Drug. Metab.* 7, 853–872. doi: 10.2174/138920006779010601

Brun, E. M., Puchades, R., and Maquieira, Á. (2011). Analytical methods for anti-doping control in sport: anabolic steroids with 4,9,11-triene structure in urine. *Trends Anal. Chem.* 30, 771–783. doi: 10.1016/j.trac.2011.01.010

Casademont, G., Pérez, B., and García Regueiro, J. A. (1996). Simultaneous determination, in calf urine, of twelve anabolic agents as heptafluorobutyryl derivatives by capillary gas chromatography-mass spectrometry. *J. Chromatogr. B* 686, 189–198. doi: 10.1016/S0378-4347(96)00211-3

Catlin, D. H., Sekera, M. H., Ahrens, B. D., Starcevic, B., Chang, Y. C., and Hatton, C. K. (2004). Tetrahydrogestrinone: discovery, synthesis, and detection in urine. *Rapid Commun. Mass Spectrom.* 18, 1245–1049. doi: 10.1002/rcm.1495

De Boer, D., Gainza Bernal, M. E., Van Ooyen, R. D., and Maes, R. A. (1991). The analysis of trenbolone and the human urinary metabolites of trenbolone acetate by gas chromatography/mass spectrometry and gas chromatography/tandem mass spectrometry. *Biol. Mass. Spectrom.* 20, 459–466. doi: 10.1002/bms.1200200805

Dunn, P. J. H., and Carter, J. F. (2018). *Good Practice Guide for Isotope Ratio Mass Spectrometry*, *2nd Edn*. Bristol: FIRMS.

Fabregat, A., Kotronoulas, A., Marcos, J., Joglar, J., Alfonso, I., Segura, J., et al. (2013). Detection, synthesis and characterization of metabolites of steroid hormones conjugated with cysteine. *Steroids* 78, 327–336. doi: 10.1016/j.steroids.2012.11.017

Fabregat, A., Pozo, Ó. J., Marcos, J., Segura, J., and Ventura, R. (2010). Quantification of testosterone and metabolites released after alkaline treatment in human urine. *Drug Test. Anal.* 2, 630–636. doi: 10.1002/dta.227

Fabregat, A., Pozo, Ó. J., Marcos, J., Segura, J., and Ventura, R. (2011). Alternative markers for the long-term detection of oral testosterone misuse. *Steroids* 76, 1367–1376. doi: 10.1016/j.steroids.2011.07.005

Gomez, C., Fabregat, A., Pozo, Ó. J., Marcos, J., Segura, J., and Ventura, R. (2014). Analytical strategies based on mass spectrometric techniques for the study of steroid metabolism. *Trends Anal. Chem.* 53, 106–116. doi: 10.1016/j.trac.2013.08.010

Goodall, A. B., and James, V. H. T. (1979). Conjugated androstenedione in human urine. *J. Steroid Biochem.* 11, 1613–1617. doi: 10.1016/0022-4731(79)90358-3

Goodall, A. B., and James, V. H. T. (1981). Observations on the nature and origin of conjugated androstenedione in human plasma. *J. Steroid Biochem.* 14, 465–471. doi: 10.1016/0022-4731(81)90358-7

Kuuranne, T., Pystynen, K. H., Thevis, M., Leinonen, A., Schänzer, W., and Kostiainen, R. (2008). Screening of *in vitro* synthesised metabolites of 4,9,11-trien-3-one steroids by liquid chromatography mass spectrometry. *Eur. J. Mass Spectrom.* 14, 181–189. doi: 10.1255/ejms.923

Mareck, U., Geyer, H., Opfermann, G., Thevis, M., and Schänzer, W. (2008). Factors influencing the steroid profile in doping control analysis. *J. Mass Spectrom.* 43, 877–891. doi: 10.1002/jms.1457

Mareck, U., Thevis, M., Guddat, S., Gotzmann, A., Bredehöft, M., Geyer, H., et al. (2004). "Comprehensive sample preparation for anabolic steroids, Glucocorticosteroids, Beta-Receptor blocking agents, selected anabolic androgenic steroids and Buprenorphine in human urine," in *Recent advances in doping analysis,* eds W. Schänzer, M. Thevis, H. Geyer, and U. Mareck. (Cologne: Sport u. Buch Strauß), 65–69.

Marques, M. A., Pereira, H. M., Padilha, M. C., and De Aquino Neto, F. R. (2007). Analysis of synthetic 19-norsteroids trenbolone, tetrahydrogestrinone and gestrinone by gas chromatography-mass spectrometry. *J. Chromatogr. A* 1150, 215–225. doi: 10.1016/j.chroma.2006.08.032

Metzler, M., and Pfeiffer, E. (2001). Genotoxic potential of xenobiotic growth promoters and their metabolites. *Apmis* 109, 89–95. doi: 10.1034/j.1600-0463.2001.d01-108.x

Parker, J. A., Webster, J. P., Kover, S. C., and Kolodziej, E. P. (2012). Analysis of trenbolone acetate metabolites and melengestrol in environmental matrices using gas chromatography-tandem mass spectrometry. *Talanta* 99, 238–246. doi: 10.1016/j.talanta.2012.05.046

Piper, T., Dib, J., Putz, M., Fusshöller, G., Pop, V., Lagojda, A., et al. (2018). Studies on the *in vivo* metabolism of the SARM YK11: identification and characterization of metabolites potentially useful for doping controls. *Drug Test. Anal.* 10, 1646–1656. doi: 10.1002/dta.2527

Piper, T., Fusshöller, G., Schänzer, W., Lagojda, A., Kuehne, D., and Thevis, M. (2019). Studies on the *in vivo* metabolism of methylstenbolone and detection of novel long term metabolites for doping control analysis. *Drug Test. Anal.* 11, 1644–1655. doi: 10.1002/dta.2736

Piper, T., Mareck, U., Geyer, H., Flenker, U., Thevis, M., Platen, P., et al. (2008). Determination of 13C/12C ratios of endogenous urinary steroids: method validation, reference population and application to doping control purposes. *Rapid Commun. Mass Spectrom.* 22, 2161–2175. doi: 10.1002/rcm.3601

Piper, T., Opfermann, G., Thevis, M., and Schänzer, W. (2010). Determination of (13)C/(12)C ratios of endogenous urinary steroids excreted as sulpho conjugates. *Rapid Commun. Mass Spectrom.* 24, 3171–3181. doi: 10.1002/rcm.4762

Piper, T., Schänzer, W., and Thevis, M. (2016a). Genotype-dependent metabolism of exogenous testosterone - new biomarkers result in prolonged detectability. *Drug Test. Anal.* 8, 1163–1173. doi: 10.1002/dta.2095

Piper, T., Schänzer, W., and Thevis, M. (2016b). Revisiting the metabolism of 19-nortestosterone using isotope ratio and high resolution/high accuracy mass spectrometry. *J. Steroid Biochem. Mol. Biol.* 162, 80–91. doi: 10.1016/j.jsbmb.2015.12.013

Pozo, O. J., Marcos, J., Ventura, R., Fabregat, A., and Segura, J. (2010). Testosterone metabolism revisited: discovery of new metabolites. *Anal. Bioanal. Chem.* 398, 1759–1770. doi: 10.1007/s00216-010-4082-0

Rzeppa, S., Heinrich, G., and Hemmersbach, P. (2015). Analysis of anabolic androgenic steroids as sulfate conjugates using high performance liquid chromatography coupled to tandem mass spectrometry. *Drug Test. Anal.* 7, 1030–1039. doi: 10.1002/dta.1895

Sano, M., Yotsui, Y., Abe, H., and Sasaki, S. (1976). A new technique for the detection of metabolites labelled by the isotope 13C using mass fragmentography. *Biol. Mass. Spectrom.* 3, 1–3. doi: 10.1002/bms.1200030102

Schänzer, W. (1996). Metabolism of anabolic androgenic steroids. *Clin. Chem.* 42, 1001–1020. doi: 10.1093/clinchem/42.7.1001

Sobolevsky, T., and Rodchenkov, G. (2015). "Detection of epitrenbolone glucuronide and cysteinyl conjugate of trenbolone may provide better retrospectivity of trenbolone abuse," in *Recent Advances in Doping Analysis,* eds W. Schänzer, M. Thevis, H. Geyer, and U. Mareck (Cologne: Sportverlag Strauss), 26–32.

Spranger, B., and Metzler, M. (1991). Disposition of 17β-trenbolone in humans. *J. Chromatogr. B* 564, 485–492. doi: 10.1016/0378-4347(91)80517-G

Tajic, M., and Kovacic, E. (1968). Free, glucuronic and sulfate testosterone, epitestosterone and adrostenedione in the urine. *Naturwissenschaften* 55:394. doi: 10.1007/BF00593305

Thevis, M., Beuck, S., Höppner, S., Thomas, A., Held, J., Schafer, M., et al. (2012). Structure elucidation of the diagnostic product ion at m/z 97 derived from androst-4-en-3-one-based steroids by ESI-CID and IRMPD spectroscopy. *J. Am. Soc. Mass Spectrom.* 23, 537–546. doi: 10.1007/s13361-011-0308-4

Thevis, M., Bommerich, U., Opfermann, G., and Schänzer, W. (2005a). Characterization of chemically modified steroids for doping control purposes by electrospray ionization tandem mass spectrometry. *J. Mass Spectrom.* 40, 494–502. doi: 10.1002/jms.820

Thevis, M., Fusshöller, G., and Schanzer, W. (2011). Zeranol: doping offence or mycotoxin? A case-related study. *Drug Test. Anal.* 3, 777–783. doi: 10.1002/dta.352

Thevis, M., Geyer, H., Mareck, U., and Schänzer, W. (2005b). Screening for unknown synthetic steroids in human urine by liquid chromatography-tandem mass spectrometry. *J. Mass Spectrom.* 40, 955–962. doi: 10.1002/jms.873

Thevis, M., Guddat, S., and Schänzer, W. (2009). Doping control analysis of trenbolone and related compounds using liquid chromatography-tandem mass spectrometry. *Steroids* 74, 315–321. doi: 10.1016/j.steroids.2008.10.004

Thevis, M., Piper, T., Horning, S., Juchelka, D., and Schänzer, W. (2013). Hydrogen isotope ratio mass spectrometry and high-resolution/high-accuracy mass spectrometry in metabolite identification studies: detecting target compounds for sports drug testing. *Rapid Commun. Mass Spectrom.* 27, 1904–1912. doi: 10.1002/rcm.6648

Tudela, E., Deventer, K., Geldof, L., and Van Eenoo, P. (2015). Urinary detection of conjugated and unconjugated anabolic steroids by dilute-and-shoot liquid chromatography-high resolution mass spectrometry. *Drug Test. Anal.* 7, 95–108. doi: 10.1002/dta.1650

WADA (2019). *2018 Anti-Doping Testing Figures*. Available online at: https://www.wada-ama.org/sites/default/files/resources/files/2018_testing_figures_report.pdf (accessed February 17, 2020).

WADA (2020). *The 2020 Prohibited List*. World Anti-Doping Agency. Available online at: https://www.wada-ama.org/sites/default/files/wada_2020_english_prohibited_list_0.pdf (accessed February 17, 2020).

Conflict of Interest: The authors declare that the research was conducted in the absence of any commercial or financial relationships that could be construed as a potential conflict of interest.

frontiers in Chemistry

METHODS
published: 05 June 2020
doi: 10.3389/fchem.2020.00439

Validation of a Bioanalytical Method for the Determination of Synthetic and Natural Cannabinoids (New Psychoactive Substances) in Oral Fluid Samples by Means of HPLC-MS/MS

Luca Calò[1], *Luca Anzillotti*[1]*, *Chiara Maccari*[2], *Rossana Cecchi*[1] and *Roberta Andreoli*[2,3]

[1] Legal Medicine, Department of Medicine and Surgery, University of Parma, Parma, Italy, [2] Laboratory of Industrial Toxicology, Department of Medicine and Surgery, University of Parma, Parma, Italy, [3] Centre for Research in Toxicology (CERT), University of Parma, Parma, Italy

OPEN ACCESS

Edited by:
Alberto Salomone,
University of Turin, Italy

Reviewed by:
Piotr Adamowicz,
Institute of Forensic Research (IFR), Poland
Emilia Marchei,
Istituto Superiore di Sanità (ISS), Italy

***Correspondence:**
Luca Anzillotti
luca.anzillotti@gmail.com

Specialty section:
This article was submitted to Analytical Chemistry, a section of the journal Frontiers in Chemistry

Received: 02 March 2020
Accepted: 27 April 2020
Published: 05 June 2020

Citation:
Calò L, Anzillotti L, Maccari C, Cecchi R and Andreoli R (2020) Validation of a Bioanalytical Method for the Determination of Synthetic and Natural Cannabinoids (New Psychoactive Substances) in Oral Fluid Samples by Means of HPLC-MS/MS. Front. Chem. 8:439. doi: 10.3389/fchem.2020.00439

New psychoactive substances (NPS) represent an important focus nowadays and are continually produced with minimal structural modifications in order to circumvent the law and increase the difficulty of identifying them. Moreover, since there are a high number of different compounds, it is arduous to develop analytical screening and/or confirmation methods that allow the identification and quantification of these compounds. The aim of this work is to develop and validate a bioanalytical method for detecting new synthetic drugs in biological samples, specifically oral fluid, using high-performance liquid chromatography coupled with mass spectrometry (HPLC-MS/MS) with minimal sample pretreatment. Oral fluid samples were simply centrifuged and denaturized with different rapid procedures before injection into the LC-MS/MS system. Calibration curves covered a linear concentration range from LOQ to 100 ng/mL. Validation parameters such as linearity, precision, accuracy, selectivity, matrix effect and thermal stability were evaluated and showed satisfactory results, in accordance with US Food & Drug Administration guidelines. The inter-day analytical bias and imprecision at two levels of quality control (QC) were within ±15% for most compounds. This method was able to identify and calculate the concentration of 10 NPS validated in this biological sample, even in the presence of matrix effect.

Keywords: new psychoactive substances, biological matrices, liquid chromatography, mass spectrometry, oral fluid, drugs of abuse, bioanalysis, method validation

INTRODUCTION

The drugs of abuse scenario is constantly changing with the rapid development of unregulated synthetic and ad-hoc-designed compounds (Anzillotti et al., 2019b; UNODC Early Warning Advisory on New Psychoactive Substances, 2020). In recent years, new psychoactive substances (NPS), including synthetic cannabinoids, as well as semi-synthetic opioids and heroin, have emerged as chemical compounds the use of which is spreading very rapidly, not only in the

United States of America but also in European countries, in addition to the use of classic drugs. Their popularity derives—especially in young generations—from their low cost and the high number of online shops. NPS are continually synthesized in illegal laboratories, and their consumption produces significant dangerous effects on human health that are still under investigation, such as agitation, aggression, and acute psychosis, as well as the potential development of dependence or cardiovascular effects (Anzillotti et al., 2019a; UNODC Early Warning Advisory on New Psychoactive Substances, 2020). In this context, the development and validation of analytical methods able to rapidly identify and correctly quantify such compounds are highly encouraged from a clinical and scientific point of view.

The purity and composition of products containing NPS are often unknown, and it can be very difficult to develop methods to identify them in biological matrices (Strano-Rossi et al., 2012, 2014; Brunt et al., 2017; Anzillotti et al., 2018, 2019b; Bianchi et al., 2019; Graziano et al., 2019; Williams et al., 2019). Although, at present, there is a rapid development of these substances of abuse, there are no current guidelines with threshold reference standard values for NPS in biological samples, to the best of our knowledge. In several countries, controls on groups of these "legal" substances are carried out using the principle of "chemical similarity" with substances already under the regulatory mechanism (United Nations Office on Drugs Crime, 2019). These substances have become a global phenomenon, with more than 120 countries and territories having reported at least one NPS (UNODC Early Warning Advisory on New Psychoactive Substances, 2020). In particular, until recently, 950 substances have been reported to the (UNODC) by governments, laboratories, and partner organizations (Rocchi et al., 2018; United Nations Office on Drugs Crime, 2019, 2020). Although synthetic cannabinoids are rapidly evolving and there are serious difficulties controlling them on the market (Coulter et al., 2011), in Europe, the European Monitoring Centre for Drugs and Drug Addiction (EMCDDA), through the EU Early Warning System, constantly monitors the use of synthetic cannabinoids. For the first time in 2008, forensic investigators in Germany and Austria took over the synthetic cannabinoid JWH018 (European Monitoring Centre for Drugs Drug Addiction, 2015). Since the 2000s, the synthetic cannabinoids were sold as mixtures for smokers, resins, and mixtures containing other psychoactive substances such as stimulants, hallucinogens, sedatives, and hypnotics. A recent development has been the discovery of synthetic cannabinoids in liquids for electronic cigarettes, now very popular among young people (European Monitoring Centre for Drugs Drug Addiction, 2017).

Therefore, the continuous challenge for forensic toxicologists is the identification of NPS in classical and alternative biological matrices such as oral fluid (Bosker and Huestis, 2009; Anizan and Huestis, 2013; Patsalos and Berry, 2013). The struggle for forensic laboratories is also due to the unknown composition of these new substances: therefore, the treatment of a patient who has taken synthetic drugs, perhaps in combination with other substances or alcohol, is quite difficult (Governo Italiano, 2017; Busardo et al., 2018). To date from a recent search of the literature, only a few studies have dealt with the determination of such compounds in oral fluid; however, thanks to current technological progress in the forensic toxicology field, a few screening tests and more selective techniques for alternative matrices have been developed, though the modern literature on analytical methodologies applied to these matrices is still limited, and a more detailed validation is often required (Gallardo and Queiroz, 2008; Strano-Rossi et al., 2012, 2014; Huestis et al., 2017; Anzillotti et al., 2018, 2019b; Bianchi et al., 2019; Graziano et al., 2019). Oral fluid has gained popularity as an alternative to classical hematic and urinary approaches in the field of workplace drug testing and the testing of drivers for being under the influence of drugs owing to its ease of collection and reduced detection time windows (Strano-Rossi et al., 2012; Edvardsen et al., 2015; Anzillotti et al., 2019b; Bianchi et al., 2019; Graziano et al., 2019). In particular, it appears to be an easier matrix to analyze and allows the rapid identification of recently developed drugs (Mercolini and Protti, 2016). No invasive sampling and easy storage are additional advantages deriving from the use of oral fluid over traditional matrices like blood or urine (Anzillotti et al., 2019b).

The aim of this article is to evaluate the best experimental conditions (in terms of sample pretreatment, technical parameters, and compound stability) in which to use oral fluid as an alternative matrix to detect these emerging drugs of abuse with a newly validated bioanalytical method.

EXPERIMENTAL

Chemicals and Reagents

Water, acetonitrile (AcCN), formic acid, and methanol (MeOH) were purchased from Sigma Aldrich (Milan, Italy).

Cannabinol (6,6,9-trimethyl-3h pentyl-6H-dibenzo[b,d] pyran-1-ol), cannabidiol (2-[(1R,6R)-3-methyl-6-(prop-1-en-2-yl) cyclohex-2-en-1-yl]-5-pentylbenzene-1,3-diol), THC (Δ9-tetrahydrocannabinol), THCCOOH (11-Nor-9-carboxy-Δ9-tetrahydrocannabinol), UR144 (1-pentyl-1H-indol- 3-yl) (2,2,3,3-tetramethylcyclopropyl)methanone, CP47497-C7 (2-[(1R,3S)-3-hydroxycyclohexyl]-5-(2-methyl-2-octanyl)phenol) and its homolog CP47497-C8 (2-(3-hydroxycyclohexyl)-5-(2-methylnonan-2-yl)phenol), AM2201 (1-([5-fluoropentyl]-1H-indol-3-yl)-(naphthalen-1-yl)methanone), JWH019 [(1-hexyl-1H-indol-3-yl)-1-naphthalenyl-methanone], JWH081 (4-methoxy-1-naphthalenyl 1-pentyl-1H-indol-3-yl) methanone), JWH122 (4-methyl-1-naphthalenyl) (1-pentyl-1H-indol-3-yl)methanone), JWH250 (1-(1-pentyl-1Hindol-3-yl)-2-(2-methoxyphenyl)-ethanone), JWH200 ([1-(2-morpholin-4-ylethyl)indol-3-yl]-naphthalen-1-ylmethanone), mephedrone or MEPH [(RS)-2-methylamino-1-(4-methylphenyl)propan-1-one], HU211 [(6As,10As)-9-(Hydroxymethyl)-6,6-dimethyl-3-(2-methyloctan-2-yl)-6a,7,10,10a-tetrahydrobenzo[c]chromen-1-ol], and Δ9-tetrahydrocannabinol-D3 (THC-D3) were also supplied from Sigma Aldrich (Milan, Italy). Standard compounds were stored according to supplier recommendations until their use. Amicon Ultra 3K devices (Millipore, Billerica, MA, USA) were used to centrifuge oral fluid samples.

Sample Collection and Preparation

Oral fluid samples were collected from 25 healthy volunteers free of drugs of abuse (both males and females), after obtaining their informed consent. The oral fluid was collected in a 15 ml plastic tube without an identification number in order to avoid any possible identification of the donor. Each sample was centrifuged at 4,000 rpm for 10 min. We mixed five different supernatants to obtain a pooled oral fluid sample. Five samples set with the minimum volume necessary for all the method validation experiments were prepared. The pooled lots were aliquoted and stored at −20°C until analysis (Gruppo Tossicologi Forensi Italiani, 2017).

All the experiments described below were prepared starting from these five pooled oral fluid samples, and each experiment was performed on all the five pooled lots independently.

Sample preparation consisted of combining 95 μL of pooled oral fluid with 5 μL of ISTD (THC-D3 at a concentration of 10 ug/mL) and 200 μL of MeOH in plastic vials; the samples were centrifuged at 10,000 rpm for 5 min, and, finally, 100 μL of supernatant was transferred to other plastic vials and injected into the HPLC-MS/MS system.

HPLC-MS/MS Equipment

The HPLC instrument was an Agilent Series 1100 (Agilent Technologies, Santa Clara, CA, USA) equipped with a degasser, a binary high-pressure gradient pump, and a thermostatted autosampler module. The MS/MS instrument was an API4000 (SCIEX, Framingham, MA USA) equipped with a TurboIonSpray interface for pneumatically assisted electrospray. Separation of the analytes and the internal standard (THC-D3) was performed using an Agilent® Pursuit XRs Ultra 2.8 C18 (100 × 2.0 mm) column, with mobile phase A consisting of an aqueous component (10 Mm formic acid in water at pH 3,75) and organic phase B (methanol/acetonitrile, 95/5 V/V) with the addition of 10 Mm formic acid, operating in an elution gradient. Elution gradient: 15% organic phase B, hold for 2 min; from 15 to 80% organic phase B in 1.5 min (linear gradient), hold for 1 min; from 80 to 100% organic phase B in 1 min (linear gradient); 100% organic phase B, hold for 5,5 min; then back to the starting condition in 0.5 min and re-equilibration for 13.5 min. The flow-rate was 0.2 ml min^{-1}. The injection volume was 2 μl, and each analysis required 25 min, including the re-equilibration time. The first (0–3 min) and the last (22–25 min) parts of the chromatographic run were diverted to waste using a 10-port valve (Valco Systems, Houston, Texas, USA).

Method Development and Validation

Mass Spectrometer Parameters

A mixture of analytes at a concentration of 0.2 μg/mL was infused in the mass spectrometer (an API 4000 Sciex coupled with an Agilent 1100 LC system, as mentioned above) both for optimizing physical parameters such as declustering potential (DP) and collision energy (CE) and for detecting characteristic analyte transitions. In Q1 mode, the MS parameters, such as gas temperature, gas flow, capillary voltage, and declustering potential, were optimized in order to obtain higher sensitivity for the $[M+H]^+$ as precursor ion. In product ion scan mode, the parameters were set to obtain the best signal to noise ratio for the fragments of each studied compound. The analyte ionization was obtained in positive mode and acquired in the Selected Reaction Monitoring (SRM) mode.

TABLE 1 | Time window setting [Retention time (RT), Q1, parent ion; declustering potential (DP), Q3, ions resulting from ion parent fragmentation, quantifier ion (Q); qualifier ion (q), collision energy (CE)] for liquid chromatography–tandem mass spectrometry analysis.

Compound	RT	$[M+H]^+$	DP	Q		q1		q2	
				m/z	CE	*m/z*	CE	*m/z*	CE
MEPH	9.8	178	50	160	20	145	30	119	30
JWH200	11.9	385	90	155	25	114	35	298	25
AM2201	12.9	360	90	155	35	127	55	144	55
JWH250	13.4	336	90	121	30	91	45	144	20
CP47497-C7	13.6	319	40	233	20	175	15	301	15
CP47497-C8	13.6	333	40	315	15	247	20	175	15
CBD	13.7	315	90	193	30	259	25	-	-
THCCOOH	13.8	345	90	193	30	299	40	327	30
JWH081	14.1	372	90	185	35	214	35	157	35
JWH122	14.3	356	90	169	35	141	35	214	55
JWH019	14.3	356	90	155	35	127	55	228	35
UR144	14.4	312	90	125	35	214	35	144	45
CBN	14.8	311	70	223	30	214	25	195	35
HU221	15.1	387	90	243	25	261	25	-	-
THC	15.3	315	90	193	30	259	30	123	30

RT, Retention Time; $[M+H]^+$, precursor ion; DP, declustering potential; Q, quantifier ion; q1 and q2, qualifier ions; CE, collision energy.

In **Table 1**, the retention times, mass spectrometer parameters, and optimized MRM transitions are summarized. The most abundant transition was chosen as the quantifier ion (Q) and the second and third, if present, most abundant transitions as qualifiers (q1 or q2). The q/Q ratio (<20%) was calculated to provide an additional identification criterion besides the retention time, as per forensic requirements.

Sample Treatment

Three different denaturation methods were compared in order to characterize the effect of sample treatment on signal intensity: (a) centrifugation of 500 μL of oral fluid with plastic centricon vials (3kDa filter) at 14,000 rpm for 15 min; (b) chemical denaturation of 100 μL of biological sample with an equal volume of AcCN, followed by centrifugation at 10,000 rpm for 5 min; (c) chemical denaturation of 50 μL of oral fluid with 100 μL of methanol, followed by centrifugation at 10000 rpm for 5 min. All three different protein denaturation procedures were applied on five pooled lots by spiking aliquots at the different calibration levels.

A pooled oral fluid sample was prepared by mixing five different oral fluid samples collected from five different healthy subjects and centrifuged at 4,000 rpm for 10 min. Each pooled sample was divided into seven different aliquots, each one spiked with the levels prepared for the calibration curve (L0-L6; see below for details). The samples, with different NPS concentrations, were further divided into three different aliquots

in order to obtain three sets of samples, each following a different denaturing treatment.

Method Validation

Method validation parameters, such as linearity, sensitivity, accuracy, precision, and thermal and storage stability, were studied following FDA guidelines. In particular, linearity, sensitivity, accuracy, and precision were calculated in water and in the pooled matrices; thermal and storage stability were calculated in matrix as well. Relative matrix effects were examined by using the approach proposed by Matuszewski: slope CV (%), the slope difference (%), and the assay CV range (%) (Matuszewski, 2006; Food Drug Administration (FDA), 2018) were obtained from five different lots of biological fluid spiked with the same calibration levels.

Pool oral fluid experiment

About 2 mL of oral fluid was collected from five volunteers, both men and women, and were mixed to make a pool of 10 mL in order to evaluate the influence of the different sources. Subsequently, the pool was used to prepare the same concentration levels. Two different conditions were tested for the calibration curve in water: 50/50 v/v MeOH/HCOOH 0.1 M and 50/50 v/v MeOH/H_2O. The oral fluid pool levels were prepared in 50/50 MeOH/HCOOH 0.1 M in both plastic and glass vials in order to evaluate whether the vial composition could interfere with analyte detection. After centrifugation (10,000 rpm for 5 min), 2 microliters of all levels were injected into the HPLC-MS/MS.

Two different levels and a blank (0, 5, and 10 ng/mL) were prepared in plastic and glass vials with different conditions: 70/30 MeOH/H_2O, 50/50 MeOH/H_2O, and 100% MeOH.

Moreover, five oral fluid pools were prepared by mixing different oral fluid samples collected from different subjects ($n = 10$). Hence, each pool was used to prepare a calibration curve (0, 1, 5, 10, 20, 50, and 100 ng/mL) with three different final conditions: 3 kDa centricon vials, 1:1 acetonitrile, and 1:2 MeOH. This trial was also replicated in water as control.

Linearity, sensibility, accuracy, and precision

The linearity of the method was calculated by preparing six calibration levels from the standard material mixture in order to obtain final concentration levels of 0, 1, 5, 10, 20, 50, and 100 ng/mL in water and further verified by homoscedastic test. To evaluate the sensitivity, the limit of detection (LOD) as a signal/noise ratio >3 (S/N>3) and the limit of quantification (LOQ) as a S/N>10 were calculated, preparing further diluted samples in water.

The between- and within-run accuracy and precision of the method based on back-calculated concentration, were evaluated by analyzing 10 solvent blank samples spiked at two different concentration levels – QC 1 (low, 5 ng/mL), QC 2 (high, 50 ng/mL) – over a 5-day validation period. The values of accuracy, CV% intraday ($n = 4$), and CV% inter-day ($n = 6$) were considered acceptable if CV% <15%. All samples prepared in water for the calculation of linearity, sensibility, accuracy, and precision were combined with a double volume of MeOH, as described in the sample preparation paragraph, before injection into the LC-MS/MS system. All of the experiments relating to the method validation parameters were repeated in the five pooled lots.

Matrix effect

The absolute matrix effect (ME) was determined as follows: set 1 was composed of five replicates of the calibration curve levels diluted in water; set 2 was composed of five oral fluid blank pooled samples fortified with analytes after protein denaturation at the same concentration as the replicates of set 1, for each analyte and concentration. ME was calculated by dividing the mean peak areas of set 2 by those of set 1 (Matuszewski et al., 2003).

The relative matrix effects were estimated by following the standard procedure proposed by Matuszewski (2006) by calculating the slope CV (%), the slope difference (%), and the assay CV range (%) obtained from five different lots of blank biological fluid pools spiked with the same calibration levels. Slope CV (%) is the precision of standard line slopes constructed in five different batches of a biofluid, expressed as a coefficient of variation. A cut-off value of lower than 3–4% has been suggested to establish whether the method is practically free from a significant relative matrix effect. Slope difference (%) is calculated as

$$\text{Slope difference (\%)} = \left(\frac{\text{Slope}_{\max} - \text{Slope}_{\min}}{\text{Slope}_{\min}}\right)\% \qquad (1)$$

and corresponds to the maximum difference in the calculated concentration of an analyte in five batches studied that originates from the relative matrix effect. Finally, "assay CV range (%)" is the range of coefficient of variation values determined at all concentrations used for constructing standard lines. It represents the overall method precision and should not exceed 8.7% in the absence of relative matrix effects (Matuszewski, 2006).

Thermal stability

Freeze/thaw cycles experiment Analyte stabilities after freeze/thaw cycles ($n = 5$) and after storage were assessed by percentage change from T0, calculated by the formula:

$$[(C_X - C_{T0})/C_{T0})] \times 100\% \qquad (2)$$

where C_{T0} is the back-calculated concentration of the T0 sample and C_X is the back-calculated concentration of the Tx samples. QC1 and QC2 samples, prepared as described above, were divided into five aliquots (I, II, III, IV, and V) and frozen at −20°C in box A for each pool. After the first cycle, all the aliquots were defrosted, and only aliquot I was transferred into box B; then, both boxes were stored at −20°C. For the second cycle, only box A was defrosted, aliquot II was transferred into box B, and box A was re-frozen, and so on until aliquot V, so that each aliquot went under a different and increased number of freeze/thaw cycles. After that, 100 μL of each sample was added to 200 μL of MeOH, which was centrifugated, and then the supernatant was injected into the HPLC-MS/MS.

Thermal stability in the short storage condition Two series of eight aliquots from the QC1 and QC2 levels were prepared and stored at room temperature and at +4°C for 0, 2, 4, 19.3, 23.5, 27.5, 43.5, and 47.5 h, respectively, to test short-term thermal and storage stability, before the longer storage at −20°C. After 1 week, 100 μL of each vial was thawed and combined with 200 μL of MeOH and centrifuged, and the supernatant was injected into the HPLC-MS/MS. In both experiments, thermal stability was tested by comparing the instrument response of the two series with that immediately frozen after the pool preparation (T = 0). For quantitative purpose, a decrease in sensibility of <15% was considered acceptable.

Storage condition

In order to evaluate whether the material composition of the vial could interfere with analyte detection, after the denaturation step, we aliquoted the samples prepared for the "matrix effect experiment," both in water and in the five different pools, in two different types of vial: glass vials and plastic vials, all for laboratory use and LC-MS/MS analyses. The samples were then injected into the HPLC-MS/MS.

RESULTS AND DISCUSSION

Denaturation Method

Optimization of sample preparation plays a crucial role in the method validation procedure, in particular when the biological matrix is rich in both inorganic and organic compounds (such as proteins) and is quite unknown in terms of quantitative analysis. A denaturation process was carried out to remove the protein component from the matrix samples, with the intent of minimizing the sample treatment as well.

The choice of the denaturation method took into account parameters such as the sensitivity, linearity, affinity of the solvent with ionization efficiency, chemical and physical matrix interactions, and sample density. Three different denaturation procedures were compared with appropriate experiments: (a) ultrafiltration with a cut-off of 3 KDa, based on a physic interaction, (b) dilution with an equal volume of AcCN, as our routine for plasma samples; (c) dilution with two volumes of MeOH, a solvent that normally increases the ionization efficiency.

To study the different behavior of the compounds as a result of the denaturation procedures, we prepared the calibration curves both in water and in five different oral fluid pools. Then, each calibration level was divided into three different aliquots, each one treated with denaturation procedures (a), (b), and (c), respectively. All samples were centrifuged, and the supernatants were injected into the LC-MS/MS system.

We observed that by using the ultrafiltration devices, only MEPH was detectable amongst all other compounds, probably since the physical denaturation was not adequate to break the interactions of the synthetic cannabinoids with the oral fluid components or the stronger affinity of aminoalkylindole compounds for oral fluid proteins with respect to the amphetamine-like compounds.

Chemical denaturation methods, obtained with AcCN or MeOH, were both adequate to detect all the compounds of interest; however, denaturation with AcCN, even if with a lower dilution factor, was less sensitive and exhibited higher analytic variability compared to the procedure with MeOH.

The accuracy of the denaturation procedure was determined as the average of the accuracies, defined as the ratio between the recalculated value and the true value, of each level and for all the compounds. For the denaturation procedure using AcCN, this accounted for 122% for samples obtained in water and 132% for spiked oral fluid ones, which were both higher than the 80–120% range assessed in the FDA guidelines. However, when MeOH was used as the solvent for protein precipitation, the accuracy for water calibrations was 115% and 116% for the same samples but with NPS mixture added to the real matrices. Moreover, the precision of the experiment, calculated as the average of CV% for all calibration levels and for all analytes, was 21.1 and 10.9% for water samples and 22.2% and 17.5% for pooled ones if denaturized with AcCN and MeOH, respectively.

In addition, comparing the response of the compounds diluted in water or spiked in pooled oral fluid, we observed a signal intensity decrease when samples were denaturized with AcCN instead of MeOH. The lower dilution factor, and the consequently higher amount of matrix components, may reduce the efficiency of the ionization process when samples are treated with AcCN instead of MeOH.

Validation Parameters in Water

Linearity, sensitivity, accuracy, precision, matrix effects, and thermal and storage stability were the criteria assessed for the method validation, following the Guidance for Industry Bioanalytical Method Validation of the FDA (2001). The accuracy and precision values were all within the acceptable limit of < 15%, except for CP47497-C7 and -C8. The linearity of the method, in the range from LOQ to 100 ng/mL, was confirmed for the compounds of interest by the calculation of correlation coefficients (R^2 > 0.991) with six levels for five repeated injections, except for CP47497-C7 and -C8 and JWH250, for which the R^2 was calculated with only four concentration levels.

Calibration curves were constructed by linear regression analysis of the area analyte versus the concentration of analytes injected (no IS) and also by linear regression analysis of the area analyte ratios analyte/IS versus the concentration of analytes injected (with IS). Moreover, Hartley's test, the Cochran test, and minimum variance tests were applied to verify hetero/homoscedasticity; all tests obtained results within limits and were comparable to tabulated parameters, certifying homoscedasticity.

The LODs and LOQs were selected based on the lowest concentration with S/ n = 3 and S/ n = 10, respectively. For JWH250, CP47497-C7, and CP47497-C8 we observed a higher LOD (> 1 ng/mL), so only QC2 accuracy and precision were calculated (Samano et al., 2014).

The inter-day mean accuracy (%) of the analytes, calculated without the use of IS and at the two spiking levels, was in the range of 85–107%, with the exception of CP47497-C8, which was 146%. The same parameter, calculated with the use of the IS,

TABLE 2 | Method validation criteria, sensitivity, accuracy, and precision (inter-day) at two quality control concentrations (5 and 50 ng/mL), calculated both without and with IS, for each compound added to water.

Water	LoD*	LoQ*	Accuracy%				Precision%			
			QC1		QC2		QC1		QC2	
Compound	*ng/mL*	*ng/mL*	*No IS*	*With IS*	*No IS*	*With IS*	*No IS*	*With IS*	*No IS*	*With IS*
MEPH	25.4	84.5	90.9	101.0	102.0	106.0	4.4	5.6	4.2	4.3
JWH200	55.7	185.0	91.6	102.0	103.0	106.0	4.0	5.3	2.8	3.0
AM2201	1.8	6.0	85.0	94.5	97.9	101.3	3.1	4.4	3.0	2.5
JWH250	378.0	1259.0	99.5	111.0	103.0	107.0	5.6	5.8	0.9	1.5
CP47497-C7	831.0	2769.0			99.0	103.0			9.8	10.0
CP47497-C8	599.0	1965.0			146.0	162.0			19.0	19.0
CBD	90.1	300.0	85.6	95.3	94.5	97.8	12.6	13.5	5.0	5.5
THCCOOH	190.0	635.0	85.7	96.0	100.0	105.0	2.5	2.8	3.9	4.6
JWH081	0.9	2.9	87.8	97.6	107.0	111.0	13.1	13.4	12.3	12.3
JWH122	1.1	3.6	88.9	98.9	106.0	110.0	4.7	5.4	2.0	2.6
JWH019	1.5	5.0	92.0	102.0	106.0	110.0	4.2	5.7	3.4	3.3
UR144	1.4	4.6	86.4	96.1	100.0	104.0	4.2	5.5	2.3	2.7
CBN	103.0	343.0	87.9	97.8	94.8	98.1	7.2	7.9	6.1	6.6
HU221	76.6	255.0	94.0	105.0	92.9	96.3	2.9	1.3	2.3	2.5
THC	102.0	342.0	86.2	95.9	94.8	98.1	2.4	4.0	2.3	2.8

LOD, Limit of detection x10^{-3}, S/N = 3; LOQ*, Limit of quantification x10^{-3}, S/N = 10; QC1, 5 ng/mL; QC2, 2, 50 ng/mL; No IS, results obtained with calibration curves constructed by linear regression analysis of the analyte area vs. the concentration of analytes injected; With IS, results obtained with calibration curves constructed by linear regression analysis of the ratio of the analyte area to the IS area vs. the concentration of analytes injected.*

was reduced to have a range of 89.7–108%, but it increased to 164% for CP47497-C8. The range of the inter-day mean precision (%) of the analytes was 0.85–13.1 and 0.60–12% when the values were calculated without considering or with considering the IS, respectively. Again, for CP47497-C8, the inter-day mean precision (19.1%) exceeded the FDA guidelines criteria of a value lower than 15%, independently from the use of IS. The accuracy and precision values were also calculated in intra-day experiments, ranging between 92–103% and being below 10%, respectively. The method validation criteria such as sensitivity, accuracy, and precision (inter-day) at two concentrations (QC1 5 ng/mL and QC2 50 ng/mL), calculated both without and with IS for each compound are reported in **Table 2**.

Data are reported both with and without IS, and the IS was chosen due to chemical structure similarity and the commercial availability of the deuterated IS; our aim was also to verify whether this approach could be applicable for routine analysis in order to define method reliability, robustness, and accuracy. In general, without IS, we observed lower accuracy with low concentration samples, as expected (85.0–99.1); on the other hand, method accuracy showed an opposite trend: for most compounds, inter- and intra-day CVs% were lower without IS, although CVs% were lower than 15%, as required by the guidelines, even with IS.

Validation Parameters in Oral Fluid

The experiments were then replicated in oral fluid; the results are summarized in **Table 3**. In general, we noticed that for JWH250, CP47497-C7, and CP47497-C8, LODs and LOQs were higher than for the other compounds, similarly to the results in water. Similar results were obtained with IS or without IS, as shown in the table; therefore, **Tables 2**, **3** show similar results.

However, particularly in terms of accuracy, the results show more variability without IS for QC1 (89.3 and 105% in water and oral fluid, respectively) and QC2 (103.2 and 115%, respectively), while with IS, these differences tend to decrease. A different outcome is seen for precision since the variability seems to be IS-dependent rather than concentration-dependent. LODs and LOQs showed better results in terms of sensibility in water samples with respect to oral fluid samples, so we were able to calculate QC1 values as well.

Matrix Effect

Table 4 shows the results obtained from both absolute (confronting water/matrix samples) and relative matrix effect experiments carried out confronting the same matrices but coming from different sources and therefore with different endogenous compounds and/or interferent concentrations.

For the absolute matrix effect (ME%), mephedrone (or MEPH) shows different chemical behavior from all of the other compounds (similar to what was shown above), highlighting a signal suppression with respect to experiments carried out in water. However, for all other compounds, these differences were minimized with the use of IS.

For the relative matrix effect, the parameters hereby calculated clearly underline the error made when interpreting results on real samples while using a calibration curve built on the same matrix but different biological individuals. The greater values, the higher is the chance of miscalculation with the standard external addition method for a quantitative result (calibration in oral fluid samples).

TABLE 3 | Method validation criteria, sensitivity, accuracy, and precision (inter-day) at two quality control concentrations (5 and 50 ng/mL), calculated both without and with IS, for each compound added to five different oral fluid pools.

Matrix	LoD*	LoQ*	Accuracy%				Precision%			
			QC1		QC2		QC1		QC2	
Compound	*ng/mL*	*ng/mL*	*No IS*	*With IS*	*No IS*	*With IS*	*No IS*	*With IS*	*No IS*	*With IS*
MEPH	173.0	575.0	97.6	91.9	104.0	103.0	4.2	6.6	3.0	6.2
JWH200	82.4	275.0	103.0	96.2	108.0	107.0	3.0	5.0	1.8	4.0
AM2201	2.8	9.2	101.0	93.4	111.0	108.0	3.5	3.1	3.7	2.7
JWH250	166.0	553.0	118.0	109.0	118.0	115.0	3.3	4.8	4.4	4.5
CP47497-C7	2275.0	7583.0			122.0	118.0			6.5	9.0
CP47497-C8	422.0	1406.0			171.0	161.0			7.1	9.8
CBD	83.6	279.0	97.4	89.4	112.0	109.0	7.0	10.1	4.8	5.9
THCCOOH	116.0	386.0	99.1	92.6	106.0	104.0	9.2	7.7	3.7	5.5
JWH081	1.6	5.5	109.0	99.7	111.0	109.0	3.7	5.5	5.0	6.1
JWH122	1.0	3.3	114.0	104.0	113.0	110.0	2.2	4.6	2.3	4.6
JWH019	5.3	17.7	112.0	104.0	113.0	110.0	3.0	5.6	3.9	4.5
UR144	2.0	6.6	108.0	99.9	110.0	107.0	2.4	5.8	3.3	6.8
CBN	146.0	487.0	102.0	92.0	112.0	108.0	10.6	11.7	8.3	12.0
HU221	173.0	575.0	113.0	105.0	111.0	108.0	6.5	7.3	7.0	5.7
THC	82.4	275.0	102.0	93.8	104.0	100.0	8.1	6.9	7.4	8.4

LOD, Limit of detection x10^{-3}, S/N = 3; LOQ*, Limit of quantification x10^{-3}, S/N = 10; QC1, 5 ng/mL; QC2, 50 ng/mL; No IS, results obtained with calibration curves constructed by linear regression analysis of the analyte area vs. the concentration of analytes injected; With IS, results obtained with calibration curves constructed by linear regression analysis of the ratio of the analyte area to the IS area vs. the concentration of analytes injected.*

Therefore, as mentioned by Matuszewski (2006) and based on data presented in this manuscript, it is proposed that the precision (CV) value of standard line slopes constructed in five different lots of a biofluid should not exceed 3–4% for the method to be considered practically free from relative matrix effect liability. In addition to high precision values of standard line slopes (<3.4%) constructed in five different lots of a biofluid, the precision values at all concentrations used for the preparation of standard curves and determined in five different lots of a biofluid did not exceed 8.7%. We observed strong relative matrix effects for different compounds,

In particular, for the parameter "Slope difference %" with respect to the "Assay CV%" range, which represented the range of coefficient of variation values determined at all concentrations used for constructing the standard lines, it suggested that the method is quite precise for quantitative aims.

Since no satisfactory results were achieved for JWH250, CP47497-C7, and -C8 (not shown in the following graphs), we focused on the results from the other compounds. As reported by other authors (Schlittenbauer et al., 2015; Ghosh, 2019) it is recommended to perform the "relative" matrix effect experiment during bio-analytical method validation, particularly when a complex biological matrix, such as oral fluid, is used for a quantitative purpose.

Thermal Stability

Freeze/Thaw Cycles

Further experiments were carried out to evaluate the influence of the freeze/thaw cycles and were therefore performed on QC1 and QC2 samples for all of the five oral fluid pools (the results are reported as mean values).

At QC1 level, for JWH019, JWH081, JWH122, and THC, we observed a signal increase related to the number of freeze/thaw cycles; while, for the other compounds a small reduction, mainly <20%, was calculated from T1 to T5 (**Figure 1A**). At higher concentration levels, QC2, all of the analytes showed the same trend, with a progressive decrease in stability (**Figure 1B**). CBD was the only compound for which the concentration seemed not to be affected by the freeze/thaw cycles; in fact, in both cases, the decrease in stability was equal to 26%.

In these experiments, it was noticed an increase in response related to the number of freeze/thaw cycles (the more, the higher response), especially for low concentration levels, where matrix effects are supposed to have a major impact.

Thermal Stability in the Short-Term Storage Condition

To obtain data on short-term thermal stability, two series of eight aliquots from QC1 and QC2 levels were added to the five oral fluid pools and were stored one at room temperature and one at +4°C for eight time intervals, 0, 2, 4, 19.3, 23.5, 27.5, 43.5, and 47.5 h, respectively, before the longer-term storage at −20°C, as shown in **Figure 2**.

Before the experiment, all samples were thawed, and 100 μL of each was combined with 200 μL of MeOH and centrifuged, and the supernatant was injected into the HPLC-MS/MS.

In **Figures 2A,B**, we report the stability trend of the QC1 and QC2 samples stored at +4°C, respectively, while in **Figures 2C,D** the trends of the same samples but stored at room temperature are shown. In general, QC2 samples were more stable than QC1

TABLE 4 | Absolute matrix effect (ME%) and relative Matrix effect, obtained on water and on five different oral fluid pools, according to the protocol proposed by Matuszewski (2006).

Compound	ME (%)[a]		SLOPE CV%[b]		SLOPE DIFFERENCE%[c]		ASSAY CV RANGE%[d]	
	NO IS	*With IS*	*NO IS*	*With IS*	*NO IS*	*With IS*	*NO IS*	*With IS*
MEPH	63.8	57.3	19.4	20.3	58.6	58.6	0.40–12.2	1.06–11.9
JWH200	121.0	109.0	13.5	21.6	38.9	69.0	0.77–15.7	0.72–11.2
AM2201	123.0	111.0	13.1	14.2	38.7	48.0	0.38–13.1	0.72–8.30
JWH250	122.0	109.0	11.4	14.1	34.6	44.3	0.35–14.2	0.33–8.56
CP47497-C7	138.0	124.0	20.5	10.2	55.6	30.5	1.81–21.2	0.42–19.1
CP47497-C8	130.0	117.0	18.8	8.7	56.5	26.4	2.15–53.1	2.36–53.3
CBD	114.0	102.0	20.6	12.8	57.7	42.7	0.12–15.3	2.54–16.6
THCCOOH	120.0	108.0	17.3	24.6	47.3	77.2	0.97–20.0	1.50-21.1
JWH081	115.0	103.0	18.1	9.8	53.0	30.3	0.38–8.30	1.59–12.7
JWH122	116.0	104.0	13.7	6.9	40.6	19.0	0.48–10.3	1.03–10.9
JWH019	113.0	101.0	15.0	8.4	38.5	25.6	0.57–11.6	0.53–15.8
UR144	115.0	103.0	15.3	9.4	42.1	27.8	0.41–13.3	0.70–16.1
CBN	123.0	111.0	18.5	4.3	59.2	11.1	0.77–19.7	1.17–26.4
HU221	129.0	117.0	14.9	10.7	37.9	34.9	1.13–12.4	2.04–18.7
THC	118.0	106.0	16.6	9.9	45.4	30.5	0.82–14.1	0.47–15.4

[a]ME%, absolute matrix effect, [b]Precision value (coefficient of variation, CV%) of slopes of standard lines constructed in five different oral fluid pools; [c]maximum difference between the highest and the lowest slope values divided by the lowest slope value and multiplied by 100; [d]range of coefficient of variation values (method precision) determined on at all concentrations used for constructing standard lines; No IS, results obtained with calibration curves constructed by linear regression analysis of the analyte area vs. the concentration of analytes injected; With IS, results obtained with calibration curves constructed by linear regression analysis of the ratio of the analyte area to the IS area vs. the concentration of analytes injected.

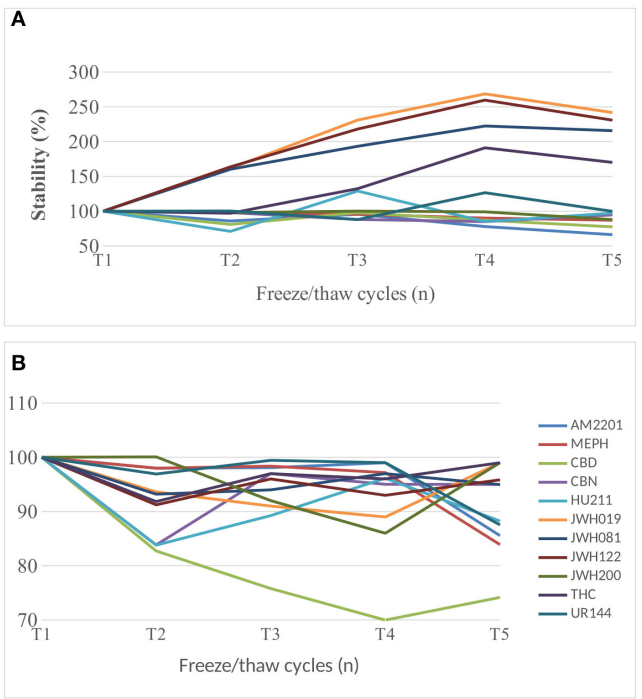

FIGURE 1 | (A) QC1 (5 ng/mL) samples in freeze/thaw cycle experiment from T1 to T5 ($n = 5$). **(B)** QC2 (50 ng/mL) samples in freeze/thaw cycle experiment from T1 to T5 ($n = 5$).

ones, and the same applies for those stored at +4°C as for the samples kept at room temperature.

Already after 24 h, QC1 samples stored at room temperature showed a decrease of <15%, while only JWH200, JWH122, JWH019, and THC registered a decrease of circa 15%, but after 48 h, JWH200 and THC resulted to be stable (<15%).

Concerning the same QC1 samples but stored at +4°C, CBD, THCCOOH, and THC showed a lower decrease in terms of signal intensity of 15%, and therefore, their behavior was considered stable.

In the QC2 samples series, different trends were noticed: in particular, MEPH, CBD, and THCCOOH already showed degradation after 24 h of storage, both at room temperature and at +4°C. When considering 48 h of storage, at room temperature JWH122, JWH019, CBN, and THC were stable, while JWH122, JWH019, UR144, CBN, and THC were stable at +4°C. **Data Sheet 1** with raw data can be found in the Supplementary Material.

Storage Condition

The effect of sample storage during the analytical session was evaluated by using the same samples prepared for the matrix experiment (Michelot et al., 2017). After the denaturation and centrifugation steps, all of the sets were divided (one calibration curve prepared in water and five in different oral fluid pools) into two lots: one in plastic vials and the other one in glass (**Figures 3**, **4**). All of the samples were injected in triplicate. **Figure 3** shows

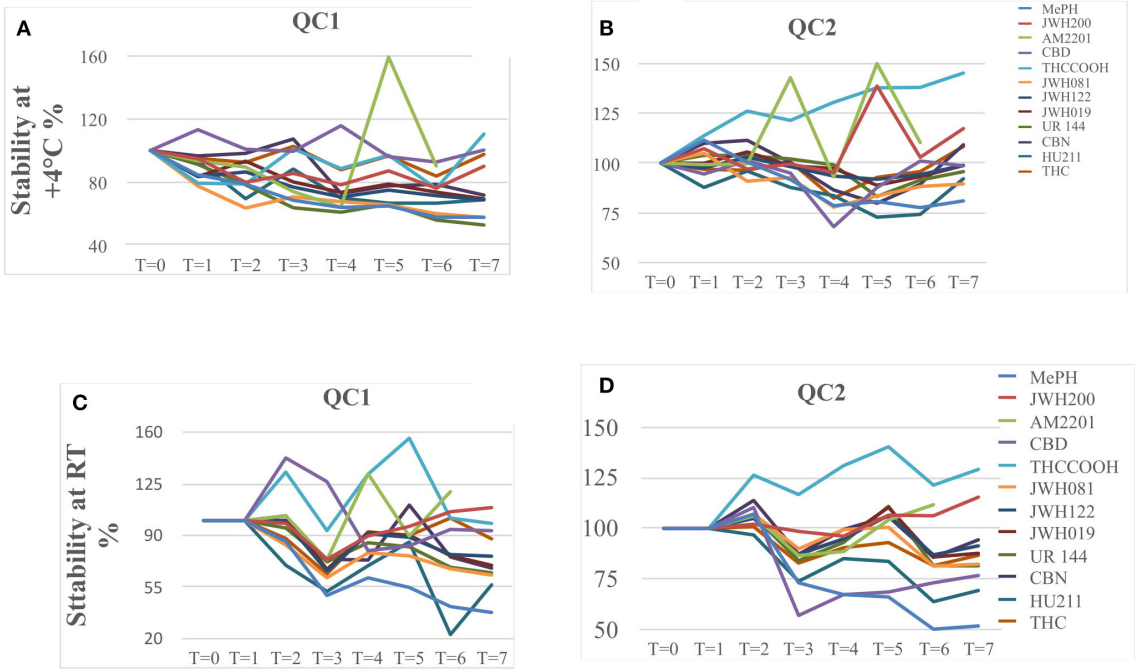

FIGURE 2 | QC1 and QC2 sample stability when stored at +4°C **(A,B)** and at room temperature **(C,D)**.

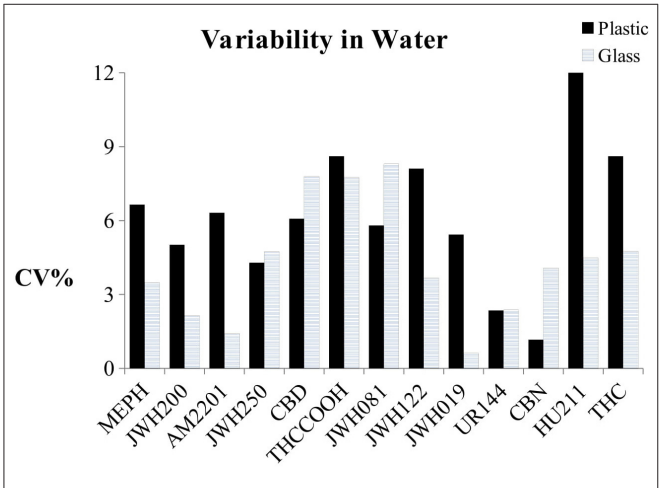

FIGURE 3 | Variability trend in water of samples stored in plastic and glass vials.

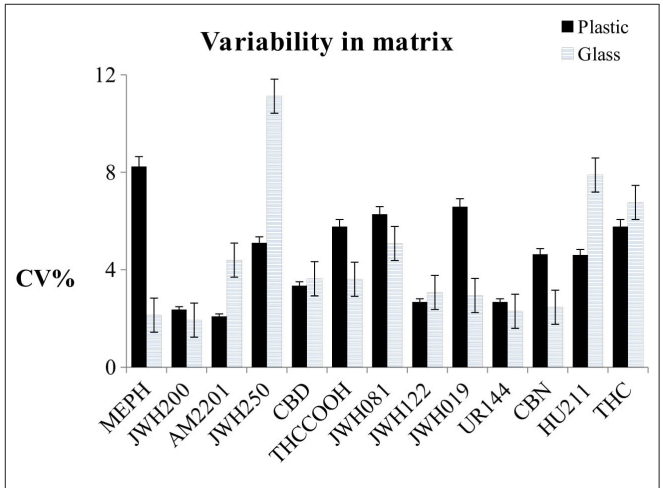

FIGURE 4 | Variability trend in oral fluid samples stored in plastic and glass vials, with uncertainty bands.

the variability trend in water of samples stored in plastic and glass vials.

In **Figure 4**, the uncertainty bands show average results from the five different pools. The variability of the storage condition was calculated as CV% of the slopes of the calibration curves for the samples prepared in water and as the mean of the CV% of the slopes of the calibration curves for the samples prepared in matrix. When the NPS mixture was spiked in water, only CBD and CBN showed higher variability if put in glass vials instead of plastic ($CV_{glass}/CV_{Plastic}$%> 15%), and the CVs% relating to JWH250, THCOOH, and UR144 were < 15% and seemed to be not dependent on the material type of the vials.

CONCLUSIONS

Although a significative relative matrix effect was demonstrated during our validation process, the method was fully validated and therefore will be applied to real samples for the determination of

10 NPS in oral fluid with minimal sample pretreatment, reducing matrix effects with the use of the appropriate IS or evaluating the matrix protein content beforehand. However, the method is sensitive, simple, and rapid, and the sample preparation is easy. Moreover, analyte stability at room temperature or lower seems to be concentration-dependent and less dependent on freeze/thaw cycles (with the exception of CBD).

While using glass vials in the validation process, a reduction in measurement variability was noted, and, therefore, the use of glass is encouraged in order to enhance accuracy and precision (apart from for JWH250 and HU211).

The method was validated following guidelines (Food Drug Administration (FDA), 2018) and was demonstrated to be applicable due to its reliability and satisfactory results in a forensic context.

DATA AVAILABILITY STATEMENT

All datasets generated for this study are included in the article/**Supplementary Material**.

ETHICS STATEMENT

The studies involving human participants were reviewed and approved by Prot. 39722 01/10/2019 Comitato Etico Area Vasta Emilia Nord. The patients/participants provided their written informed consent to participate in this study.

AUTHOR CONTRIBUTIONS

LC: analytical experiments, data analysis and method validation. LA: data review, editing and reviewing of the manuscript, corresponding author. CM: graphics and data analysis. RC: reviewer of analytical experiments and manuscript. RA: reviewer of the manuscript, coordinator of the group, data reviewer and data interpretation.

SUPPLEMENTARY MATERIAL

The Supplementary Material for this article can be found online at: https://www.frontiersin.org/articles/10.3389/fchem.2020.00439/full#supplementary-material

REFERENCES

Anizan, S., and Huestis, M. A. (2013). The potential role of oral fluid in antidoping testing. *Clin. Chem*. 60, 307–322. doi: 10.1373/clinchem.2013.209676

Anzillotti, L., Calò, L., Giacalone, M., Banchini, A., and Cecchi, R. (2018). Determination of methadone and eight new psychoactive substances in hair samples by gas chromatography/mass spectrometry. *J. Forensic Sci. Med*. 4, 184–91. doi: 10.4103/jfsm.jfsm_22_18

Anzillotti, L., Marezza, F., Calò, L., Andreoli, R., Agazzi, S., Bianchi, F., et al. (2019b). Determination of synthetic and natural cannabinoids in oral fluid by solid-phase microextraction coupled to gas chromatography/mass spectrometry: a pilot study. *Talanta* 201, 335–341. doi: 10.1016/j.talanta.2019.04.029

Anzillotti, L., Marezza, F., Calò, L., Banchini, A., and Cecchi, R. (2019a). A case report positive for synthetic cannabinoids: are cardiovascular effects related to their protracted use? *Leg Med.* 41:101637. doi: 10.1016/j.legalmed.2019.101637

Bianchi, F., Agazzi, S., Riboni, N., Erdal, N., Hakkarainen, M., Ilag, L. L., et al. (2019). Novel sample-substrates for the determination of new psychoactive substances in oral fluid by desorption electrospray ionization-high resolution mass spectrometry. *Talanta* 202, 136–144. doi: 10.1016/j.talanta.2019.04.057

Bosker, W. M., and Huestis, M. A. (2009). Oral fluid testing for drugs of abuse. *Clin. Chem*. 55, 1910–1931. doi: 10.1373/clinchem.2008.108670

Brunt, T. M., Atkinson, A. M., Nefau, T., Martinez, M., Lahaie, E., Malzcewski, A., et al. (2017). Online test purchased new psychoactive substances in 5 different European countries: a snapshot study of chemical composition and price. *Int. J. Drug Policy* 44, 105–114. doi: 10.1016/j.drugpo.2017.03.006

Busardo, F.P. Pichini, S. Pellegrini, M., Montana, A., Lo Faro, A. F. Zaami, S., Graziano, S. (2018). Correlation between blood and oral fluid psychoactive drug concentrations and cognitive impairment in driving under the influence of drugs. *Curr. Neuropharmacol*. 16, 84–96. doi: 10.2174/1570159X15666170828162057

Coulter, C., Garnier, M., and Moore, C. (2011). Synthetic cannabinoids in oral fluid. *J. Anal. Toxicol.* 35, 424–430. doi: 10.1093/anatox/35.7.424

Edvardsen, H. M., Moan, I. S., Christophersen, A. S., and Gjerde, H. (2015). Use of alcohol and drugs by employees in selected business areas in Norway: a study using oral fluid testing and questionnaires. *J. Occup. Med. Toxicol*. 16:46. doi: 10.1186/s12995-015-0087-0

European Monitoring Centre for Drugs and Drug Addiction (2015). *Synthetic Cannabinoids and "Spice" Drug Profile*. Available online at: http://www.emcdda.europa.eu/publications/drug-profiles/synthetic-cannabinoids (accessed May 26, 2020).

European Monitoring Centre for Drugs and Drug Addiction (2017). *Perspectives on Drugs: Synthetic Cannabinoids in Europe*. Available online at: http://www.emcdda.europa.eu/topics/pods/synthetic-cannabinoids_en (accessed May 26, 2020).

Food and Drug Administration (FDA), Bioanalytical Method Validation Guidance (2018). Available online at: https://www.fda.gov/regulatory-information/search-fda-guidance-documents/bioanalytical-method-validation-guidance-industry (accessed May 26, 2020).

Gallardo, E., and Queiroz, J. A. (2008). The role of alternative specimens in toxicological analysis. *Biomed. Chromatogr*. 22, 795–821. doi: 10.1002/bmc.1009

Ghosh, C. (2019). Relative matrix effects: a step forward using standard line slopes and ANOVA analysis. *Arab. J. Chem*. 12, 1378–1386. doi: 10.1016/j.arabjc.2014.11.019

Governo Italiano (2017). *Dipartimento delle Politiche Antidroga, Relazione al Parlamento*. Available online at: http://www.politicheantidroga.gov.it/media/2153/relazione-al-parlamento_2017.pdf (accessed May 26, 2020).

Graziano, S., Anzillotti, L., Mannocchi, G., Pichini, S., and Busardò, F. P. (2019). Screening methods for rapid determination of new psychoactive substances (NPS) in conventional and non-conventional biological matrices. *J. Pharm. Biomed Anal*. 30, 170–179. doi: 10.1016/j.jpba.2018.10.011

Gruppo Tossicologi Forensi Italiani (2017). Gruppo Tossicologi Forensi Italiani. *Linee guida per le strutture dotate di laboratori per gli accertamenti di sostanze d'abuso con finalità tossicologico-forensi e medico-legali su campioni biologici prelevati da vivent*. Available online at: https://www.gtfi.it/linee-guida/ (accessed May 26, 2020).

Huestis, A. M., Brandt, D. S., Rana, S., Auwärter, V., and Baumann, M. H. (2017). Impact of novel psychoactive substances on clinical and forensic toxicology and global public health. *Clin. Chem*. 63, 1564–1569. doi: 10.1373/clinchem.2017.274662

Matuszewski, B. K. (2006). Standard line slopes as a measure of a relative matrix effect in quantitative HPLC-MS bioanalysis. *J. Chromatogr. B*. 2, 293–300. doi: 10.1016/j.jchromb.2005.11.009

Matuszewski, B. K., Constanzer, M. L., and Chavez-Eng, C. M. (2003). Strategies for the assessment of matrix effect in quantitative bioanalytical methods based on HPLC-MS/MS. *Anal. Chem*. 75, 3019–3030. doi: 10.1021/ac020361s

Mercolini, L., and Protti, M. (2016). Biosampling strategies for emerging drugs of abuse: towards the future of toxicological and forensic analysis. *J. Pharmaceut. Biomed.* 130, 202–219. doi: 10.1016/j.jpba.2016.06.046

Michelot, H., Fu, S., Stuart, B., Shimmon, R., Raymond, T., Crandell, T., et al. (2017). Effect of drug precursors and chemicals relevant to clandestine laboratory investigation on plastic bags used for collection and storage. *Forensic Sci. Int*. 273, 106–112. doi: 10.1016/j.forsciint.2017.02.007

Patsalos, P. N., and Berry, D. J. (2013). Therapeutic drug monitoring of antiepileptic drugs by use of saliva. *Ther. Drug Monit*. 35, 4–29. doi: 10.1097/FTD.0b013e31827c11e7

Rocchi, R., Simeoni, M. C., Montesano, C., Vannutelli, G., Curini, R., Sergi, M., et al. (2018). Analysis of new psychoactive substances in oral fluids by means of microextraction by packed sorbent followed by ultra-highperformance liquid chromatography–tandem mass spectrometry. *Drug Test Anal.* 10, 865–873. doi: 10.1002/dta.2330

Samano, L. K., Poklis, J. L., Lichtman, A. H., and Poklis, A. (2014). Development of a high-performance liquid chromatography–tandem mass spectrometry method for the identification and quantification of CP-47,497, CP-47,497-C8 and JWH-250 in mouse brain. *J. Anal. Toxicol.* 38, 307–314. doi: 10.1093/jat/bku043

Schlittenbauer, L., Seiwert, B., and Reemtsma, T. (2015). Matrix effects in human urine analysis using multi-targeted liquidchromatography–tandem mass spectrometry. *J. Chromatogr. A* 1415, 91–99. doi: 10.1016/j.chroma.2015.08.069

Strano-Rossi, S., Anzillotti, L., Castrignanò, E., Romolo, F. S., and Chiarotti, M. (2012). Ultra high performance liquid chromatography-electrospray ionization-tandem mass spectrometry screening method for direct analysis of designer drugs, "spice" and stimulants in oral fluid. *J. Chromatogr. A* 1258, 37–42. doi: 10.1016/j.chroma.2012.07.098

Strano-Rossi, S., Odoardi, S., Fisichella, M., Anzillotti, L., Gottardo, R., and Tagliaro, F. (2014). Screening for new psychoactive substances in hair by ultrahigh performance liquid chromatography-electrospray ionization tandem mass spectrometry. *J. Chromatogr. A* 1372, 145–156. doi: 10.1016/j.chroma.2014.10.106

United Nations Office on Drugs and Crime (2019). *Early Warning Advisory on New Psychoactive Substance. What Are NPS*?. Available online at: https://www.unodc.org/LSS/Page/NPS (accessed May 26, 2020).

United Nations Office on Drugs and Crime (2020). *Current NPS Threats*. Available online at: https://www.unodc.org/documents/scientific/Current_NPS_Threats_Volume_II_Web.pdf (accessed May 26, 2020).

UNODC Early Warning Advisory on New Psychoactive Substances (2020). Available online at: https://www.unodc.org/LSS/Page/NPS (accessed May 26, 2020).

Williams, M., Martin, J., and Galettis, P. (2019). A validated method for the detection of synthetic cannabinoids in oral fluid. *J. Anal. Toxicol.* 43, 10–17. doi: 10.1093/jat/bky043

Conflict of Interest: The authors declare that the research was conducted in the absence of any commercial or financial relationships that could be construed as a potential conflict of interest.

frontiers in Chemistry

ORIGINAL RESEARCH
published: 17 July 2020
doi: 10.3389/fchem.2020.00539

How to Study the Metabolism of New Psychoactive Substances for the Purpose of Toxicological Screenings—A Follow-Up Study Comparing Pooled Human Liver S9, HepaRG Cells, and Zebrafish Larvae

*Lea Wagmann[1], Fabian Frankenfeld[1], Yu Mi Park[2,3], Jennifer Herrmann[2,4], Svenja Fischmann[5], Folker Westphal[5], Rolf Müller[2,4], Veit Flockerzi[6] and Markus R. Meyer[1]**

[1] Department of Experimental and Clinical Toxicology, Institute of Experimental and Clinical Pharmacology and Toxicology, Center for Molecular Signaling (PZMS), Saarland University, Homburg, Germany, [2] Department of Microbial Natural Products (MINS), Helmholtz Institute for Pharmaceutical Research Saarland (HIPS), Saarland University, Saarbrücken, Germany, [3] Environmental Safety Group, Korea Institute of Science and Technology (KIST) Europe, Saarbrücken, Germany, [4] German Center for Infection Research (DZIF), Partner Site Hannover–Braunschweig, Saarbrücken, Germany, [5] State Bureau of Criminal Investigation Schleswig–Holstein, Kiel, Germany, [6] Department of Experimental and Clinical Pharmacology, Institute of Experimental and Clinical Pharmacology and Toxicology, Center for Molecular Signaling (PZMS), Saarland University, Homburg, Germany

OPEN ACCESS

Edited by:
Alberto Salomone, University of Turin, Italy

Reviewed by:
Svante Vikingsson, Swedish National Board of Forensic Medicine, Sweden
Samuel D. Banister, University of Sydney, Australia

***Correspondence:**
Markus R. Meyer
markus.meyer@uks.eu

Specialty section:
This article was submitted to Analytical Chemistry, a section of the journal Frontiers in Chemistry

Received: *27 February 2020*
Accepted: *26 May 2020*
Published: *17 July 2020*

Citation:
Wagmann L, Frankenfeld F, Park YM, Herrmann J, Fischmann S, Westphal F, Müller R, Flockerzi V and Meyer MR (2020) How to Study the Metabolism of New Psychoactive Substances for the Purpose of Toxicological Screenings—A Follow-Up Study Comparing Pooled Human Liver S9, HepaRG Cells, and Zebrafish Larvae. Front. Chem. 8:539. doi: 10.3389/fchem.2020.00539

The new psychoactive substances (NPS) market continues to be very dynamic. A large number of compounds belonging to diverse chemical groups continue to emerge. This makes their detection in biological samples challenging for clinical and forensic toxicologists. Knowledge of the metabolic fate of NPS is crucial for developing comprehensive screening procedures. As human studies are not feasible due to ethical concerns, the current study aimed to compare the NPS' metabolic pattern in incubations with pooled human liver S9 fraction (pHLS9), human liver HepaRG cells, and zebrafish larvae. The latter model was recently shown to be a promising preclinical surrogate for human hepatic metabolism of a synthetic cannabinoid. However, studies concerning other NPS classes are still missing and therefore an amphetamine-based *N*-methoxybenzyl (NBOMe) compound, a synthetic cathinone, a pyrrolidinophenone analog, a lysergamide, as well as another synthetic cannabinoid were included in the current study. Liquid chromatography coupled to Orbitrap-based high-resolution tandem mass spectrometry was used to analyze metabolic data. Zebrafish larvae were found to produce the highest number of phase I but also phase II metabolites (79 metabolites in total), followed by HepaRG cells (66 metabolites). Incubations with pHLS9 produced the least metabolites (57 metabolites). Furthermore, the involvement of monooxygenases and esterases in the metabolic phase I transformations of 4F-MDMB-BINACA was elucidated using single-enzyme incubations. Several cytochrome P450 (CYP) isozymes were shown to contribute, and CYP3A5 was involved in all CYP-catalyzed reactions, while amide and ester hydrolysis were catalyzed by the human carboxylesterase (hCES)

isoforms hCES1b and/or hCES1c. Finally, metabolites were compared to those present in human biosamples if data were available. Overall, the metabolic patterns in HepaRG cells provided the worst overlap with that in human biosamples. Zebrafish larvae experiments agreed best with data found in human plasma and urine analysis. The current study underlines the potential of zebrafish larvae as a tool for elucidating the toxicokinetics of NPS in the future.

Keywords: drugs of abuse, zebrafish, metabolism study, isozyme mapping, LC-HRMS/MS, toxicological screening

INTRODUCTION

New psychoactive substances (NPS) are a global issue posing a remarkable challenge to drug policy and a risk to public health. The number of deaths attributed to NPS dramatically increased during the last years, and most NPS appeared to induce more severe adverse effects than classic drugs such as heroin, cannabis, and amphetamine (Kronstrand et al., 2018). Symptoms associated with NPS intake might range from central nervous system toxicity leading to seizures, acute psychosis, aggression, to cardiotoxicity, and liver toxicity resulting in, e.g., arrhythmias and system failures (Kronstrand et al., 2018). NPS products are easily available, mainly via Internet shops selling new compounds as so-called "legal highs" or "research chemicals" (Brandt et al., 2014). Little or no scientific information are available about the effects of NPS and how best to counteract them. Besides, users are often unaware of the content and the dosage of the psychoactive substances contained in NPS products and potentially exposed to additional serious health risks (UNODC, 2019).

Furthermore, the NPS market is very dynamic and characterized by the large numbers of new substances belonging to several chemical groups (EMCDDA, 2019; UNODC, 2019). Between 2009 and 2016, 739 different NPS were reported to the United Nations Office on Drugs and Crime's Early Warning Advisory (UNODC, 2019). The diversity of compounds available on the market makes the detection of NPS in biological samples challenging for clinical and forensic toxicologists (Wagmann and Maurer, 2018). High-resolution mass spectrometry "is on the way to become the gold standard in non-targeted screening procedures due to its high flexibility, sensitivity, and selectivity" (Maurer and Meyer, 2016; Meyer and Maurer, 2016). The matrix of choice for comprehensive screening purposes is urine, which can be obtained non-invasively, provides large volumes, and the drugs as well as their metabolites are usually concentrated (Peters, 2014). However, lipophilic NPS are often extensively metabolized and the analytical strategy should also be focused on metabolites particularly in urine screening (Wagmann and Maurer, 2018). Thus, metabolism studies are mandatory for developing comprehensive screening methods. Metabolites may be identified in samples obtained from authentic cases. However, authentic human biosamples are often not available and controlled human studies are not feasible due to ethical concerns and lack of preclinical safety data (Meyer, 2016). To overcome this issue, metabolites can be generated using various *in vitro* or *in vivo* models (Meyer, 2018; Wagmann and Maurer, 2018; Diao and Huestis, 2019). Zebrafish (*Danio rerio*) has become a popular model organism. It shares morphological, physiological, and histological characteristics with mammals. For instance, several cytochrome P450 (CYP) enzymes in zebrafish have direct orthologs in humans. It is therefore expected that zebrafish drug metabolism may be similar to that in mammals (De Souza Anselmo et al., 2017). Not only the adult zebrafish, but also zebrafish larvae were used to generate xenobiotic metabolites (Diao and Huestis, 2019). The larvae are not considered as animals until 5 days post-fertilization (dpf) according to the European Directive 2010/63/EU. Despite this, they provide benefits of intact organisms (EU, 2010; Van Wijk et al., 2016). In 2019, Richter et al. used the new synthetic cannabinoid 7′N-5F-ADB (also known as 5F-MDMB-P7AICA and methyl 2-[1-(5-fluoropentyl)-1*H*-pyrrolo[2,3-b]pyridine-3-carboxamido]-3,3-dimethylbutanoate) to further develop the zebrafish larvae model, with the aim to be used as a preclinical surrogate for human hepatic NPS metabolism (Richter et al., 2019a). Results obtained with the larvae model were then compared to those of established *in vitro* incubations using pooled human liver S9 fraction (pHLS9) or the human hepatoma cell line HepaRG. Data of the model systems were also compared to human urinary metabolites (Richter et al., 2019a). Incubations with pHLS9 produced the lowest number of metabolites, while zebrafish larvae and HepaRG cell incubations provided the most comprehensive spectrum of human urinary 7′N-5F-ADB metabolites (Richter et al., 2019a,b). The authors concluded that zebrafish larvae seemed to be a promising model for studying the toxicokinetics of NPS, but further studies comparing different NPS classes were needed (Richter et al., 2019a). Therefore, the aim of the current study was to evaluate five NPS of different classes in a similar manner. Their chemical structures are given in **Figure 1**. The amphetamine-based NBOMe 3,4-DMA-NBOMe (also known as 3,4-dimethoxyamphetamine-NBOMe and 1-[3,4-dimethoxy]-*N*-[*ortho*-methoxybenzyl]propane-2-amine), the synthetic cathinone ephylone (also known as *N*-ethylnorpentylone and *N*-ethylpentylone), the synthetic cannabinoid 4F-MDMB-BINACA (also known as methyl 2-[1-(4-fluorobutyl)-1*H*-indazole-3-carbonyl]amino-3,3-dimethylbutanoate and 4-fluoro MDMB-BUTINACA), the pyrrolidinophenone analog 4F-PHP (also known as 4-fluoro-alpha-pyrrolidinohexiophenone, 4-fluoro-alpha-pyrrolidinohexanophenone, 4-F-α-PHP, and 4F-alpha-PHP), and the lysergamide 1P-LSD (1-propionyl-*d*-lysergic acid diethylamide) were included. The five NPS were already shown to be extensively metabolized and therefore suitable for the current comparative metabolism study (Caspar et al., 2018b;

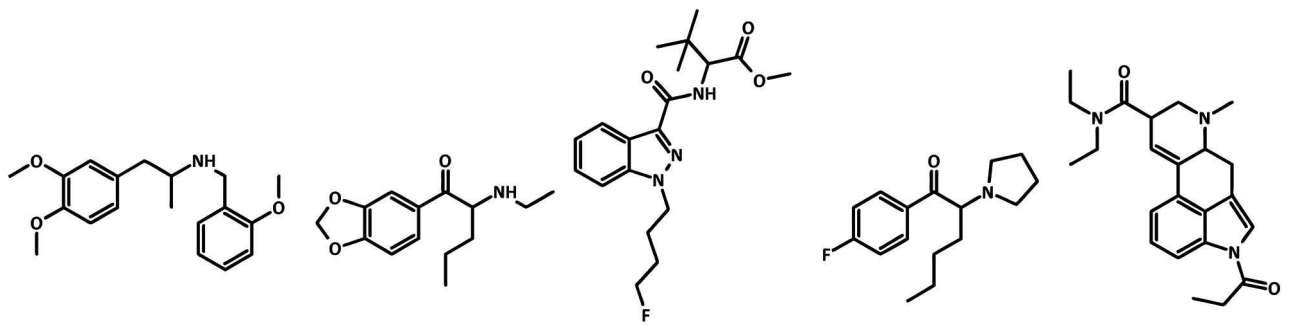

FIGURE 1 | Chemical structures of the five new psychoactive substances included in the current study.

Haschimi et al., 2019; Krotulski et al., 2019; Wagmann et al., 2019b,c). Caspar et al. used pHLS9 incubations and rat urine to investigate the metabolism of 3,4-DMA-NBOMe (Caspar et al., 2018b; Wagmann et al., 2019b,c). Wagmann et al. identified metabolites of ephylone and 4F-PHP in human blood and urine as well as in pHLS9 incubations (Caspar et al., 2018b; Wagmann et al., 2019b,c). The metabolic fate of 4F-MDMB-BINACA was investigated using human biosamples and incubations with pooled human liver microsomes (pHLM) (Haschimi et al., 2019; Krotulski et al., 2019) and results of *in vitro* incubations with pHLS9 and 1P-LSD were also described (Caspar et al., 2018b; Wagmann et al., 2019b,c).

In the current study, liquid chromatography coupled to Orbitrap-based high-resolution tandem mass spectrometry (LC-HRMS/MS) was used to analyze metabolic data after incubations with zebrafish larvae and HepaRG cells. The metabolites were compared to those detected in pHLS9 incubations, which were already described for four out of five compounds (Caspar et al., 2018b; Wagmann et al., 2019b,c). 4F-MDMB-BINACA pHLS9 incubations should be done in this study. The detected metabolites were compared to those in human biosamples if data were available. To further extend the knowledge about the metabolism of 4F-MDMB-BINACA, monooxygenases and esterases involved in its phase I metabolism should be identified in activity screenings.

MATERIALS AND METHODS

Reagents, Chemicals, and Enzymes

4F-MDMB-BINACA was provided by the EU-funded project ADEBAR (IZ25-5793-2016-27) for research purposes. 3,4-DMA-NBOMe, ephylone, 4F-PHP, and 1P-LSD were available from previous studies (Caspar et al., 2018b; Wagmann et al., 2019b,c). The hydrochloride of racemic 3,4-DMA-NBOMe was provided by the State Bureau of Criminal Investigation Schleswig-Holstein (Kiel, Germany) for research purposes, ephylone and 4F-PHP were obtained from an online vendor of NPS based in the Netherlands, and 1P-LSD was provided by Synex Synthetics (Maastricht, the Netherlands). The identity as well as purity of the NPS were confirmed by high-performance liquid chromatography (HPLC), infrared spectroscopy, and MS/MS. $NADP^+$ was obtained from Biomol (Hamburg, Germany), trimipramine-*d*3 was from LGC (Wesel, Germany), and dithiothreitol, reduced glutathione, superoxide dismutase, magnesium chloride ($MgCl_2$), dipotassium hydrogen phosphate (K_2HPO_4), potassium dihydrogen phosphate (KH_2PO_4), Tris hydrochloride, isocitrate dehydrogenase, isocitrate, 3′-phosphoadenosine-5′-phosphosulfate (PAPS), *S*-(5′-adenosyl)-L-methionine (SAM), dimethyl sulfoxide (DMSO), acetyl coenzyme A, diazepam-*d*5, and ammonium formate (analytical grade) were from Merck KGaA (Darmstadt, Germany). Uridine 5′-diphospho-glucuronosyltransferase (UGT) reaction mixture solution A (25 mM UDP glucuronic acid), UGT reaction mixture solution B (250 mM Tris–HCl, 40 mM $MgCl_2$, and 0.125 mg/ml alamethicin), pHLS9 (20 mg protein/ml), pHLM (20 mg microsomal protein/ml, 330 pmol total CYP/mg protein), the baculovirus-transfected insect cell microsomes (Supersomes) containing 1 nmol/ml of the human complementary DNA-expressed cytochrome P450 (CYP) isozymes CYP1A2, CYP2A6, CYP2B6, CYP2C8, CYP2C9 (2 nmol/ml), CYP2C19, CYP2D6, CYP2E1 (2 nmol/ml), CYP3A4, CYP3A5 (2 nmol/ml), flavin-containing monooxygenase 3 (FMO 3, 5 mg protein/ml), and recombinant human carboxylesterases hCES1b, hCES1c, and hCES2 were obtained from Corning (Amsterdam, the Netherlands). All enzyme containing preparations were thawed at 37°C after delivery, aliquoted, snap-frozen in liquid nitrogen, and stored at −80°C until use. Williams Medium E, HPRG670 supplement, GlutaMAX, cryopreserved and differentiated HepaRG cells, and 96-well plates coated with type I collagen were obtained from Life Invitrogen (Darmstadt, Germany). Zebrafish embryos were obtained from in-house bred adult zebrafish (approval no. 2.4.1.1-H, Landesamt für Verbraucherschutz, Saarland, Germany) of the AB wild-type line, and 6-well plates and 96-well plates were obtained from Sarstedt (Nümbrecht, Germany). Acetonitrile (LC-MS grade), methanol (LC-MS grade), formic acid (LC-MS grade), and all other reagents and chemicals (analytical grade) were purchased by VWR (Darmstadt, Germany).

Incubations With pHLS9 and 4F-MDMB-BINACA

According to published procedures (Richter et al., 2017b, 2019b; Caspar et al., 2018b; Wagmann et al., 2019b,c), the final incubation volume per reaction tube was 150 µl, with a final protein concentration of 2 mg/ml. The given concentrations represent final concentrations. A preincubation for 10 min at 37°C with UGT reaction mixture solution B (containing alamethicin, 25 µg/ml), $MgCl_2$ (2.5 mM), $NADP^+$ (0.6 mM), isocitrate (2.5 mM), isocitrate dehydrogenase (0.8 U/ml), superoxide dismutase (100 U/ml), acetyl coenzyme A (0.1 mM), phosphate buffer (90 mM, pH 7.4), and pHLS9 (2 mg/ml) was done. Afterwards, UGT reaction mixture solution A (containing UDP glucuronic acid, 2.5 mM), PAPS (40 µM), SAM (1.2 mM), dithiothreitol (1 mM), and glutathione (10 mM) were added, as well as 25 µM 4F-MDMB-BINACA to start the reactions. The mixture was incubated for 360 min. Total amount of organic solvent in incubation mixtures was <2% (Chauret et al., 1998). After 60 min, an aliquot of the reaction mixture (60 µl) was transferred in another reaction tube containing 20 µl of ice-cold acetonitrile to terminate the reactions. The remaining aliquot (90 µl) was incubated for an additional 300 min, and then the reactions were stopped by adding 30 µl of ice-cold acetonitrile. Thereafter, the reaction tubes were cooled at −20°C for 30 min prior to centrifugation at 18,407 × *g* for 2 min. The supernatants (50 µl) were transferred into autosampler vials, and 1 µl was injected onto the LC-HRMS/MS system. Control samples without pHLS9 and blank samples without substrate were prepared to confirm the absence of non-metabolically formed and interfering compounds, respectively. All incubations were performed in duplicate.

In vivo Maximum-Tolerated Concentration Studies in Zebrafish Larvae

Internal protocols based on published standard methods (Westerfield, 2007) were used to perform zebrafish husbandry and the maximum-tolerated concentration (MTC) testing was based on a previous study (Richter et al., 2019a). Danieau's medium [17 mM NaCl, 2 mM KCl, 0.12 mM $MgSO_4$, 1.8 mM $Ca(NO_3)_2$, 1.5 mM HEPES, pH 7.1–7.3, and 1.2 µM methylene blue] at 28°C was used to raise zebrafish larvae of the AB wild-type strain. For MTC testing, 96-well plates were used with 100 µl of medium and one larva per well. Drug exposition was started 4 dpf using 0, 0.01, 0.1, 1, 10, 50, or 100 µM final concentrations of 3,4-DMA-NBOMe, ephylone, 4F-MDMB-BINACA, 4F-PHP, or 1P-LSD, respectively. The drug exposure in the incubator at 28°C lasted 24 h. The final DMSO concentration was 1% (*v/v*) for all experiments. Monitoring of the larvae was done using a LEICA M205 FA stereo microscope (Leica Mikrosysteme Vertrieb GmbH, Wetzlar, Germany) to detect developmental defects and/or decreased survival rates. Fifteen larvae were used for each experiment.

Zebrafish Larvae Exposure

In accordance with a previous study (Richter et al., 2019a) with minor modifications, substances were administrated to the zebrafish larvae at 4 dpf via the Danieau's medium with final substrate concentrations of 25 µM (4F-MDMB-BINACA) or 100 µM (3,4-DMA-NBOMe, ephylone, 4F-PHP, and 1P-LSD), respectively, and a final DMSO concentration of 1% (*v/v*). Six-well plates were used and 10 larvae were placed in each well containing 2,000 µl of Danieau's medium supplemented with one of the NPS. After an incubation period of 24 h at 28°C, the larvae were collected separated from the surrounding medium. All larvae of one well (10 larvae) were washed twice with 1,000 µl of Danieau's medium. Afterwards, they were euthanized by placing the tubes in ice water for 15 min. After removing the residual medium, the larvae were snap-frozen in liquid nitrogen followed by lyophilization and stored at −20°C until extraction. Twenty larvae (from two wells) were extracted using 50 µl of methanol, shaken for 2 min, and centrifuged for 2 min at 18,407 × *g*. Thirty microliters of the supernatants was transferred into autosampler vials and 1 µl was injected onto the LC-HRMS/MS system. Medium samples without larvae were collected to identify non-metabolically formed compounds. Blank larvae samples without the NPS were prepared to confirm the absence of interfering compounds. All incubations were done in triplicate.

Incubations With HepaRG Cells

Cell culture experiments using differentiated human hepatocellular carcinoma HepaRG cells were carried out as recently described (Richter et al., 2019a,c). Cells were handled under sterile conditions. A laminar flow bench class II (Thermo Scientific Schwerte, Germany) and an incubator (Binder, Tuttlingen, Germany) with 95% air humidity and 5% CO_2 atmosphere at 37°C were used. The concentrations given in the following are final concentrations. Collagen-coated 96-well plates were used and the HepaRG cells were seeded in a density of 72,000 cells/well (a 100-µl aliquot cell suspension/well) in thaw and seed medium, consisting of Williams E medium supplemented with penicillin (100 U/ml), streptomycin (100 µg/ml), GlutaMAX, and HPRG670. Four hours after cell seeding, 50 µl of the supernatants was removed from each well. Afterwards, 50 µl of the thaw and seed medium containing 3,4-DMA-NBOMe, ephylone, 4F-MDMB-BINACA, 4F-PHP, or 1P-LSD (50 or 500 µM resulting in final concentrations of 25 or 250 µM), respectively, was added. Each well also contained 0.5% (*v/v*) DMSO. After drug exposure of 24 h, 50 µl of the supernatants was precipitated using the same volume of acetonitrile containing 0.1% (*v/v*) formic acid. The mixtures were vortexed, cooled for 30 min at −20°C, and centrifuged at 18,407×*g* for 2 min. Eighty microliters of the mixture was transferred into an autosampler vial and 1 µl was injected onto the LC-HRMS/MS system. Control samples without substrate and blank samples without HepaRG cells were prepared in the same manner to confirm the absence of interfering compounds or non-metabolically formed compounds, respectively. All incubations were performed in triplicate.

Monooxygenases Activity Screening of 4F-MDMB-BINACA

According to an established protocol (Wagmann et al., 2016), the final volume per reaction tube was 50 µl with a final 4F-MDMB-BINACA concentration of 25 µM and enzyme concentrations

of 50 pmol/ml for CYP1A2, CYP2A6, CYP2B6, CYP2C8, CYP2C9, CYP2C19, CYP2D6, CYP2E1, CYP3A4, and CYP3A5, respectively, or 0.25 mg protein/ml for FMO3. Furthermore, the reaction mixture contained 90 mM phosphate buffer (pH 7.4), superoxide dismutase (200 U/ml), isocitrate (5 mM), $MgCl_2$ (5 mM), isocitrate dehydrogenase (0.5 U/ml), and $NADP^+$ (1.2 mM). The phosphate buffer was replaced with Tris buffer (90 mM) for incubations with CYP2A6 and CYP2C9 according to the manufacturer's recommendation. All incubations were performed at 37°C for 30 min and terminated by adding 50 µl of ice-cold acetonitrile. Afterwards, the mixtures were centrifuged at 18,407×*g* for 5 min, 70 µl of the supernatants was transferred into autosampler vials, and 1 µl was injected onto the LC-HRMS/MS system. Positive control incubations were performed with pHLM (1 mg microsomal protein/ml), and negative controls without enzyme were prepared to identify non-metabolically formed compounds. All incubations were done in duplicate.

Esterases Activity Screening of 4F-MDMB-BINACA

Experiments were performed in accordance with a previous study (Meyer et al., 2015) with minor modifications. The final volume per reaction tube was 100 µl with a final 4F-MDMB-BINACA concentration of 100 µM and enzyme concentration of 0.2 mg protein/ml for hCES1b, hCES1c, and hCES2. Incubations with pHLM and pHLS9 (0.2 mg protein/ml, each) were performed in a similar manner. Additionally, incubations with human plasma (50 µl pooled human plasma, 40 µl phosphate buffer, and 10 µl substrate) were performed. The reactions were started by adding the enzyme-containing preparation and terminated with an equal volume of ice-cold acetonitrile containing diazepam-*d*5 (100 µM) as an internal standard. Only plasma incubations were terminated by addition of a three-fold volume of ice-cold acetonitrile. The reaction mixtures were centrifuged at 18,407×*g* for 15 min, and then supernatants were transferred to autosampler vials, and 5 µl was injected onto the LC-HRMS/MS system. Negative control incubations without enzyme were prepared to identify non-metabolically formed compounds. All incubations were done in duplicate.

Preparation of Human Biosamples After Intake of 4F-MDMB-BINACA

Human blood and urine collected after a suspected intake of drugs of abuse were submitted to the authors' laboratory for regular clinical toxicological analysis. The blood sample was centrifuged, and plasma was separated. The authors' standard liquid–liquid extraction for human plasma screening was used (Maurer et al., 2016). Briefly, 1,000 µl of plasma was mixed with 100 µl of internal standard (0.01 µg/µl trimipramine-*d*3 in methanol) and extracted with 5,000 µl of a mixture of diethyl ether:ethyl acetate (1:1, *v/v*) after addition of 2,000 µl of saturated sodium sulfate solution. Phase separation was mediated by centrifugation. The organic layer was transferred into a flask and evaporated to dryness at 60°C under reduced pressure. The aqueous residue was then alkalized with 500 µl of 1 M sodium hydroxide and extracted a second time with 5,000 µl of the diethyl ether:ethyl acetate mixture. The organic extract was transferred to the same flask and evaporated as described before. The combined residues were dissolved in 100 µl of methanol and transferred into an autosampler vial, and 5 µl was injected onto the LC-HRMS/MS system. An aliquot of the human urine sample (100 µl) was prepared according to a previous study by precipitation with 500 µl of acetonitrile (Wissenbach et al., 2011). The mixture was shaken and centrifuged (18,407×*g*, 2 min). After transfer of the supernatant into an autosampler vial, it was evaporated to dryness at 70°C under a gentle stream of nitrogen. The residue was dissolved in 50 µl of a mixture of eluent A and B (see LC-HRMS/MS conditions, 1:1, *v/v*) and 5 µl was injected onto the LC-HRMS/MS system.

LC-HRMS/MS Apparatus and Conditions

According to a previous study (Richter et al., 2019a), a Thermo Fisher Scientific (TF, Dreieich, Germany) Dionex UltiMate 3000 Rapid Separation (RS) UHPLC system with a quaternary UltiMate 3000 RS pump and an UltiMate 3000 RS autosampler controlled by the TF Chromeleon software version 6.8 was used. The LC system was coupled to an Orbitrap-based TF Q-Exactive Plus equipped with a heated electrospray ionization II (HESI-II) source. Calibration was done prior to analysis with a Positive Cal Mix (Supelco, Bellefonte, PA, USA) at a flow rate of 3 µl/min using a syringe pump. The conditions of the LC system were as follows: TF Accucore PhenylHexyl column (100 × 2.1 mm, 2.6 µm particle size); gradient elution with 2 mM ammonium formate solution containing 0.1% (*v/v*) formic acid (eluent A) and 2 mM ammonium formate solution in acetonitrile/methanol (50:50, *v/v*) containing 0.1% (*v/v*) formic acid, and 1% (*v/v*) water (eluent B). The flow rate was set to 0.5 ml/min (0–11.5 min) and 0.8 ml/min (11.5–13.5 min). The following gradient was used: 0–1.0 min hold 1% B, 1–10 min to 99% B, 10–11.5 min hold 99% B, 11.5–13.5 min hold 1% B. The HESI-II source conditions were as follows: ionization mode, positive; heater temperature, 320°C; ion transfer capillary temperature, 320°C; sheath gas, 60 arbitrary units (AU); auxiliary gas, 10 AU; spray voltage, 4.00 kV; and S-lens RF level, 50.0. Mass spectrometry experiments were performed using high-resolution (HR) full scan mode and a targeted MS^2 mode with an inclusion list for each NPS. The inclusion list contained *m/z* values of metabolites, which were likely to be formed for example hydroxy, oxo, carboxy, dealkyl, demethylenylated, and defluorinated metabolites (phase I) as well as sulfates and glucuronides (phase II) and combinations of them. Full scan settings were as follows: resolution, 35,000; automatic gain control (AGC) target, 3e6; maximum injection time (IT), 120 ms; scan ranges, 3,4-DMA-NBOMe *m/z* 100–700, ephylone *m/z* 200–600, 4F-MDMB-BINACA *m/z* 150–700, 4F-PHP *m/z* 200–600, and 1P-LSD *m/z* 250–700. The settings for the targeted MS^2 mode with the respective inclusion lists were as follows: resolution, 17,500; AGC target, 2e5; maximum IT, 250 ms; loop count, 5; isolation window, 1.0 *m/z*; stepped normalized collision energy (NCE), 17.5, 35, 52.5%; pick others, enabled. ChemSketch 2018 2.1 (ACD/Labs, Toronto, Canada) was used to draw the structures of the hypothetical metabolites and for the calculations of the exact masses. Xcalibur Qual Browser version 4.1.31.9 (TF) was used for data handling. The

mass tolerance between calculated and measured mass was adjusted to 5 ppm. For identification of metabolites, HR full scan data were screened for potential exact precursor ion (PI) masses of expected metabolites. Metabolites were tentatively identified by comparing the corresponding $HRMS^2$ spectrum to that of the parent compound.

RESULTS AND DISCUSSION

Identification of 4F-MDMB-BINACA Phase I and II Metabolites in pHLS9 Incubations

Only the reference material of the parent compound 4F-MDMB-BINACA was available. Therefore, postulated metabolic transformations could not be confirmed using chemical standards, and all the metabolites were claimed to be tentatively identified. This was also true for the other investigated NPS. All tentatively identified metabolites of 4F-MDMB-BINACA along with their absolute peak areas in pHLS9 incubations after 1 or 6 h of incubations are listed in **Table 1**. The given areas were taken from one replicate of the pHLS9 incubations ($n = 2$). The second replicate provided the same pattern of metabolite abundances. $HRMS^2$ spectra of the parent compound and the metabolites discussed in detail in the following are depicted in **Figure 2**, while $HRMS^2$ spectra of all other 4F-MDMB-BINACA metabolites are depicted in the **Electronic Supplementary Material** (ESM). The metabolites were sorted by increasing *m/z*. In case of isomers with identical *m/z*, metabolites were sorted by increasing retention time. Each metabolite was assigned to a unique metabolite ID. The calculated exact masses, not the measured masses, will be used in the following. In total, 15 phase I and two phase II metabolites of 4F-MDMB-BINACA were detected in pHLS9 incubations (see **Table 2**). Haschimi et al. performed 4F-MDMB-BINACA incubations with pHLM instead of pHLS9 without co-substrates of phase II metabolic reactions and identified 11 phase I metabolites (Haschimi et al., 2019). All these metabolites were also detected in pHLS9 incubations with one exception, namely, a 4F-MDMB-BINACA metabolite formed after ester hydrolysis and hydroxylation of the butyl chain.

The $HRMS^2$ spectrum of 4F-MDMB-BINACA (PI at *m/z* 364.2031, $C_{19}H_{27}O_3N_3F^+$) showed the subsequent fragmentation of the ester moiety due to an initial methanol loss (−32.0262 u, CH_4O) forming the fragment ion (FI) at *m/z* 332.1769 ($C_{18}H_{23}O_2N_3F^+$) followed by a loss of CO (−27.9949 u), resulting in the FI at *m/z* 304.1820 ($C_{17}H_{23}ON_3F^+$). The most abundant FI at *m/z* 219.0928 ($C_{12}H_{12}ON_2F^+$) corresponded to a cleavage of the amide moiety between the carbonyl carbon atom and the nitrogen atom. The FI at *m/z* 237.1034 ($C_{12}H_{14}O_2N_2F^+$) represented a mass shift of +18.0106 u corresponding to the mass of water. Richter et al. postulated a rearrangement reaction for 5F-ADB potentially also explaining the current finding. 5F-ADB obtained a similar structure, but with a fluoro pentyl chain instead of the fluoro butyl chain of 4F-MDMB-BINACA. Ester cleavage followed by nucleophilic attack of the oxygen at the indazole nitrogen in position 2 may lead to cyclization (Richter et al., 2019b). Further cleavage of the amide bond and the ester bond may result in the FI at *m/z* 237.1034. The same shift was detected for the FIs at *m/z* 145.0396 ($C_8H_5ON_2^+$) and 163.0502 ($C_8H_7O_2N_2^+$), formed after cleavage of the amide bond between the carbonyl carbon atom and the nitrogen atom and elimination of the fluoro butyl chain.

Due to the large number of metabolites tentatively identified in this study, only some 4F-MDMB-BINACA metabolites with fragmentation patterns that were representative for the other metabolites could be described in detail. After ester hydrolysis (MB8, PI at *m/z* 350.1874, $C_{18}H_{25}O_3N_3F^+$), an initial loss of water (−18.0105 u, H_2O) was observed resulting in the FI at *m/z* 332.1769 ($C_{18}H_{23}O_2N_3F^+$), instead of a loss of methanol as described for the parent compound 4F-MDMB-BINACA, but also followed by a loss of CO. A similar fragmentation pattern was already described for other carboxylic acids (Niessen and Correa, 2016; Wagmann et al., 2019a). All other FIs were the same as those detected in the $HRMS^2$ spectrum of 4F-MDMB-BINACA.

Two metabolites with the PI at *m/z* 366.1824 (MB13, MB14, $C_{18}H_{25}O_4N_3F^+$) were identified as products of ester hydrolysis plus hydroxylation. Both spectra obtained an initial water loss resulting in the FI at *m/z* 348.1718 ($C_{18}H_{23}O_3N_3F^+$) supporting the assumption of prior ester hydrolysis. Furthermore, the mass shift of +15.9949 u between the FI at *m/z* 320.1769 ($C_{17}H_{23}O_2N_3F^+$) and 304.1820 ($C_{17}H_{23}ON_3F^+$) in the spectrum of the parent compound indicated an additional oxygen atom at the fluoro butyl chain, the indazole ring, or the *tert*-butyl group. In case of MB13, FIs at *m/z* 237.1034, 219.0928, 163.0502, and 145.0396 were detected, according to the $HRMS^2$ spectrum of the parent compound, indicating unchanged fluoro butyl and indazole parts. Therefore, MB13 was hydroxylated at the *tert*-butyl group. In case of MB14, the FIs at *m/z* 253.0983, 235.0877, 179.0451, and 161.0346 represented the aforementioned FIs shifted by +15.9949 u (oxygen), indicating that the indazole part of MB14 was hydroxylated, but the exact position could not be determined based on the fragmentation pattern.

The PI at *m/z* 348.1718 of MB6 ($C_{18}H_{23}O_3N_3F^+$) provided a mass shift of −2.0157 u regarding the PI of MB8 (ester hydrolysis). This was postulated to be an ester hydrolysis followed by dehydrogenation (Haschimi et al., 2019; Krotulski et al., 2019). Another possibility would be the formation of a lactone after hydroxylation of the *tert*-butyl part, with or without former ester hydrolysis as postulated for MDMB-FUBINACA (Kavanagh et al., 2017). The formation of the lactone was expected to be more likely due to the FI at *m/z* 320.1769 ($C_{17}H_{23}O_2N_3F^+$), which was also detected for MB13 (ester hydrolysis + hydroxylation of the *tert*-butyl part) and MB16 (hydroxylation of the *tert*-butyl part), but not MB8 (ester hydrolysis), and the FI at *m/z* 113.0597 ($C_6H_9O_2^+$), a 4,4-dimethyl-2-oxotetrahydrofuran-3-ylium ion, formed by cleavage of the bond between amide nitrogen and alpha carbon of the lactone part. In accordance with the observations of Kavanagh et al. (2017), MB6 was not ionizable in negative ionization mode, which contrasts with the characteristic behavior of carboxylic acids such as MB8 (ester hydrolysis).

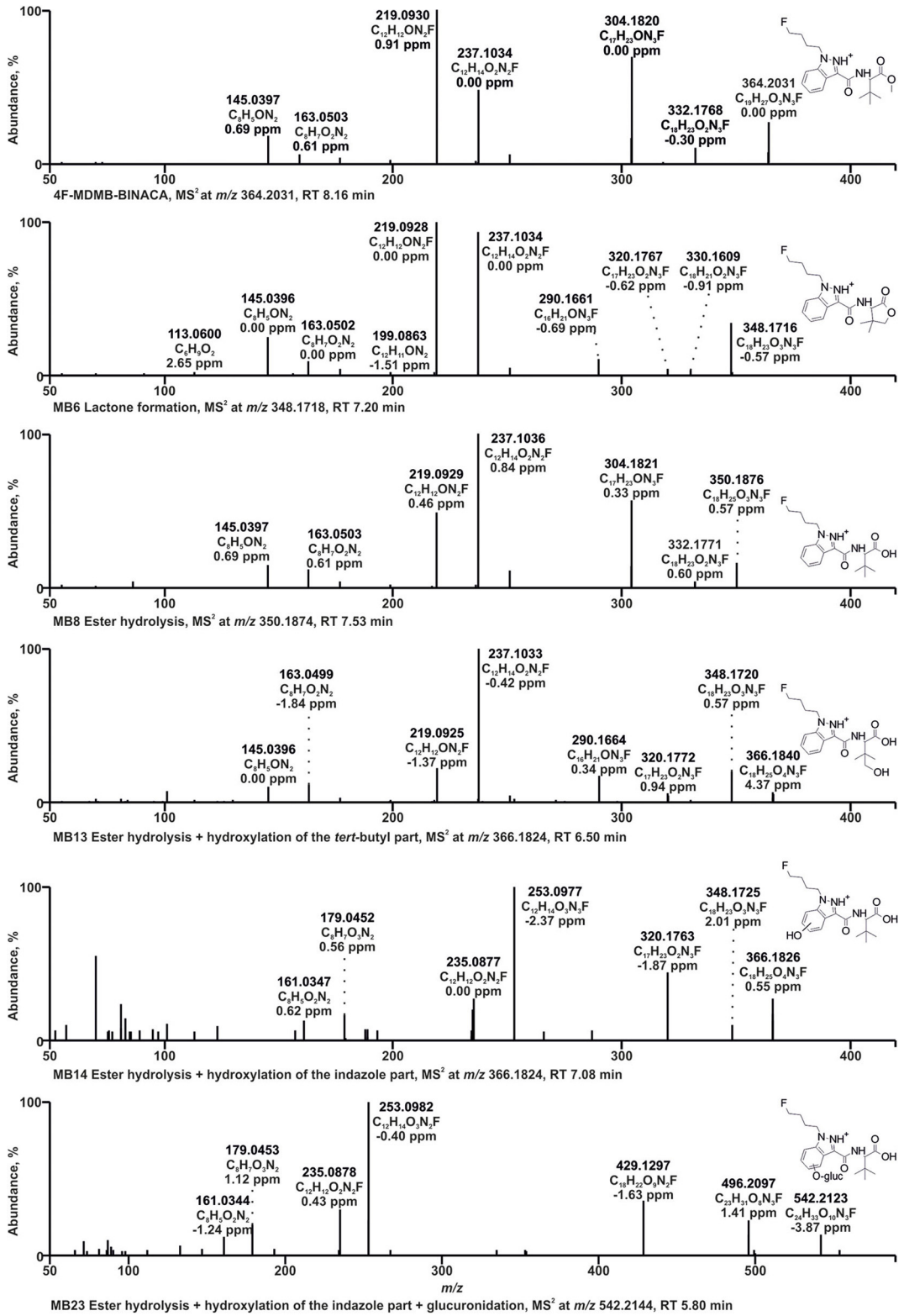

FIGURE 2 | HRMS^2 spectra of 4F-MDMB-BINACA and some of its metabolites detected in incubations with pooled human liver S9 fraction, HepaRG cells, and/or zebrafish larvae. Metabolite IDs correspond to **Table 1**. MB, 4F-MDMB-BINACA metabolite; RT, retention time.

TABLE 1 | Absolute peak areas of 4F-MDMB-BINACA and its phase I and II metabolites in incubations with pooled human liver S9 fraction (pHLS9, $n = 2$), HepaRG cells ($n = 3$), and zebrafish larvae ($n = 3$) taken from one replicate, each, along with the unique metabolite ID, observed metabolic reaction, and calculated exact mass.

Metabolite ID	Metabolic reaction	Calculated exact masses, *m/z*	pHLS9 1 h [25 μM]	pHLS9 6 h [25 μM]	HepaRG [25 μM]	HepaRG [250 μM]	Zebrafish larvae [25 μM]
4F-MDMB-BINACA	- (parent compound)	364.2031	**9.37E+08**	**2.17E+08**	**1.28E+08**	**5.18E+08**	**2.89E+09**
MB1	Amide hydrolysis	237.1034	n.d.	n.d.	3.34E+04	3.82E+06	n.d.
MB2	Lactone formation + *N*-dealkylation	274.1186	n.d.	n.d.	n.d.	n.d.	5.13E+05
MB3	Ester hydrolysis + *N*-dealkylation	276.1343	9.07E+05	1.27E+06	3.99E+05	6.92E+06	n.d.
MB4	*N*-Dealkylation	290.1499	**5.62E+06**	2.82E+05	n.d.	9.55E+06	7.45E+06
MB5	Lactone formation + oxidative defluorination	346.1761	n.d.	1.26E+06	n.d.	2.40E+05	9.42E+05
MB6	Lactone formation	348.1718	n.d.	**5.21E+07**	n.d.	2.48E+06	**1.29E+08**
MB7	Ester hydrolysis + oxidative defluorination	348.1918	n.d.	**1.91E+06**	**1.25E+06**	**1.34E+07**	5.96E+04
MB8	Ester hydrolysis	350.1874	**1.01E+08**	**2.77E+08**	**5.16E+07**	**1.63E+09**	**1.73E+07**
MB9	Lactone formation + oxidative defluorination + oxidation to carboxylic acid	360.1554	n.d.	1.57E+05	n.d.	n.d.	2.53E+06
MB10	Ester hydrolysis + oxidative defluorination + oxidation to carboxylic acid	362.1710	n.d.	n.d.	1.68E+05	8.32E+05	5.72E+04
MB11	Oxidative defluorination	362.2074	**4.27E+06**	3.89E+05	9.30E+04	6.93E+06	2.92E+06
MB12	Lactone formation + hydroxylation of the *tert*-butyl part	364.1667	n.d.	n.d.	n.d.	n.d.	1.68E+06
MB13	Ester hydrolysis + hydroxylation of the *tert*-butyl part	366.1824	7.30E+03	6.42E+05	n.d.	**3.13E+07**	4.57E+05
MB14	Ester hydrolysis + hydroxylation of the indazole part	366.1824	4.94E+04	3.04E+05	n.d.	n.d.	n.d.
MB15	Oxidative defluorination + oxidation to carboxylic acid	376.1867	2.16E+06	**3.34E+06**	1.15E+04	8.00E+06	**2.60E+07**
MB16	Hydroxylation of the *tert*-butyl part	380.1980	1.70E+05	n.d.	n.d.	n.d.	5.98E+06
MB17	Hydroxylation of the butyl chain	380.1980	9.01E+05	5.84E+04	n.d.	2.95E+06	n.d.
MB18	Hydroxylation of the indazole part isomer 1	380.1980	3.75E+05	n.d.	n.d.	n.d.	4.77E+05
MB19	Hydroxylation of the indazole part isomer 2	380.1980	**7.16E+06**	4.56E+04	n.d.	n.d.	n.d.
MB20	Hydroxylation of the indazole part + sulfation	460.1548	n.d.	n.d.	n.d.	n.d.	2.06E+06
MB21	Ester hydrolysis + oxidative defluorination + glucuronidation	524.2239	n.d.	n.d.	**4.18E+05**	7.56E+05	n.d.
MB22	Ester hydrolysis + glucuronidation	526.2196	n.d.	n.d.	**2.56E+07**	**3.25E+07**	n.d.
MB23	Ester hydrolysis + hydroxylation of the indazole part + glucuronidation	542.2144	n.d.	1.34E+05	n.d.	n.d.	n.d.
MB24	Oxidative defluorination + oxidation to carboxylic acid + glucuronidation	552.2188	n.d.	n.d.	n.d.	n.d.	2.34E+05
MB25	Hydroxylation of the *tert*-butyl part + glucuronidation	556.2301	n.d.	n.d.	n.d.	n.d.	**1.75E+07**
MB26	Hydroxylation of the indazole part + glucuronidation	556.2301	5.96E+05	7.68E+05	n.d.	1.48E+06	1.96E+06

The five largest areas per model are given in bold. MB, 4F-MDMB-BINACA metabolite; n.d., not detected.

Glucuronidation was identified by the increase of 176.0320 u ($C_6H_8O_6$) in the parent mass. MB23 with the PI at *m/z* 542.2144 ($C_{24}H_{33}O_{10}N_3F^+$) was identified as product of ester hydrolysis, hydroxylation of the indazole part, and glucuronidation. MB14 represented the corresponding phase I metabolite. MB14 and MB23 provided the same fragmentation pattern below *m/z* 366.1824 (PI of MB14), but differences in the abundance of several FIs. The FI at *m/z* 496.2089 ($C_{23}H_{31}O_8N_3F^+$) in the $HRMS^2$ spectrum of MB23 represented the FI at *m/z* 320.1769 ($C_{17}H_{23}O_2N_3F^+$) conjugated with glucuronic acid. Therefore, the glucuronic acid moiety was most likely bound to the hydroxy group at the indazole part and not to the carboxylic acid.

According to the recommendation of Richter et al., two incubation time points were analyzed to detect initial metabolic steps as well as late phase metabolites (Richter et al., 2017b). As no reference standards of the metabolites were available, their quantification was not possible. Only their abundance could be compared to each other. However, it must be noticed that the highest concentration is not always reflected by the highest abundance, which is influenced by the ionizability of a compound. The most abundant metabolite in pHLS9 incubations after 1 and 6 h was MB8 (ester hydrolysis). After 1 h of incubation, it was followed by MB19 (hydroxylation of the indazole part isomer 2) and MB4 (*N*-dealkylation). After 6 h of incubation, MB6 (lactone formation) and MB15 (oxidative defluorination + oxidation to carboxylic acid) represented the second and third most abundant metabolites, respectively.

Incubations with pHLS9 following the same procedure were already performed for 3,4-DMA-NBOMe, ephylone, 4F-PHP, and 1P-LSD, and the results and their fragmentation patterns

TABLE 2 | Number of phase I and II metabolites of the five tested NPS detected in incubations with pooled human liver S9 fraction (pHLS9), HepaRG cells, and zebrafish larvae.

	pHLS9 [25 μM]	HepaRG [25 μM]	HepaRG [250 μM]	Zebrafish larvae
4F-MDMB-BINACA				
Phase I	15	7	12	14
Phase II	2	2	3	4
3,4-DMA-NBOMe				
Phase I	6 (Caspar et al., 2018b)	6	10	9
Phase II	5 (Caspar et al., 2018b)	4	7	7
Ephylone				
Phase I	5 (Wagmann et al., 2019b)	2	4	5
Phase II	8 (Wagmann et al., 2019b)	4	6	4
4F-PHP				
Phase I	6 (Wagmann et al., 2019b)	5	6	8
Phase II	2 (Wagmann et al., 2019b)	0	1	3
1P-LSD				
Phase I	8 (Wagmann et al., 2019c)	14	15	22
Phase II	0 (Wagmann et al., 2019c)	1	2	3
Total				
Phase I	40	34	47	58
Phase II	17	11	19	21

were described elsewhere (Caspar et al., 2018b; Wagmann et al., 2019b,c).

In vivo Maximum-Tolerated Concentration Studies in Zebrafish Larvae

To exclude toxic effects of the investigated NPS on zebrafish larvae, which might prevent metabolic transformations, the MTC was evaluated. The survival rates of zebrafish larvae (4 dpf) after 24-h treatment with the NPS added to the medium at the concentrations of 0, 0.01, 0.1, 1, 10, 50, or 100 μM are given in **Table 3**. In case of 3,4-DMA-NBOMe, ephylone, 4F-PHP, and 1P-LSD, survival rates were 100% for all tested concentrations and no malformations were observed. Therefore, a concentration of 100 μM was considered to be non-toxic for zebrafish larva 4 dpf and chosen for metabolism studies. The MTC study with 4F-MDMB-BINACA showed survival rates of 73% and 53% at 50 and 100 μM, respectively. No malformations were observed. Further zebrafish studies were performed with only 25 μM 4F-MDMB-BINACA, and larvae were monitored in terms of survival and malformations, to ensure nontoxicity of the chosen concentration.

TABLE 3 | Survival rates of zebrafish larvae (4 dpf) after 24-h treatment with various concentrations of 3,4-DMA-NBOMe, ephylone, 4F-MDMB-BINACA, 4F-PHP, or 1P-LSD, respectively.

Concentration, μM	Survival rate, %				
	3,4-DMA-NBOMe	Ephylone	4F-MDMB-BINACA	4F-PHP	1P-LSD
0	100	100	100	100	100
0.01	100	100	100	100	100
0.1	100	100	100	100	100
1	100	100	100	100	100
10	100	100	100	100	100
50	100	100	73	100	100
100	100	100	53	100	100

Fifteen larvae were tested per concentration level and test compound, respectively.

Identification of Metabolites in Incubations With HepaRG Cells and Zebrafish Larvae and Comparison to Metabolites Identified in Incubations With pHLS9

Zebrafish were found to have similar metabolic enzymes to mammals and to be able to perform both phase I (such as oxidations, *N*-demethylations, *O*-demethylations, or *N*-dealkylations) and phase II metabolic reactions (for example, sulfations, glucuronidations, or methylations) (De Souza Anselmo et al., 2017; Matos et al., 2019). As whole organisms, zebrafish larvae may also overcome the limitations of *in vitro* model systems (Van Wijk et al., 2016). Concerning *in vitro* metabolism studies, human liver tissue-derived primary hepatocytes are considered as "gold standard," but provide several disadvantages such as complex isolation procedures, high variability in the enzyme expression, and limited availability (Guillouzo et al., 2007; Godoy et al., 2013). Relevant alternative *in vitro* systems are sought after and especially HepaRG cells were found to be a suitable alternative to primary human hepatocytes (Lubberstedt et al., 2011; Godoy et al., 2013).

HepaRG cells represent immortalized human liver cells derived from a tumor. They were shown to remain capable of expressing most of the liver-specific functions, including the major CYPs involved in drug metabolism, but were derived from a CYP2D6 poor metabolizer patient (Guillouzo et al., 2007). Neither HepaRG cells nor zebrafish larvae experiments demand the supplementation of co-substrates of metabolic reactions representing their main advantage over pHLS9 incubations (Richter et al., 2017a). However, handling of cells as well as zebrafish larvae is time-consuming and requires special laboratory equipment and qualified personnel. Furthermore, zebrafish larvae experiments required a higher total amount of the NPS then HepaRG incubations. Incubations with pHLS9 could be performed with the lowest NPS amount, which might be beneficial in cases only small volumes of substances are available.

Based on the results of the MTC study, a 4F-MDMB-BINACA concentration of 25 μM was added to the zebrafish larvae medium and neither malformations nor dead larvae were

observed after 24 h of incubation. Thus, 25 μM 4F-MDMB-BINACA was considered as non-toxic for zebrafish larvae (4 dpf). Focusing on the detection of metabolites, a previous study demonstrated the extraction of zebrafish larvae to be superior to the precipitation of the surrounding medium (Richter et al., 2019a). In case of HepaRG cell incubations, the precipitated cell culture medium was shown to be an appropriate matrix for identification of metabolites (Richter et al., 2017a, 2019a,c). HepaRG cell experiments were conducted using two different concentrations (25 and 250 μM, respectively) in accordance with a previous study (Richter et al., 2019c). All tentatively identified metabolites of 4F-MDMB-BINACA along with their absolute peak areas in HepaRG cells incubations or zebrafish larvae are listed in **Table 1**. The given areas were taken from one replicate of the HepaRG incubations ($n = 3$) or zebrafish larvae experiments ($n = 3$). The other replicates provided the same pattern of metabolite abundances. $HRMS^2$ spectra of the parent compound and the metabolites are depicted in **Figure 2** or **Figure S1** in the ESM.

Nine metabolites (7 phase I, 2 phase II) were detected in the HepaRG cell culture medium using a 4F-MDMB-BINACA concentration of 25 μM and 15 metabolites (12 phase I, 3 phase II) were detected using 250 μM 4F-MDMB-BINACA (see **Table 2**). All metabolites identified after administration of 25 μM 4F-MDMB-BINACA to HepaRG cells could also be detected after administration of 250 μM as well as six additional metabolites. Most abundant metabolites were MB8 (ester hydrolysis) followed by MB7 (ester hydrolysis + oxidative defluorination) and MB22 (ester hydrolysis + glucuronidation). Eighteen metabolites (14 phase I, 4 phase II) were detected in zebrafish larvae (see **Table 2**). MB8 (ester hydrolysis), MB6 (lactone formation), and MB15 (oxidative defluorination + oxidation to carboxylic acid) provided the highest abundance. In conclusion, zebrafish larvae led to the identification of the highest number of 4F-MDMB-BINACA metabolites among the investigated models. In comparison to HepaRG cells, zebrafish larvae produced more phase I, but also II metabolites. Incubations with pHLS9 produced one phase I metabolite more but two phase II metabolites less than zebrafish larvae.

All tentatively identified metabolites of 3,4-DMA-NBOMe, ephylone, 4F-PHP, and 1P-LSD in HepaRG cell incubations and zebrafish larvae are listed in **Tables S1**–**S4** (ESM), which also contain the metabolites detected in pHLS9 incubations described in literature. Detailed information on their MS fragmentation patterns may also be found in literature (Caspar et al., 2018b; Wagmann et al., 2019b,c). $HRMS^2$ spectra of the parent compounds and the metabolites recorded during the current study are depicted in **Figures S2**–**S5** (ESM). In accordance with the results for 4F-MDMB-BINACA, zebrafish larvae also produced the highest number of phase I and II metabolites of 4F-PHP and 1P-LSD. Concerning 3,4-DMA-NBOMe, most metabolites were formed by HepaRG cells with 250 μM substrate concentration, while pHLS9 incubations produced the highest number of ephylone metabolites.

Summarizing the results of all five investigated NPS (see **Table 2**), the highest number of metabolites could be detected in zebrafish larvae (79 metabolites in total, 58 phase I, 21 phase II). However, some metabolites were exclusively formed by zebrafish larvae (e.g., MB2, MB12, MN9, and MP3), possibly indicating species differences between humans and zebrafish. HepaRG cells after administration of 250 μM substrate were identified as the second most efficient metabolizing model (66 metabolites in total, 47 phase I, 19 phase II), followed by pHLS9 incubations (57 metabolites in total, 40 phase I, 17 phase II). In the current study, HepaRG cells produced more metabolites after application of 250 μM NPS in comparison to 25 μM. However, as the investigated NPS were not tested for toxicity in HepaRG cells prior to the experiments, incubation of two different concentrations is also recommended for future studies.

Monooxygenases Activity Screening of 4F-MDMB-BINACA

The involvement of monooxygenases in the metabolic phase I transformations of 4F-MDMB-BINACA was elucidated using single-enzyme incubations. Single-enzyme incubations allowed the evaluation of the involvement of an individual isoform, which is important to assess the risk of interindividual differences based on polymorphisms or interactions with co-consumed drugs (of abuse) or food ingredients due to inhibition or induction (Meyer, 2016). Ten different CYP isoenzymes and FMO3 were used representing monooxygenases known to be involved in the human hepatic metabolism of xenobiotics (Wagmann et al., 2016). Incubations with pHLM, containing all these isozymes in their natural composition, were used as positive controls. Results are given in **Table 4**. The initial monooxygenases activity screenings of 3,4-DMA-NBOMe, ephylone, 4F-PHP, and 1P-LSD were described elsewhere (Caspar et al., 2018a; Wagmann et al., 2019b,c). CYP3A4 was described to be involved in the *N*-dealkylation and CYP2C19 and CYP2D6 in the *O*-demethylation and hydroxylation of 3,4-DMA-NBOMe (Caspar et al., 2018a; Wagmann et al., 2019b,c). Ephylone and 4F-PHP were both metabolized by CYP1A2, CYP2B6, CYP2C19, and CYP3A4 (Caspar et al., 2018a; Wagmann et al., 2019b,c), while 1P-LSD was *N*-dealkylated and hydroxylated exclusively by CYP3A4 (Caspar et al., 2018a; Wagmann et al., 2019b,c).

CYP1A2, CYP2C8, CYP2C19, CYP3A4, and CYP3A5 were shown to be involved in the metabolic phase I reactions of 4F-MDMB-BINACA. CYP3A5 was involved in all observed metabolic steps with the exception of the amide hydrolysis (MB1) and the ester hydrolysis (MB8). Both hydrolysis steps were found to be not catalyzed by the investigated monooxygenases but, interestingly, only detected in pHLM incubations. The elimination of the fluoro butyl chain (MB4) was catalyzed by CYP1A2, CYP2C19, CYP3A4, and CYP3A5. The lactone formation (MB6) was catalyzed by CYP3A4 and CYP3A5, demonstrating that previous ester hydrolysis was not essential for formation of MB6. The oxidative defluorination (MB11) was detected in incubations with CYP2C8 and CYP3A5. Hydroxylated metabolites (MB16–MB19) were formed by CYP1A2, CYP2C19, CYP3A4, and CYP3A5. Due to the high number of CYP

TABLE 4 | Detection of the 4F-MDMB-BINACA phase I metabolites (metabolite IDs correspond to **Table 1**) in *in vitro* incubations containing 1 out of 11 monooxygenase isozymes, respectively, or pooled human liver microsomes (pHLM).

Enzyme preparation	Metabolite ID and metabolic reaction								
	MB1 (Amide hydrolysis)	MB4 (*N*-Dealkylation)	MB6 (Lactone formation)	MB8 (Ester hydrolysis)	MB11 (Oxidative defluorination)	MB16 (Hydroxylation of the *tert*-butyl part)	MB17 (Hydroxylation of the butyl chain)	MB18 (Hydroxylation of the indazole part isomer 1)	MB19 (Hydroxylation of the indazole part isomer 2)
CYP1A2	–	+	–	–	–	–	–	–	+
CYP2A6	–	–	–	–	–	–	–	–	–
CYP2B6	–	–	–	–	–	–	–	–	–
CYP2C8	–	–	–	–	+	–	–	–	–
CYP2C9	–	–	–	–	–	–	–	–	–
CYP2C19	–	+	–	–	–	–	+	+	+
CYP2D6	–	–	–	–	–	–	–	–	–
CYP2E1	–	–	–	–	–	–	–	–	–
CYP3A4	–	+	+	–	–	–	+	+	–
CYP3A5	–	+	+	–	+	+	+	+	+
FMO3	–	–	–	–	–	–	–	–	–
pHLM	+	+	+	+	+	+	+	+	+

Incubations were performed in duplicate. CYP, cytochrome P450; FMO, flavin-containing monooxygenase; +, detected; –, not detected.

TABLE 5 | Detection of the 4F-MDMB-BINACA metabolites after amide hydrolysis (MB1) or ester hydrolysis (MB8, metabolite IDs correspond to **Table 1**) in *in vitro* incubations containing one out of three human carboxylesterase isozymes (hCES), respectively, pooled human liver microsomes (pHLM), pooled human liver S9 fraction (pHLS9), or pooled human blood plasma (pHBP).

Enzyme preparation	Metabolite ID	
	MB1	MB8
hCES1b	–	+
hCES1c	+	+
hCES2	–	–
pHLM	+	+
pHLS9	+	+
pHBP	–	–

Incubations were performed in duplicate; +, detected; –, not detected.

isozymes found to be involved in the phase I metabolism, it is unlikely that polymorphisms or inhibition of a single isozyme will have a high impact on the biotransformation of 4F-MDMB-BINACA *in vivo*.

Esterase Activity Screening of 4F-MDMB-BINACA

In order to investigate the involvement of esterases in the metabolism of 4F-MDMB-BINACA, an esterase activity screening was performed using three recombinant human carboxylesterases, pHLM, pHLS9, and pooled human blood plasma. The results are listed in **Table 5**. Carboxylesterases are membrane-bound phase I drug-metabolizing enzymes that can hydrolyze a variety of xenobiotics (Wang et al., 2011). Ester hydrolysis of 4F-MDMB-BINACA (MB8) was shown to be catalyzed by hCES1b and hCES1c. This was consistent with a previous study by Meyer et al., describing that drugs of abuse with small alcohol parts were mainly hydrolyzed by hCES1 isoforms (Meyer et al., 2015). Amide hydrolysis (MB1) was shown to be catalyzed by hCES1c. MB1 and MB8 were also detected in incubations with pHLM and pHLS9, but not in incubations with pooled human blood plasma. The human liver preparations of pHLM and pHLS9 are known to contain carboxylesterases, mainly hCES1 isoforms, but also hCES2 in lower levels (Wang et al., 2011). Pooled human blood plasma contains no carboxylesterases, but the four non-specific esterases such as butyrylcholinesterase, paraoxonase, acetylcholinesterase, and albumin esterase (Li et al., 2005). MB1 was not identified in the prior pHLS9 incubations for identification of phase I and II metabolites of 4F-MDMB-BINACA. This was most probably caused by low formation levels of MB1 in these incubations due to the predominance of other metabolic pathways. Genetic polymorphisms of hCES1 have been shown to affect the metabolism of several drugs (Di, 2019). Therefore, interindividual differences in the hydrolysis of 4F-MDMB-BINACA cannot be excluded.

Comparison to Metabolites Identified in Human Biosamples

Zebrafish larvae were identified as a model system producing the highest number of metabolites of the five investigated NPS. However, a high number of metabolites does not necessarily mean that a model system is the most suitable one for developing analytical procedures for human biosamples. The metabolites identified during a metabolism study must be implemented in screening procedures for human biosamples aiming to detect the intake of NPS for example in a clinical or forensic toxicological context. The consideration of metabolites as targets is crucial particularly in urine screening (Wagmann and Maurer, 2018), but the detection of NPS can only be successful if the implemented metabolites were the same as the ones present in human biosamples. The implementation should not be motivated by the abundance of the metabolite. Each model system has limitations and a minor metabolite detected in a model system may be a major metabolite in humans. Metabolites tentatively identified in pHLS9, HepaRG cells, and zebrafish larvae incubations were compared to those detected in human biosamples to determine the measure of concordance.

Human blood and urine samples of a male individual after suspected intake of drugs of abuse were submitted to the authors' laboratory for regular toxicological analysis. The patient was initially found unconscious and taken to the hospital. A comprehensive toxicological screening in plasma and urine was performed including numerous therapeutic drugs, drugs of abuse, NPS, and their metabolites. The toxicological screening detected not only 4F-MDMB-BINACA but also amitriptyline and quetiapine at therapeutic levels in the patient's biosamples. No targeted analysis for detection of γ-hydroxybutyrate (GHB), which would also be able to cause deep sedation, was performed due to the patient's symptoms and the case history.

The reconstructed chromatograms of the *m/z* of 4F-MDMB-BINACA and its metabolites derived from the HR full scan of the plasma and urine sample analysis are given in **Figure 3**. The most abundant signals in descending order in the plasma sample were assigned to the parent compound 4F-MDMB-BINACA, MB8 (ester hydrolysis), MB6 (lactone formation), and MB16 (hydroxylation of the *tert*-butyl part). Time point and dosage of the 4F-MDMB-BINACA intake were unknown, but the presence of the parent compound and the patient's

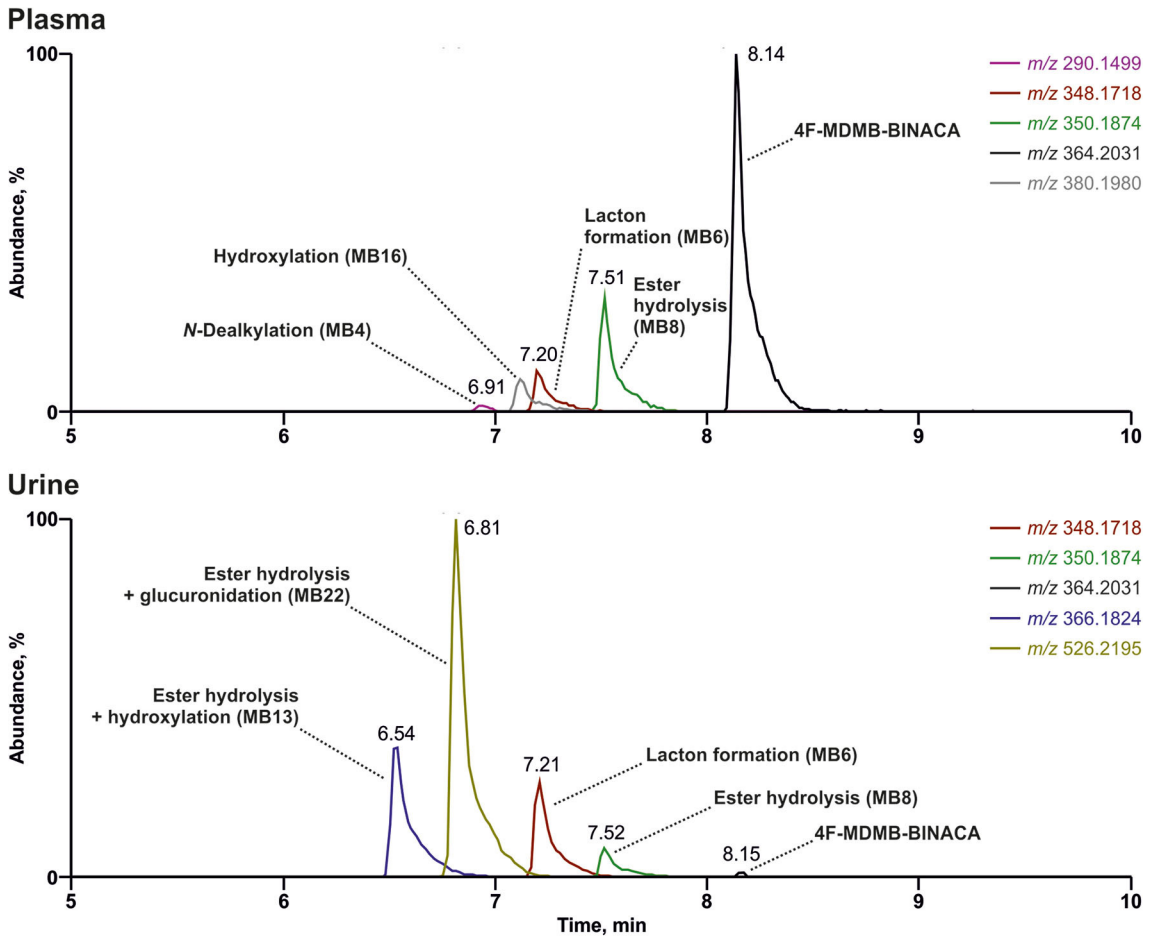

FIGURE 3 | Reconstructed chromatograms of the mass-to-charge ratios of 4F-MDMB-BINACA and its metabolites in high-resolution full scan derived from an authentic human plasma and urine sample after unknown dose and time point of 4F-MDMB-BINACA intake. Colored figure may be viewed online.

TABLE 6 | Relative number of matches (%) with the four most abundant signals detected in human plasma and urine samples after intake of 4F-MDMB-BINACA, ephylone, or 4F-PHP compared to incubations with pooled human liver S9 fraction (pHLS9), HepaRG cells, and zebrafish larvae.

	pHLS9 [25 μM]	HepaRG [25 μM]	HepaRG [250 μM]	Zebrafish larvae
4F-MDMB-BINACA				
Plasma	100	50	75	100
Urine	75	50	100	75
Ephylone (Wagmann et al., 2019b)				
Plasma	100	75	100	100
Urine	100	75	100	100
4F-PHP (Wagmann et al., 2019b)				
Plasma	75	50	50	100
Urine	75	25	50	75
Total	88	54	79	92

health status suggested a recent intake. The most abundant signals in the urine sample were assigned to MB22 (ester hydrolysis + glucuronidation), MB13 (ester hydrolysis + hydroxylation of the *tert*-butyl part), MB6 (lactone formation), and MB8 (ester hydrolysis). However, the parent compound was barely detectable in urine. Therefore, MB6, MB8, and MB22 are particularly recommended as targets for comprehensive screening procedures, if the sample preparation of urine does not contain conjugate cleavage. Otherwise, MB22 does not have to be included. The approaches used by Haschimi et al. and Krotulski et al. included conjugate cleavage in urine and both only described phase I metabolites of 4F-MDMB-BINACA (Haschimi et al., 2019; Krotulski et al., 2019). Haschimi et al. identified 13 metabolites in 17 human urine samples and recommended MB6 and MB8 as reliable urinary markers (Haschimi et al., 2019). Krotulski et al. identified nine 4F-MDMB-BINACA metabolites in four blood and four urine samples and only recommended to include MB8 as well as MB11 in toxicological screening procedures (Krotulski et al., 2019).

Table 6 summarizes the concordance of the four most abundant signals in the current patient's plasma or urine with the 4F-MDMB-BINACA metabolites identified in pHLS9, HepaRG cells, and zebrafish larvae experiments. Concerning plasma, all four compounds reflecting the four most abundant signals were detectable in pHLS9 incubations and zebrafish larvae (100%), while only two (50%) or three compounds (75%) were detectable in HepaRG cell experiments depending on the used NPS concentration. HepaRG cells with 250 μM 4F-MDMB-BINACA formed all four most abundant metabolites in urine (100%), while pHLS9 and zebrafish larvae formed three metabolites (75%) and HepaRG with 25 μM 4F-MDMB-BINACA formed only two of them (50%). These findings were in accordance with the previous study focusing on another synthetic cannabinoid. Richter et al. reported HepaRG cells to form the highest number of the most abundant human urinary metabolites of 7′N-5F-ADB, followed by zebrafish larvae and pHLS9 incubations (Richter et al., 2019a).

Data concerning detectability of ephylone and 4F-PHP in human biosamples were also available and taken from a recent publication (Wagmann et al., 2019b). Ephylone, ME1 (*N*-deethylation), ME2 (demethylenation), ME3/4 (demethylenation + methylation), as well as the corresponding glucuronic acid conjugates of ME2 (ME11/12) and ME3/4 (ME13/14) represented the highest ephylone-related signals in human plasma and/or urine. In case of 4F-PHP, the parent compound, MP2 (reduction), MP3 and MP4 (hydroxylation + oxidation to ketone or lactam), and MP10 (reduction + glucuronidation) led to the signals with the highest abundance (Wagmann et al., 2019b). As given in **Table 6**, pHLS9, HepaRG cells with 250 μM NPS, and zebrafish larvae experiments provided perfect agreement with the four most abundant ephylone-related signals in plasma and urine (100%). Zebrafish larvae experiments were also perfectly suited for detection of the four most abundant 4F-PHP-related signals in human plasma (100%). The accordance with human urine was the same for pHLS9 and zebrafish larvae experiments, but both models only led to the detection of three out of the four most abundant signals (75%). Overall, zebrafish larvae experiments provided the most comprehensive concordance of detected NPS-related compounds with those present in the human biosamples plasma and urine (92%). Incubations with pHLS9 came as second best (88%) followed by HepaRG cell incubations with 250 μM NPS (79%). These findings underline the suitability of zebrafish larvae for toxicokinetic studies of NPS. As zebrafish larvae represent intact organisms, their possible application is beyond metabolism studies, e.g., investigations on distribution or excretion patterns of NPS. However, the most easily manageable model investigated in this study, the pHLS9 incubations, also provided a good overlap with metabolites detected in human biosamples and can also be considered as an appropriate *in vitro* metabolism model for developing toxicological screening procedures.

Unfortunately, only very limited data concerning detectability of 3,4-DMA-NBOMe and 1P-LSD in human biosamples were available. Nevertheless, Caspar et al. recommended 3,4-DMA-NBOMe after *O*-demethylation (MN5 or MN6) or *O,O*-didemethylation (MN2) of the amphetamine part as well as their glucuronides (MN20 or MN21 and MN17) as urine screening targets for 3,4-DMA-NBOMe after oral application to rats. HepaRG cells and zebrafish larvae produce MN5, MN6, MN20, and MN21, while Caspar et al. only detected one isomer (MN5 or MN6 and MN20 or MN21), but also MN2 and MN17 in pHLS9 incubations (Caspar et al., 2018b).

It is likely that 1P-LSD is hydrolyzed to LSD *in vivo* (Brandt et al., 2016; Grumann et al., 2019; Halberstadt et al., 2019; Wagmann et al., 2019c). Grumann et al. reported that 1P-LSD could not be detected in serum and urine samples of an intoxicated patient after assumed consumption of a blotter containing 1P-LSD. However, they were able to find LSD in both matrices, but no information on the presence of 1P-LSD-specific metabolites in the biosamples was given (Grumann et al., 2019). Halberstadt et al. were able to detect 1P-LSD, LSD, and several metabolites in rat plasma after subcutaneous administration to rats. Some metabolites were found to be

1P-LSD specific as they still contained the 1-propionyl moiety (Halberstadt et al., 2019).

Finally, some limitations of the present study must be considered. First, only biosamples of one individual after intake of 4F-MDMB-BINACA or ephylone and 4F-PHP were used for comparison and interindividual metabolism differences cannot be excluded. The same is true for species differences between humans and zebrafish concerning the metabolism of 3,4-DMA-NBOMe and 1P-LSD, as human biosamples were not available. In addition, different NPS concentrations were used for the different metabolism models based on experience and MTC study results.

CONCLUSIONS

The three metabolism models, by name pHLS9 incubations, HepaRG cells, and zebrafish larvae, formed numerous metabolites of the five NPS. Zebrafish larvae were found to produce the highest number of metabolites. The 4F-MDMB-BINACA, ephylone, and 4F-PHP metabolites formed by zebrafish larvae also provided the highest concordance with the four most abundant signals in human biosamples. Nevertheless, all metabolism models produced metabolites similar to those detected in authentic biosamples. Furthermore, several CYP isozymes as well as hCES1b and hCES1c were shown to be involved in the phase I metabolic reactions of 4F-MDMB-BINACA. Interindividual differences, presumably mainly based on hCES1 polymorphisms, cannot be excluded. The current study underlines the potential of zebrafish larvae as a tool for elucidating the toxicokinetics of NPS in the future.

DATA AVAILABILITY STATEMENT

Datasets generated for this study are included in the article/**Supplementary Material** or available upon reasonable request.

ETHICS STATEMENT

Ethical review and approval was not required for the study on human participants in accordance with the local legislation and institutional requirements. Written informed consent for participation was not required for this study in accordance with the national legislation and the institutional requirements.

AUTHOR CONTRIBUTIONS

LW and MM established the study design and planned the experiments. FF and LW were responsible for the experimental execution. JH, YP, and RM were responsible for Zebrafish larvae experiments. VF and LW were responsible for HepaRG cell experiments. SF and FW provided reference standard of 4F-MDMB-BINACA. LW and FF wrote the first draft of the manuscript. All authors contributed to manuscript revision, read, and approved the submitted version.

ACKNOWLEDGMENTS

We would like to thank the EU-funded project ADEBAR (IZ25-5793-2016-27), Niels Eckstein (University of Applied Sciences Kaiserslautern, Germany), Simon D. Brandt (Liverpool John Moores University, UK), and Alexander Stratford (Synex Synthetics BV, the Netherlands) for the supply of chemical standards, as well as Heidi Löhr, Armin A. Weber, Selina Hemmer, and Tanja M. Gampfer for their support. We acknowledge support by the Deutsche Forschungsgemeinschaft (DFG, German Research Foundation) and Saarland University within the funding programme Open Access Publishing.

SUPPLEMENTARY MATERIAL

The Supplementary Material for this article can be found online at: https://www.frontiersin.org/articles/10.3389/fchem.2020.00539/full#supplementary-material

REFERENCES

Brandt, S. D., Kavanagh, P. V., Westphal, F., Stratford, A., Elliott, S. P., Hoang, K., et al. (2016). Return of the lysergamides. Part I: analytical and behavioural characterization of 1-propionyl-d-lysergic acid diethylamide (1P-LSD). *Drug Test. Anal.* 8, 891–902. doi: 10.1002/dta.1884

Brandt, S. D., King, L. A., and Evans-Brown, M. (2014). The new drug phenomenon. *Drug Test. Anal.* 6, 587–597. doi: 10.1002/dta.1686

Caspar, A. T., Meyer, M. R., and Maurer, H. H. (2018a). Human cytochrome P450 kinetic studies on six N-2-methoxybenzyl (NBOMe)-derived new psychoactive substances using the substrate depletion approach. *Toxicol. Lett.* 285, 1–8. doi: 10.1016/j.toxlet.2017.12.017

Caspar, A. T., Meyer, M. R., Westphal, F., Weber, A. A., and Maurer, H. H. (2018b). Nano liquid chromatography-high-resolution mass spectrometry for the identification of metabolites of the two new psychoactive substances N-(ortho-methoxybenzyl)-3,4-dimethoxyamphetamine and N-(ortho-methoxybenzyl)-4-methylmethamphetamine. *Talanta* 188, 111–123. doi: 10.1016/j.talanta.2018.05.064

Chauret, N., Gauthier, A., and Nicoll-Griffith, D. A. (1998). Effect of common organic solvents on in vitro cytochrome P450-mediated metabolic activities in human liver microsomes. *Drug Metab. Dispos.* 26, 1–4.

De Souza Anselmo, C., Sardela, V. F., Matias, B. F., De Carvalho, A. R., De Sousa, V. P., Pereira, H. M. G., et al. (2017). Is zebrafish (Danio rerio) a tool for human-like metabolism study? *Drug Test. Anal.* 9, 1685–1694. doi: 10.1002/dta.2318

Di, L. (2019). The impact of carboxylesterases in drug metabolism and pharmacokinetics. *Curr. Drug Metab.* 20, 91–102. doi: 10.2174/1389200219666180821094502

Diao, X., and Huestis, M. A. (2019). New synthetic cannabinoids metabolism and strategies to best identify optimal marker metabolites. *Front. Chem.* 7:109. doi: 10.3389/fchem.2019.00109

EMCDDA (2019). European Drug Report 2019. *Publications of the European Union*. Available online at: http://www.emcdda.europa.eu/edr2019_en

EU (2010). "Directive 2010/63/EU of the European Parliament and of the Council of 22 September 2010 on the protection of animals used for scientific purposes Text with EEA relevance", in *Official Journal of the European Union*. European Union. L276/33–79.

Godoy, P., Hewitt, N. J., Albrecht, U., Andersen, M. E., Ansari, N., Bhattacharya, S., et al. (2013). Recent advances in 2D and 3D *in vitro* systems using primary hepatocytes, alternative hepatocyte sources and non-parenchymal liver cells and their use in investigating mechanisms of hepatotoxicity, cell signaling and ADME. *Arch. Toxicol.* 87, 1315–1530. doi: 10.1007/s00204-013-1078-5

Grumann, C., Henkel, K., Stratford, A., Hermanns-Clausen, M., Passie, T., Brandt, S. D., et al. (2019). Validation of an LC-MS/MS method for the quantitative analysis of 1P-LSD and its tentative metabolite LSD in fortified urine and serum

samples including stability tests for 1P-LSD under different storage conditions. *J. Pharm. Biomed. Anal.* 174, 270–276. doi: 10.1016/j.jpba.2019.05.062

Guillouzo, A., Corlu, A., Aninat, C., Glaise, D., Morel, F., and Guguen-Guillouzo, C. (2007). The human hepatoma HepaRG cells: a highly differentiated model for studies of liver metabolism and toxicity of xenobiotics. *Chem. Biol. Interact.* 168, 66–73. doi: 10.1016/j.cbi.2006.12.003

Halberstadt, A. L., Chatha, M., Klein, A. K., Mccorvy, J. D., Meyer, M. R., Wagmann, L., et al. (2019). Pharmacological and biotransformation studies of 1-acyl-substituted derivatives of d-lysergic acid diethylamide (LSD). *Neuropharmacology* 172:107856. doi: 10.1016/j.neuropharm.2019.107856

Haschimi, B., Mogler, L., Halter, S., Giorgetti, A., Schwarze, B., Westphal, F., et al. (2019). Detection of the recently emerged synthetic cannabinoid 4F-MDMB-BINACA in "legal high" products and human urine specimens. *Drug Test. Anal.* 11, 1377–1386. doi: 10.1002/dta.2666

Kavanagh, P., Grigoryev, A., and Krupina, N. (2017). Detection of metabolites of two synthetic cannabimimetics, MDMB-FUBINACA and ADB-FUBINACA, in authentic human urine specimens by accurate mass LC–MS: a comparison of intersecting metabolic patterns. *Forensic Toxicol.* 35, 284–300. doi: 10.1007/s11419-017-0356-y

Kronstrand, R., Guerrieri, D., Vikingsson, S., Wohlfarth, A., and Green, H. (2018). Fatal poisonings associated with new psychoactive substances. *Handb. Exp. Pharmacol.* 252, 495–541. doi: 10.1007/164_2018_110

Krotulski, A. J., Mohr, A. L. A., Kacinko, S. L., Fogarty, M. F., Shuda, S. A., Diamond, F. X., et al. (2019). 4F-MDMB-BINACA: a new synthetic cannabinoid widely implicated in forensic casework. *J. Forensic. Sci.* 64, 1451–1461. doi: 10.1111/1556-4029.14101

Li, B., Sedlacek, M., Manoharan, I., Boopathy, R., Duysen, E. G., Masson, P., et al. (2005). Butyrylcholinesterase, paraoxonase, and albumin esterase, but not carboxylesterase, are present in human plasma. *Biochem. Pharmacol.* 70, 1673–1684. doi: 10.1016/j.bcp.2005.09.002

Lubberstedt, M., Muller-Vieira, U., Mayer, M., Biemel, K. M., Knospel, F., Knobeloch, D., et al. (2011). HepaRG human hepatic cell line utility as a surrogate for primary human hepatocytes in drug metabolism assessment *in vitro*. *J. Pharmacol. Toxicol. Methods* 63, 59–68. doi: 10.1016/j.vascn.2010.04.013

Matos, R. R., Martucci, M. E. P., De Anselmo, C. S., Alquino Neto, F. R., Pereira, H. M. G., and Sardela, V. F. (2019). Pharmacokinetic study of xylazine in a zebrafish water tank, a human-like surrogate, by liquid chromatography Q-Orbitrap mass spectrometry. *Forensic Toxicol.* 38, 108–121. doi: 10.1007/s11419-019-00493-y

Maurer, H. H., and Meyer, M. R. (2016). High-resolution mass spectrometry in toxicology: current status and future perspectives. *Arch. Toxicol.* 90, 2161–2172. doi: 10.1007/s00204-016-1764-1

Maurer, H. H., Pfleger, K., and Weber, A. A. (2016). *Mass Spectral Data of Drugs, Poisons, Pesticides, Pollutants and their Metabolites*. Weinheim: Wiley-VCH.

Meyer, M. R. (2016). New psychoactive substances: an overview on recent publications on their toxicodynamics and toxicokinetics. *Arch. Toxicol.* 90, 2421–2444. doi: 10.1007/s00204-016-1812-x

Meyer, M. R. (2018). Toxicokinetics of NPS: update 2017. *Handb. Exp. Pharmacol.* 252, 441–459. doi: 10.1007/164_2018_102

Meyer, M. R., and Maurer, H. H. (2016). Review: LC coupled to low- and high-resolution mass spectrometry for new psychoactive substance screening in biological matrices - where do we stand today? *Anal. Chim. Acta* 927, 13–20. doi: 10.1016/j.aca.2016.04.046

Meyer, M. R., Schutz, A., and Maurer, H. H. (2015). Contribution of human esterases to the metabolism of selected drugs of abuse. *Toxicol. Lett.* 232, 159–166. doi: 10.1016/j.toxlet.2014.10.026

Niessen, W. M., and Correa, R. A. (2016). *Interpretation of MS-MS Mass Spectra of Drugs and Pesticides*. Hoboken, NJ: John Wiley and Sons. doi: 10.1002/9781119294269

Peters, F. T. (2014). Recent developments in urinalysis of metabolites of new psychoactive substances using LC-MS. *Bioanalysis* 6, 2083–2107. doi: 10.4155/bio.14.168

Richter, L. H. J., Flockerzi, V., Maurer, H. H., and Meyer, M. R. (2017a). Pooled human liver preparations, HepaRG, or HepG2 cell lines for metabolism studies of new psychoactive substances? A study using MDMA, MDBD, butylone, MDPPP, MDPV, MDPB, 5-MAPB, and 5-API as examples. *J. Pharm. Biomed. Anal.* 143, 32–42. doi: 10.1016/j.jpba.2017.05.028

Richter, L. H. J., Herrmann, J., Andreas, A., Park, Y. M., Wagmann, L., Flockerzi, V., et al. (2019a). Tools for studying the metabolism of new psychoactive substances for toxicological screening purposes - A comparative study using pooled human liver S9, HepaRG cells, and zebrafish larvae. *Toxicol. Lett.* 305, 73–80. doi: 10.1016/j.toxlet.2019.01.010

Richter, L. H. J., Maurer, H. H., and Meyer, M. R. (2017b). New psychoactive substances: studies on the metabolism of XLR-11, AB-PINACA, FUB-PB-22, 4-methoxy-alpha-PVP, 25-I-NBOMe, and meclonazepam using human liver preparations in comparison to primary human hepatocytes, and human urine. *Toxicol. Lett.* 280, 142–150. doi: 10.1016/j.toxlet.2017.07.901

Richter, L. H. J., Maurer, H. H., and Meyer, M. R. (2019b). Metabolic fate of the new synthetic cannabinoid 7'N-5F-ADB in rat, human, and pooled human S9 studied by means of hyphenated high-resolution mass spectrometry. *Drug Test. Anal.* 11, 305–317. doi: 10.1002/dta.2493

Richter, L. H. J., Menges, J., Wagmann, L., Brandt, S. D., Stratford, A., Westphal, F., et al. (2019c). *In vitro* toxicokinetics and analytical toxicology of three novel NBOMe derivatives: phase I and II metabolism, plasma protein binding, and detectability in standard urine screening approaches studied by means of hyphenated mass spectrometry. *Forensic Toxicol.* 38, 141–159. doi: 10.1007/s11419-019-00498-7

UNODC (2019). *World Drug Report 2019*. Available online at: https://wdr.unodc.org/wdr2019/ (accessed October 07, 2018).

Van Wijk, R. C., Krekels, E. H. J., Hankemeier, T., Spaink, H. P., and Van Der Graaf, P. H. (2016). Systems pharmacology of hepatic metabolism in zebrafish larvae. *Drug Discov. Today Dis. Models* 22, 27–34. doi: 10.1016/j.ddmod.2017.04.003

Wagmann, L., Hempel, N., Richter, L. H. J., Brandt, S. D., Stratford, A., and Meyer, M. R. (2019a). Phenethylamine-derived new psychoactive substances 2C-E-FLY, 2C-EF-FLY, and 2C-T-7-FLY: investigations on their metabolic fate including isoenzyme activities and their toxicological detectability in urine screenings. *Drug Test. Anal.* 11, 1507–1521. doi: 10.1002/dta.2675

Wagmann, L., Manier, S. K., Eckstein, N., Maurer, H. H., and Meyer, M. R. (2019b). Toxicokinetic studies of the four new psychoactive substances 4-chloroethcathinone, N-ethylnorpentylone, N-ethylhexedrone, and 4-fluoro-alpha-pyrrolidinohexiophenone. *Forensic Toxicol.* 38, 59–69. doi: 10.1007/s11419-019-00487-w

Wagmann, L., and Maurer, H. H. (2018). Bioanalytical methods for new psychoactive substances. *Handb. Exp. Pharmacol.* 252, 413–439. doi: 10.1007/164_2017_83

Wagmann, L., Meyer, M. R., and Maurer, H. H. (2016). What is the contribution of human FMO3 in the N-oxygenation of selected therapeutic drugs and drugs of abuse? *Toxicol. Lett.* 258, 55–70. doi: 10.1016/j.toxlet.2016.06.013

Wagmann, L., Richter, L. H. J., Kehl, T., Wack, F., Bergstrand, M. P., Brandt, S. D., et al. (2019c). *In vitro* metabolic fate of nine LSD-based new psychoactive substances and their analytical detectability in different urinary screening procedures. *Anal. Bioanal. Chem.* 411, 4751–4763. doi: 10.1007/s00216-018-1558-9

Wang, J., Williams, E. T., Bourgea, J., Wong, Y. N., and Patten, C. J. (2011). Characterization of recombinant human carboxylesterases: fluorescein diacetate as a probe substrate for human carboxylesterase 2. *Drug Metab. Dispos.* 39, 1329–1333. doi: 10.1124/dmd.111.039628

Westerfield, M. (2007). *The Zebrafish Book a Guide for the Laboratory Use of Zebrafish Danio* (Brachydanio) Rerio*. Eugene, OR: University of Oregon Press.

Wissenbach, D. K., Meyer, M. R., Remane, D., Philipp, A. A., Weber, A. A., and Maurer, H. H. (2011). Drugs of abuse screening in urine as part of a metabolite-based LC-MSn screening concept. *Anal. Bioanal. Chem.* 400, 3481–3489. doi: 10.1007/s00216-011-5032-1

Conflict of Interest: The authors declare that the research was conducted in the absence of any commercial or financial relationships that could be construed as a potential conflict of interest.

frontiers in Chemistry

ORIGINAL RESEARCH
published: 24 July 2020
doi: 10.3389/fchem.2020.00624

Gas Chromatography—Fourier Transform Infrared Spectroscopy for Unambiguous Determination of Illicit Drugs: A Proof of Concept

Tania M. G. Salerno[1], *Paola Donato*[2], *Giampietro Frison*[3], *Luca Zamengo*[3] *and Luigi Mondello*[1,4,5,6]*

[1] BeSep S.r.l., c/o Department of Chemical, Biological, Pharmaceutical and Environmental Sciences, University of Messina, Messina, Italy, [2] Department of Biomedical, Dental, Morphological and Functional Imaging Sciences, University of Messina, Messina, Italy, [3] Laboratory of Environmental Hygiene and Forensic Toxicology, DMPO Department, AULSS 3, Venice, Italy, [4] Department of Chemical, Biological, Pharmaceutical and Environmental Sciences, University of Messina, Messina, Italy, [5] Chromaleont S.r.l., c/o Department of Chemical, Biological, Pharmaceutical and Environmental Sciences, University of Messina, Messina, Italy, [6] Research Unit of Food Science and Nutrition, Department of Science and Technology for Humans and the Environment, Campus Bio-Medico University of Rome, Rome, Italy

OPEN ACCESS

Edited by:
Alberto Salomone, University of Turin, Italy

Reviewed by:
Alex Krotulski, The Center for Forensic Science Research and Education (CFSRE), United States
Mohammad Sharif Khan, Dartmouth College, United States

***Correspondence:**
Luigi Mondello
lmondello@unime.it

Specialty section:
This article was submitted to Analytical Chemistry, a section of the journal Frontiers in Chemistry

Received: *19 May 2020*
Accepted: *15 June 2020*
Published: *24 July 2020*

Citation:
Salerno TMG, Donato P, Frison G, Zamengo L and Mondello L (2020) Gas Chromatography—Fourier Transform Infrared Spectroscopy for Unambiguous Determination of Illicit Drugs: A Proof of Concept. Front. Chem. 8:624. doi: 10.3389/fchem.2020.00624

The increasing number of synthetic molecules constantly introduced into the illicit drug market poses a great demand in terms of separation and identification power of the analytical tools. Therefore, forensic laboratories are challenged to develop multiple analytical techniques, allowing for the reliable analysis of illicit drugs. This goal is accomplished by means of spectroscopy measurements, usually after a separation step, consisting of liquid (LC) or gas (GC) chromatography. Within the wide range of hyphenated techniques, the coupling of GC to Fourier Transform Infrared Spectroscopy (FTIR) provides a powerful identification tool, also allowing discriminating between isobars and isomers. In this research, the effectiveness of GC-FTIR is demonstrated, in achieving structure elucidation of 1-pentyl-3-(1-naphthoyl)indole, commonly known as JWH-018, a synthetic cannabinoid identified as component of illegal "incense blends." Moreover, solid deposition FTIR enabled for boosting the sensitivity of the technique, over conventional flow (light pipe) cells, scaling down the limit of identification to the ng scale. Calibration curves for JWH-018 standard were obtained in the 20–1,000 ng range, and the limit of detection and limit of quantification were assessed as equal to 4.3 and 14.3 ng, respectively. Finally, the proposed methodology has been adopted for the identification of active principles in a real "street" sample seized by the law enforcement, consisting of an herbal matrix containing four different synthetic cannabinoids belonging to the JWH class. The correct identification of such compounds, with a high degree of chemical similarity, demonstrated the usefulness of the proposed approach for reliable analysis of complex mixtures of illicit drugs, as viable alternative to widespread mass spectrometry-based approaches.

Keywords: gas chromatography, Fourier Transform Infrared Spectroscopy, solid deposition interface, illicit drugs, synthetic cannabinoids, forensic analysis

INTRODUCTION

Since their appearance in the illicit drug market, the number of new psychoactive substances (NPS) is growing at an alarming fast rate; as a consequence, the task of analysis and identification of NPS is posing a big challenge for forensic scientists on one side, and regulatory bodies, for the design and delivery of effective evidence-based responses to drug problems (Zuba, 2014; Lee et al., 2019).

In its latest report, the European Monitoring Center for Drugs and Drug Addiction (EMCDDA) revealed a market that is both resilient and reflective of developments taking place at the global level; the value of the NPS market is unknown actually, however 55 new substances were reported to the European Union Early Warning System (EWS) in 2018, bringing the total number of NPS monitored to 731 (EMCDDA, 2019). Undoubtedly, the shaping and implementation of policy responses and law enforcement activity have contributed to slow-down in appearance of NPS, with respect to the previous decade. However, NPS continue to pose serious cross-border threats to health, with potent synthetic opioids (mainly fentanyls), synthetic cannabinoids and designer benzodiazepines appearing on the market, associated with reports of health emergencies and deaths. Moreover, drug overdoses are commonly associated with the intake (deliberate or not) of multiple substances and thus, health threats and diagnosis may be overlooked without the disposal of adequate forensic and toxicological data. As a consequence, introducing comprehensive screening and increasing the reliability of testing is a central focus for many countries, who have made significant investments in this area. Unfortunately, drug designers are working incessantly to synthesize non-controlled analogs of the drugs of abuse, aiming to get around the existing anti-drug laws, by introducing slight modifications to the chemical structures (UNODC, 2018; Kraenenburg et al., 2019). The constant introduction of new drugs in turn creates a need for reference material to confirm structural elucidation of uncommon or newly encountered substances (Brandt et al., 2014).

In this context, researchers have put considerable efforts in developing advanced chromatographic instrumentation and techniques, aiming to achieve reliable identification of organic compounds in complex mixtures. Approaches based on high-resolution gas chromatography coupled to mass spectrometry (HRGC-MS) are the workhorse analytical tool employed in forensics laboratories, affording the selectivity and sensitivity required for most analytes commonly encountered in seized drugs; however, these hyphenated techniques presents inherent weak points which relate to both the GC and MS counterparts (International, 2015, 2017; Scientific Working Group for the Analysis of Seized Drugs (SWGDRUG), 2019). The data afforded by GC-MS are in fact affected by measurement uncertainties, of different magnitude and sources, of which analysts must be aware: first the uncertainty of measurement for GC retention time, expressed as absolute or relative time units (compared to a known reference standard). Second, the uncertainty of measurement of relative abundances of MS ions obtained by electron impact (EI) ionization; in both cases, specific acceptance criteria recommended by different governing bodies are not uniform (Davidson et al., 2018; Kelly and Bell, 2018).

Whereas, generally accepted as the gold standard of forensic drug analysis, yet GC-MS in some cases suffers from clear limitations, for the identification of co-eluting regioisomeric forms of synthetic drugs of identical elemental composition and yielding identical fragmentation patterns. In some circumstances, positional isomers, and diastereomers may be separated chromatographically, but identification cannot be attained, univocally, on the sole basis of the retention behavior. Whenever structural assignment is mandatory, a further analytical step may be required, consisting of compound isolation or targeted organic synthesis (followed by purification/concentration, eventually) prior to further characterization (Abiedalla et al., 2019; Kraenenburg et al., 2019).

To this concern, the combination of high-resolution gas chromatography (HRGC) to Fourier Transform Infrared Spectroscopy (FTIR) provides a unique tool, through the combination of high efficient separation, and highly specific identification. GC-FTIR allows to quick identifying functional groups in unknown substances, based on the retention behavior of the analytes and the IR absorption bands. Relying on distinct chemical properties, IR may well complement the information afforded by mass spectrometry (MS), in achieving structural identification of volatile and semi-volatile molecules. Moreover, by measuring small energy differences based on rotational and vibrational amplitudes between individual molecular bonds, FTIR spectroscopy enables to overcome one limitation of MS detection, in discriminating regioisomeric compounds (Kempfert, 1988; Almalki et al., 2019).

First attempts to interface a gas chromatograph to IR spectroscopy date back to four decades ago (Griffiths et al., 2008); however the real milestone came in the late 1960s, with the replacement of conventional gratings or dispersive elements with interferometers and FT mathematics (Low and Freeman, 1967). Though exploiting the clear advantage of speed of analysis, yet those hyphenated instruments used high-capacity GC columns and were operated in the stopped-flow mode (Low, 1971; Shaps and Varano, 1977). A flow-through gas cell, known as the light pipe (LP), was used as an interface to deliver vapor-phase IR spectra of eluting solutes (Visser, 2002), with the addition of a flow of make-up gas to compensate for the greater internal diameter of the LP device over that of the GC column (typically, 1.5 vs. 0.32 mm i.d.). In such a way, the chromatographic resolution was kept, even at the cost of longer residence time of the analytes in the interface and, thus, a decrease in the sensitivity. The latter was further impaired by the higher temperature required in the interface for the less volatile GC components, creating background noise in the spectrum (Brown et al., 1985). Indeed, the coupling of GC and FTIR has always posed the need to compromise between sensitivity, and speed. The narrow bandwidths of GC peaks often did not allow for adequate detector sampling, to record a useful spectrum; on the other hand, the amount of analyte required in most cases overwhelmed the GC column capacity. Later on, sample trapping techniques have been developed, aiming to achieve lower detection limits than those

afforded by LPs: the matrix isolation (MI) interface (Reedy et al., 1985), and the direct deposition interface (DD) (Fuoco et al., 1986). Both consisted of cryogenic devices allowing for mobile-phase elimination by trapping the GC-separated compounds eluting from the sub-ambient temperature to 11 K (MI) or 77 K (DD). All cold trapping interfaces rely on the use of high vacuum (needed to prevent interferences from environmental water and carbon dioxide), and leak-tight interface housing. In MI, also a cage of 1–2% of argon is added to the carrier gas for freezing the analytes. A critical comparison between light-pipe and sample trapping interfacing methods has been made by Schneider and Demirgian (1986), also discussing *pros* and *cons* in terms of applicability to sample analysis. The light-pipe interface provided a relatively quick and inexpensive way to obtain library-searchable vapor-phase spectra, in real time and in a non-destructive way, from GC eluted components. Whereas, MI interfaces implied a two-step process, since collection of IR spectra from the trapped analytes occurred after the collection was completed. In DD interface, the immobilized spots pass through an external IR beam a few seconds after the deposition, and multiple scans can be taken, as long as the cryogenic conditions are maintained. Both deposition techniques afford at least two orders of magnitude more sensitivity than the LP devices, with the resolution increased from 8 to 4 cm^{-1}. As a result of the sharper absorption bands compared with those obtained from free rotating molecules in the gas-phase, also the specificity was increased, in terms of differentiation between closely related molecules. Such features pave the way for the use of solid deposition GC-FTIR as a viable alternative to GC-MS approaches in forensic laboratories, for the reliable identification of NPS such as synthetic cathinones, cannabinoids, phencyclidine analogs, etc.

Originally developed for achieving the desired selectivity toward the cannabinoid receptors CB1 and CB2, synthetic cannabinoids or cannabimimetics were used in the clinical practice to deliver high therapeutic activity (anti-inflammatory and analgesic properties) from unwanted side effects (psychotropic activity). Unfortunately, the information generated by the scientific community has been promptly misused by clandestine laboratories, and these compounds have quickly found their way into the recreational drug market. The detailed pharmacological activities of these analogs are not known, which makes easy access and use of these drugs very dangerous to human health; moreover, synthetic cannabinoids are typically full agonists on the CB1 receptor, thus leading to maximum activation, even at significantly lower doses. Besides their higher potency with respect to the conventional drugs, long half-lives, and formation of active metabolites represent additional hazards deriving from illegal use of cannabimimetics (Bretteville-Jensen et al., 2013; ElSohly et al., 2014). The latter encompasses a wide range of chemical structures, and new analogs are constantly introduced on the market after the preceding drug comes under regulation; this poses additional challenges to drug law enforcement and forensic scientists. Analytical techniques developed so far for the detection and/or quantification of synthetic cannabinoids include colorimetric, immunochemical, and chromatographic methods (Namera et al., 2015).

In this research, the feasibility of using GC-FTIR with solid deposition of the analyte is shown, to achieve unambiguous structure elucidation of 1-pentyl-3-(1-naphthoyl)indole, commonly known as JWH-018, a synthetic cannabinoid identified as component of illegal "incense blends." Furthermore, the results obtained from the analysis of a seized sample containing several synthetic cannabinoids were compared to those afforded by GC-EI-MS, in terms of identification of unknown components. Detection and identification of unknown NPS in real samples is a major concern when legal or regulatory issues are involved; quantification of targeted analytes may be required, eventually. In a similar way as for MS-based identification, IR spectral data are searched into commercial or custom-made libraries, containing hundreds to thousands IR spectra of standard compounds. When reference materials are measured one at the time, in pure form or constant matrix, then LOD would be sufficient to describe the performance of the measuring system. In this study, another validation parameter was investigated, i.e., the limit of identification (LOI), defined as the lowest analyte concentration that yields a library searchable IR spectrum. In this concern, LOI is related to LOD in that a detectable signal is entailed, but this must also allow for a correct identification to be made, from a defined database. Most often overlooked in similar studies, LOI is a key parameter in determining the possibility for reliable identification of an unknown compound, contained at a certain amount in a given sample, and often in the presence of a noisy background. In a very straightforward way, LOI is sometimes estimated by simply doubling the LOD value (Lanzarotta et al., 2017).

MATERIALS AND METHODS

Standards and Chemicals

Ethyl acetate and methanol pure grade GC-MS solvents were obtained from Merck Life Science (Merck KGaA, Darmstadt, Germany). The following certified reference material (purity ≥98%): 1-naphthalenyl(1-pentyl-1H-indol-3-yl) -methanone (JWH-018), 1-naphthalenyl(1-hexyl-1H-indol-3-yl)-methanone(JWH-019), 1-naphthalenyl(1-butyl-1H-indol-3-yl) -methanone(JWH-073), were purchased from Cayman Chemical (Ann Arbor, MI, USA) as 1 mg/mL solutions.

Standard and Sample Preparation

Working solutions of JWH-018 in ethyl acetate were prepared in the concentration range 10–1,000 μg/mL (six concentration levels: 10, 20, 50, 100, 500, 1,000) and analyzed in triplicate. For construction of the calibration curve and for determining the experimental limit of identification (LOI) and the limit of quantification (LOQ), linearity was found in the 20–1,000 μg/mL range. A vegetable matrix sold illegally (and seized in northern Italy) suspected to contain synthetic cannabinoids was extracted at ambient temperature through sonication with methanol (47 mg sample in 1 mL of solvent) and filtered prior to injection into the GC-FTIR system.

Gas Chromatography

GC analyses were performed on a Nexis GC-2030 gas chromatograph equipped with AOC-20i auto sampler (Shimazdu, Kyoto, Japan). All GC separations were carried out on a Supelco SLB-5ms column (30 m L × 0.25 mm i.d., 0.25 μm d_f) (Merck KGaA, Darmstadt, Germany), under the same conditions. Injections were performed in splitless mode (1.50 min sampling time), with an injection volume of 1 μL and an injector temperature of 280°C. Helium (purity 99.99%) was used as carrier gas in constant linear velocity of 30 cm/s, and a pressure of 109 kPa at the begin of the ramp temperature. The oven temperature was programmed as follows: 100°C for 2 min, then ramp to 350°C at 15°C/min. The final temperature was held for 5.0 min, resulting in total GC run times of 24.0 min. The end of the column was connected to a deactivated fused silica capillary through a micro Siltite μ-union (Trajan Scientific and Medical, Milton Keynes, UK) and inserted into a heated transfer line connected to the IR interface. The transfer line and restrictor temperatures were set at 280°C. Blanks were run in between samples to assure that the liner and column were free of contamination.

GC-FTIR Interface

The transfer line exiting the GC oven was connected into a DiscovIR solid phase FTIR detector (Spectra-Analysis Instrument Inc., Marlborough, MA, USA). The restrictor was positioned directly above a ZnSe disk, which was chilled down to −50°C by means of liquid nitrogen, and cleaned daily with acetone. The DiscovIR FTIR instrument was equipped with a Mercury-Cadmium-Telluride (MCT) cryogenically cooled detector. Solid phase IR spectra of the GC eluted compounds were recorded in real time from 100 μm × 100 μm spots in the 650–4,000 cm^{-1} range, with a resolution of 4 cm^{-1} and a scan rate of 2 Hz, at a disc rotation speed of 3 mm/min.

GC-FTIR Data Acquisition and Processing

The GC instrument was controlled by the LabSolution software (Shimazdu, Kyoto, Japan). GC-FTIR data acquisition and processing were performed using the Thermo Galactic GRAMS/AI spectroscopy and chromatography software ver. 9.3 provided within the instrument. Compounds were identified through the library search program (Spectral ID), using a first derivative correlation algorithm, by comparison within a custom-made solid phase IR spectral library containing IR spectral data of around 600 synthetic cannabinoids and other NPS (namely, Controlled and Prohibited Substances ver. 1.0). The results expressed by the software in 0–1 units (were 0 represents the maximum value for similarity or quality score), was converted for simplicity and uniformity with other search software into 1–100% units (where 100 represents the maximum quality score), by using the formula: Quality score = (1-GRAMS value)*100.

GC-MS

GC-MS analyses were performed on a GCMS-QP2020 NX instrument, equipped with AOC-20 auto sampler and EI source (Shimazdu, Kyoto, Japan). The experimental conditions were the same as those employed for GC-FTIR analyses, except for the injection, which was performed in split mode (1:50), with an injection volume of 0.3 μL (injector temperature of 280°C). MS parameters were as follows: full scan mode in the 40–650 m/z range, ion source temperature: 250°C, interface temperature: 200°C.

Blanks were run in between samples to assure that the liner and column were free of contamination.

Data acquisition and processing was performed by LabSolutions GCMSsolution software ver. 4.41 (Shimazdu, Kyoto, Japan). Compounds were identified by comparison within SWGDRUG MS Library ver. 3.6 (available at http://www.swgdrug.org/ms.htm), containing over 3,000 EI mass spectra of drugs and drug-related compounds.

RESULTS AND DISCUSSION

The use of GC-FTIR as an effective tool for forensic drug identification has been already demonstrated 30 years ago, in terms of specificity needed to differentiate between closely related isomers, including cocaine/pseudococaine, phentermine/metamphetamine (Kempfert, 1988). In contrast to data afforded by widespread MS detection, the uniqueness of IR spectra allows to quickly discriminate between isomers other than optical isomers without the need for preliminary purification/derivatization, as proven for a number of different drug categories, including cannabinoids (Smith et al., 2014, 2018; Belal et al., 2018; DeRuiter et al., 2018; Lee et al., 2019). Since the disclosure of their existence in herbal mixtures (Auwarter et al., 2009), N-alkyl indole-3-carbonyl derivatives

TABLE 1 | Akyl-3-acyl-indole derivatives of the JWH series.

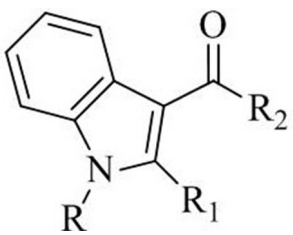

Common name	Formula	R	R_1	R_2
JWH-018	$C_{24}H_{23}NO$	*n-Pentyl*	*H*	*1-Naphtyl*
JWH-019	$C_{25}H_{25}NO$	*n-Hexyl*	*H*	*1-Naphtyl*
JWH-073	$C_{23}H_{21}NO$	*n-Butyl*	*H*	*1-Naphtyl*
JWH-020	$C_{26}H_{27}NO$	*n-Heptyl*	*H*	*1-Naphtyl*
JWH-015	$C_{23}H_{21}NO$	*n-Propyl*	CH_3	*1-Naphtyl*
JWH-250	$C_{23}H_{21}NO$	*n-Pentyl*	*H*	*2-Methoxy-benzyl*
JWH-019 N (6-fluorohexyl) isomer	$C_{25}H_{24}FNO$	*5-Fluoro-n-pentyl*	*H*	*2-Iodo-phenyl*
JWH-018 N (3-methylbutyl) isomer	$C_{24}H_{23}NO$	*n-3-Methylbutyl*	*H*	*1-Naphtyl*

targeting cannabinoid receptors have been largely abused, and have accounted for a major portion of new psychoactive substances put illegally on the market. Many of these synthetic molecules result from modifications of the parent molecule1-naphthalenyl(1-pentyl-1H-indol-3-yl)-methanone shown in **Table 1**, commonly known as JWH-018, such as: the substitution of the indole core ring with other systems (pyrrole, indazole and carbazole), the introduction of acyl groups different than naphthalenyl at the 3-position of indole ring, or the modification of the alkyl chain at the 1-position (different chain length, chain branching, fluoroalkyl groups). The obvious goal of these slight structural changes is to create analogs which are regarded as beyond the scope of the regulation.

Optimization of Solid Phase GC-FTIR

The first step of this research consisted in optimization of the analysis conditions for JWH-018, with regard to the parameters affecting the hyphenation of the two techniques, and FTIR detection as the end goal. The calculation of IR response vs. time was done with the use of the standard software package which utilizes a Gram-Schmidt reconstruction (GSR), resulting in the GC-FTIR chromatogram in **Figure 1** (inset). It can be appreciated how the result of this reconstruction process closely resembles that of a total ion chromatogram from a GC-MS system.

The overall performance of the GC-FTIR technique relies on the deposition of the GC-eluted compounds contained in a carrier gas stream onto the ZnSe disc; thus, one main factor affecting the quality of an IR spectrum is the disc temperature, which can be adjusted by the amount of liquid nitrogen supplied from a Dewar. If insufficient chilling is provided to the disc, trapping of the analytes would be incomplete, with a detrimental effect on the sensitivity of the technique, to a different extent depending on the volatility of the molecules. For the low volatile compounds under study, the maximum analyte recovery in the solid state was obtained at a disc temperature of −50°C. Under the selected experimental conditions, JWH-018 was eluted from the 30 m SLB-5ms column at a retention time just above 20 min as shown in the inset in **Figure 2**. One microliter splitless injection of the ethyl acetate JWH-018 standard solution, corresponding to 1 μg injected on column, gave a chromatographic base peak width of 26 s (52 data points), at an optimum disc rotation speed of 3 mm/min. A proper visual description of the analyte peak requires a discrete number of data points across the same peak, as dictated by the detector acquisition rate and the chromatographic peak width; in temperature-programmed GC analyses, the latter may be affected by large carrier-gas velocity changes, to a variable extent. To this concern, matching the disc rotation speed to the amount of analyte being delivered by the deposition tip is crucial to proper interrogate the deposited solid, avoiding losses in the sensitivity if the time required for complete analyte deposition is not allotted.

On the other hand, slowing down the disc rotation rate excessively would inevitable come at the cost of sacrificed (chromatographic) resolution, which is of utmost concern in FTIR spectra.

The FTIR transmittance spectrum of JWH-018, recorded in the 650–4,000 cm^{-1} at a resolution of 4 cm^{-1} is shown in **Figure 2**. In the 3,000 wavenumber region, two medium intensity IR bands at 2,955 and 2,931 cm^{-1} and a weaker band at 2,872 cm^{-1} arise from the aliphatic C-H stretching, while a single minor band at 3,059 cm^{-1} represents the aromatic C-H stretching. A strong carbonyl absorption band is visible in the wavenumber region around 1,620 cm^{-1}; noticeably this C-O stretching appears as a doublet, due to the higher spectral resolution of the GT-FTIR (solid phase) interface employed,

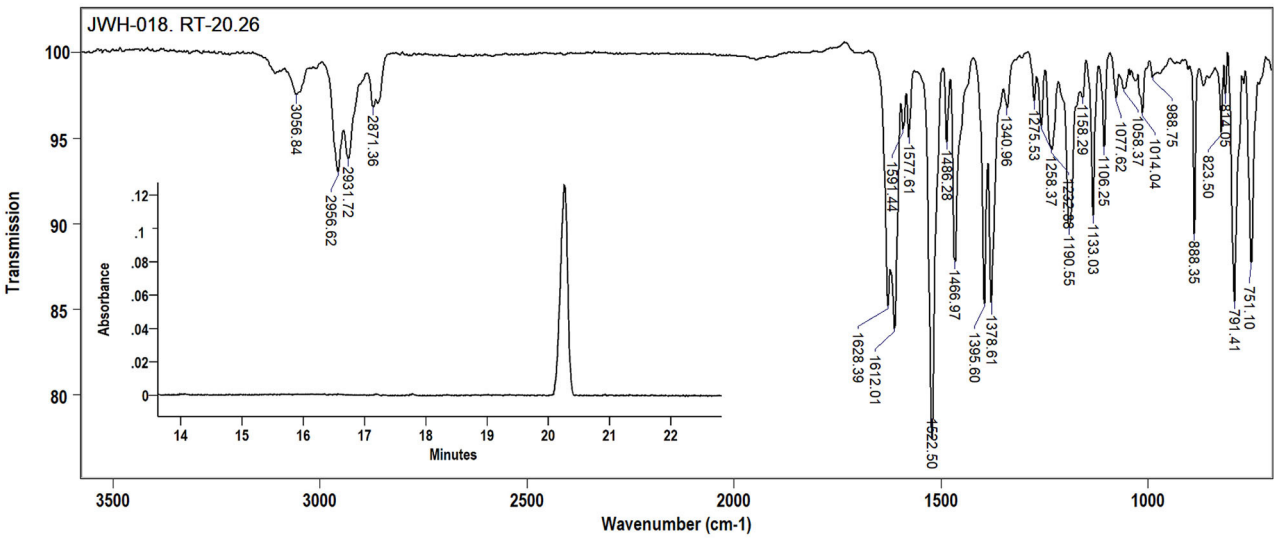

FIGURE 1 | Solid-phase mid-IR spectrum for JWH-018 (1-naphthalenyl(1-pentyl-1H-indol-3-yl)-methanone) at 4 cm^{-1} resolution. Inset: the Grams-Schimdt reconstructed GC-FTIR chromatogram (SLB-5ms, 30 m L × 0.25 mm i.d., 0.25 μm d_f).

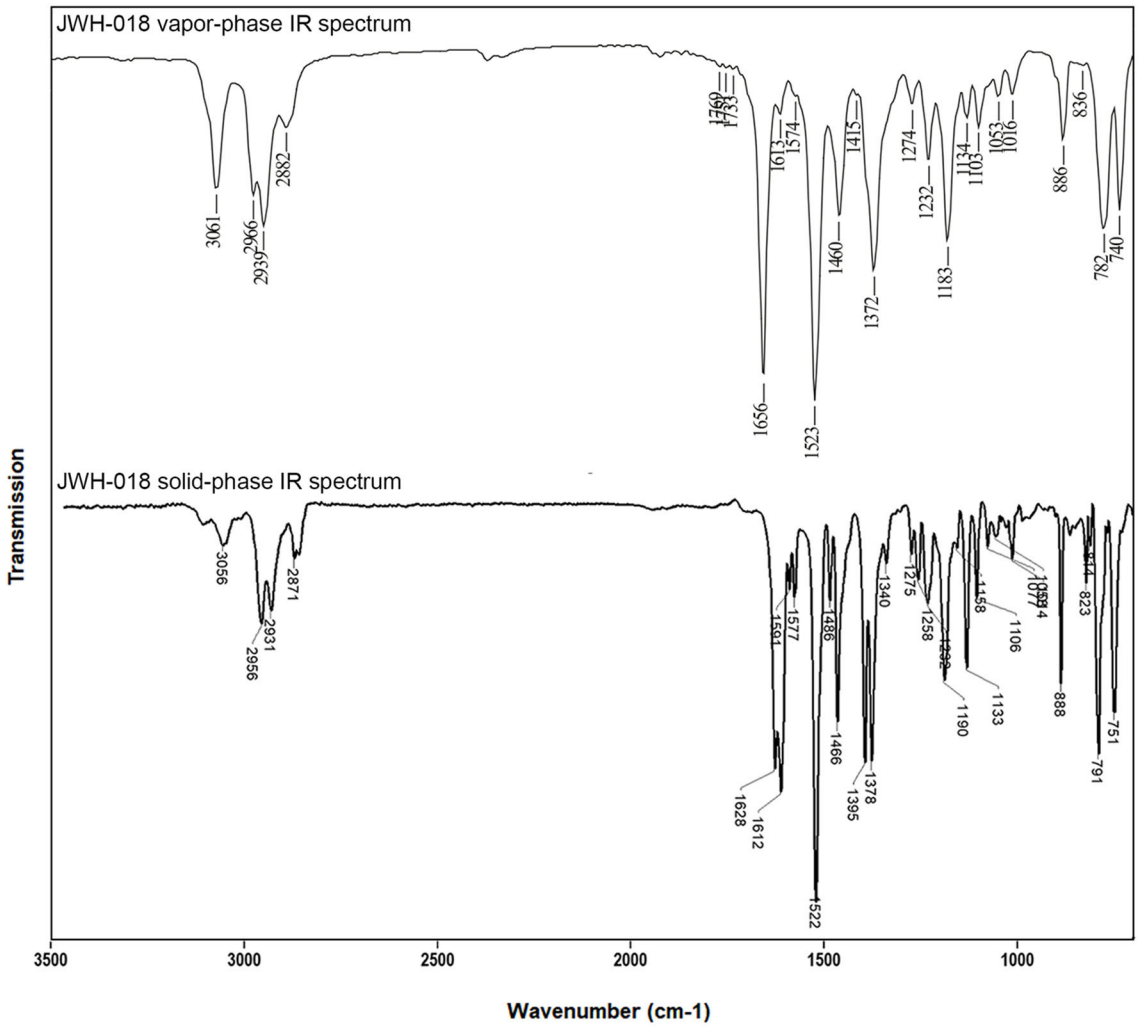

FIGURE 2 | Vapor-phase **(top)** and solid-phase **(bottom)** mid-IR spectra for JWH-018 (1-naphthalenyl(1-pentyl-1H-indol-3-yl)-methanone), at a resolution of 8 and 4 cm^{-1}, respectively. Top part of this figure has been reprinted from Spectrochimica Acta Part A: Molecular and Biomolecular Spectroscopy, 196, Lewis W. Smith, Amber Thaxton-Weissenfluh,Younis Abiedalla, Jack De Ruiter, Forrest Smith, C. Randall Clark, Correlation of vapor phase infrared spectra and regioisomeric structure in synthetic cannabinoids, page 10, Copyright 2018, with permission from Elsevier.

compared to that of light-pipe (gas phase) devices employed elsewhere (Smith et al., 2018). As absorption bands are broadened by molecular rotation or intermolecular forces, the fine structure of the IR spectrum is lost; moreover, the high temperatures required in the light-pipe method cause the absorption bands to be broadened and the spectral specificity reduced. The differences in IR data quality afforded by the two different techniques can be easily appreciated in **Figure 2**, showing a visual comparison of mid-IR spectra for JWH-018 by using LP and solid phase GC-FTIR interfaces.

Calibration curves for JWH-018 were obtained from triplicate injections of five concentration levels in the 20–1,000 mg/mL range, by plotting the chromatographic peak area as a function of the analyte concentration. The IR response vs. amount injected was linear over the range investigated (linear regression: y = 4E-05x - 0.0004, $R^2 = 0.996$) and the figures of merit determined in terms of limit of detection (LOD) and limit of quantification (LOQ), with an average e relative standard deviation (RSD%) per calibration point of 5.42. A LOD value of 4.3 ng was defined, as the sample amount yielding a peak equal to three times the peak-to-peak noise level without any post-run treatment, thus mimicking the situation in which a complete unknown is to be identified, in a real sample application. The low end of the linear detection range (LDR) was defined as the LOQ value of 14.3 ng, as the sample amount yielding a peak equal to 10 times the peak-to-peak noise level. The high end of the LDR could be determined as the highest concentration retaining linearity, without overloading the inlet liner or column, resulting in poor peak shape or carryover between consecutive runs. However, this figure could be not determined experimentally, since it would be higher than the concentration of the standard solution provided by the manufacturer.

It must be specified at this point, that the LOD and LOQ values for the solid-phase GC-FTIR technique were estimated from plots of the chromatographic peak area vs. analyte concentration, in a non- targeted way. This approach more fits the need for unknown drug identification and quantification in real samples; however a targeted approach based on absorbance measurement of the most intense IR peak as a function of time would yield different figures of merit, as regards increased selectivity and sensitivity (Lanzarotta et al., 2017).

Identification Through Solid-Phase Library Search

The sharp absorption bands in FTIR spectra obtained from solid deposited analytes give the ability to differentiate between similar compounds, and may well complement the type of data provided by GC-MS analysis, in achieving reliable identification. However, results based on qualitative review of the IR data by the analyst are heavily subjective and may lead to different outcomes; for this reason, it is desirable to implement more objective algorithm-based criteria, based on quantitative data evaluation. Hereby, the quality score (QS) or quality match factor (QMF) was adopted, as an unbiased criterion to differentiate between IR spectra and achieve unambiguous compound identification upon library search.

The results obtained by searching the IR spectral data for JWH-018 into a custom-made library containing IR spectral data of synthetic cannabinoids and other psychoactive substances (supplied by the vendor) demonstrated that the compounds can be differentiated and identified with no ambiguity, through the evaluation of QMF (**Figure 3**).

As it can be seen in the results from library search in **Figure 3** (bottom), JWH-018 was correctly identified with a similarity around 0.005, which corresponds to a QMF of 99.5% [QMF= (1-GRAMS value)*100]. Noticeably, JWH-018 gave a QMF below 90% (ranging from 89.9 to 81.2%) when it was matched to the wrong compounds, including one regioisomer (Hit 5). A visual comparison of the IR spectra of Hits 1–6, shown in the bottom part of **Figure 4**, reveals a high degree of similarity, the only differences being related to the different length of the N-alkyl chain. These are reflected in the aliphatic C-H stretching bands in the 2,900 cm^{-1} region and C-H bending bands in the wavenumber region below 1,200 cm^{-1}. The terminal halogen substituted derivative (6-fluorohexyl, hit 6) shows changes in the aliphatic triplet pattern around 3,000 cm^{-1} to almost a

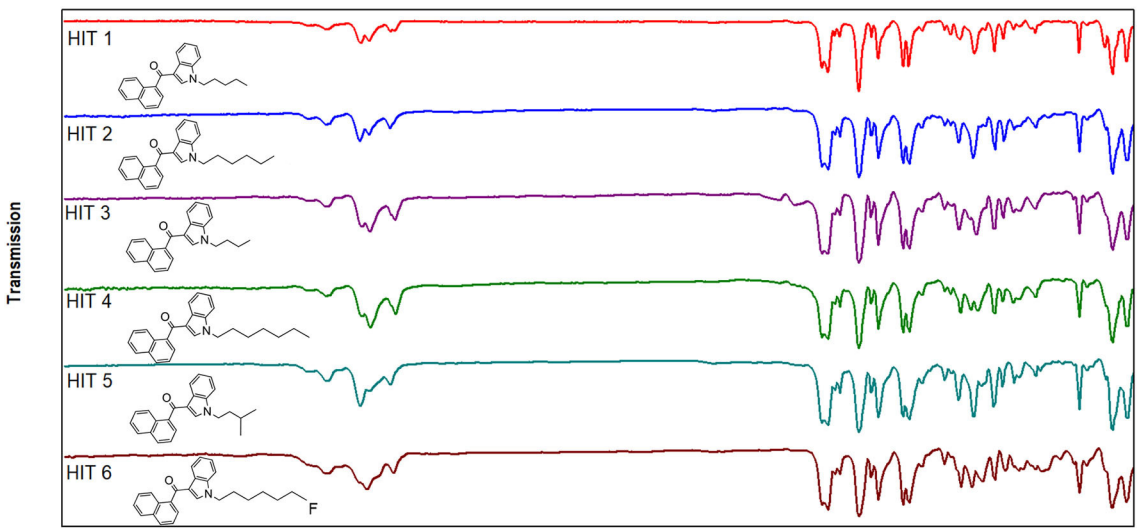

HIT	QUALITY	COMPOUND NAME	LIBRARY
1	0.0050827	JWH-018	Controlled & Prohibited Substances 1.0
2	0.100952	JWH-073	Controlled & Prohibited Substances 1.0
3	0.105353	JWH-019	Controlled & Prohibited Substances 1.0
4	0.142832	JWH-020	Controlled & Prohibited Substances 1.0
5	0.150306	JWH-018 N-(3-methylbutyl) isomer	Controlled & Prohibited Substances 1.0
6	0.188372	JWH-019 N-(6-fluorohexyl) isomer	Controlled & Prohibited Substances 1.0

FIGURE 3 | Software window showing the library search results obtained for JWH-018 IR spectral data. **(Top)** IR spectra of JWH and its structural analogs (Hits 1–6). **(Bottom)** QMF obtained for JWH-018 against correct and incorrect matches. Quality is expressed in 0–1 units (with 0 representing the maximum value for similarity or quality score).

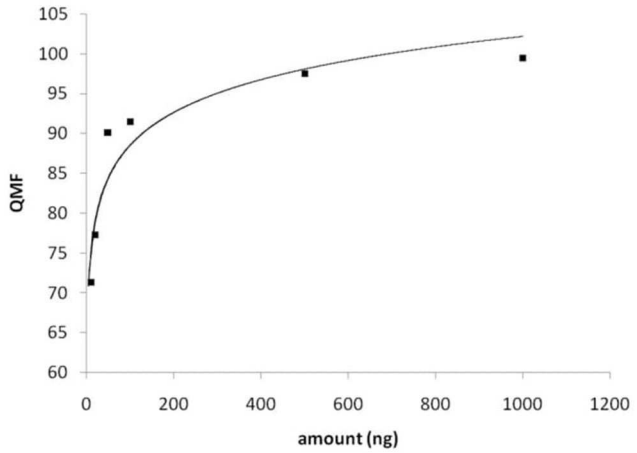

FIGURE 4 | Plot of the QMF values obtained for library search of JWH-018, as a function of the amount measured.

TABLE 2 | QMF for JWH-018 and its related compounds.

Compound	QMF to the analog compound		
	JWH-018	**JWH-073**	**JWH-019**
JWH-018	**99.5**	89.4	86.2
JWH-073	89.9	**96.9**	83.8
JWH-019	89.5	81.8	**94.8**

*Results rendered by algorithm-based search criteria in 0–1 units were converted into 1–100% units [QMF = (1-GRAMS value)*100]. In bold are the QMF of the compound itself.*

single band with weak shoulder inflections, due to the loss of the terminal methyl group of the N-alkyl tail substituent; moreover C-F stretching bands are in the fingerprint region of 1,000–1,300 cm^{-1}. Nonetheless, these small spectral differences are successfully captured by the QMF values obtained for the different matches, demonstrating the usefulness of the technique to differentiate between closely related molecules of the JWH series. Among all the JWH-018 analogs, the JWH-073 and JWH-019 gave the closest match (Hits 7 and following gave QMF below 80% and are not shown), thus they were analyzed separately to further validate the results. The resulting QMF of the three compounds matched again each other are presented in **Table 2**; thus, a QS or QMF of 0.1 (90%) could be assumed for a correct identification, given the high specificity of the spectral data, to reduce the likelihood for false positives and increase confidence in the results.

Hereby, as a more trustworthy approach, the IR spectra recorded for JWH-018 solutions at concentration levels investigated for the LDR, were searched into the solid-phase FTIR library. A plot of the QMF values obtained of the compound itself, showed a logarithmic dependence from the amount measured, as in **Figure 4**. Based on the criterion established before, the minimum amount of substance yielding a library searchable IR spectrum (QMF $\geq$ 90%), is just below 50 ng.

Solid Phase GC-FTIR and GC-EI-MS Analysis of a Seized Sample

NPS are increasingly sold and consumed as mixtures of several different active principles, whose pharmacodynamics and adverse effects are almost unknown, and with large intra- and inter-product concentration variabilities. This poses a challenge for forensic laboratories, as they are frequently asked to promptly identify unknown substances, both for the court and/or to orient emergency treatments in intoxication cases (Zamengo et al., 2014).

To assess the applicability of the technique for analysis of a real sample, a vegetable matrix, suspected to contain one or more synthetic cannabinoids, was extracted by sonication and injected into the GC-FTIR and GC-EI-MS systems; analyses were made in triplicate.

The GC-FTIR and GC-MS chromatograms of the extracted drug sample are shown in **Figure 5**. Four major components belonging to the JWH series were separated on a 30 m length of non-polar bonded and highly crosslinked silphenylene polymer column, virtually equivalent in polarity to a poly (5% diphenyl/95% dimethyl siloxane) column, which is commonly applied in forensic drug analysis. These synthetic cannabinoids were later identified as: 1-(1-pentyl-1H-indol-3-yl)-2-(2-methoxyphenyl)-ethanone (JWH-250), (2-methyl-1-propyl-1H-indol-3-yl)-1-naphthalenyl-methanone (JWH-015), (1-butyl-1H-indol-3-yl)-1-naphthalenyl-methanone (JWH-073), and 1-naphthalenyl(1-pentyl-1H-indol-3-yl)-methanone (JWH-018); their chemical structures are given in **Table 1**.

It is worth mentioning at this point that a method for untargeted analysis was developed, and the GC program temperature optimized to achieve baseline separation of all possible cannabinoid constituents in unknown samples. Moreover, this program allowed for calculation of the Linear Retention Indices of synthetic cannabinoids, upon injection of a C4–C40 alkane reference mixture (data not included in the work). The use of a higher initial temperature, or a much steeper ramp, would allow to speed up elution of the compounds of interest, absolutely; however it was not the scope of this work.

The GC-MS technique afforded superior resolution and sensitivity within the same analysis time, in part due to faster detector scan rate (100 Hz) with respect to the FTIR counterpart (2 Hz). An additional minor peak showed up in the GC-MS chromatogram after the compounds of interest, at t_R of 22.5 min (**Figure 6**-bottom), which could not be detected by GC-FTIR. In contrast, the upper GC-FTIR trace reveals three minor peaks, eluting in the 12–14 min retention time window (**Figure 5**-top), which were not recorded by GC-MS. This latter evidence is, in the authors' opinion, intrinsic to the distinct technologies, in fact FTIR may be regarded as "compound independent," in that once GC eluted analytes from the tip are deposited as solid spots onto the disk, FTIR spectra may be recorded. In other words, no disparity in ionization may affect the spectral result.

The analysis of street drug samples relies strictly on the specificity of the technique for the target substance of abuse, and thus on the capability to discriminate between a plethora

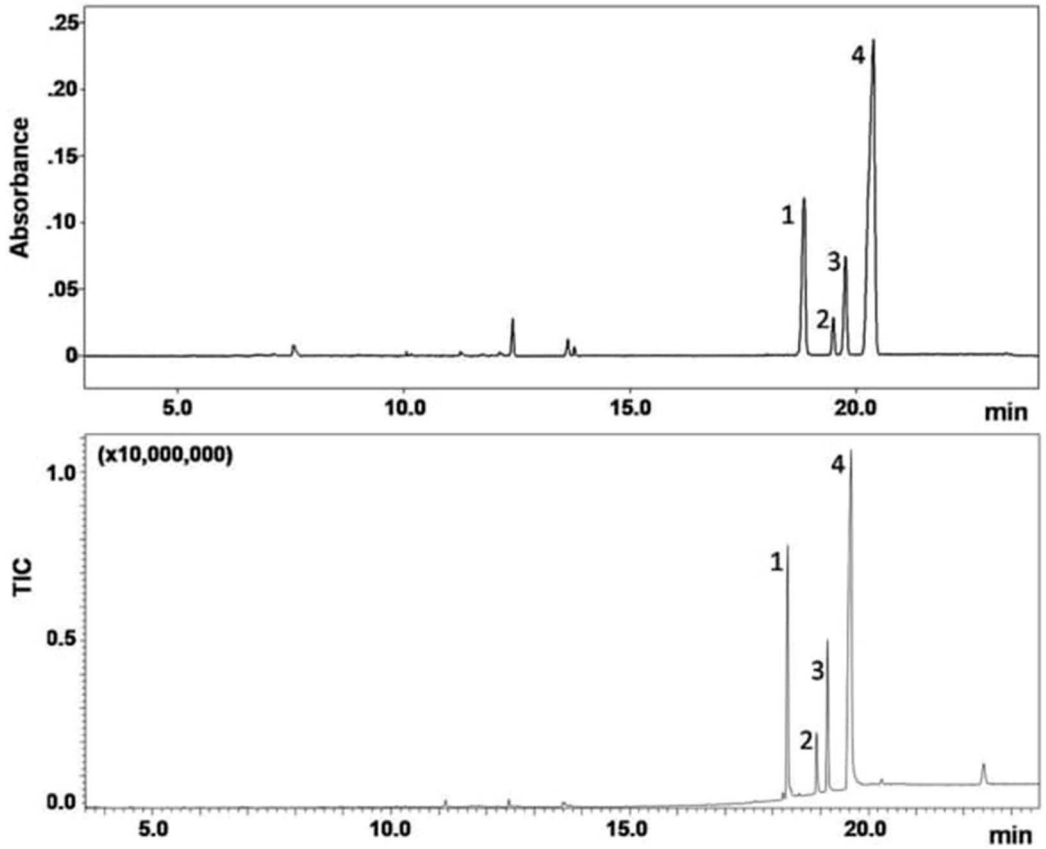

FIGURE 5 | GC-FTIR **(top)** and GC-EI-MS **(bottom)** analysis of a seized sample. Column: SLB-5ms (30 m L × 0.25 mm i.d., 0.25 μm d_f), carrier gas: helium at 1.1 mL/min (30 cm/s, 109 kPa); oven: 100°C for 2 min, to 350°C at 15°C/min (held for 5.0 min); injection: 1 μL splitless (GC-FTIR) or 0.3 μL split 1:50 (GC-MS) at 280°C. Peak identification: JWH-250 (1), JWH-015 (2), JWH-073 (3), JWH-018 (4).

of possible "co-formulants" with nearly identical chemical structures. In this study, the results obtained by GC-FTIR and GC-EI-MS were evaluated, to assess the capabilities of the two techniques, in allowing for ultimate identification of the seized sample components. To this purpose, IR and MS spectral data were searched into a custom-made solid phase FTIR library, containing IR spectral data of around 600 synthetic cannabinoids and other NPS, and the SWGDRUG MS Library ver. 3.6 (available at http://www.swgdrug.org/ms.htm), containing over 3,000 EI mass spectra of drugs and drug-related compounds. The resulting QMF values obtained by the two techniques are listed in **Table 3**, reported as the correct matches for each compound identified.

The FTIR spectra obtained by solid-deposition interface in all cases succeeded to discriminate between the different substances, with QMF values ranging from 91 to 98%, thus confirming validity of the criterion of QMF of 90 and above to ascertain unequivocal identification of the correct molecule. The QMF values obtained in a similar way upon library search of MS spectral data were for all the correct matches lower, with a maximum QMF of 96 and a minimum QMF of 89, with the last result being lower than the minimum acceptance criterion.

A further concern in library search is the QMF differential between the correct and the (closest) incorrect matches, in that it allows for confident structure identification to be achieved, even if the spectrum of a target analyte is not included in the specific library. To this regard, the case of the first eluting sample component, labeled as peak #1 at t_R around 18 min (chromatograms in **Figure 5**), is noteworthy. This compound was identified by library search of EI-MS data, as shown in **Figure 6**, as JWH-250, with a QMF of 96 (Hit #1). While this would be regarded as quite satisfactory for assessing identification, however it must be noted that Hit #2 and Hit #3, representing the closest incorrect matches for JWH-302 and JWH-201, respectively, shows nearly identical QMF value, *viz.* 95 and 94. In this situation, very little information is available for the specific differentiation of regioisomers having identical nominal and observed masses, and even abundant fragment ions obtained by EI occur at equivalent masses: 1-(1-pentyl-1H-indol-3-yl)-2-(2-methoxyphenyl)-ethanone (JWH-250), 2-(3-methoxyphenyl)-1-(1-pentyl-1H-indol-3-yl)-ethanone (JWH-302), 2-(4-methoxyphenyl)-1-(1-pentyl-1H-indol-3-yl)-ethanone (JWH-201), with Molecular Formula $C_{22}H_{25}NO_2$.

Likewise, the results obtained by library search of solid-phase FTIR data, shown in **Figure 7**, fully prove the capability of the technique in affording the specificity of information required.

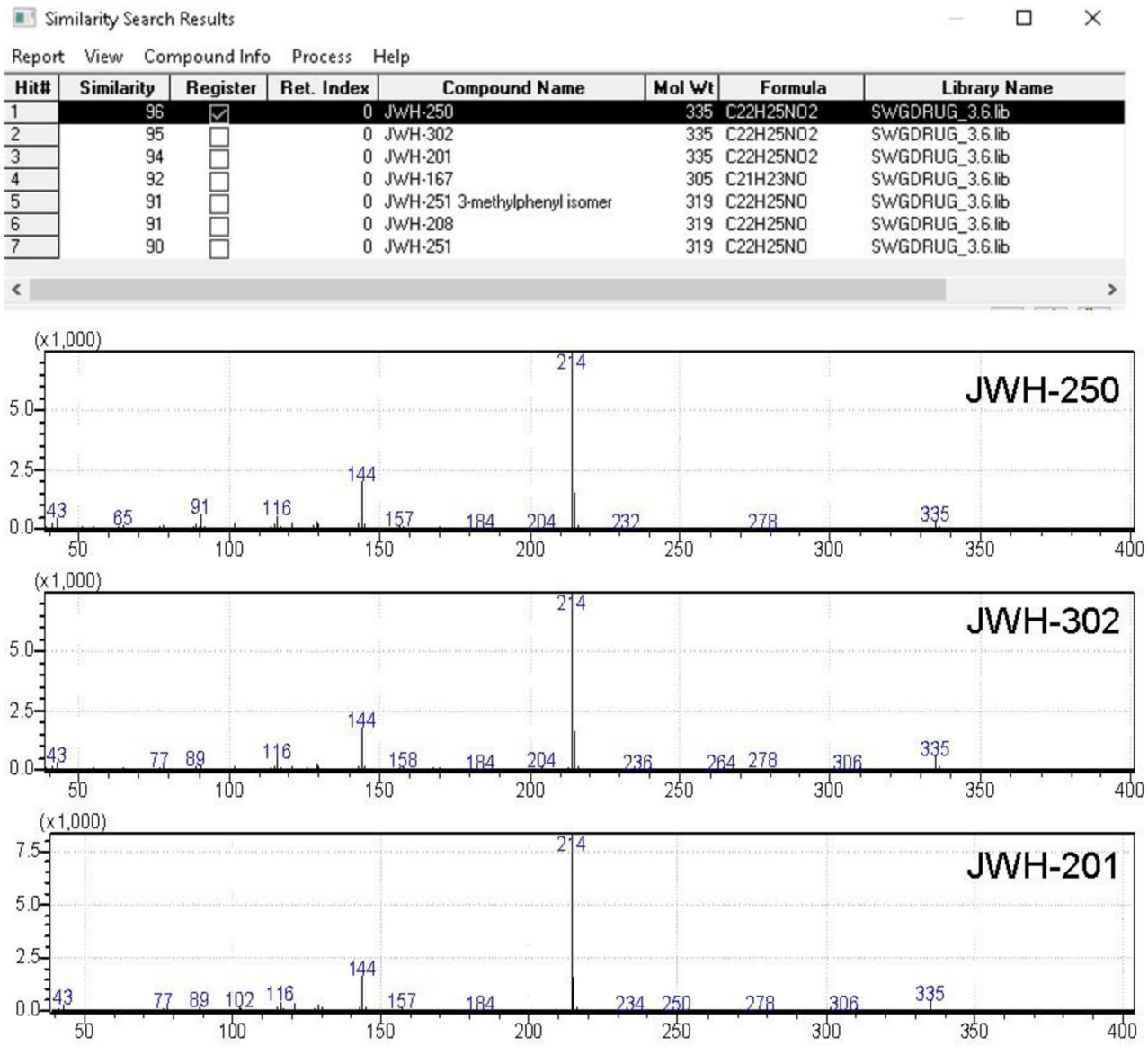

FIGURE 6 | Software window showing the library search results obtained for JWH-250 EI-MS spectral data. QMF obtained for against correct and incorrect matches are shown in column #2.

TABLE 3 | QMF for the compounds identified in a seized sample.

Compound	QMF to the analog compound	
	GC-FTIR	GC-MS
JWH-250	98.0	96
JWH-015	91.5	89
JWH-073	95.6	90
JWH-018	96.7	92

*Results rendered by algorithm-based search criteria in 0–1 units were converted into 1–100% units [QMF = (1-GRAMS value)*100].*

It can be seen that regioisomeric compounds ranked as Hit #1(JWH-250), Hit #9 (JWH-302), and Hit #10 (JWH-201), with a QMF value of 98.0 for the correct match, vs. 44.0 and 39.0 for the two incorrect matches (**Figure 7**-bottom). The high discrimination power of solid-phase FTIR may be appreciated from a visual comparison of the IR spectra stacked in **Figure 7** (top), where changes in positional bonding result in unique patterns, especially in the complex fingerprint region, that allow for differentiation among the three regioisomers.

CONCLUSIONS

The effectiveness of solid-phase GC-FTIR is demonstrated, as an alternative tool to widespread MS-based approaches, for achieving unequivocal identification of NPS. The use of a solid deposition interface enabled for boosting the resolution and

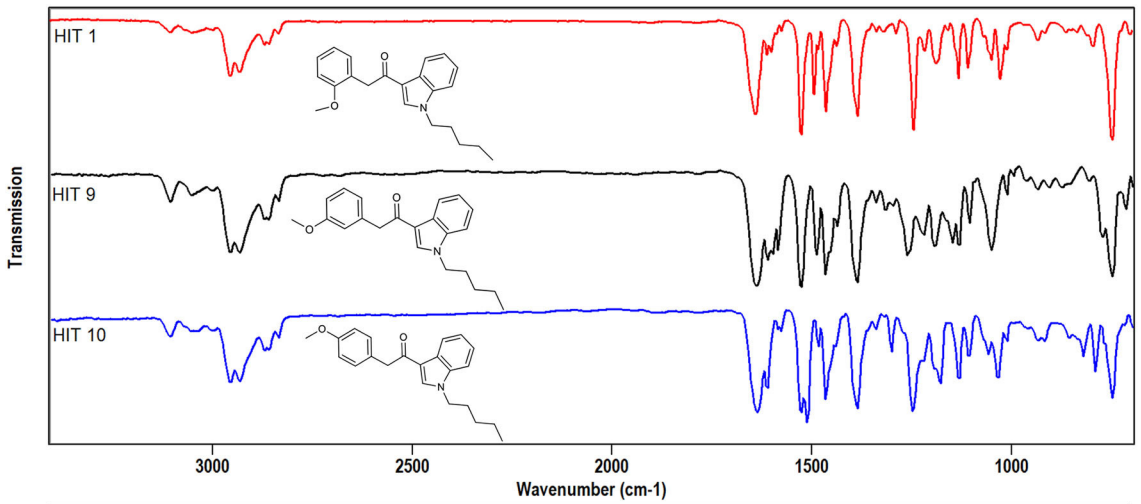

HIT	QUALITY	COMPOUND NAME	LIBRARY
1	0.0194001	JWH-250	Controlled & Prohibited Substances 1.0
2	0.231392	RCS-8	Controlled & Prohibited Substances 1.0
3	0.497327	JWH-251	Controlled & Prohibited Substances 1.0
4	0.499484	JWH-251 3-methylphenyl isomer	Controlled & Prohibited Substances 1.0
5	0.522278	JWH-203	Controlled & Prohibited Substances 1.0
6	0.540957	JWH-203 4-chlorophenyl isomer	Controlled & Prohibited Substances 1.0
7	0.542045	JWH-251 4-methylphenyl isomer	Controlled & Prohibited Substances 1.0
8	0,557779	JWH-203 3-chlorophenyl isomer	Controlled & Prohibited Substances 1.0
9	0.559322	JWH-302	Controlled & Prohibited Substances 1.0
10	0.609446	JWH-201	Controlled & Prohibited Substances 1.0

FIGURE 7 | Software window showing the library search results obtained for JWH-250 IR spectral data. **(Top)** IR spectra of JWH-250 and its regioisomers JWH-302, JWH-201 (Hits 9, 10). **(Bottom)** QMF obtained for JWH-250 against correct and incorrect matches. Quality is expressed in 0–1 units (with 0 representing the maximum value for similarity or quality score).

sensitivity of the technique, over gas phase cells, scaling down the limit of identification to the ng scale. Results obtained from the analysis of an illicit street drug sample showed that GC-MS alone would in this case not afford the reliable identification of the unknown compounds, with the exclusion of the other possible regioisomeric molecules. The lack in MS specificity, along with the likelihood for chromatographic co-elutions, and the possible scarcity of available reference material would make drug identification challenging. Thus, the individual identification of any one of these substances and the exclusion of possible misidentification will depend heavily upon chromatographic methods. Likewise, solid-phase GC-FTIR succeeded in allowing for confident identification of all the compounds in a forensic drug sample, given the ability to eliminate regioisomers as possible interfering or co-eluted substances. This additional specificity of FTIR comes at the price of lower sensitivity (at the ng scale) with respect to the MS counterpart (at the pg scale), nonetheless this may be not a primary concern in forensic science, since illicit drugs usually contain up to milligrams of psychoactive substances.

DATA AVAILABILITY STATEMENT

The raw data supporting the conclusions of this article will be made available by the authors, without undue reservation.

AUTHOR CONTRIBUTIONS

LM: conception and design. TS: acquisition of data. TS, PD, GF, and LZ: analysis and interpretation of data. PD: drafting the article. All authors: contributed to the article and approved the submitted version.

REFERENCES

Abiedalla, Y., Smith, L. W., Abdel-Hay, K. M., Neel, L., Belal, T. S., Thaxton-Weissenfluh, A., et al. (2019). Spectroscopic differentiation and chromatographic separation of regioisomeric indole aldehydes: synthetic cannabinoids precursors. *Forensic Chem*. 12, 78–90. doi: 10.1016/j.forc.2018.12.004

Almalki, A. J., Clark, C. R., and DeRuiter,. J. (2019). GC–MS analysis of regioisomeric substituted N-benzyl-4-bromo-2,5-dimethoxyphenethylamines. *Forensic Chem*. 14, 100164–100174. doi: 10.1016/j.forc.2019.100164

Auwarter, V., Dresen, S., Weinmann, W., Muller, M., and Putz, M., Ferreiro, N. (2009). 'Spice' and other herbal blends: harmless incense or cannabinoid designer drugs? *J. Mass. Spectrom*. 44, 832–837. doi: 10.1002/jms.1558

Belal, T. S., Thaxton-Weissenfluh, A., DeRuiter, J., Smith, F., Abiedalla, Y., Abdel-Hay, K. M., et al. (2018). Differentiation of methylated indole ring regioisomers of JWH-007: GC-MS and GC-IR studies. *Forensic Chem*. 7, 1–9. doi: 10.1016/j.forc.2017.11.001

Brandt, S. D., King, L. A., and Evans-Brown, M. (2014). The new drug phenomenon. *Drug Test. Anal*.6, 587–597. doi: 10.1002/dta.1686

Bretteville-Jensen, A. L., Tuv, S. S., Bilgrei, O. R., Fjeld, B., and Bachs, L. (2013). Synthetic cannabinoids and cathinones: prevalence and markets. *Forensic Sci*. Rev. 25, 8–26.

Brown, R. S., Cooper, J. R., and Wilkins, C. L. (1985). Light pipe temperature and other factors affecting signal in gas chromatography/Fourier transform infrared spectrometry. *Anal. Chem*. 57, 2275–2279. doi: 10.1021/ac00289a023

Davidson, J. T., Lumb, B. J., Nano, G., and Jackson, G. P. (2018). Comparison of measured and recommended acceptance criteria for the analysis of seized drugs using Gas Chromatography-Mass Spectrometry (GC-MS). *Forensic Chem*. 10, 15–26. doi: 10.1016/j.forc.2018.07.001

DeRuiter, J., Smith, F., Abiedalla, Y., Neel, L., and Clark, C. R. (2018). GC-MS and GC-IR analysis of regioisomeric cannabinoids related to 1-(5-fluoropentyl)-3-(1-naphthoyl)-indole. *Forensic Chem*. 10, 48–57. doi: 10.1016/j.forc.2018.07.005

ElSohly, M. A., Gul, W., Wanas, A. S., and Radwan, M. M. (2014). Synthetic cannabinoids: analysis and metabolites. *Life Sci*. 97, 78–90. doi: 10.1016/j.lfs.2013.12.212

EMCDDA (2019) *EMCDDA Operating Guidelines for the European Union Early Warning System on New Psychoactive Substances*. Lisbon: EMCDDA. Available online at: http://www.emcdda.europa.eu/publications/guidelines/operating-guidelines-for-the-european-union-early-warning-system-on-new-psychoactive-substances_en

Fuoco, R., Shafer, K. H., and Griffiths, P. R. (1986). Capillary gas chromatography/Fourier transform infrared microspectrometry at sub ambient temperature. *Anal. Chem*. 58, 3249–3254. doi: 10.1021/ac00127a073

Griffiths, P. R., Heaps, D. A., and Brejna, P. R. (2008). The gas chromatography/infrared interface: past, present, and future. *Appl. Spectrosc*. 62, 259A−270A. doi: 10.1366/000370208786049213

International, A. (2015). *Standard Practice for Quality Assurance of Laboratories Performing Seized-Drug Analysis*.

International, A. (2017). *Standard Practice for Identification of Seized Drugs*.

Kelly, K., and Bell, S. (2018). Evaluation of the reproducibility and repeatability of GCMS retention indices and mass spectra of novel psychoactive substances. *Forensic Chem*. 7, 10–18. doi: 10.1016/j.forc.2017.11.002

Kempfert,. K. (1988). Forensic drug analysis by GC/FT-IR. *Appl. Spectrosc*. 42, 845–849. doi: 10.1366/0003702884429003

Kraenenburg, R. F., García-Cicourel, A. R., Kukurin, C., Janssen, H.-G., Schoenmakers, P. J., and van Asten, A. C. (2019). Distinguishing drug isomers in the forensic laboratory: GC–VUV in addition to GC–MS for orthogonal selectivity and the use of library match scores as a new source of information. *Forensic Sci. Int*. 302, 109900–109914. doi: 10.1016/j.forsciint.2019.109900

Lanzarotta, A., Lorenz, L., Voelker, S., Falconer, T. M., and Batson, J. S. (2017). Forensic drug identification, confirmation, and quantification using a fully integrated gas chromatography–Fourier transform infrared–mass spectrometer (GC-FT-IR-MS). *Appl. Spectrosc*. 72, 750–756. doi: 10.1177/0003702817746964

Lee, H. Z. S., Koh, H. B., Tan, S., Goh, B. J., Lim, R., Lim, J. L. W., et al. (2019). Identification of closely related new psychoactive substances (NPS) using solid deposition gas-chromatography infra-red detection (GC–IRD) spectroscopy. *Forensic Sci. Int*. 299, 21–33. doi: 10.1016/j.forsciint.2019.03.025

Low, M. J. D. (1971). Infrared Fourier Transform spectroscopy in flavor analysis. IV. Spectra of gas chromatography fractions. *J. Agric. Food Chem*. 19, 1124–1127. doi: 10.1021/jf60178a013

Low, M. J. D., and Freeman, S. K. (1967). Measurements of infrared spectra of gas-liquid chromatography fractions using multiple-scan interference spectrometry. *Anal. Chem*. 39, 194–198. doi: 10.1021/ac60246a025

Namera, A., Kawamura, M., Nakamoto, A., Saito, T., and Nagao, M. (2015). Comprehensive review of the detection methods for synthetic cannabinoids and cathinones. *Forensic Toxicol*. 33,175–194. doi: 10.1007/s11419-015-0270-0

Reedy, G. T., Ettinger, D. G., Schneider, J. F., and Bourne, S. (1985). High-resolution gas chromatography/matrix isolation infrared spectrometry. *Anal. Chem*. 57, 1602–1609. doi: 10.1021/ac00285a024

Schneider, J. F., and Demirgian, J. C. (1986). A comparison of GC/IR interfaces: the light pipe versus matrix isolation. *J. Chromatogr. Sci*. 24, 330–333. doi: 10.1093/chromsci/24.8.330

Scientific Working Group for the Analysis of Seized Drugs (SWGDRUG) (2019). *Recommendations Edition 8.0*. Available online at: http://swgdrug.org/Documents/SWGDRUG%20Recommendations%20Version%208_FINAL_ForPosting_092919.pdf

Shaps, R. H., and Varano, A. (1977). Stop-flow GC/IR analysis. *Industr. Res*. 2, 86–89.

Smith, F. T., DeRuiter, J., Abdel-Hay, K., and Clark, C. R. (2014). GC–MS and FTIR evaluation of the six benzoyl-substituted-1-pentylindoles: isomeric synthetic cannabinoids. *Talanta* 129, 171–182. doi: 10.1016/j.talanta.2014.05.023

Smith, L. W., Thaxton-Weissenfluh, A., Abiedalla, Y., DeRuiter, J., Smith, F., and Clark, C. R. (2018). Correlation of vapor phase infrared spectra and regioisomeric structure in synthetic cannabinoids. *Spectrochim. Acta A*. 196, 375–384. doi: 10.1016/j.saa.2018.02.052

UNODC (2018). *Understanding the Synthetic Drug Market: The NPS Factor, Global SMART Update Volume* 19.

Visser, T. (2002). FT-IR detection in gas chromatography. *TRAC Trend Anal. Chem*. 21, 627–636. doi: 10.1016/S0165-9936(02)00812-9

Zamengo, L., Frison, G., Bettin, C., and Sciarrone, R. (2014). Understanding the risks associated with the use of new psychoactive substances (NPS): high variability of active ingredients concentration, mislabelled preparations, multiple psychoactive substances in single products. *Toxicol. Lett*. 229, 220–228. doi: 10.1016/j.toxlet.2014.06.012

Zuba, D. (2014). New psychoactive substances - a contemporary challenge for forensic toxicologists. *Probl. Forensic Sci*. 100, 359–385.

Conflict of Interest: The authors declare that the research was conducted in the absence of any commercial or financial relationships that could be construed as a potential conflict of interest.

The handling Editor declared a past co-authorship with the authors GF and LZ.

frontiers in Chemistry

ORIGINAL RESEARCH
published: 27 August 2020
doi: 10.3389/fchem.2020.00737

Opium Alkaloids in Harvested and Thermally Processed Poppy Seeds

Michelle G. Carlin, John R. Dean and Jennifer M. Ames†*

Department of Applied Sciences, Northumbria University, Newcastle upon Tyne, United Kingdom

The opium alkaloids (morphine, codeine, thebaine, noscapine, and papaverine) have been detected on poppy seeds; they are widely used by the food industry for decoration and flavor but can introduce opium alkaloids into the food chain. Of the opium alkaloids found on poppy seeds, morphine, and codeine are the most pharmacologically active and have been detected in biological matrices collected in workplace and roadside drug testing resulting in positive opiate results. The European Food Safety Authority introduced an acute reference dose of 10 μg morphine/kg of body weight as a safe level for morphine in food products. In this work, it was found that in harvested poppy seeds, and thermally processed poppy seeds (with and without a food matrix), if used in normal levels would not exceed the recommended acute reference dose. It was also shown that the levels of all alkaloids reduce when thermally processed, in comparison with harvested, untreated seeds.

Keywords: poppy seeds, morphine, codeine, thebaine, noscapine, papaverine, workplace/roadside drug testing

OPEN ACCESS

Edited by:
Alberto Salomone,
University of Turin, Italy

Reviewed by:
Serap Annette Female Akgur,
Ege University, Turkey
Mohammad Sharif Khan,
Dartmouth College, United States

****Correspondence:***
Michelle G. Carlin
m.carlin@northumbria.ac.uk

†Present address:
Jennifer M. Ames,
Jenny Ames Consulting Ltd, Reading,
United Kingdom

Specialty section:
This article was submitted to Analytical Chemistry, a section of the journal Frontiers in Chemistry

Received: *02 March 2020*
Accepted: *17 July 2020*
Published: *27 August 2020*

Citation:
Carlin MG, Dean JR and Ames JM (2020) Opium Alkaloids in Harvested and Thermally Processed Poppy Seeds. Front. Chem. 8:737. doi: 10.3389/fchem.2020.00737

INTRODUCTION

Papaver somniferum L. the opium poppy originated in Sumer, a region in ancient Mesopotamia (modern day Iraq and Kuwait) around 5000 BC (Aragón-Poce et al., 2002). Much has been written with respect to the opium poppy and many relate not only to the cultivation and harvest of this crop but to the investigations of the chemistry of the plant and its medicinal uses as well as the wars that have been fought over opium (Duke, 1973; Kapoor, 1995; Bernath, 1999; Miller and Tran, 2000; Aragón-Poce et al., 2002; Askitopoulou et al., 2002; Martinez-Fernández et al., 2002; Schiff, 2002; Bozan and Temelli, 2008; Cordell, 2013; Windle, 2013).

In the 21st century, the two main legitimate uses of the opium poppy are as a source of alkaloid compounds for the pharmaceutical industry and as a source of poppy seeds for the food industry (Gumuscu et al., 2008). Of the plant family Papaveraceae (common name poppy) the genus *Papaver* has two species containing morphine, codeine, thebaine, noscapine (also called narcotine), and papaverine (**Figure 1**): *Papaver somniferum L.* and *Papaver setigerum D.C* (Garnock-Jones and Scholes, 1990; Yoshimatsu et al., 2005; Mohsin et al., 2012). Thebaine has been reported in *Papaver orientale L. and Papaver bracteatum* Lindl. but no biosynthetic interconversion to codeine and morphine has been found in these species (Stermitz and Rapoport, 1961). Although it is known that alkaloid compounds can be found in both *Papaver somniferum L.* and *Papaver setigerum D.C.* the former has considerably higher levels of the

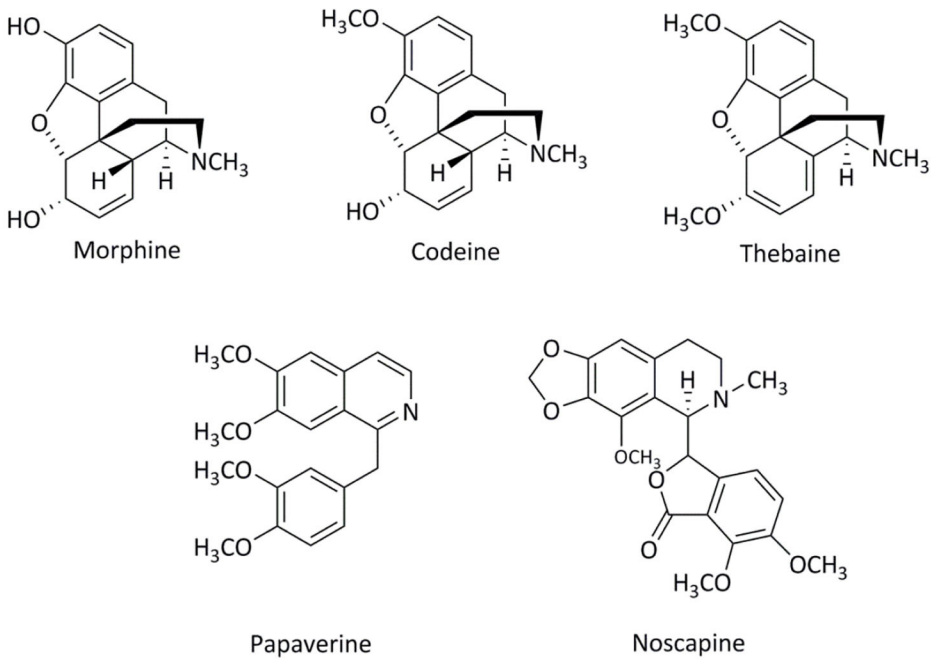

FIGURE 1 | Chemical structures of the major opium alkaloids.

five major alkaloids, by percent weight, of opium than that present in *setigerum* (**Table 1**).

Papaver somniferum L. is an annual crop cultivated worldwide but is legitimately grown by the pharmaceutical and food industries in Australia, Canada, Central and Southern America, Czechoslovakia (now the Czech Republic and Slovakia), France, Holland, Hungary, India, Iran, Poland, Romania, Spain, Turkey, and (the former) Yugoslavia (Bernath, 1999; International Narcotics Board, 2016).

Papaver somniferum L. is an herbaceous plant which is harvested for its latex 5–10 days after the flowering petals fall from the plant (Schiff, 2002). The dried latex product is called opium from which morphine and other alkaloid compounds can be extracted. However, if left to fully mature, the plant will form poppy seeds within the capsule which can be mechanically harvested and collected by a sieving process (Kapoor, 1995; Schiff, 2002).

Harvesting methods have been shown to greatly affect the level of alkaloids in the final opium product (Mahdavi-Damghani et al., 2010). If the opium is harvested too early in the process the product is found to be watery and if too late the opium contains significantly lower levels of alkaloids (Mahdavi-Damghani et al., 2010).

Papaver somniferum L. is cultivated for the pharmaceutical industry but a by-product of the process of harvesting poppy straw is poppy seeds (International Narcotics Board, 2016). This source of poppy seeds is used by the food industry and are included in cakes, on bread products and sold to supermarkets and specialist shops for use in cooking/baking recipes. It was initially thought that the seeds and any products derived from them would not contain any alkaloid compounds due to the fact that the seeds develop after the latex (Duke, 1973; Schiff, 2002). However, in the late 1970's, it was noted that poppy seeds contained alkaloids found in opium (Grove et al., 1976). Meadway et al. (1998) highlighted that it was possible to fail a urine drug test after the consumption of a bread product containing poppy seeds (Meadway et al., 1998). Since then, it has become increasingly apparent that the presence of alkaloids in the food chain is a problem and can potentially lead to serious repercussions (Garnock-Jones and Scholes, 1990; Cassella et al., 1997; Bonicamp and Santana, 1998; Meadway et al., 1998; Sproll et al., 2006; Cone and Huestis, 2007; Lachenmeier et al., 2010; Chen et al., 2014; Smith et al., 2014). In Germany in particular, where poppy seeds are used and readily incorporated into food products, measures have been taken to reduce the amount of morphine present in poppy seeds intended for the food chain. It has been reported that poppy seeds used for decorative purposes can contain up to 100 mg/kg of morphine however, German authorities have recommended a limit of 20 mg/kg (Sproll et al., 2007). The European Food Safety Authority (EFSA) have published information relating to alkaloids in food products and provided a risk assessment with respect to public health (EFSA, 2011). The Report highlighted the requirement to estimate the dietary morphine exposure. Based on information provided from three European countries it was estimated that daily intake of morphine ranged from 3–90 μg/kg body weight per day. It was also hypothesized, using the same data that portions of food items having high poppy seed content could provide morphine exposure in the range 38–200 μg/kg body weight per portion for adults. From evaluation of extensive scientific literature sources,

TABLE 1 | Alkaloid content by % weight of opium in *Papaver setigerum* and *Papaver somniferum*.

	Papaver subspecies	
Alkaloid	***Setigerum****	***Somniferum*⁺ %**
Morphine	2.3%	7.65–25.15
Codeine	2.6%	1.21–6.37
Thebaine	Detected but not quantified	0.97–6.38
Papaverine	4.7%	0.51–5.33
Noscapine	10.2%	4.03–15.22

**as determined by electrophoresis (Panicker et al., 2007), ⁺as determined by HPLC (Krenn et al., 1998).*

TABLE 2 | Poppy seed source and country of origin.

Poppy seed source reference	Country of origin stated on label
#1	China
#2	Unknown
#3	Turkey
#4	Unknown
#5	Holland
#6	Netherlands
#7	Unknown
#8	Netherlands

the EFSA panel concluded that it was possible for an individual to suffer effects from ingestion of poppy seed products. Importantly it has also been shown that washing, and other pre-treatments, of the seeds can reduce morphine levels by up to 90%; it is believed that the alkaloid content of poppy seeds is due to external contamination from the pod previously containing the latex and not from the inside of the seeds (Sproll et al., 2006). It is known that the ingestion of poppy seeds has caused positive opiate drug test results with positive opiate results have been found in urine, blood, and oral fluid (Cassella et al., 1997; Bonicamp and Santana, 1998; Meadway et al., 1998; Rohrig and Moore, 2003; Wong et al., 2005; Carlin, 2009; Jankovičová et al., 2009; Lachenmeier et al., 2010; Chen et al., 2014).

In this study, the aim was to establish if thermal processing methods, the food matrix employed and the source of poppy seeds would affect the levels of opium alkaloids identified pre- and post-baking. The main reason for this was to establish if normal food preparation techniques, employed when using poppy seeds, would ultimately affect the opium alkaloids reaching the food chain. Ultimately this will influence drug-testing results or have a potential clinical impact on an individual.

EXPERIMENTAL

Chemicals, Reagents and Poppy Seeds

Organic solvents (acetonitrile, chloroform, isopropyl alcohol, diethyl ether, and methanol) of HPLC grade were purchased from Sigma-Aldrich (Poole, Dorset). Deuterated morphine (100 $\mu g/mL^{-}$ in methanol was purchased from Sigma Aldrich (Poole, Dorset). Liquid nitrogen was obtained from BOC Industrial Gases (Manchester). Poppy seeds were purchased from a number of retail outlets in the UK with the country of origin identified where available (**Table 2**).

LC-MS Instrument

HPLC was performed using an LC Surveyor system (Thermo Finnigan, Hemel Hempsted, UK) which was equipped with a pump, auto-sampler, and column heater. Mass spectrometry was performed using an LCQ advantage (Thermo Finnigan, Hemel Hempsted, UK) ion trap mass spectrometer. An Allure pentafluorophenyl phase with a propyl spacer (PFPP) column

TABLE 3 | Mobile phase composition and gradient program for HPLC.

Mobile phase composition

Solvent A: Water + 2 mM ammonium formate + 0.2% formic acid, pH 2.4

Solvent B: Acetonitrile + 2 mM ammonium formate + 0.2% formic acid, pH4.8

Time (mins)	%A	%B	Flow rate (μL/min)
0.00	90	10	350
2.00	90	10	350
10.00	10	90	350
11.00	10	90	350
12.00	90	10	350
14.00	90	10	350

TABLE 4 | Analyte specific parameters for LCQ Advantage mass spectrometer from HPLC.

Compound	*m/z*	Monitored transition mass *(m/z)*	Collision Energy (eV)
Morphine	286	286 → 201, 229	33
Morphine-d3	289	289 → 201, 229	30
Codeine	300	300 → 215, 243, 282	32
Thebaine	312	312 → 183, 249, 281	28
Papaverine	340	340 → 202	36
		202 → 171	32
Noscapine	414	414 → 220, 353	29

5 μm, 50 × 2.1 mm fitted with an Allure PFPP 10.0 × 2.1 mm guard column (both Restek, Buckinghamshire, UK) were employed. The HPLC was run using a gradient method (**Table 3**) with the column thermostated to 40°C and the autosampler tray held at 8°C.

The mass spectrometer was operated in positive mode ionization with the specific instrument parameters shown in **Table 4** (Carlin et al., 2017).

Figure 2 shows the extracted ion chromatograms for each of the alkaloids being analyzed in this work, including deuterated morphine as an internal standard. An overall run time of 12 min was employed, with all analytes of interest eluting before 10 min.

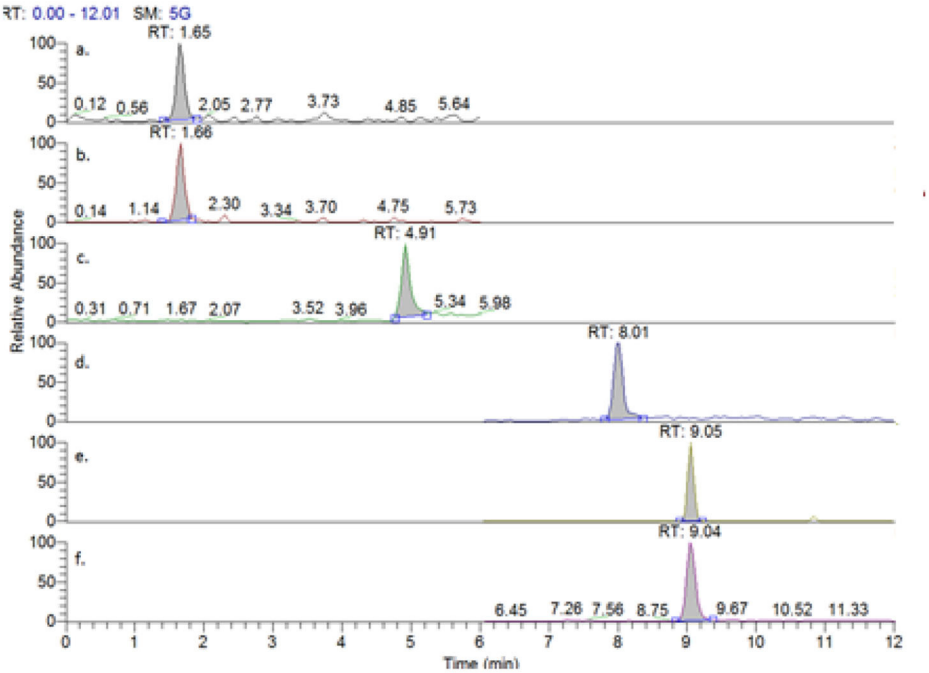

FIGURE 2 | Extracted chromatograms from a mixed injection of (a) morphine, (b) morphine-d3, (c) codeine, (d) thebaine, (e) papaverine, and (f) noscapine.

TABLE 5 | Validation parameters for morphine, codeine, thebaine, papaverine, and noscapine.

Compound	Linear equation	R^2	Concentration range (ng/mL)	LOQ (ng/mL)	LOD (ng/mL)	Precision %CV	Repeatability %CV
Morphine	y = 0.0047x−0.0100	0.9957	0–200	10	1.5	1.1	2.9
Codeine	y = 0.014x−0.0675	0.9976	0–200	10	2	2.7	4.8
Thebaine	y = 0.0214x−0.2152	0.9915	0–200	10	2	1.5	4.5
Papaverine	y = 0.019x−0.1795	0.9952	0–400	10	2	1.8	5.8
Noscapine	y = 0.0735x−0.6081	0.9985	0 – 500	10	1.5	3.6	4.6

Method Validation

In the validation of the LC-MS method, calibration models were prepared by using the concentration versus the ratio of the drug peak area/internal standard peak area. A minimum of six calibration points, plus a blank, were used with the concentration range and associated linear equations and R^2 values (**Table 5**). A calibration set was analyzed alongside every data set. The limit of detection (LOD) for this method was determined to be <2 ng/mL and the limit of quantitation (LOQ) was determined to be 10 ng/mL. Precision and accuracy were found to be less than 6% for all alkaloids. Analyte specific validation data is shown in **Table 5**.

Alkaloid Extraction From Poppy Seeds

Seven solvents, which covered a broad range of polarity index values (**Table 6**) and a solvent mix, chloroform: isopropanol (90:10, v/v), were investigated with respect to alkaloid extraction efficiency.

For each solvent, extractions were carried out at a different pH's (i.e., pH 3.5, pH 5.0, pH 7.0, and pH 9.0) to obtain the optimum extraction conditions for the alkaloids from the poppy seeds. To avoid contamination by plastic residues from pipette tips by the solvents, glass pipettes were employed.

Poppy seeds from a portion of the #1 seeds were homogenized using a spice blender and approximately 200 mg of the seeds were weighed into glass Durham tubes (four tubes for each of the solvents). For each solvent, the pH was altered to produce a solution of poppy seeds and solvent (1 mL) at the specified pHs. To each solution, deuterated internal standard (morphine-d_3) was added. The tubes were then capped and placed into an ultrasonic bath for 10 min, centrifuged at 4,000 rpm for 10 min. The appropriate layer was transferred to a clean glass tube, where it was dried down under nitrogen at 40°C and reconstituted in 100 µL of aqueous mobile phase: extracts were filtered using a 0.22 µm nylon syringe filter before being transferred to a glass insert held in an auto-sampler vial for the LC-MS instrument.

Calibration solutions were prepared in the mobile phase on the day of analysis for each of the extractions. The resultant equations from the calibration were used to determine the concentration of the solution of poppy seeds; the final alkaloid levels in ng/g were determined by taking into account the dilution factor from the solvent and the original weight of the poppy seeds used. The reason that calibration curves were produced on each analysis day was that it was shown in previous extractions, that small sub-samples of poppy seeds from the same packet/batch showed much variation of the concentration of the alkaloids present. This is in keeping with the findings of other researchers, who identified a variation in opium alkaloids within a batch and between batches of poppy seeds analyzed (Bozan and Temelli, 2008; López et al., 2018).

Preparations of Poppy Seeds and Bakery Products

Poppy Seed Muffins

Mini poppy seed muffins were prepared by mixing together 175 g of self-raising flour, 112 g of caster sugar, 50 g of poppy seeds, ½ teaspoon of bicarbonate of soda, 70 g of melted butter, two small eggs, the zest of one lemon, and 175 mL of skimmed milk. The ingredients were mixed into a batter and added to each of the dimples of mini-muffin trays purchased from Lakeland (Ambleside, Cumbria). The trays were then placed into an electric oven set to 180°C and left to cook for 15 min. The final weight of poppy seeds in each mini-muffin was approximately 1.8 g. They were then left to cool to room temperature. Each poppy seed muffin weighed ∼20 g. The poppy seed muffins were immersed in liquid nitrogen, crushed using a mortar and pestle and transferred to a spice blender for homogenisation prior to extraction and analysis by LC-MS. The LC-MS method employed has been previously reported in the literature (Carlin et al., 2017). The liquid nitrogen method was found to be easiest to apply to the muffins: this was due to the fact that the poppy seeds were incorporated into the sponge of the muffin. Trying to extract each poppy seed from the matrix proved very time consuming and was also considered that any alkaloids that may have interacted with the muffin matrix may also be included in results. Less fatty emulsion was also formed during the extraction method, when liquid nitrogen was employed.

TABLE 6 | Extraction solvents and associated polarity index values.

Solvent	Polarity index (snyder)[1]
Diethyl ether	2.8
Dichloromethane	3.1
Chloroform	4.1
Isopropanol	4.3
Acetonitrile	5.8
Methanol	6.6
Water	9
Chloroform/isopropanol (90:10, v/v)	Unknown

[1] *Snyder's Polarity Index Values of Common Laboratory Solvents. Available online at: http://www.sanderkok.com/techniques/hplc/eluotropic_series_extended.html#1.*

Poppy Seed Topped Rolls

A comparative study was carried out to establish if there was a difference between alkaloid levels resulting from poppy seeds incorporated into the matrix of the muffin to those resulting from poppy seeds coated onto a bread roll. The dough for the rolls was prepared using 280 g of strong white bread flour, 1½ tablespoons of sugar, one teaspoon of salt, ¾ teaspoon of fast action yeast, two tablespoons of skimmed milk powder, 150 mL of water, and two tablespoons of oil. The dough was mixed in a commercially available Morphy Richards compact bread maker (using the "dough" program). The dough was then split into 4 equal portions and each one was pressed into poppy seeds. The rolls were then placed into an oven at 190°C and left to cook for 25 min, according to the recipe of the bread mix. The rolls were left to cool to room temperature and the poppy seeds were scraped from the surface using a metal spatula and homogenized in a spice blender prior to extraction and analysis by LC-MS.

TABLE 7 | Range and mean weight of alkaloids (ng/g) in poppy seeds.

	Morphine		Codeine		Thebaine		Noscapine	
Poppy seed source reference	Mean weight (ng/g)	Range (ng/g)	Mean weight (ng/g)	Range (ng/g)	Mean weight (ng/g)	Range (ng/g)	Mean weight (ng/g)	Range (ng/g)
#1	1233	233–3,197	2,308	1,426–4,520	1,251	285–2,480	ND	ND
#2	29,652	2,638–63,994	8,507	474–23,307	42,950	1,977–133,493	ND	ND
#3	121	ND–769	157	ND–651	ND	ND	ND	ND
#4	ND	ND	72	52–106	ND	ND	ND	ND
#5	5,840	864–10,837	2,610	ND–5,441	6,363	841–12,561	534	ND–2,970
#6	1,620	141–4,223	153	61–349	112	ND–343	ND	ND
#7	1,059	ND–4,754	5,688	236–14,607	ND	ND	2,224	291–10,700
#8	62	ND–312	117	94–157	ND	ND	ND	ND

ND, not detected.

Thermally Processed Poppy Seeds

In order to assess if the muffin matrix had any effect on the level of alkaloids found in the poppy seeds, raw poppy seeds from different suppliers were placed on a baking tray and heating at 180°C for 15 min: they were then left to cool to room temperature, homogenized in a spice blender prior to extraction and analysis by LC-MS.

RESULTS AND DISCUSSION

Extraction Method

The resulting chromatograms from the poppy seed extractions were obtained for each of the alkaloid compounds and were compared with respect to the presence of alkaloid and internal standard peaks, peak shape, and interferences from the matrix/solvent combination. It was found that at the extremes of the polarity scale (diethyl ether, dichloromethane, and water), the chromatograms produced were complex and with poor peak shape for the alkaloids; these observations were independent of pH.

In contrast, the optimum result, in terms of alkaloid presence and peak shape, was obtained using the solvent mixture i.e., chloroform: isopropanol (90:10, v/v) at pH 3.5. For this reason, this extraction solvent mixture was used for all subsequent extraction's.

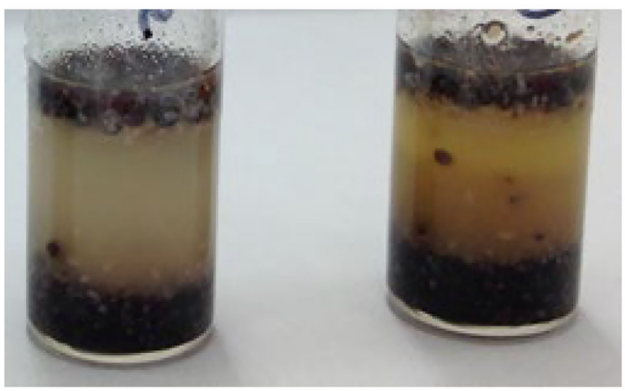

FIGURE 3 | Sample tubes containing poppy seed muffin and extraction solvent, post agitation, and centrifugation.

Harvested Poppy Seeds

From each batch of poppy seeds, a minimum of six different portions (weighing ∼200 mg) were extracted and analyzed. For each source, the mean weight of each of the alkaloids in poppy seeds was calculated. When the levels of morphine in poppy seeds from each of the different sources was compared (**Table 7**), it was found that there was much variation within batch but also between sources of poppy seeds. For example, no morphine was identified in any of the 15 randomly selected portions of seeds from source #4 however from source #2, when 15 randomly selected portions of these seeds were analyzed, the levels of morphine ranged from 2,638–63,994 ng/g. The range is provided to show the extent of the variation and is in keeping with other publications of this nature (López et al., 2018). There is much variation in the extracted opiate compounds, which is primarily due to the environmental differences of the seeds (Katrine et al., 2018; Lahiri et al., 2018). The country of origin for both of these poppy seed sources is unknown.

When the same comparison was carried out for codeine (**Table 7**) it was also found that there was much variation within different portions of the same batch and between sources of poppy seeds as was the case with morphine. Source #2, which was found to have a level of morphine much higher than the other sources, was also found to have a higher level of codeine. No other similarities can be drawn from the data. When this same comparison was carried out for thebaine (**Table 7**) it was found that of the poppy seeds analyzed, 50% of the source seeds did not contain thebaine. It was also found that the same source with the highest levels of morphine and codeine also exhibited the highest levels of thebaine.

Noscapine was identified in only two of the eight sources of poppy seeds (**Table 7**). It was found that the seeds from source #7 contained the highest levels of noscapine of the two sources where noscapine was identified. When the levels of the other alkaloids present in source #7 seeds, it was found that morphine (ND−4,754 ng/g) and codeine (2,361–14,607 ng/g) were also

TABLE 8 | Comparison of levels of alkaloids identified in harvested poppy seeds, seeds from the surface of bread rolls and seeds heated with no matrix.

		Harvested		Seeds on bread roll		Heated (no matrix)	
Source reference	**Alkaloid**	**Mean (ng/g)**	**Range (ng/g)**	**Mean (ng/g)**	**Range (ng/g)**	**Mean (ng/g)**	**Range (ng/g)**
#1	Morphine	545	8–1,888	11	ND−33	63	ND−304
	Codeine	82	ND−284	3	ND−27	5	ND−54
#6	Morphine	217	ND−431	1	ND−11	ND	ND
	Codeine	175	ND−418	3	ND−21	ND	ND
	Papaverine	11	ND−64	ND	ND	ND	ND
	Noscapine	34	ND−80	ND	ND	ND	ND
#8	Morphine	25	ND−96	ND	ND	15	ND−49
	Codeine	30	ND−81	5	ND - 19	11	ND−52

ND, not detected.

identified at levels in the higher range with the respect to the other sources. Papaverine was detected in some of the analyzed seeds but peaks were so small that it was not possible to quantify them. Source #2 was found to contain morphine (2,638–63,994 ng/g), codeine (474–23,307 ng/g) and thebaine (1,977–133,493 ng/g) at levels higher in comparison to other sources. It has been identified that sub-varieties of *Papaver somniferum L.* will have different alkaloid content and compositions (EFSA, 2011; Stranska et al., 2013). However, this taxonomic information was not available from the suppliers of the seeds.

It has been known since 1920 (Annett, 1920) that factors, such as the season in which the plants are grown, weather conditions, and quality and type of fertilizer used can greatly affect the levels of alkaloids biosynthesised by *Papaver somniferum L.* In turn, the levels of alkaloids found in opium latex will also be affected. No data currently exist that compares levels of alkaloids in opium latex and alkaloids from the same plant but it is assumed that the levels would correlate. On this basis, the country of origin, where the plant was grown in the field (e.g., in the shade or direct sunlight) and the quality of the soil can all affect the levels of alkaloids in the poppy seeds (Moeller et al., 2004; Sproll et al., 2006). This means that if a batch of poppy seeds is harvested from one field, naturally there will be variation in the levels of alkaloids from each of the plants. It has also been shown that the alkaloids present in the opium latex may contaminate the poppy seeds as part of the growing process and that a batch of poppy seeds is the combination of multiple fields in one country: all of these factors may explain why there is such variation within batch and between sources of poppy seeds.

Harvested Versus Thermally Processed Poppy Seeds

A comparison was carried out to establish if there was a difference in the levels of alkaloids identified between harvested poppy seeds, as described above, poppy seeds which were baked on top of a bread roll, poppy seeds incorporated into a muffin matrix, and poppy seeds heated in an oven in the absence of bread/muffin matrix. For each supermarket source of harvested poppy seeds, poppy seeds heated without matrix, and poppy seeds scraped from the bread roll, 15 randomly selected portions from each packet weighing ∼200 mg were extracted and analyzed while for the poppy seed muffins, ∼400 mg of homogenized poppy seed/muffin mixture was extracted. However, the muffin matrix greatly interfered with the extraction process. During the extraction process, a fatty emulsion was formed which affected further sample preparation techniques (**Figure 3**). These aliquots were filtered twice prior to being transferred into HPLC vials however when the chromatograms were analyzed for these muffin extractions, no alkaloids were identified. For this reason, it was not possible to include the poppy seed muffins extract results in the comparison between harvested poppy seeds, thermally processed seeds on their own and poppy seeds on the top of bread buns. In addition, seed portions from three randomly selected sources were extracted and analyzed with the results shown in **Table 8**. Again, as was established with extractions of harvested poppy seeds there was much variation in the alkaloids identified and in the levels of those alkaloids present, Deuterated morphine was added prior to extraction of the alkaloids from the seeds and percentage extractions were incorporated into the calculations.

What was identified from this data was that whether the seeds were heated on the surface of the bread roll or were heated with no bread matrix, the levels of alkaloids (if detected) were considerably lower than in the harvested seeds. Koleva et al. (2012) reported that morphine content could be reduced by 10–50% in the process of baking while Sproll et al. (2007) reported that the process of grinding and baking could reduce the morphine content of poppy seeds by up to 84%.

When comparing the results from the current work to levels published in the literature (**Table 9**) it can be seen that these findings are in-keeping with those published by Sproll et al. (2006) however, their maximum concentrations for each of the alkaloids compared, was found to be higher than in the current study. This group of researchers employed an LC/MS/MS method for the detection of morphine, codeine, papaverine, and noscapine in poppy seeds. The work published by Grove et al. (1976) appears to show much lower levels for morphine and codeine and only these two alkaloids were included in this study. However, this could have been due to the sensitivity of the GC-MS instrument employed, the lack of information regarding the presence of other alkaloids present in poppy seeds at this time as the work reported by Grove et al. was published in 1976 when analytical instruments, such as GC-MS were not as sensitive as they are today.

The levels of alkaloids identified in the current work are generally lower than those found by Sproll et al. (2006) but this could be due to the same factors that may influence the

TABLE 9 | Comparison of alkaloids identified in poppy seeds.

	Current work	Grove et al. (1976)	Sproll et al. (2006)
Compound	**Range (ng/g)**		
Morphine	ND–63,994	600–2,300	1,000–270,000
Codeine	ND–23,307	100–500	ND–56,000
Thebaine	ND–133,493	NI	NI
Papaverine	ND	NI	ND
Noscapine	ND–10,700	NI	ND–21,000

ND, not detected; NI, not included in the study.

TABLE 10 | Comparison of alkaloids identified on harvested and thermally processed poppy seeds.

		Harvested	Seeds on bread roll	Heated (no matrix)
Source reference	**Alkaloid**	**(ng)**	**(ng)**	**(ng)**
#1	Morphine	5,666–11,330	49.5–59.4	912–1824
	Codeine	850–1700	40.5–48.6	324–648
#6	Morphine	1290–2590	16.5–19.8	–
	Codeine	1250–2500	31.5–37.8	–
	Papaverine	192–380	–	–
	Noscapine	240–480	–	–
#8	Morphine	290–580	–	147–294
	Codeine	240–490	28.5–34.2	156–312

levels of alkaloids in poppy seeds previously highlighted. This research has shown that alkaloid variation exists depends on the specific alkaloids, their source and thermal processing. It was clear from the data obtained in this current work, and from other studies published in the literature, that there is much variation in the levels of alkaloids identified in poppy seeds. This variation can be attributed to a variety of natural parameters, such as weather and soil conditions, but also in the way that the seeds are harvested (Lachenmeier et al., 2010). Processing methods prior to packaging and even the baking process has been shown to greatly affect the level of alkaloids (Sproll et al., 2007). The findings of this study correlate with the studies published in the literature.

When poppy seeds are consumed on a bun or roll, it has been estimated that each roll contains 1–4 g of poppy seeds (Lachenmeier et al., 2010). Due to the reduction of the levels of alkaloids in the baking process, it has been estimated that if the poppy seeds contained 100,000 ng/g of morphine, the amount of seeds ingested would not cause any significant effect on an individual (Sproll et al., 2006).

Assuming that the average salad contains 3–6 g (1–2 teaspoons) of poppy seeds and the average bread bun has between 1.5–1.8 g of poppy. In addition, if 3–6 g of heated ("toasted") poppy seeds would be used in a salad, the following values were calculated (based on the data obtained from **Table 8** and using the highest value of each alkaloid determined).

The EFSA Panel on Contaminants in the Food Chain defined an acute reference dose (ARfD) of 10 μg morphine/kg (10,000 ng morphine/kg) of body weight (EFSA, 2011). If one assumes a 70 kg body weight of an "average" adult, it is possible to safely ingest 700 μg (700,000 ng) of morphine. This value cannot be used when relating to young children, the elderly or individuals of poor health (Sproll et al., 2006). With respect to the values of morphine obtained in this work for harvested seeds, seeds on top of a bread roll and seeds heated with no matrix (**Table 10**) and taking into account the weights of poppy seeds used in a variety of food products mentioned above, the morphine ingested will not exceed the ARfD determined by the EFSA.

Recently, the EFSA published an update on these guidelines (Katrine et al., 2018). This update related to the detection of morphine, codeine, oripavine, noscapine, and papaverine in poppy seed samples whereas, the previous report related only to the levels of morphine entering the food chain. Codeine values were given in relation to morphine equivalents, using a conversion factor of 0.2. Noscapine and papaverine were considered in the most recent publication however, the data that was available to the EFSA did not allow for a hazard characterization but they did conclude that the presence of these compounds would not present a health concern. In relation to the presence of thebaine and oripavine (not included in the work of this paper), it was concluded that there was insufficient data to make any assessment. Based on these updated EFSA findings, the presence of the morphine and codeine in the poppy seeds analyzed in this work, would still would still fall below the recommendations outlined.

Currently, there are no guidelines on how poppy seeds entering the food chain should be treated prior to use (López et al., 2018). There is also little or no information on packaging of poppy seeds regarding what, if any, treatment has taken place prior to packaging. Since the ingestion of poppy seeds has been used as reasons for failure of workplace drug testing and roadside drug testing, more should be done to ensure as much information as is possible is available on the preparation methods of the seeds.

DATA AVAILABILITY STATEMENT

The datasets generated for this study are available on request to the corresponding author.

ETHICS STATEMENT

This work was approved by the Northumbria University Ethics committee. The university holds a UK Home Office Drug License for the storage and use of controlled drug standards and for the extraction of alkaloids from poppy seeds.

AUTHOR CONTRIBUTIONS

The laboratory work, analysis of data and writing was carried out predominantly by MC. JD and JA helped in the design and review of data and interpretation and all parties contributed to the writing and review of the article. All authors contributed to the article and approved the submitted version.

FUNDING

This work was funded with the support from the Department of Applied Sciences, Northumbria University.

ACKNOWLEDGMENTS

This work was carried out and submitted as part of a Ph.D., program by MC (Carlin, 2015). The work was carried out by JA while working at Northumbria University, United Kingdom.

REFERENCES

Annett, H. E. (1920). Factors influencing alkaloidal content and yield of latex in the opium poppy (*Papaver somniferum*). *Biochem. J.* 14, 618–636. doi: 10.1042/bj0140618

Aragón-Poce, F., Martinez-Fernández, E., Márquez-Espinós, C., Pérez, A., Mora, R., and Torres, L. M. (2002). History of opium. *Int. Congr. Ser.* 1242, 19–21. doi: 10.1016/S0531-5131(02)00600-3

Askitopoulou, H., Ramoutsaki, I. A., and Konsolaki, E. (2002). Archaeological evidence on the use of opium in the minoan world. *Int. Congr. Ser.* 1242, 23–29. doi: 10.1016/S0531-5131(02)00769-0

Bernath, J (ed). (1999). *Poppy: The Genus Papaver (Medicinal and Aromatic Plants - Industrial Profiles)*. Boca Raton, FL: CRC Press.

Bonicamp, J. M., and Santana, I. L. (1998). Can a poppy seed food addict pass a drug test? *Microchem. J.* 58, 73–79. doi: 10.1006/mchj.1997.1536

Bozan, B., and Temelli, F. (2008). Chemical composition and oxidative stability of flax, safflower and poppy seed and seed oils. *Bioresour. Technol.* 99, 6354–6359. doi: 10.1016/j.biortech.2007.12.009

Carlin, M. (2009). Forensic science: roadside drug testing. *Meas. Control* 42, 306–309. doi: 10.1177/002029400904201003

Carlin, M. G. (2015). *Development and Evaluation of an LC-ESI-MS Method for the Simultaneous Detection of Five Major Opium Alkaloids*. Northumbria University.

Carlin, M. G., Dean, J. R., Bookham, J. L., and Perry, J. J. B. (2017). Investigation of the acid/base behaviour of the opium alkaloid thebaine in LC-ESI-MS mobile phase by NMR spectroscopy. *R. Soc. Open Sci.* 4:170715. doi: 10.1098/rsos.170715

Cassella, G., Wu, A. H. B., Shaw, B. R., and Hill, D. W. (1997). The analysis of thebaine in urine for the detection of poppy seed consumption. *J. Anal. Toxicol.* 21, 376–383. doi: 10.1093/jat/21.5.376

Chen, P., Braithwaite, R. A., George, C., Hylands, P. J., Parkin, M. C., Smith, N. W., et al. (2014). The poppy seed defense: a novel solution. *Drug Test. Anal.* 6, 194–201. doi: 10.1002/dta.1590

Cone, E. J., and Huestis, M. A. (2007). Interpretation of oral fluid tests for drugs of abuse. *Ann NY Acad Sci.* 1098, 51–103. doi: 10.1196/annals.1384.037

Cordell, G. A. (2013). Fifty years of alkaloid biosynthesis in phytochemistry. *Phytochemistry* 91, 29–51. doi: 10.1016/j.phytochem.2012.05.012

Duke, J. (1973). Utilization of *Papaver*. *Econ. Bot.* 27, 390–400. doi: 10.1007/BF02860692

EFSA (2011). Scientific Opinion on the risks for public health related to the presence of opium alkaloids in poppy seeds. *EFSA J.* 9, 1–150. doi: 10.2903/j.efsa.2011.2405

Garnock-Jones, P. J., and Scholes, P. (1990). Alakloid content of *Papaver somniferum subsp. setigerum* from New Zealand. *N. Zeal. J. Biol.* 28:367–369. doi: 10.1080/0028825X.1990.10412320

Grove, M. D., Spencer, G. F., Wakeman, M. V., and Tookey, H. L. (1976). Morphine and codeine in poppy seed. *J. Agr. Food Chem.* 24, 896–897. doi: 10.1021/jf60206a022

Gumuscu, A., Arslan, N., and Sarihan, E. O. (2008). Evaluation of selected poppy (*Papaver somniferum L.*) lines by their morphine and other alkaloids contents. *Eur Food Res Technol.* 226, 1213–1220. doi: 10.1007/s00217-007-0739-0

International Narcotics Board (2016). *Supply of Opiate Raw Materials and Demand for Opiates for Medical and Scientific Purposes*.

Jankovičová, K., Ulbrich, P., and Fuknová M. (2009). Effect of poppy seed consummation on the positive results of opiates screening in biological samples. *Legal Med.* 11 (Suppl. 1), 416–418. doi: 10.1016/j.legalmed.2009.03.002

Kapoor, L. D. (1995). *Opium Poppy: Botany, Chemistry and Pharmacology*. Boca Raton, FL: Food Products Press.

Katrine, K. H., Jan, A., Lars, B., Margherita, B., Beat, B., Sandra, C., et al. (2018). Update of the scientific opinion on opium alkaloids in poppy seeds. *EFSA J.* 16:e05243. doi: 10.2903/j.efsa.2018.5243

Koleva, I. I., van Beek, T. A., Soffers, A. E. M. F., Dusemund, B., and Rietjens, I. M. C. M. (2012). Alkaloids in the human food chain – Natural occurrence and possible adverse effects. *Mol. Nutr. Food Res.* 56, 30–52. doi: 10.1002/mnfr.201100165

Krenn, L., Glantschnig, S., and Sorgner, U. (1998). Determination of the five major opium alkaloids by reversed-phase high-performance liquid chromatography on a base-deactivated stationary phase. *Chromatographia* 47, 21–24. doi: 10.1007/BF02466781

Lachenmeier, D. W., Sproll, C., and Musshoff, F. (2010). Poppy seed foods and opiate drug testing - where are we today? *Ther. Drug Monit.* 32, 11–18. doi: 10.1097/FTD.0b013e3181c0eee0

Lahiri, R., Lal, R. K., Srivastava, N., and Shanker, K. (2018). Genetic variability and diversity in Indian germplasm of opium poppy (*Papaver somniferum L.*). *J. Appl. Res. Med. Aroma. Plants* 8, 41–46. doi: 10.1016/j.jarmap.2017.10.001

López, P., Pereboom-de Fauw, D. P. K. H., Mulder, P. P. J., Spanjer, M., de Stoppelaar, J., Mol, H. G. J., et al. (2018). Straightforward analytical method to determine opium alkaloids in poppy seeds and bakery products. *Food Chem.* 242, 443–450. doi: 10.1016/j.foodchem.2017.08.045

Mahdavi-Damghani, A., Kamkar, B., Al-Ahmadi, M. J., Testi, L., Muñoz-Ledesma, F. J., and Villalobos, F. J. (2010). Water stress effects on growth, development and yield of opium poppy (*Papaver somniferum L.*). *Agric. Water Manag.* 97, 1582–1590. doi: 10.1016/j.agwat.2010.05.011

Martinez-Fernández, E., Aragón-Poce, F., Márquez-Espinós, C., Pérez-Pérez, A., Pérez-Bustamante, F., and Torres-Morera, L. M. (2002). The history of opiates. *Int. Congr. Ser.* 1242, 75–77. doi: 10.1016/S0531-5131(02)00781-1

Meadway, C., George, S., and Braithwaite, R. (1998). Opiate concentrations following the ingestion of poppy seed products - evidence for 'the poppy seed defence'. *Forensic Sci. Int.* 96, 29–38. doi: 10.1016/S0379-0738(98)00107-8

Miller, R. J., and Tran, P. B. (2000). More mysteries of opium revealed: 300 years of opiates. *Trends Pharmacol. Sci.* 21, 299–304. doi: 10.1016/S0165-6147(00)01516-9

Moeller, M. R., Hammer, K., and Engel, O. (2004). Poppy seed consumption and toxicological analysis of blood and urine samples. *Forensic Sci. Int.* 143, 183–186. doi: 10.1016/j.forsciint.2004.03.027

Mohsin, H. F., Wahab, I. A., Nasir, N. I. M., Zulkefl, N. H., and Nasir, N. I. S. M. (2012). The chemical investigation of *Papaver* seeds. *Int. J. Adv. Sci. Eng. Inform. Technol.* 2, 38–41. doi: 10.18517/ijaseit.2.4.211

Panicker, S., Wigno, H. L., and Ziska, L. H. (2007). Quantitation of the major alkaloids in opium from *Papaver setigerum*. *Microgram J.* 5, 13–19. Available online at: https://www.semanticscholar.org/paper/Quantitation-of-the-Major-Alkaloids-in-Opium-from-Panicker-Wojno/2dda9d97ce9483a117dbdba2b9338b5cba20f180

Rohrig, T. P., and Moore, C. (2003). The determination of morphine in urine and oral fluid following ingestion of poppy seeds. *J. Anal. Toxicol.* 27, 449–452. doi: 10.1093/jat/27.7.449

Schiff, P. L. (2002). Opium and its alkaloids. *Am. J. Pharm. Educ.* 66, 186–194. Available online at: https://pdfs.semanticscholar.org/03b1/b950aac345b24842803a0df94f15dae7380c.pdf

Smith, M. L., Nichols, D. C., Underwood, P., Fuller, Z., Moser, M. A., LoDico, C., et al. (2014). Morphine and codeine concentrations in human urine following controlled poppy seeds administration of known opiate content. *Forensic Sci. Int.* 241, 87–90. doi: 10.1016/j.forsciint.2014.04.042

Sproll, C., Perz, R. C., Buschmann, R., and Lachenmeier, D. W. (2007). Guidelines for reduction of morphine in poppy seed intended for food purposes. *Eur. Food Res. Technol.* 226, 307–310. doi: 10.1007/s00217-006-0522-7

Sproll, C., Perz, R. C., and Lachenmeier, D. W. (2006). Optimized LC/MS/MS analysis of morphine and codeine in poppy seed and evaluation of their fate during food processing as a basis for risk analysis. *J. Agr. Food Chem.* 54, 5292–5298. doi: 10.1021/jf0608975

Stermitz, F. P., and Rapoport, H. (1961). The biosyntheis of opium alkaloids. Alkaloid Interconversions in *Papaver somniferum* and *P. orientale*. *J. Am. Chem. Soc.* 83, 4045–4050. doi: 10.1021/ja01480a022

Stranska, I., Skalicky, M., Novak, J., Matyasova, E., and Hejnak, V. (2013). Analysis of selected poppy (*Papaver somniferum L.*) cultivars: pharmaceutically important alkaloids. *Ind. Crops Prod.* 41, 120–126. doi: 10.1016/j.indcrop.2012.04.018

Windle, J. (2013). Harms caused by China's 1906–17 opium suppression intervention. *Int. J. Drug Policy*. 24, 498–505. doi: 10.1016/j.drugpo.2013.03.001

Wong, R. C., Tran, M., and Tung, J. K. (2005). Oral fluid drug tests: effects of adulterants and foodstuffs. *Forensic Sci. Int.* 150, 175–180. doi: 10.1016/j.forsciint.2005.02.023

Yoshimatsu, K., Kiuchi, F., Shimomura, K., and Makino, Y. (2005). A rapid and reliable solid-phase extraction method for high-performance liquid chromatographic analysis of opium alkaloids from *Papaver* plants. *Chem. Pharm. Bull.* 53, 1446–1450. doi: 10.1248/cpb.53.1446

Conflict of Interest: The authors declare that the research was conducted in the absence of any commercial or financial relationships that could be construed as a potential conflict of interest.

frontiers in Chemistry

ORIGINAL RESEARCH
published: 25 September 2020
doi: 10.3389/fchem.2020.00693

Comprehensive Protocol for the Identification and Characterization of New Psychoactive Substances in the Service of Law Enforcement Agencies

*Ewa Bulska[1], Robert Bachliński[2], Michał K. Cyrański[1], Magdalena Michalska-Kacymirow[1], Wioletta Kośnik[1], Paweł Małecki[1], Karol Grela[1] and Michał A. Dobrowolski[1]**

[1] Faculty of Chemistry, Biological and Chemical Research Center, University of Warsaw, Warsaw, Poland, [2] Central Forensic Laboratory of the Police, Warsaw, Poland

OPEN ACCESS

Edited by:
Grzegorz Zadora,
University of Silesia of Katowice, Poland

Reviewed by:
Marco Vincenti,
University of Turin, Italy
Wei-Lung Tseng,
National Sun Yat-sen University, Taiwan
Bogumila Byrska,
Institute of Forensic Research (IFR), Poland

***Correspondence:**
Michał A. Dobrowolski
miked@chem.uw.edu.pl

Specialty section:
This article was submitted to Analytical Chemistry, a section of the journal Frontiers in Chemistry

Received: 06 March 2020
Accepted: 03 July 2020
Published: 25 September 2020

Citation:
Bulska E, Bachliński R, Cyrański MK, Michalska-Kacymirow M, Kośnik W, Małecki P, Grela K and Dobrowolski MA (2020) Comprehensive Protocol for the Identification and Characterization of New Psychoactive Substances in the Service of Law Enforcement Agencies. Front. Chem. 8:693. doi: 10.3389/fchem.2020.00693

A non-routine, comprehensive protocol for characterization of emerging new psychoactive substances (NPS) including chemical structures, impurities, as well as crystal structures, has been developed to facilitate the work of law enforcement agencies. A set of NPS has been synthesized, identified, and characterized by various analytical methods in order to be used as certified reference standards (CRMs). Seven selected compounds (5-IT, NM-2201, MT-45, AB-CHMINACA, UR-144, 5F-PB-22, and 4-CMC) were synthesized on the laboratory scale, then the process was upscaled to semi-technical. All products were analyzed by electrospray Q/TOF-MS/MS for molecular structure identification. The presence of by-products, as well as metal impurities, arising from the performed syntheses, were characterized by reversed phase liquid chromatography (RP-HPLC) with DAD and Q/TOF-MS detection and inductively-coupled plasma with quadrupole mass spectrometer (ICP-QMS), respectively. Additionally, the crystal structures of UR-144, NM-2201, 5F-PB-22, and 4-CMC have been determined by single-crystal and powder X-ray diffraction.

Keywords: new psychoactive substance (NPS), synthetic cannabinoid (SC), X-ray diffraction, ES Q/TOF MS/MS, LC-Q/TOF

INTRODUCTION

New psychoactive substances (NPS) are a large group of chemical compounds that have been available on the world market since the beginning of the twenty-first century[1,2]. They differ in composition, but have one common feature: they affect the central nervous system (CNS) of a human in a similar manner to previously known "classical" drugs. These substances are both synthetic and obtained from plants. They are known by many names: designer drugs, legal highs, bath salts, party pills, etc.

[1]European Monitoring Centre for Drugs and Drug Addiction. Available online at: http://www.emcdda.europa.eu/publications/edr/trends-developments/2019

[2]United Nations Office on Drugs and Crime. *Global SMART Programme*. Available online at: https://www.unodc.org/LSS/Page/NPS/GlobalSmart

According to their chemical structures, they can be divided into several main groups: synthetic cannabinoids, cathinones, phenylethylamines, tryptamines, benzodiazepines, piperidines, pyrrolidines, and opioids. The majority of new drugs on the market in Poland (and throughout Europe)[1] are synthetic cannabinoids, introduced as a legal alternative to marijuana[3], and cathinones, legal substitutes for amphetamines (DeRuiter et al., 1994).

The interest in synthesizing cannabinoids began with the synthesis of dl-Δ^1-tetrahydrocannabinol in 1965 (Mechoulam and Gaoni, 1965). Later, several research groups and commercial companies focused on synthesizing compounds with cannabimimetic activity. At first, only classical cannabinoids [e.g., HU-210 (Howlett et al., 1990) and Levonantradol (Koe, 1981)] were obtained. Non-classical cannabinoids [e.g., CP-47,497 and CP-59,540 (Melvin et al., 1984; Compton et al., 1992)] and AAIs (Huffman et al., 1994) were developed at the end of the twenty-first century after the so-called cannabinoid receptors CB1 (Matsuda et al., 1990) and CB2 (Munro et al., 1993) were identified and cloned. Since then, scientific interest in these compounds has increased leading to the synthesis of over 100 substances with high or medium affinity to the CB1 receptor[3].

Differently substituted *n*-alkyl indole or indazole-3-carbonyl derivatives are distributed around the world as synthetic cannabinoids. They appeared on the market in Europe around 2006 and were first detected toward the end of 2008. In 2018 a further 11 new synthetic cannabinoids were reported for the first time, bringing the total number reported to the EU Early Warning System to 190 (EU Drug Markets Report, 2019). This makes the synthetic cannabinoids the largest group of substances monitored by the EMCDDA, and reflects the overall demand for cannabis within Europe and the rapid pace by which manufacturers can produce and supply new cannabinoids to circumvent drug laws, and similar reports are coming from the other parts of the world[4] The race between illegal laboratories and law enforcement agencies is never-ending. Newly substituted compounds appear on the drug market just after their predecessors fall under regulation, meaning there is an essential need to develop rapid, effective, and easy to apply scientific techniques for the purposes of law enforcement.

Liquid chromatography combined with mass spectrometry (LC/MS) and tandem mass spectrometry (LC/MS/MS) has become a powerful tool for the identification and characterization of psychoactive substances as well as degradants, metabolites, and process impurities (Eckers et al., 1997). Among the many methods available, particularly noteworthy is liquid chromatography coupled to high-resolution quadrupole time-of-flight mass spectrometry (LC-Q/TOF) (Fornal et al., 2013). This technique enables the tentative identification of an unknown compound based on the prediction of its chemical formula from accurate ion mass measurement and characteristic isotopic pattern (Aszyk and Kot-Wasik, 2016). This technique is characterized by high sensitivity, selectivity, and versatility. Moreover, it is considered a very great tool for the identification of species and can be very useful when reference standards are not available. Additionally, the sample amount needed for the analysis is very small, and sample preparation is straightforward—it is just dissolved and analyzed (Eckers et al., 1997; Lee et al., 2009). The analytical protocol developed by this study was successfully used for the identification of various metabolites with a view to doping control (Kwiatkowska et al., 2018; Grucza et al., 2019). Modern LC-Q/TOF mass spectrometers offer high chromatographic and mass resolutions and high mass accuracy measurements of both parent and fragment ions and provide sufficient information to detect and identify compounds, even in complex matrices (Eckers et al., 1997). In this work, we used the high potential of LC-Q/TOF mass spectrometry for the effective identification of new psychoactive substances in our research.

The X-ray diffraction technique is not commonly used in NPS analysis, especially synthetic cannabinoids. This is mainly due to their physical form (plant or resin) found on the worldwide black market. Here we present crystal structures and diffraction patterns of three synthetic cannabinoids: UR-144, NM-2201, and 5F-PB-22; obtained by single-crystal and powder X-ray diffraction. The crystal structure of UR-144 was reported before (Banister et al., 2015) but has not been deposited in the Cambridge Structural Database (CSD) (Groom et al., 2016). We redetermined it at a lower temperature (sometimes a possible reason for phase transitions) and deposited all the structures in the CSD before publishing this article.

Only a few articles reporting crystal structures of synthetic cannabinoids have been published [e.g., (Hongfeng et al., 2005; Huffman et al., 2005; Nycz et al., 2010; Hong et al., 2011; Banister et al., 2013)]. There is a large need to develop the CSD further for new psychoactive substances. It may serve as a very quick and reliable source for identifying illicit substances, as it is a common tool, especially for the people working in the government laboratories.

In this article, the authors describe a carefully developed non-routine analytical protocol toward the comprehensive characterization of NPS. Selected physicochemical techniques make it possible to obtain the complementary information of NPS, namely those considered as emerging substances found on the illegal drug market. Completely characterized compounds could serve as reference substances to facilitate the work of law enforcement agencies. Thus, the combination of analytical instrumental techniques and X-ray diffraction may allow for rapid and credible studies of evidence collected at the crime scene. Moreover, such protocols could enable forensic scientists to gather supporting information that may be used for judicial purposes as incontestable proof.

[3] *United Nations Office on Drugs and Crime, Synthetic Cannabinoids in Herbal Products*. Available online at: http://www.unodc.org/documents/scientific/Synthetic_Cannabinoids.pdf

[4] *UNODC Laboratory and Scientific Section Portals*. Available online at: https://www.unodc.org/LSS/Announcement/Details/249b6412-8faf-46f1-8269-3dbd31d3bd40

MATERIALS AND METHODS

Synthesis of Compounds

We have synthesized seven NPS widely circulating on worldwide black markets[1,2] and belonging to 4 diverse groups: synthetic

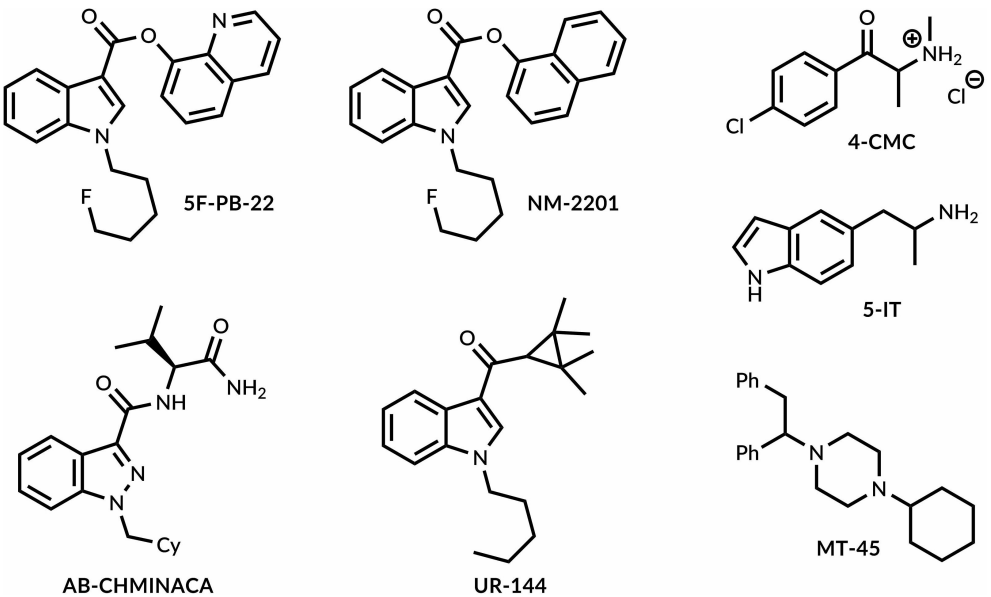

FIGURE 1 | Designer drugs synthesized in this study.

cannabinoids, cathinones, phenethylamine, and piperazine derivatives (**Figure 1**).

Syntheses of 5F-PB-22, NM-2201, and UR-144 were accomplished according to a modified Kassiou et al. procedure (Banister et al., 2015) (**Supplementary Schemes S1, S2** in the Electronic **Supplementary Material**, ESI). The key intermediate—*N*-(5-fluoropentyl)-indole-3-carboxylic acid—was obtained from indole in three steps (*N*-alkylation, acylation with trifluoroacetic acid anhydride, and hydrolysis of the corresponding trifluoromethyl ketone) with 88% overall yield. Subsequent esterification led to 5F-PB-22 and NM-2201 in 91 and 72% yield, respectively. UR-144 was obtained in good 58% overall yield in two steps (*N*-alkylation and acylation with 2,2,3,3-tetramethylcyclopropanecarboxylic acid) from commercially available indole.

Synthesis of 4-CMC was accomplished according to a modified Bak et al. procedure (Bak et al., 2019) (**Supplementary Scheme S3** in the ESI). The reaction was performed starting from commercially available 4-chloropropiophenone in a series of α-bromination and amination reactions and the desired product was obtained in a 68% overall yield.

Synthesis of MT-45 was performed according to a modified Umemoto et al. procedure (Natsuka et al., 1975) (**Supplementary Scheme S4** in the ESI). Here, the sequence of oxazolidine formation, Grignard reaction, and amination led to MT-45 in 46% overall yield.

Synthesis of 5-IT employed a modified Szabo *et al.* procedure (Troxler et al., 1968) (**Supplementary Scheme S5** in the ESI). Condensation of indole-5-carboxaldehyde with nitroethane, followed by lithium aluminum hydride reduction resulted in 5-IT in 75% overall yield.

Synthesis of AB-CHMINACA was accomplished according to a modified Kassiou et al. procedure (Longworth et al., 2016) (**Supplementary Scheme S6** in the **Supporting Information**). Protection of 1*H*-Indazole-5-carboxylic acid as methyl ester, followed by alkylation with (bromomethyl)cyclohexane and deprotection allows obtaining a key intermediate, *N*-(cyclohexylmethyl)indazole-5-carboxylic acid. Subsequent amidation with valinamide hydrochloride resulted in AB-CHMINACA in 58% overall yield.

Sample Description

The investigations were carried out for the selected NPS (UR-144, MT-45, 4-CMC, NM-2201, 5-IT, AB-CHMINACA, 5F-PB-22) synthesized on the laboratory scale as well as after upscaling to semi-technical. Groups of samples were named as "laboratory sample" (A) and "semi-technical' sample" (B).

Sample Preparation for Chemical Analysis

Laboratory (A) and semi-technical (B) samples were prepared as follows: approximately 1 mg of the individual product (compound of interest) was dissolved in 1 ml of acetonitrile (ACN), followed by a series of dilutions in ACN:H_2O (1:1) solution, depending on the detection method used (MS; MS/MS; UV-Vis).

Identification of Compounds After Synthesis

To identify the specific compounds, a main product of synthesis, the exact mass was measured and the parent ion was fragmented using a Q/TOF mass spectrometer (6540; Agilent) with direct sample introduction (syringe pump). The parameters of the mass spectrometer were as follows: ionization type: electrospray; ionization: positive ion mode; voltage on the capillary: 3,500 V;

TABLE 1 | HPLC setup parameters.

Solvent A	Ammonium formate 1 g/L in 10% ACN
Solvent B	Ammonium formate 1 g/L in 90% ACN
Column	LumiSep C18, 100 x 2.1, 3.0 μm
Velocity of mobile phase	0.5 mL/min
Injection	2.00 μL
Column temperature	35° C
Detector	DAD: 254 nm, 230 nm and 295 nm; ESI-MS-Q/TOF

TABLE 2 | Gradient elution program for HPLC separation.

Time [min]	% A	% B
0.0	100	0
3.00	100	0
8.00	0	100
8.01	100	0
15.00	100	0

gas temperature: 300° C; drying gas flow: 8 L/min; nebulizer: 35 psi; shielding gas temperature: 350° C; shield gas flow: 11 L/min; fragmentor voltage: depending on the compound 100 or 175 V; voltage on the collecting cone: 65 V; collision energy: 10, 20 and 40; mass range for MS scan mode: 100–950 m/z; mass range for MS/MS mode: 40–600 m/z.

Melting Points

Melting points were determined for UR-144, NM-2201, and 5F-PB-22 using a Mettler Toledo MP70 Melting Point System. They were 73.5, 122, and 87°, respectively.

Organic Impurities

It is essential to identify the impurities arising from the synthesis process for any items that may serve as a certified reference standard. To separate the main compounds and their potential impurities, reversed phase high-performance liquid chromatography (RP-HPLC) was used followed by a diode array detector (DAD) and a high-resolution mass spectrometer (Q/TOF-MS). An HPLC apparatus with a DAD detector (1290; Agilent) and a Q/TOF mass spectrometer (6540; Agilent) was used for that purpose. Chromatograms with DAD detection were recorded at three wavelengths (254, 230, and 295 nm). **Tables 1**, **2** present the parameters of the chromatographic separation, detectors, and gradient elution program. **Table 3** presents the parameters of the mass spectrometer.

Inorganic Impurities

To assess the elemental impurities, which can be introduced during the synthesis of all investigated products, ICP-QMS (NexIon 300D, Perkin-Elmer) was used. All compounds were subjected to microwave-assisted mineralization (Milestone MultiWave) before measurements. The validation of the analytical procedure was performed with the use of tetracycline and amoxicillin pure compounds as well as after the addition of known amounts of multi-element standards. **Table 4** presents the parameters of the ICP-MS conditions.

TABLE 3 | Experimental parameters for the MS/MS identification experiments.

Ionization: electrospray
Mode of ionization: positive
Voltage on capillary: 3,500 V
Gas temperature (1): 300° C
Gas flow (1): 8 L/min
Nebuliser pressure: 35 psi
Gas temperature (2): 350° C
Gas flow (2): 11 L/min
Voltage on fragmentor: 175 V
Voltage on skimmer: 65 V
Collision energy: 10, 20, and 40
Mass range for MS scan mode: 100–950 m/z
Mass range for MSMS mode: 40–600 m/z

TABLE 4 | Optimal measurement conditions for elemental analysis by ICP-MS.

Parameter	Description
Spray chamber	Scott, Quartz
Atomizer	Coaxial (Mainhardt)
Plasma torch	Quartz
Sampling cone	Nickel
The forming cone	Nickel
Frequency of the generator	40 MHz
Resolution of mass signals	(0.7 ± 0.05) a.m.u.
Generator power	1,000 W
Deflector voltage	−9 V
Voltage on the analog detector	−1,800 V
Voltage on the pulse detector	950 V
Plasma gas flow	15.00 L/min
Auxiliary gas flow	1.2 L/min
The flow of atomizing gas	0.89 L/min
Stop time	50 ms
The number of sweeps	20
Number of repetitions	3-5
Solution dispensing speed	1 mL/min

Compound Characteristics

As indicated above, all the compounds were synthesized at the University of Warsaw. We were able to obtain crystals of UR-144 (**1**), NM-2201 (**2**), 5F-PB-22 (**3**), and 4-CMC suitable for X-ray experiments by slow evaporation from ethanol. Single crystals were measured at 130 (2) K on a Bruker D8 Venture Photon100 diffractometer with a TRIUMPH monochromator and MoK_α fine-focus sealed tube ($\lambda = 0.71073$ Å). The structure of 4-CMC has been deposited earlier at ambient conditions (Nycz et al., 2016). We redetermined it at low temperature (to check for possible phase transitions) but, as we would like to focus on crystal structures of synthetic

TABLE 5 | Crystal data and structure refinement for: UR-144 (1), NM-2201 (2), 5F-PB-22 (3).

Compound	(1)	(2)	(3)
Empirical formula	$C_{21}H_{29}N_1O_1$	$C_{24}H_{22}F_1N_1O_2$	$C_{23}H_{21}F_1N_2O_2$
Formula weight	311.45	375.43	376.43
Temperature [K]	130	130	130
Space group	$P2_1/n$	$P2_1/c$	$P\text{-}1$
Unit cell dimensions			
a [Å]	12.0920(5)	12.0583(6)	8.388(5)
b [Å]	10.7612(4)	13.5389(8)	10.309(7)
c [Å]	13.9030(5)	11.4574(6)	11.853(6)
α [°]	90	90	68.75(3)
β [°]	93.743(2)	95.100(2)	86.52(2)
γ [°]	90	90	79.24(3)
Volume V [Å^3]	1805.26(12)	1863.09(17)	938.5(9)
Z [molecules/cell]	4	4	2
$D_{calculated}$ [g cm^{-3}]	1.146	1.338	1.332
Absorption coefficient μ/ mm^{-1}	0.069	0.091	0.092
θ range for data collection [°]	2.31-25.00	2.27-25.00	2.15-25.50
Limiting indices	$-14 \leq h \geq 14$	$-14 \leq h \geq 14$	$-10 \leq h \geq 10$
	$-12 \leq k \geq 12$	$-16 \leq k \geq 16$	$-12 \leq k \geq 12$
	$-16 \leq l \geq 16$	$-13 \leq l \geq 13$	$-14 \leq l \geq 14$
Reflections collected/unique	25,423/3,170	21,433/3,279	27,748/3,491
Data/parameters	3,170/214	3,279/254	3,491/348
Goodness of Fit	1.047	1.152	1.125
Final R index ($I > 2\sigma$)	0.0348	0.0401	0.0390
wR^2	0.0830	0.0803	0.0855
Largest diff. Peak and hole [Å^{-3}]	0.232 and −0.184	0.212 and −0.192	0.248 and −0.267
CCDC	1842294	1842293	1842292

cannabinoids in this article, for details please refer to the Electronic **Supplementary Information** (ESI).

The crystals were positioned 40, 50, and 100 mm from the CCD camera for (**1**), (**2**), and (**3**), respectively. A total of 1,613, 340, and 1,101 frames were measured with exposure times of 8.96, 0.28, and 0.31 h for (**1**), (**2**), and (**3**). Data were collected using the APEX2 program (APEX2, 2013), integrated with the Bruker SAINT software package (SAINT, 2013), and corrected for absorption effects using the multi-scan method (SADABS) (SADABS, 2012). The structures were solved and refined using the SHELX Software Package (Sheldrick, 2015) with the atomic scattering factors taken from the International Tables (International Tables for Crystallography, 1992). Crystal data and structure refinement are specified in **Table 5**. The structure of (**3**) is disordered with a fluorine atom at two alternative sites with 75–25% occupancies. The figures were generated with Mercury (ver. 4.2.0) (Macrae et al., 2006).

CCDC 1842292-1842294, 1943878 contains the supplementary crystallographic data for this paper. These data can be obtained free of charge via http://www.ccdc.cam.ac.uk/conts/retrieving.html.

Powder X-ray diffraction measurements were performed at room temperature on a Bruker D8 Discover diffractometer ($CuK_{\alpha1}$ and $CuK_{\alpha2}$ radiation in a *ca.* 2:1 intensity ratio). The samples were placed in sealed quartz capillaries (0.5 mm diameter).

RESULTS AND DISCUSSION

Identification of Products of Synthesis

The first approach was to perform the identification of all synthesized compounds obtained on both the laboratory and semi-technical scales. This was done according to the common, validated scheme, exemplified by the 5F-PB-22. The mass spectrum (MS) and fragmentation spectrum (MS/MS) are presented along with the proposed fragmentation path in **Figure 2**, for 5F-PB-22 obtained on the semi-technical scale (B). The careful evaluation of all spectra indicates the presence of a pseudomolecular ion $[M+H]^+$ at 377.1660 m/z units, dimer of pseudomolecular ion $[2M+H]^+$ at 753.3247 m/z units and the product of in-source fragmentation of the pseudmolecuar ion with m/z 232.1130 units. Below, the product ion spectra of the pseudomolecular ion $[M+H]^+$ (377.1660 m/z), acquired at a collision energy of 10 eV, is also shown with its proposed fragmentation path. The information gained from these ion product spectra confirms that the compound is 5F-PB-22.

Mass spectra for other compounds obtained on the semi-technical scale are presented in the supplementary material as follows: 5-IT (B)—**Supplementary Figure 18**, NM-2201 (B)—**Supplementary Figure 19**, AB-CHMINACA (B)—**Supplementary Figure 20,** and UR-144 (B)—**Supplementary Figure 21**.

To deduce the mass of the compound of interest from the mass spectra registered at MS/MS, the accuracy of measurements was established (**Table 6**). The mass accuracy (MA), expressed as part per millions (ppm) was calculated as follows:

$$MA = (M_{exp} - M_{theoret})/M_{theoret} \times 10^6$$

The results indicate that the accuracy of the mass measurements is high and enables satisfactory identification of the compounds of interest.

Finally, the evaluation of the mass spectra, toward the identification of the specific compound was performed for all investigated products of synthesis. Then, those products that were identified as expected underwent further characterization for their organic and inorganic impurities as well as crystal structures. This was considered necessary, to use them as standard compounds for judicial purposes.

Organic Impurities

The composition of synthesized products of psychoactive substances was also examined to determine possible organic impurities, which could be the by-products of the synthesis processes on both laboratory and semi-technical scales. For this purpose, a procedure for the separation of the tested compounds (main products of synthesis) and their potential impurities has been developed using liquid chromatography coupled with a high-resolution mass spectrometer (Q/TOF-MS). To exemplify

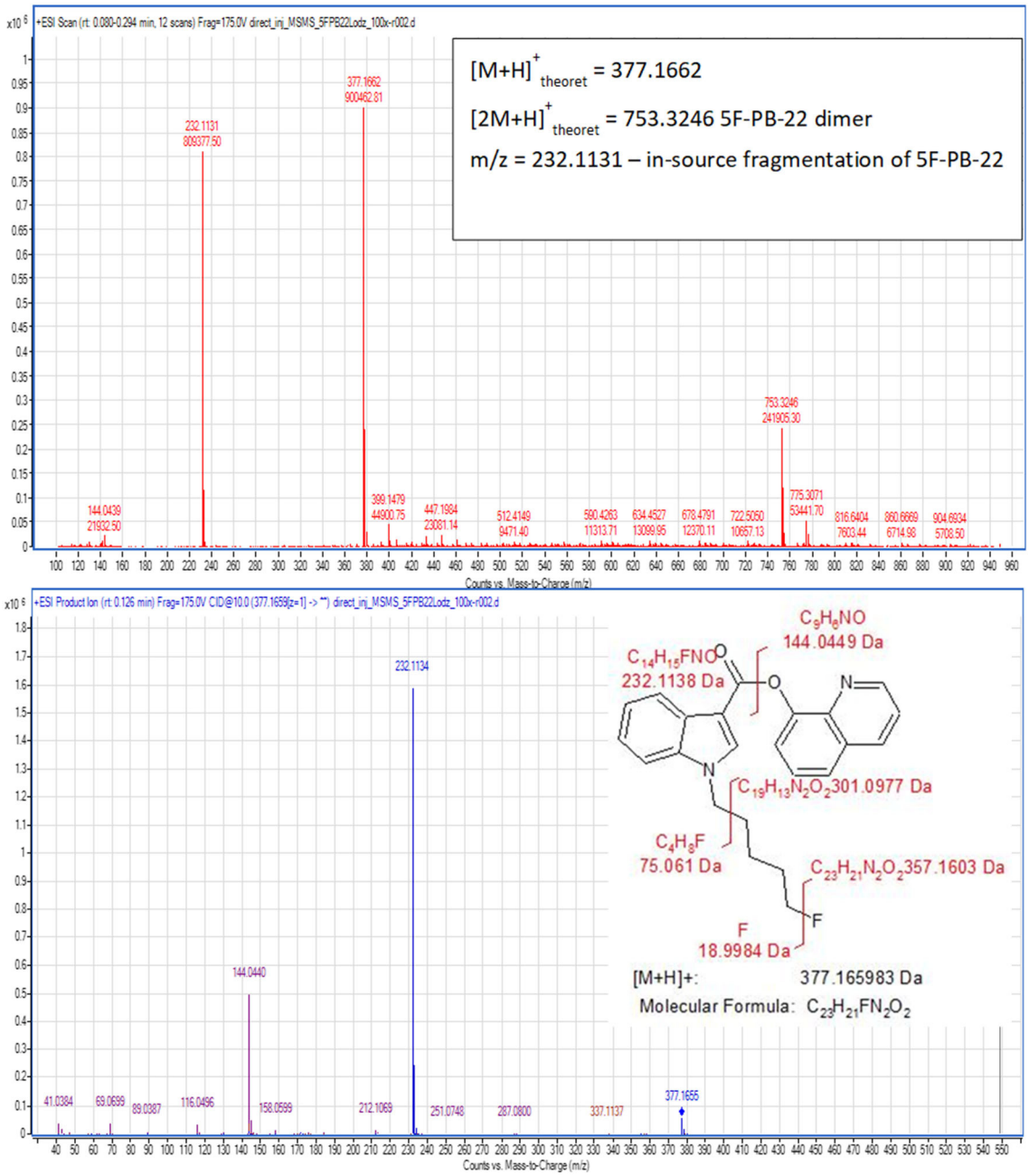

FIGURE 2 | Mass spectra for 5F-PB-22 (B).

the process, chromatograms of 5F-PB-22 on the laboratory (A) and semi-technical scales (B) are shown in **Figures 3**, **4**.

The other chromatograms obtained with the use of optimized separation parameters presented in **Tables 1**–**3** and the UV spectra of the individual compounds are presented in the ESI (**Supplementary Figures 22**–**28**).

The results show that the products of synthesis performed either on the laboratory or semi-technical scale are high-purity organic compounds. Those results prove that they can be considered as high-purity reference materials.

Inorganic Impurities

Although the organic impurities are the most important aspects considered for standard compounds with defined purity, in the course of this work it was essential to conduct the entire characterization of the obtained substances. For this purpose, the inorganic impurities, namely the elemental composition of the synthesis product were evaluated. The measurements were performed with ICP-MS and the following, most abundant isotopes were monitored: ^{51}V, ^{52}Cr, ^{55}Mn, ^{59}Co, ^{60}Ni, ^{63}Cu, ^{66}Zn, ^{88}Sr, ^{95}Mo, ^{101}Ru, ^{105}Pd, ^{107}Ag, ^{111}Cd, ^{137}Ba, ^{195}Pt, ^{205}Tl, ^{208}Pb,

TABLE 6 | The accuracy of measurements established for compounds obtained on the semi-technical scale.

Compound	Formula	$M_{theoret}$ (calculated m/z [M+H])	M_{exp} (measured m/z [M+H])	MA (mass accuracy) [ppm]
5F-PB-22 (B)	$C_{23}H_{21}FN_2O_2$	377.1659	377.1662	0.8
5-IT (B)	$C_{11}H_{14}N_2$	175.1230	175.1227	1.7
NM-2201 (B)	$C_{24}H_{22}FNO_2$	376.1707	376.1682	6.6
AB-CHMINACA (B)	$C_{20}H_{28}N_4O_2$	357.2285	357.2295	2.8
UR-144 (B)	$C_{21}H_{29}NO$	312.2322	312.2323	0.3

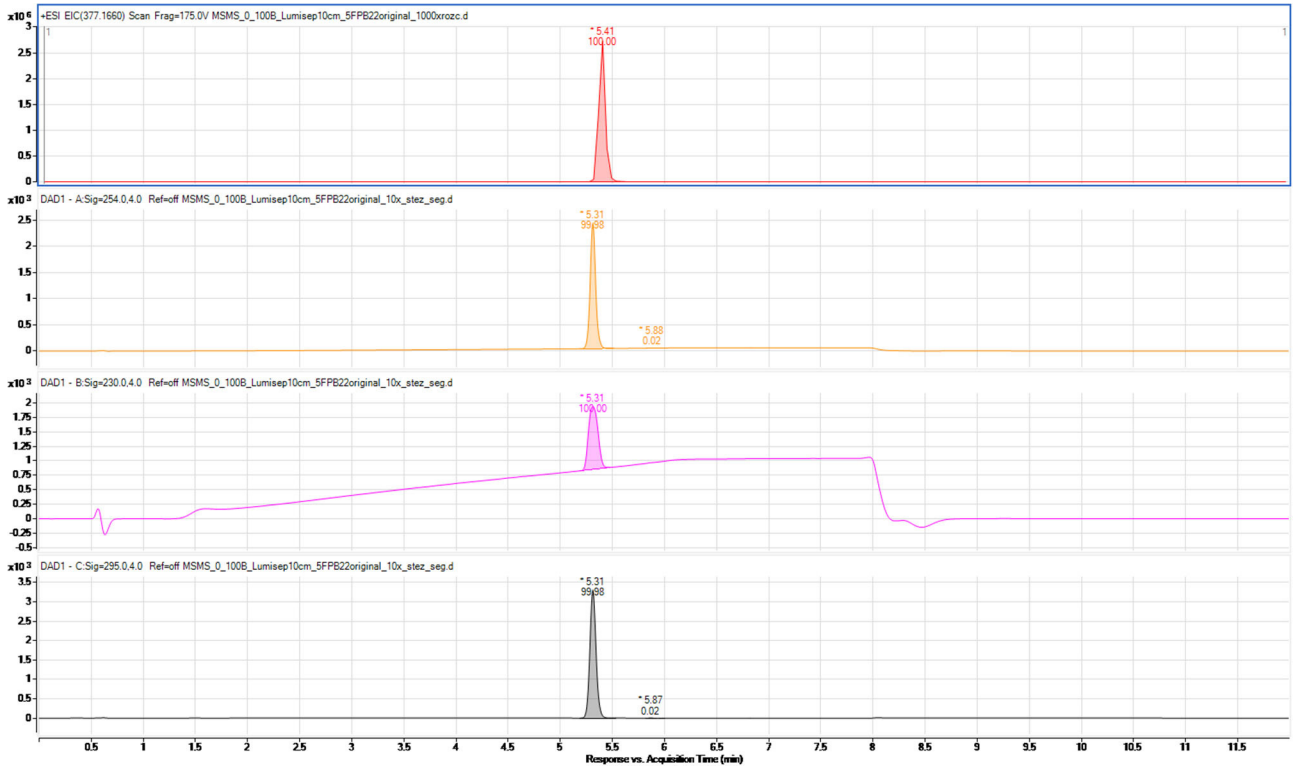

FIGURE 3 | Chromatogram of 5F-PB-22 synthesized on the laboratory scale (A). MS detection (extracted ion chromatogram) and UV-Vis at three wavelengths (254, 230, and 295 nm).

^{202}Hg. The values of the limit of detection (LOD) and limit of quantification (LOQ) are listed in **Table 7**.

The accuracy of the measurement condition was evaluated by the recovery either of spiked sample isotopes or of the elements measured in the presence of a defined matrix (tetracycline and amoxicillin solutions), which for all listed elements were no worse than 98 ± 5%.

All products of synthesis were examined for purities. Only those being characterized as pure with regard to organic impurities and those in which the content of listed elements was below the limit of detection (as presented in **Table 7**) were considered to be sufficient for crystallographic characterization.

To conclude, quantitative analysis of the elemental compositions indicated the high-purity of all synthesized substances, regardless of the scale of synthesis, which is essential to consider those substances as candidates for being Certified Reference Materials of established purity.

X-ray Diffraction

(1-Pentyl-1H-indol-3-yl) (2,2,3,3-tetramethylcyclopropyl) methanone, UR-144 (**1**) crystallizes in a monoclinic system, space group $P2_1/n$, with one molecule in an asymmetric part of the unit cell (**Figure 5**). The indole moiety is almost planar; the angle between the mean planes of the rings is 1.0°. The alkyl carbon chain is bent with respect to the nitrogen atom by 113.2° (C4-C5-N1). The structure is stabilized mostly by weak van der Waals interactions, but also weak C-H…π interactions in the crystal lattice. The latter involves the hydrogen atoms at C5 or C6 toward the centroid of the phenyl ring of the neighboring

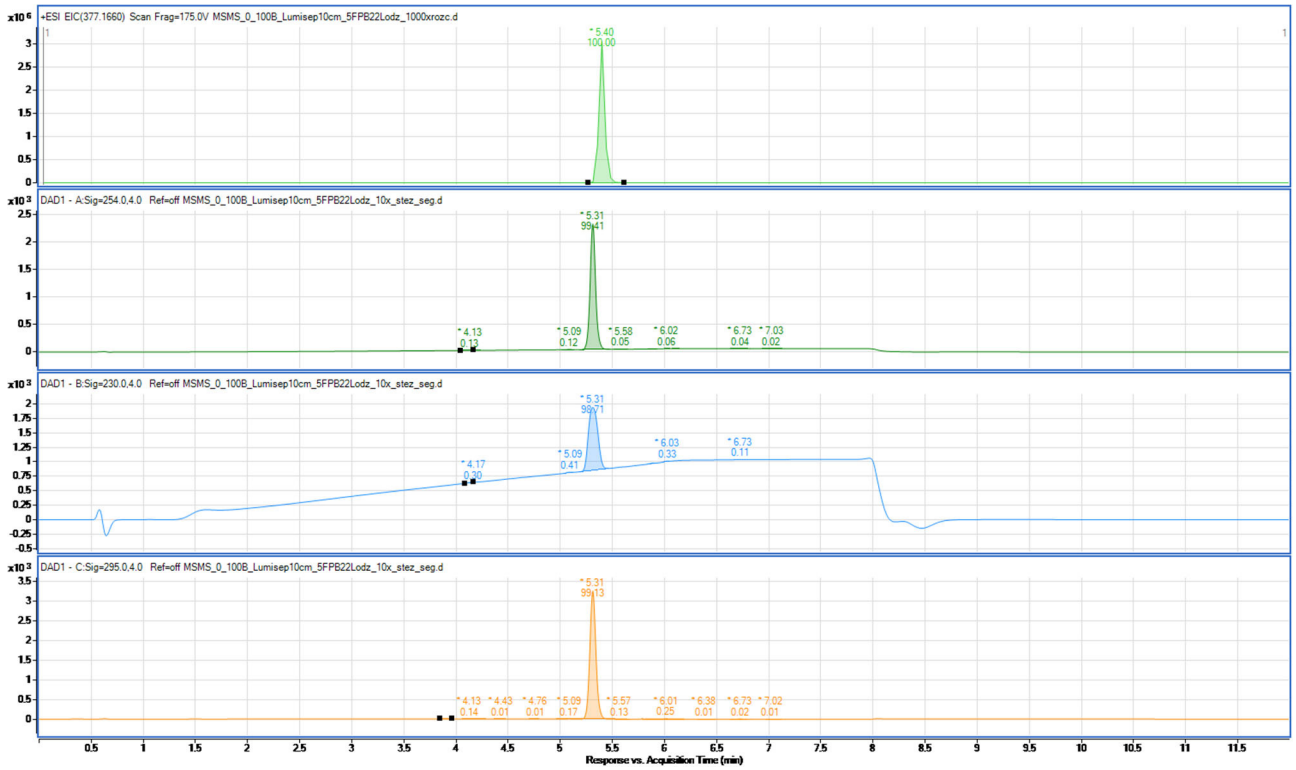

FIGURE 4 | Chromatogram of 5F-PB-22 synthesized on the semi-technical scale (B). MS detection (extracted ion chromatogram) and UV-Vis at three wavelengths (254, 230, and 295 nm).

TABLE 7 | The detection (LOD) and quantification (LOQ) limits for selected elements [mg/kg].

	Pd	Pt	Ru	Zn	Cd	Co	Mn	Cu	Mo
LOD	0.037	0.028	0.059	1.23	0.032	0.062	0.257	0.562	0.184
LOQ	0.066	0.040	0.099	1.36	0.056	0.107	0.318	0.677	0.235
	Ni	**Pb**	**Hg**	**V**	**Ba**	**Sr**	**Cr**	**Ag**	**Tl**
LOD	0.544	0.168	0.074	0.215	0.887	0.239	0.238	0.025	0.004
LOQ	0.885	0.210	0.115	0.258	0.937	0.267	0.340	0.044	0.006

molecule (3.038 and 3.047 Å, respectively). The crystal packing and short interactions are shown in **Figure 6**.

Naphthalen-1-yl 1-(5-fluoropentyl)-1H-indole-3-carboxylate, NM-2201 (**2**) crystallizes in a monoclinic system, space group $P2_1/c$, with one molecule in an asymmetric part of the unit cell (**Figure 7**). The indole moiety is almost planar; the angle between the mean planes of the rings is 1.4°. The alkyl carbon chain is bent with respect to the nitrogen atom by 112.1° (C4-C5-N1). The structure is stabilized by weak C5-H…O2 hydrogen bonds (with the distance of 2.677Å), but also C-H…F interactions. For the latter, the interaction with the fluorine atom is bifurcated and the appropriate C4-H…F and C12-H…F distances equal to 2.502 and 2.574 Å, respectively. The crystal packing and short interactions are shown in **Figure 8**.

Quinolin-8-yl 1-(5-fluoropentyl)-1H-indole-3-carboxylate, 5F-PB-22 (**3**) crystallizes in a triclinic system, space group P-1, with one molecule in an asymmetric part of the unit cell (**Figure 9**). The structure is disordered with a fluorine atom at two alternative sites with 75-25% occupancies. The indole moiety is almost planar; the angle between the mean planes of the rings is 2.0°. The alkyl carbon chain is bent with respect to the nitrogen atom by 113.2° (C4-C5-N1). The structure is stabilized by weak hydrogen bonds between the hydrogen at C7 and the nitrogen atom N2 (2.588 Å). Interestingly, the neighboring molecules form a kind of stack with overlapping pyrrole rings (distance between the centroids equal to 3.451 Å). The molecules also form weak hydrogen bonds between one of the hydrogens at C1 and the oxygen atom O2 (2.633 Å). Finally, there are C-H…F interactions in the crystal lattice involving the hydrogen atom at C23 of the quinoline moiety and the disordered fluorine atom of the neighboring molecule (2.645 and 2.574 Å, respectively). The crystal packing and short interactions are shown in **Figure 10**.

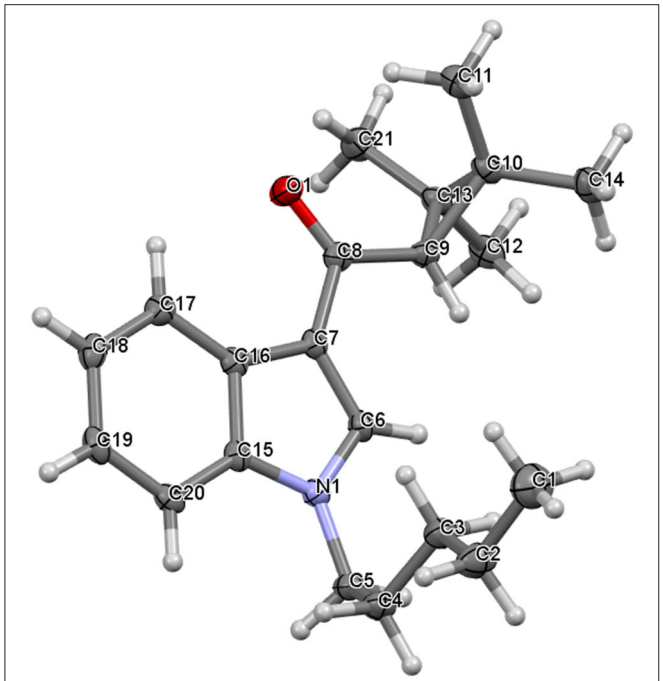

FIGURE 5 | The molecular structure of UR-144 showing atom numbering and displacement ellipsoids at the 50% probability level.

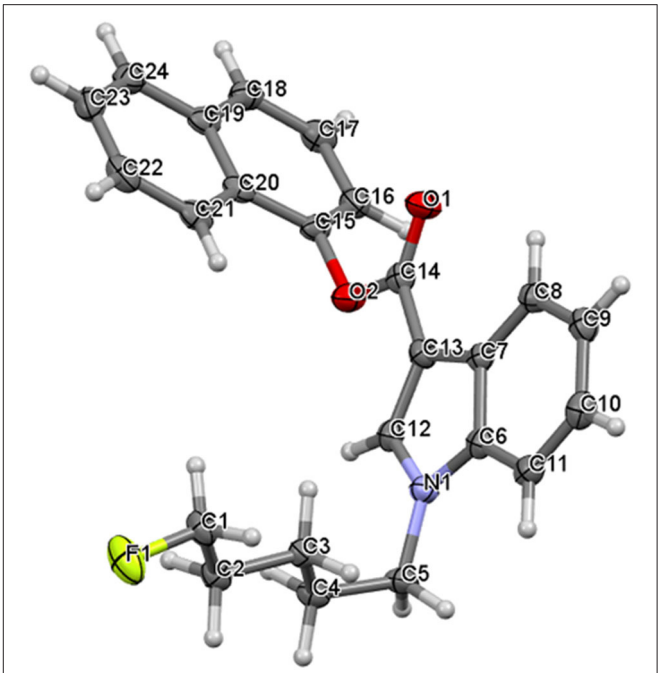

FIGURE 7 | The molecular structure of NM-2201 showing atom numbering and displacement ellipsoids at the 50% probability level.

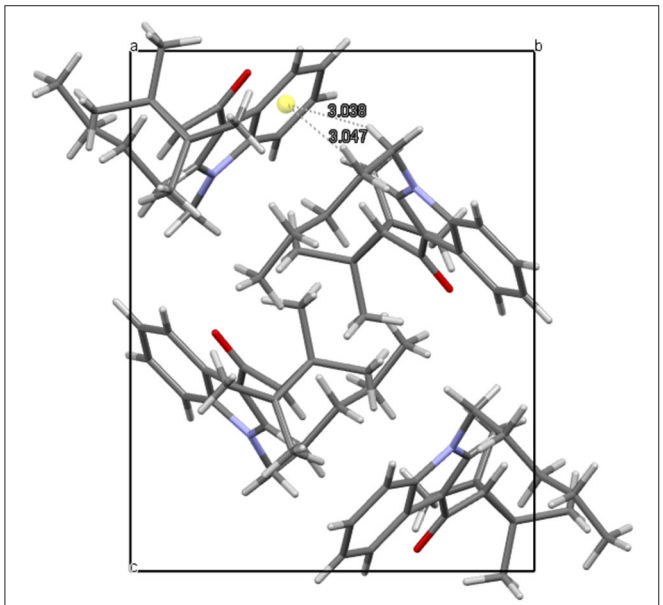

FIGURE 6 | Crystal packing and short interactions in the crystal structure of UR-144. View along [100] direction.

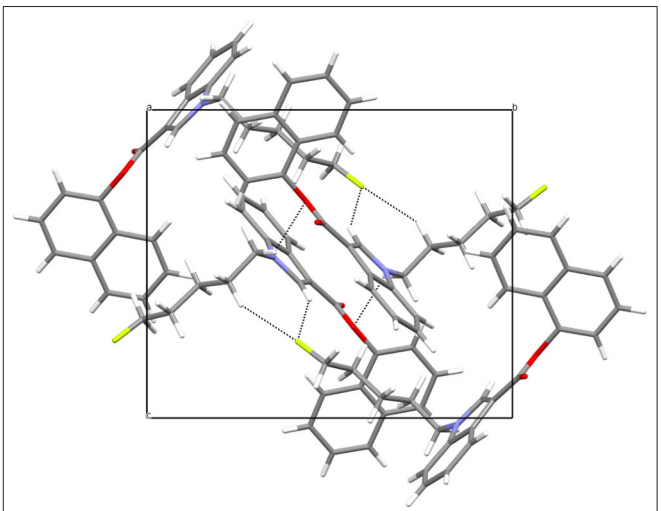

FIGURE 8 | Crystal packing and short interactions in the crystal structure of NM-2201. View along [100] direction.

Additionally, the compounds (**1**), (**2**), and (**3**) have been measured by powder X-ray diffraction. It is a fast method to characterize the compound once we have solved its crystal structure (solving the crystal structure from powder diffraction data is possible, but not trivial and time consuming). Using generally available software it is straightforward to export powder diffraction patterns from the single crystal structure and compare it with an experimentally measured sample. The examples are shown for UR-144, NM-2201, and 5F-PB-22 in **Figures 11–13**. Despite the disorder in structure (**3**), the agreement in reflection positions for both powder patterns is very good. A small shift is caused by the different temperatures of the measurements (see the compound

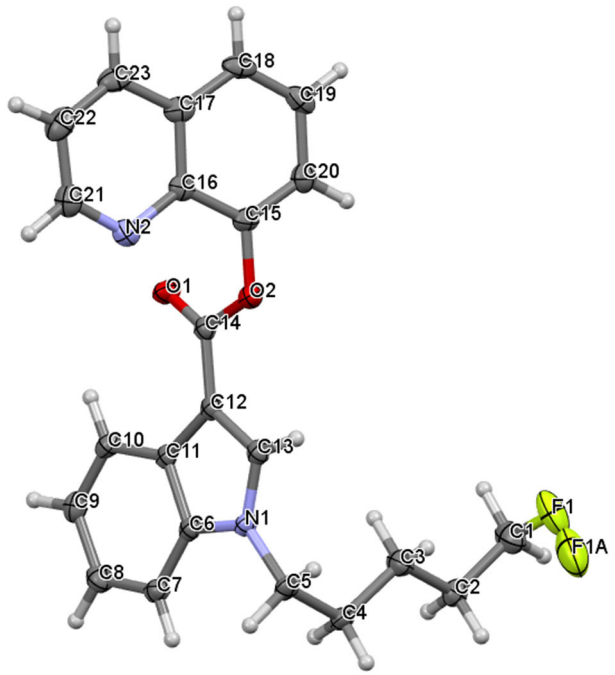

FIGURE 9 | The molecular structure of 5F-PB-22 showing atom numbering and displacement ellipsoids at the 50% probability level. Fluorine atom at two alternative sites with 75–25% occupancy.

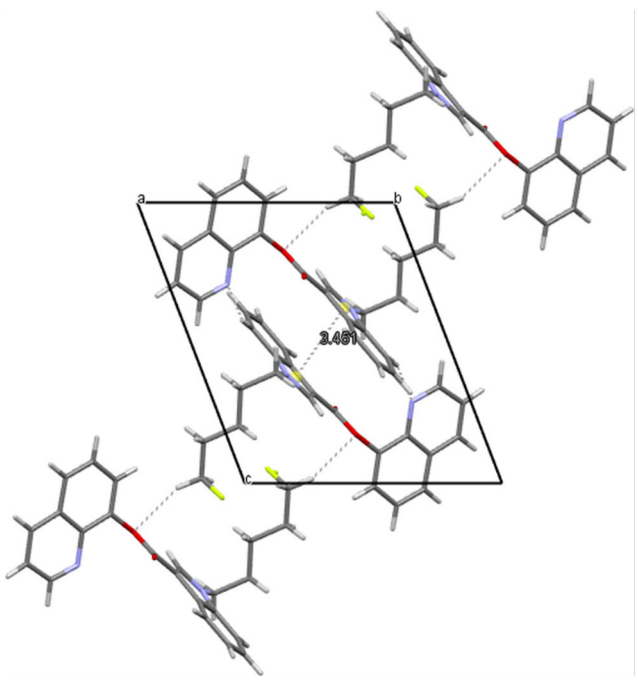

FIGURE 10 | Crystal packing and short interactions in the crystal structure of 5F-PB-22. View along [100] direction.

characteristic section). The same analysis can be done for unknown powder and any crystal structure deposited in the Cambridge Structural Database (Groom et al., 2016). The great advantage of forensic requirements is that X-ray diffraction methods are non-destructive.

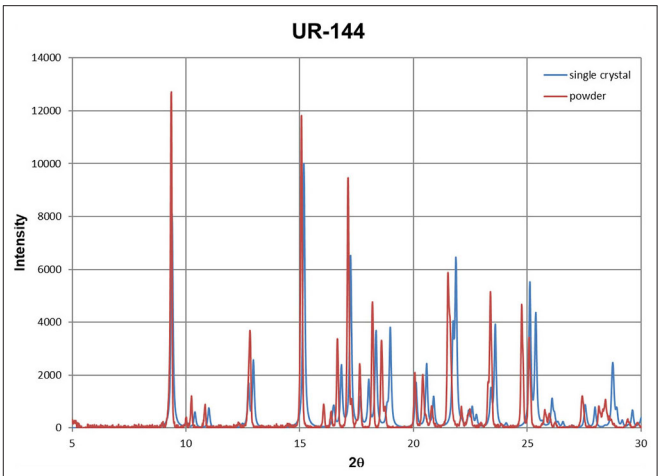

FIGURE 11 | Powder diffraction patterns for UR-144, obtained from single crystal data (blue) and powder sample (red).

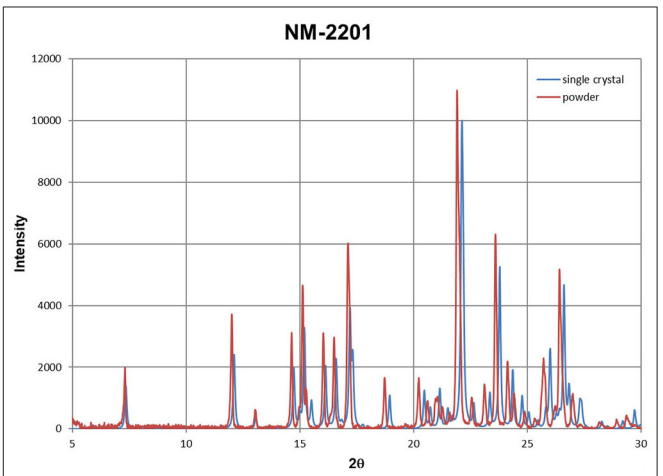

FIGURE 12 | Powder diffraction patterns for NM-2201 obtained from single crystal data (blue) and powder sample (red).

CONCLUSIONS

The market for NPS is systematically growing. Successive addition of new compounds to the list of the substances being controlled all over the world does not discourage illegal laboratories from synthesizing novel deadly drugs. Therefore, there is a growing need to develop rapid and versatile analytical protocols as well as complementary techniques, which enable the provision of specific characterization for criminal investigations, thus preventing such illegal activity. In this article, we have presented a cooperative study toward the synthesis and characterization of selected NPS, with their intended application as CRMs for future use by law enforcement agencies.

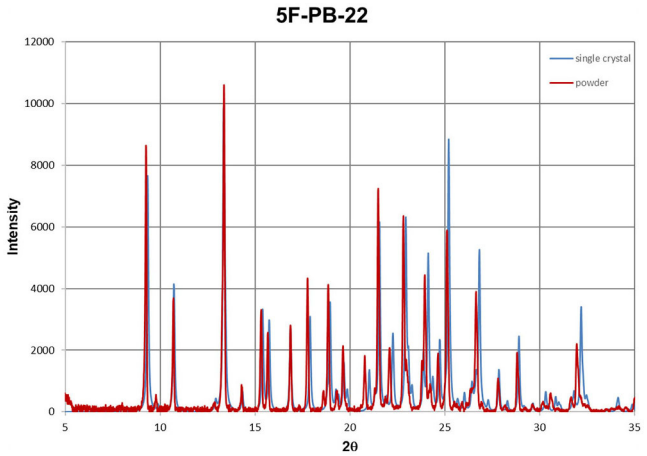

FIGURE 13 | Powder diffraction patterns for 5F-PB-22 obtained from single crystal data (blue) and powder sample (red).

We would like to highlight that the proposed non-routine analytical protocols for comprehensive characterization of NPS combining carefully selected physicochemical techniques, enables the generation of complementary information for selected NPS, namely those considered as emerging substances found on the illegal drug market.

We have successfully synthesized 7 NPS, those being known on the drug-market. An analytical procedure that combines chromatographic separation with the simultaneous identification of synthesized products using mass spectrometry with a Q/TOF type analyzer has been developed. The identity of the analyzed psychoactive substances was confirmed, and their purities have been determined.

Moreover, crystal structures of synthetic cannabinoids UR-144, NM-2201, 5F-PB-22 are presented in this article. A comparison between crystal and powder samples showed very good agreement. There are not many structures that we can qualify as new psychoactive substances among over one million deposited in CSD, so a lot must be done to facilitate the work of forensic scientists. X-ray diffraction methods, not commonly used by forensic scientists especially for synthetic cannabinoids, are non-destructive. This may be crucial for the evidence collected at the crime scene.

The completely characterized substances could serve as reference standards, which are intended to facilitate the work of law enforcement agencies. Thus, the combination of analytical instrumental techniques and X-ray diffraction may allow for rapid and credible studies of evidence collected at the crime scene. Moreover, such protocols enabling forensic scientists to gather supporting information may be used for judicial purposes as incontestable proof.

DATA AVAILABILITY STATEMENT

The datasets generated for this study can be found in the The Cambridge Crystallographic Data Center, CCDC 1842292-1842294, 1943878.

AUTHOR CONTRIBUTIONS

Syntheses of the compounds were performed by WK, PM and KG, the products were analyzed by electrospray Q/TOF-MS/MS, reversed-phase liquid chromatography (RP-HPLC) followed by detection with DAD detector. Q/TOF-MS and inductively coupled plasma with quadrupole mass spectrometer (ICP-QMS) by MM-K and EB, X-ray data collection and analyses were performed by MD and MC. RB was the holder of Grant No. DOB-BIO6/16/44/2014. The first draft of the manuscript was written by MD. All authors commented on previous versions of the manuscript, read, and approved the final manuscript, and contributed to the study conception and design.

FUNDING

This work was supported by the National Center for Research and Development (NCBR) under Grant No. DOB-BIO6/16/44/2014. The X-ray structures were determined in the Advanced Crystal Engineering Laboratory (aceLAB) at the Faculty of Chemistry, University of Warsaw; established by generous support from the Polish Ministry of Science and Higher Education (grant No. 614/FNiTP/115/2011).

SUPPLEMENTARY MATERIAL

The Supplementary Material for this article can be found online at: https://www.frontiersin.org/articles/10.3389/fchem.2020.00693/full#supplementary-material

REFERENCES

APEX2. (2013). *Bruker AXS Inc*. Madison Wisconsin USA.

Aszyk, J., and Kot-Wasik, A. (2016). The use of HPLC-Q-TOF-MS for comprehensive screening of drugs and psychoactive substances in hair samples and several "legal highs" products. *Monatsh. Chem.* 147, 1407–1414. doi: 10.1007/s00706-016-1773-z

Bak, A., Kozik, V., Kozakiewicz, D., Gajcy, K., Strub, D. J., Swietlicka, A., et al. (2019). Novel benzene-based carbamates for AChE/BChE inhibition: synthesis and ligand/structure-oriented SAR study. *Int. J. Mol. Sci.* 20:1524. doi: 10.3390/ijms20071524

Banister, S. D., Stuart, J., Kevin, R. C., Edington, A., Longworth, M., Wilkinson, S. M., et al. (2015). Effects of bioisosteric fluorine in synthetic cannabinoid designer drugs JWH-018, AM-2201, UR-144, XLR-11, PB-22, 5F-PB-22, APICA, and STS-135. *ACS Chem. Neurosci.* 6, 1445–1458. doi: 10.1021/acschemneuro.5b00107

Banister, S. D., Wilkinson, S. M., Longworth, M., Stuart, J., Apetz, N., English, K., et al. (2013). The synthesis and pharmacological evaluation of adamantane-derived indoles: cannabimimetic drugs of abuse. *ACS Chem. Neurosci.* 4, 1081–1092. doi: 10.1021/cn400035r

Compton, D. R., Johnson, M. R., Melvin, L. S., and Martin, B. R. (1992). Pharmacological profile of a series of bicyclic cannabinoid analogs:

classification as cannabimimetic agents. *J. Pharmacol. Exp. Ther*. 260, 201–209.

DeRuiter, J., Hayes, L., Valaer, A., and Clark, C. R. (1994). Methcathinone and designer analogues: synthesis, stereochemical analysis, and analytical properties. *J. Chromatogr. Sci*. 32, 552–564. doi: 10.1093/chromsci/32.12.552

Eckers, C., Haskins, N., and Langridge, J. (1997). the use of liquid chromatography combined with a quadrupole time-of-flight analyser for the identification of trace impurities in drug substance. *Rapid Commun. Mass Spectrom*. 11, 1916–1922. doi: 10.1002/(SICI)1097-0231(199711)11:17<1916::AID-RCM96>3.0.CO;2-8

EU Drug Markets Report. (2019). Available online at: http://www.emcdda.europa.eu/system/files/publications/12078/20192630_TD0319332ENN_PDF.pdf

Fornal, E., Stachniuk, A., and Wojtyla, A. (2013). LC-Q/TOF mass spectrometry data driven identification and spectroscopic characterisation of a new 3,4-methylenedioxy-N-benzyl cathinone (BMDP). *J. Pharm. Biomed. Anal*. 72, 139–144. doi: 10.1016/j.jpba.2012.09.019

Groom, C. R., Bruno, I. J., Lightfoot, M. P., and Ward, S. C. (2016). The cambridge structural database. *Acta Cryst. B* 72, 171–179. doi: 10.1107/S2052520616003954

Grucza, K., Kowalczyk, K., Wicka, M., Szutowski, M., Bulska, E., and Kwiatkowska, D. (2019). The use of a valid and straightforward method for the identification of higenamine in dietary supplements in view of anti-doping rule violation cases. *Drug Test. Anal*. 11, 912–917. doi: 10.1002/dta.2602

Hong, X., Hong-Shun, S., Feng-Mao, L., and Jian-qing, D. (2011). 1-Butyl-3-(1-naphthoyl)-1*H*-indole. *Acta Crystallogr. Sect. E Struct. Rep. Online* 67:o1349. doi: 10.1107/S1600536811016631

Hongfeng, D., Gifford, A. N., Zvonok, A. M., Cui, G., Li, X., Fan, P., et al. (2005). Potent cannabinergic indole analogues as radioiodinatable brain imaging agents for the CB1 cannabinoid receptor. *J. Med. Chem*. 48, 6386–6392. doi: 10.1021/jm050135l

Howlett, A. C., Champion, T. M., Wilken, G. H., and Mechoulam, R. (1990). Stereochemical effects of 11-OH-delta-8-tetrahydrocannabinol-dimethylheptyl to inhibit adenylate cyclase and bind to the cannabinoid receptor. *Neuropharmacology* 29, 161–165. doi: 10.1016/0028-3908(90)90056-W

Huffman, J. W., Dai, D., Martin, B. R., and Compton, D. R. (1994). Design, synthesis and pharmacology of cannabimimetic indoles. *Bioorg. Med. Chem. Lett.* 4, 563–566. doi: 10.1016/S0960-894X(01)80155-4

Huffman, J. W., Zengin, G., Wu, M. J., Lu, J., Hynd, G., Bushell, K., et al. (2005). Structure-activity relationships for 1-alkyl-3-(1-naphthoyl)indoles at the cannabinoid CB(1) and CB(2) receptors: steric and electronic effects of naphthoyl substituents. New highly selective CB(2) receptor agonists. *Bioorg. Med. Chem.* 13, 89–112. doi: 10.1016/j.bmc.2004.09.050

International Tables for Crystallography. (1992). *Volume C: Mathematical, Physical and Chemical Tables*. Dordrecht; Boston, MA; London: Kluwer Academic Publishers.

Koe, B. K. (1981). Levonantradol, a potent cannabinoid-related analgesic, antagonizes haloperidol-induced activation of striatal dopamine synthesis. *Eur. J. Pharmacol.* 70, 231–235. doi: 10.1016/0014-2999(81)90219-3

Kwiatkowska, D., Kowalczyk, K., Grucza, K., Szutowski, M., Bulska, E., and Wicka, M. (2018). Detection of bemitil and its metabolite in urine by means of LC-MS/MS in view of doping control analysis. *Drug Test. Anal*. 10, 1682–1688. doi: 10.1002/dta.2524

Lee, K. H., Ho, C. S., Iu, P. H. Y., Lai, S. J. P., Shek, C. C., Lo, Y., et al. (2009). Development of a broad toxicological screening technique for urine using ultra-performance liquid chromatography and time-of-flight mass spectrometry. *Anal. Chim. Acta* 649, 80–90. doi: 10.1016/j.aca.2009.06.068

Longworth, M., Banister, S. D., Mack, B. C. J., Glass, M., Connor, M., and Kassiou, M. (2016). The 2-alkyl-2H-indazole regioisomers of synthetic cannabinoids AB-CHMINACA, AB-FUBINACA, AB-PINACA, and 5F-AB-PINACA are possible manufacturing impurities with cannabimimetic activities. *Forensic Toxicol*. 34, 286–303. doi: 10.1007/s11419-016-0316-y

Macrae, C. F., Edgington, P. R., McCabe, P., Pidcock, E., Shields, G. P., Taylor, R., et al. (2006). Mercury visualization and analysis of crystal structures. *J. Appl. Crystallogr*. 39, 453–457. doi: 10.1107/S002188980600731X

Matsuda, L. A., Lolait, S. J., Brownstein, M. J., Young, A. C., and Bonner, T. I. (1990). Structure of a cannabinoid receptor and functional expression of the cloned cDNA. *Nature* 346, 561–564. doi: 10.1038/346561a0

Mechoulam, R., and Gaoni, Y. (1965). A total synthesis of DL-Delta-1-tetrahydrocannabinol, the active constituent of hashish. *J. Am. Chem. Soc*. 87, 3273–3275. doi: 10.1021/ja01092a065

Melvin, L. S., Johnson, M. R., Harbert, C. A., Milne, G. M., and Weissman, A. (1984). A cannabinoid derived prototypical analgesic. *J. Med. Chem*. 27, 67–71. doi: 10.1021/jm00367a013

Munro, S., Thomas, K. L., and Abu-Shaar, M. (1993). Molecular characterization of a peripheral receptor for cannabinoids, *Nature* 365, 61–65. doi: 10.1038/365061a0

Natsuka, K., Nakamura, H., Uno, H., and Umemoto, S. (1975). 1-substituted 4-(1,2-diphenylethyl)piperazine derivatives and their analgesic activities. 1. *J. Med. Chem.* 18, 1240–1244. doi: 10.1021/jm00246a014

Nycz, J. E., Malecki, G., Zawiazalec, M., Pazdziorek, T., and Skop, P. (2010). 1-Pentyl-3-(4-methoxy-1-naphthoyl)indole and 2-(2-methoxy-phenyl)-1-(1-pentyl-1H-indol-3-yl)-ethanone: X-ray structures and computational studies. *J. Mol. Struct*. 984, 125–130. doi: 10.1016/j.molstruc.2010.09.016

Nycz, J. E., Pazdziorek, T., Malecki, G., and Szala, M. (2016). Identification and derivatization of selected cathinones by spectroscopic studies. *Forensic Sci. Int*. 266, 416–426. doi: 10.1016/j.forsciint.2016.06.034

SADABS. (2012). *Bruker AXS Inc*. Madison Wisconsin USA.

SAINT. (2013). *Bruker AXS Inc*. Madison Wisconsin USA.

Sheldrick, G. M. (2015). Crystal structure refinement with SHELXL, acta. *Crystallogr. Sect. C Struct. Chem*. 71, 3–8. doi: 10.1107/S2053229614024218

Troxler, F., Harnisch, A., Bormann, G., Seemann, F., and Szabo, L. (1968). Synthesen von indolen mit (2-aminoäthyl)-, (2-aminopropyl)-oder alkanolamin-seitenketten am sechsring. 5. mitt. über synthetische indol-verbindungen [1]. *Helv. Chim. Acta.* 51, 1616–1628. doi: 10.1002/hlca.19680510717

Conflict of Interest: The authors declare that the research was conducted in the absence of any commercial or financial relationships that could be construed as a potential conflict of interest.

frontiers in Chemistry

ORIGINAL RESEARCH
published: 30 September 2020
doi: 10.3389/fchem.2020.00672

Application of X-Ray Powder Diffraction for Analysis of Selected Dietary Supplements Containing Magnesium and Calcium

*Izabela Jendrzejewska**

Institute of Chemistry, Faculty of Science and Technology, University of Silesia, Katowice, Poland

It is estimated that ∼50% of medications and dietary supplements offered in the Internet are counterfeit. X-ray diffraction is one of the techniques which may be successfully applied to identify various chemical compounds in polycrystalline mixtures such as dietary supplements, but also medications, narcotics or designer drugs. X-ray diffraction enables the understanding of compositions of such mixtures. For the tests, 22 dietary supplements which should contain magnesium and calcium compounds, available in pharmacies, groceries, Internet shops, as well as in shops for sportspersons, were selected. Identification of crystalline substances present in the tested sample consists in determination of inter-planar distances d_{hkl} of investigated substances and determination of intensity of the obtained diffraction lines, and then in comparing them with values contained in diffraction databases. In this study, the ICDD-PDF2 database was used. The most important criterion in qualitative analysis, confirming the presence of a given phase, is the conformity of positions of diffraction lines in the recorded diffraction image with those in the reference image. Reflection shifts for the individual 2θ angles compared with the data from the database should not exceed 0.2°. In most cases, X-ray analysis of the investigated dietary supplements proved the presence of magnesium and calcium compounds declared by the manufacturer, as well as allowing the identification of auxiliary substances present in the tested products. In the case of two magnesium-containing dietary supplements, the magnesium compounds declared by the manufacturer were not found. Our studies confirmed the effectiveness of X-ray structural analysis and proved the possibility of distinguishing counterfeit preparations from authentic products, as well as to use this method for the quality control of such pharmaceutical preparations.

Keywords: dietary supplements analysis, counterfeit pharmaceutics, X-ray study, Bragg's low, diffraction data, X-ray phase analysis

OPEN ACCESS

Edited by:
Alberto Salomone,
University of Turin, Italy

Reviewed by:
Roberta Risoluti,
Sapienza University of Rome, Italy
Juan Manuel Lázaro-Martínez,
University of Buenos Aires, Argentina

***Correspondence:**
Izabela Jendrzejewska
izabela.jendrzejewska@us.edu.pl

Specialty section:
This article was submitted to Analytical Chemistry, a section of the journal Frontiers in Chemistry

Received: *25 February 2020*
Accepted: *29 June 2020*
Published: *30 September 2020*

Citation:
Jendrzejewska I (2020) Application of X-Ray Powder Diffraction for Analysis of Selected Dietary Supplements Containing Magnesium and Calcium. Front. Chem. 8:672. doi: 10.3389/fchem.2020.00672

INTRODUCTION

In recent years, there has been an increasing number of fatal cases resulting from taking counterfeit medical and therapeutical products, and dietary supplements. WHO and FDA experts estimate that counterfeit products may constitute ∼10% of the global medicinal drug market. It is thought that the following groups are the largest among counterfeit drugs: antibiotics (28%); hormones

(including steroid hormones, 18%); anti-asthmatics and anti-allergics (8%); antimalarials (7%); analgesics and antipyretics (6%); other medications (14 therapeutical classes, 33%) (Maurin et al., 2007; Singh et al., 2009; Venhuis et al., 2011). Also counterfeiters are also interested in popular medicines, such as aspirin. In 2013, 1.2 million aspirin tablets were confiscated in France, and it was a product that did not contain the active substance at all. In the USA, three batches of product containing only water, which were to replace a good, effective, and commonly used oncological drug, were confiscated (World Health Organisation, 2006).

Apart from these, dietary supplements are also massively forged. Because of the fact that they are classified as foodstuffs, their common availability and an increase in the interest for this type of product may be observed at present. More than 10,000 dietary supplements are available on the Polish market. These products contain more than 500 components in total. Use of many of them has no factual substantiation. The majority of plant products, nutrients and dietary supplements is not tested for the quality of the components used. Dietary supplements containing structural analogs of and chemical compounds very similar to those comprised in medicinal drugs, are particularly dangerous. They have much stronger undesirable effects usually and even cause death (World Health Organisation, 2018). That is why it is important to control their chemical composition, using the available test methods (Stypułkowska et al., 2011).

For the study, popular and frequently purchased dietary supplements containing magnesium and calcium were chosen. The goal of the paper consists in the identification of calcium and magnesium compounds declared by manufacturers as components of given supplements, as well as an attempt of determination whether the product is authentic or not.

MATERIALS AND METHODS

Materials

Twenty-two dietary supplements containing calcium and magnesium were purchased in pharmacies, shops, filling stations, and via the Internet, and then subjected to tests using X-ray radiation. All analyzed products are gathered in **Table 1**. In the table, the data reported by manufacturers (magnesium and calcium contents), and the form of the chemical compound are taken into account.

The table does not include auxiliary substances such as starch, talc, magnesium stearate, citric acid, etc., because of the fact that the main goal of the paper is the identification of calcium and magnesium compounds as "active substances" in the analyzed dietary supplements. On the other hand, strong diffraction lines, originating from auxiliary substances, such as ascorbic acid, citric acid, magnesium stearate, alanine, starch, are marked in the diffraction patterns. It pertains particularly to multivitamin preparations, in which the intensity of diffraction lines originating from magnesium and calcium compounds is lower than that of the strongest lines present in the diffraction pattern.

TABLE 1 | Analyzed dietary supplements.

No.	Product name (*manufacturer*)	Magnesium content in 1 tablet/sachet [mg]	Form of magnesium
Analyzed magnesium-containing dietary supplements			
1.	Falvit *Bausch Health*	112.5	Magnesium oxide
2.	Vitalsss Plus Multivitamin *Natur Product Pharma*	57.0	Magnesium carbonate
3.	Vitalsss Plus Magnez *Natur Product Pharma*	200.0	Magnesium carbonate
4.	Asparoc Apteo *Synoptis Pharma*	17.0	Magnesium carbonate
5.	Vitalsss Plus Magnez + Witamina B_6 *Natur Product Pharma*	187.5	Magnesium oxide
6.	Magnez OTX *OTXcare*	60.0	Magnesium carbonate
7.	Magnez B_6 skurcz *INV Poland*	100.0	Magnesium citrate
8.	Dr. Max$^+$ Magnez + VitB_6 *ARENAPHARMA SP. Z O.O.*	60.0	Magnesium lactate Magnesium oxide
9.	Mex Muscle Excellence *MEX Nutrition*	150.0	Magnesium citrate
10.	Thermo Pump *Power Sports Polska*	100.0	Magnesium citrate
11.	7 Nutrition Bomb Pre-workout *TRICEPS Polska*	30.0	Magnesium citrate
12.	Magnesium *KFD Nutrition*	125.0	Magnesium citrate
Analyzed calcium-containing dietary supplements			
13.	Calcium plusssz *Polski Lek*	300	Calcium carbonate
14.	Molekin Osteo *NATUR PRODUKT PHARMA*	300	Algae Calcium (*Lithothamnium* sp.) Calcium carbonate
15	Calcium in foil ZDROVIT *NATUR PRODUKT PHARMA*	300	Calcium carbonate
16.	Calcium in foil + vit.C ZDROVIT *NATUR PRODUKT PHARMA*	300	Calcium carbonate
17.	Calcium 500 D *POLFA Łódz*	500	Calcium lactogluconate
18.	Calcium Alergo Plus *POLFA Łódz*	300	Calcium lactate Calcium carbonate
19.	Kalcikinon *VALENTIS*	300	Calcium carbonate
20.	Calcium 400 mg + witamina D3 *VITALIS*	300	Calcium carbonate
21.	Vitrum osteo *Takeda Pharma*	500	Calcium carbonate
22.	Calcium GLUCONICUM *Farmapol*	45	Calcium gluconate

Methods

Diffractometric Method

X-ray radiation has the ability to diffract, or dissipate off the rays on atoms of crystals. A reflection of a beam of parallel rays

occurs on a series of parallel lattice planes (*hkl*). The radiation will be amplified when the angle of incidence (θ) is equal to the angle of reflection (θ). To amplify the reflected radiation, the path difference (Δs) must be equal to a total multiple of the wavelength (nλ), as only then, the wave are in phase. The scheme of X-ray diffraction is shown in Epp (2016).

The amplification condition will be met if:

$$n\lambda = 2d_{hkl}sin\theta \quad (1)$$

where: n—reflection order, λ—wavelength, d_{hkl}—interplanary distance, θ—angle of reflection.

The Equation (1), namely the Bragg-Wulff equation, describes the geometrical condition for X-ray diffraction (XRD) on lattice planes having interplanary distances of d_{hkl}. An important advantage of the method consists in the fact that not only the θ angle, at which the X-rays are being reflected is measured, but also the intensities of the observed diffraction pattern lines. The diffraction pattern is obtained in the form of a plot of the intensity (count number) *vs.* the 2θ (deflection angle) (**Figure 1**).

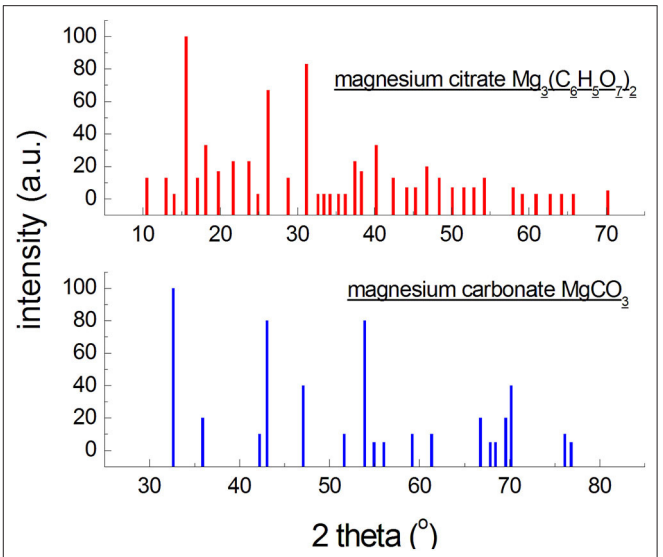

FIGURE 1 | Diffraction patterns generated based on the data from the ICDD database for an organic and an inorganic magnesium salt.

X-Ray Structural Analysis

X-ray phase analysis plays an important role in the analysis of almost all solids, including medications and medicinal preparations. As a non-destructive method, it is used for: (a) identification of unknown compounds, (b) investigation of polymorphism, solvation and salt form identification, (c) determination of physico-chemical properties, (d) detection of impurities and anomalies in medications (Thatcher and Briner, 1986; Stephenson, 2005; Chauhan and Chauhan, 2014; Das et al., 2014). X-ray phase analysis enables both qualitative and quantitative analyses of polycrystalline substances. Each crystalline substance has a characteristic X-ray diffraction pattern with specific locations of diffraction lines and their intensities. Such polycrystalline diffraction patterns are so complex that it is not possible to have identical diffraction images for various substances. Therefore, diffraction patterns may play the role of "fingerprints" in the identification of substances. A diffraction pattern may be considered as a set of interplanary distances d_{hkl} and line intensities corresponding to them. It is important that every phase included in the composition of the mixture is independent in the process of creation of the diffraction pattern, which is a sum of diffraction patterns of the co-existent phases. To carry out the qualitative phase analysis, one should compare the obtained diffraction pattern (2θ angles, d_{hkl} interplanary distances, and diffraction line intensities) with a corresponding standard, found in a proper database. A diffraction line shift of $<0.2^\circ$ is a normal phenomenon while analyzing a polycrystalline substance. It is connected with a random arrangement of grains in a polycrystalline sample. On the other hand, shifts larger than 0.2° at a given diffraction angle 2θ indicate a different crystal structure. Counterfeit pharmaceuticals contain various types of auxiliary substances (excipients) with different crystal structures than those of substance present in authentic products (Kugler, 2003; Rendle, 2003). Based on this assumption, a product for which the obtained diffraction lines are shifted by more than 0.2°, should be considered suspect (USP Pharmacopeial Convention, 2011; DeWitt, 2015). This rule is published in the general chapter of the <941> ascertaining that if the shifts of diffraction lines in an XRD image of the tested products are larger than 0.2° for a given 2θ diffraction angle while compared to the XRD image for an authentic product, these products meet the counterfeit criteria (DeWitt, 2015). Also, counterfeit drugs and supplements may be distinguished from authentic ones by studying their general XRD images. Additional lines, lack of lines, as well as line shifts will be observed in diffraction patterns of counterfeit products. This method enables the application of X-ray phase analysis as a technique for distinguishing counterfeit pharmaceuticals from authentic ones in legal chemistry.

The obtained diffraction pattern contains information on the angle of reflection θ and wavelength λ, so, using the Bragg Equation (1), the interplanary distance d_{hkl} may be calculated (Bojarski and Łagiewka, 1988). The obtained values of the interplanary distances d_{hkl} characterize a given phase and are independent from the radiation type, while the line intensities are closely related to it. Due to this method, identification of components of crystalline phases containing the tested material is possible, and simultaneously, qualitative analysis of the sample takes place.

There is a dependence between the intensity $J^{j,0}_{hkl}$ of any j phase reflection, having the mass absorption coefficient μ^*_j, and the intensity of the same reflection, J^j_{hkl}, in the case when the phase j with a mass share m_j is present in a polyphasic mixture with a mass coefficient μ^*, shown by the following formula:

$$J^j_{hkl} = J^{j,0}_{hkl}\frac{\mu^*_j}{\mu^*}m_j \quad (2)$$

As can be seen from the formula (2), the intensity of a recorded reflection of a given phase depends on its amount in the mixture

m_j and the $J_{hkl}^{j,0}$ value, or its crystal structure (Bojarski and Łagiewka, 1988).

Identification of phases in polyphasic mixtures (and dietary supplements should be considered such) depends on crystal structure of a given phase, characters of the co-existing phases, and instrumental factors. X-ray photographs of crystalline phases having a high symmetry (regular, tetragonal, hexagonal systems) contain a relatively low number of diffraction reflections, but of high intensities. It allows for identifying them even at their contents below 1%. It is assumed that the X-ray detection limit is in the range of 0.1–1% by wt. per phase, while the limit of detection (LOD) is assumed as ∼1% (Bojarski and Łagiewka, 1988)[1].

On the other hand, X-ray photographs of low-symmetry phases (triclinic, monoclinic systems) contain large numbers of reflections, but of low intensities, leading to worse detection limits. Phases composed of atoms of elements having high atomic numbers will exhibit higher intensities of reflections than those composed of light elements (**Figure 1**). It is a consequence of atomic dissipation factor, increasing with the increase in the atomic number of the element. Thus, the X-ray detection limit will be more favorable for compounds with a high symmetry, and unfavorable for compounds with a low symmetry composed of light elements. It should be noted that more than 2/3 of organic compounds crystallize in low-symmetry systems, and the strongest diffraction lines are observed at small angles (**Figure 1**). The content of a given crystalline phase may be lower than this limit, so it will not be identified, but it does not mean it is absent. The detection limit is affected also by size of the crystallites and perfection of the crystal lattice. Defected lattices and crystallite sizes below 0.1 μm cause broadening and weakening of intensities of the reflections, hindering identification. The change in the limit of detection of a crystalline phase, depending on the type of the mixture, wherein this phase is present, consists in a change in the ration between the absorption coefficient of the phase and the mixture as a whole, μ_j^*/μ^*, and in a superposition of reflections of the concomitant phases. The detection limit of phase *j*, having an absorption coefficient μ_j^*, will be more favorable in a mixture with a low absorption coefficient than in a mixture with a high value of absorption coefficient (formula 2) (Bojarski and Łagiewka, 1988).

Quantitative analysis is based on the diffraction line intensity expressed as formula (3):

$$J_{hkl} = C|F_{hkl}|^2 \cdot LP \cdot p \cdot A \quad (3)$$

where: C—constant, F_{hkl}–structural factor, LP—Lorentz, and polarization factor, p—plane multiplicity factor, A—absorption factor.

Depending on the number of phases in the mixture and their relationships, several typical methods of quantitative analysis are distinguished: (i) direct comparison of reflection intensities, (ii) internal standard method, (iii) external standard method, (iv) Chung method. It is important that reflections having adequate intensities are chosen. These should be the strongest, well separated reflections, located in a small angle range. Precision of quantitative X-ray analysis depends on many factors, therefore this method is affected by errors related to the structure of the phase being determined and the preparation of the sample. Precision of this method ranges from tenths of per cent to several per cent, depending on the analyzed mixture (Bojarski and Łagiewka, 1988).

Sample Analysis of Dietary Supplements

Our studies were focused on a qualitative analysis of selected dietary supplements containing calcium and magnesium compounds. Samples of dietary supplements were very finely ground in an agate mortar, until a homogeneous fine powder was obtained. The tests were carried out using a PW1050 polycrystalline diffractometer with a PW1729 generator from Philips. Bragg-Brentano focusing of diffractive radiation was applied. The total duration of the analysis of each supplement amounted to 48 h, the angular range of the goniometer: 5°÷135°, CuKα1 radiation (λ = 1.54056 Å), filter—Ni. During the experiment, a full scan in the angle range of 5°–120° was carried out, with an angular step of 0.05°, and the scanning time was 0.1 s. The next measurement was configured so that the angle range matched to the given preparation subjected to the analysis. When the tested sample did not exhibit any peaks above 80°, the second measurement was recorded in the 2θ angle range of 5°÷80° or 10°÷80°. Parameters of the second measurement were as follows: 0.02° angular step and 0.02 s scanning time, affecting the quality of the diffraction pattern distinctly. The measurement was carried out twice or thrice to eliminate all errors.

RESULTS AND DISCUSSION

Identification of calcium and magnesium compounds contained in the tested supplements was performed based on the data from the ICDD PDF−2 database (Release 2008, **Table A1**). For each tested substance, qualitative phase analysis was carried out. It consisted in a comparison of the experimental diffraction data such as *2θ* diffraction angles, d_{hkl} interplanary distances, and relative intensities, with the data from the ICDD database. Values of d_{hkl} interplanary distances were calculated based on the Bragg-Wulff equation. The results gathered in tables and shown in the figures are grouped according to the magnesium or calcium compound contained in the tested dietary supplement.

Phase Analysis of Dietary Supplements Containing Magnesium

Figure 2 illustrates polycrystalline diffraction patterns for the following dietary supplements: *Asparoc APTEO Vitalsss Plus Multiwitamina, Vitalsss Plus Mg + K,* and *Magnez OTX*. In all diffraction patterns, diffraction lines characteristic for magnesium carbonate ($MgCO_3$) are present. Their intensity is small, confirming the small amount of $MgCO_3$ declared by the manufacturer (**Table 1**). The largest amount of $MgCO_3$ is contained in Vitalsss Plus Magnesium (200 mg) and it is evident in the diffraction pattern, where the lines originating from

[1]https://serc.carleton.edu/research_education/geochemsheets/techniques/XRD.html (accessed September 06, 2020).

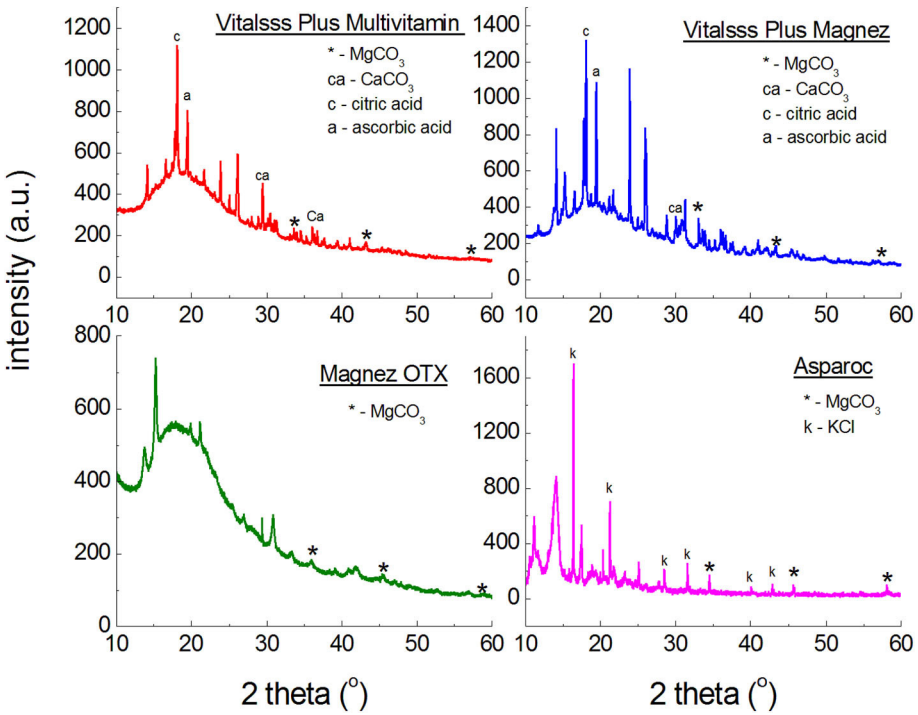

FIGURE 2 | X-ray powder diffraction spectra of dietary supplements containing magnesium carbonate ($MgCO_3$).

TABLE 2 | Comparison of experimental data with the data from the ICDD database for the following dietary supplements: *Vitalsss Plus Multiwitamina, Vitalsss Plus Magnez, Magnez OTX, Asparoc* containing magnesium carbonate ($MgCO_3$).

No. of diffraction line	2θ (°) exp.	2θ (°) ICDD	Intensity	Δ2θ	d_{hkl} (Å) exp.	d_{hkl} (Å) ICDD	hkl
Asparoc APTEO **($MgCO_3$ PDF 01–070–8513)**							
1.	34.4519	34.5963	100	0.1446	2.60	2.59	104
2.	44.7239	44.8843	55	0.1604	2.02	2.02	113
3.	58.0396	57.8903	23	0.1493	1.59	1.61	116
Vitalsss Plus Multiwitamina, Vitalsss Plus Magnez **($MgCO_3$ PDF 01–070–8513)**							
1.	34.4527	34.5963	100	0.1736	2.60	2.59	104
2.	44.7412	44.8843	55	0.1431	2.02	2.02	113
Magnez OTX **($MgCO_3$ PDF 01–070–8515)**							
1.	35.8432	35.6711	100	0.1721	2.51	2.51	104
2.	45.6132	45.9207	70	0.3075	1.98	1.97	113
3.	58.7563	58.8903	30	0.1340	1.57	1.57	116

$MgCO_3$ have the highest intensity in comparison to the other dietary supplements with $MgCO_3$.

The comparison of experimental values of the 2θ angle with the data from the ICDD database for magnesium carbonate showed that the peak shifts are smaller than 0.2° (**Table 2**). It proves that the same crystalline form of $MgCO_3$, thus the same product, is present in every tested dietary supplement, meaning that the tested preparation are authentic.

Figure 3 presents diffraction patterns of dietary supplements containing magnesium oxide (MgO). In the diffraction patterns of *Falvit* and *Dr. Max*$^{+}$ *Magnez* + *VitB*$_6$ (**Figure 2**), three of the strongest diffraction lines characteristic for magnesium oxide MgO are clearly evident. For *Vitalsss Plus Magnez*, only one line originating from MgO was identified, at the 2θ corresponding to the strongest line for MgO. Intensity of this line was significantly lower than that of the MgO line in *Falvit* preparation, however, the amount of MgO in *Vitalsss Plus Magnez* is higher in comparison with that in *Falvit* (**Table 1**). It indicates that the amount of magnesium oxide in the former preparation is lower than the manufacturer declares.

Comparing the experimental 2θ values and the calculated values of interplanary distances d_{hkl} gathered in **Table 3** with the data from the ICDD database, their very good accordance may be confirmed. The shifts of the reflections for the individual

diffraction angles 2θ compared to the reference data are smaller than 0.2°, confirming the authenticity of the product.

Figure 4 presents diffraction patterns of dietary supplements with magnesium citrate. For *Magnez B_6 skurcz*, 4 well-evident diffraction lines were identified, while for *Magnesium KFD Nutrition* only one line is visible for an angle close to the 2θ value, at which the strongest line from magnesium citrate is observed. The line has a lower intensity than, approximately, the corresponding line for *Magnez B_6 skurcz*, despite the fact that the amount of magnesium citrate is relatively larger in *Magnesium KFD Nutrition* (**Table 1**). It may indicate a significantly smaller amount of magnesium citrate in *Magnesium KFD Nutrition* than the amount declared by the manufacturer.

The experimental data (2θ angle values and the calculated values of d_{hkl} interplanary distances) for *Magnez B_6 skurcz* are in a good accordance with the data from the ICDD database (**Table 4**). The $\Delta 2\theta$ differences for the individual diffraction angles 2θ while compared with the ICDD data are smaller than

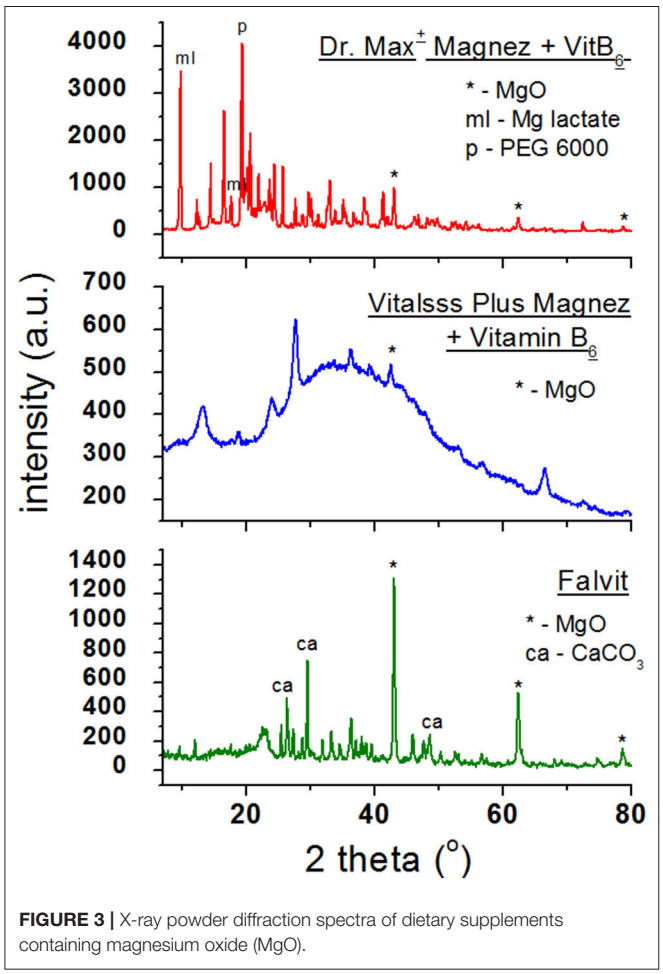

FIGURE 3 | X-ray powder diffraction spectra of dietary supplements containing magnesium oxide (MgO).

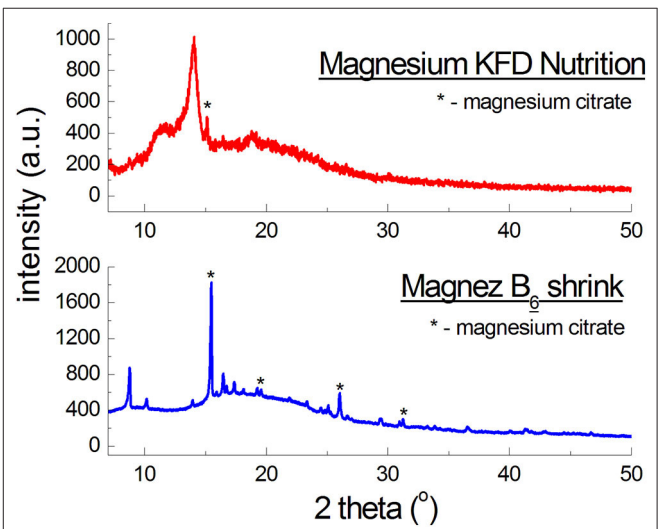

FIGURE 4 | X-ray diffraction pattern for dietary supplements containing magnesium citrate [$Mg_3(C_6H_5O_7)_2$].

TABLE 3 | Comparison of experimental data with the data from the ICDD database for dietary supplements *Falvit* and *Vitalsss Plus Mg + vit. B_6* containing magnesium oxide (MgO) and *Dr. Max$^+$ Magnez + VitB$_6$* containing also magnesium lactate ($C_6H_{10}MgO_6 3H_2O$) apart from magnesium oxide (MgO).

No. of diffraction line	2θ (°) exp.	2θ (°) ICDD	Intensity	Δ2θ	d_{hkl} (Å) exp.	d_{hkl} (Å) ICDD	hkl
***Falvit* (MgO PDF 00–001–1235)**							
1.	43.0245	43.0368	100	0.0123	2.10	2.10	111
2.	62.3951	62.2582	75	0.1369	1.49	1.49	220
3.	78.9413	79.0768	15	0.1355	1.21	1.21	222
***Vitalsss Plus Mg + vit. B_6* (MgO PDF 00–001–1235)**							
1.	42.8321	43.0368	100	0.2047	2.10	2.10	111
***Dr. Max$^+$ magnesium + VitB$_6$* (MgO PDF 00–001–1235)**							
1.	42.9623	43.0368	100	0.0763	2.10	2.11	200
2.	62.4159	62.2582	52	0.1577	1.49	1.49	220
3.	78.8806	79.0768	15	0.1962	1.21	1.21	222
***Dr. Max$^+$ Magnez + VitB$_6$* ($C_6H_{10}MgO_6 3H_2O$ PDF 00–001–0061)**							
1.	9.4976	9.3015	100	0.1961	9.30	9.50	–
2.	17.5541	17.3739	80	0.1802	5.05	5.10	–

TABLE 4 | Results of analysis of experimental data and data from the ICDD database for the following dietary supplements: *Magnez B_6 skurcz* and *Magnesium KFD Nutrition* and for sportspersons: *Mex Muscle Excellence* and *Thermo Pump* [magnesium citrate $Mg_3(C_6H_5O_7)_2$, PDF 00–001–0186].

No. of diffraction line	2θ (°) exp.	2θ (°) ICDD	Intensity	Δ2θ	d_{hkl} (Å) exp.	d_{hkl} (Å) ICDD	hkl
Magnez B_6 skurcz							
1.	15.3818	15.5331	100	0.1513	5.76	5.70	–
2.	18.1052	18.0889	33	0.0163	4.90	4.90	–
3.	26.1338	26.1884	67	0.0546	3.41	3.40	–
4.	31.2150	31.1370	83	0.0780	2.86	2.87	–
Magnesium KFD Nutrition							
1.	15.1703	15.5331	100	0.3628	5.83	5.70	–
Mex Muscle Excellence							
1.	15.0362	15.5331	100	0.2969	5.89	5.70	–
2.	26.1465	26.1884	67	0.0419	3.40	3.40	–
3.	31.1596	31.1370	83	0.0226	2.87	2.87	–
Thermo Pump							
1.	15.2275	15.5331	100	0.3103	5.81	5.70	–
2.	26.4399	26.1884	67	0.2515	3.37	3.40	–
3.	31.0575	31.1370	83	0.0795	2.88	2.87	–

0.2°, which may prove that the tested preparation is authentic. On the other hand, for *Magnesium KFD Nutrition*, the $\Delta 2\theta$ value is higher than 0.2°, possibly indicating irregularities in the composition of this supplement, e.g., a lack of magnesium citrate, an amount lower than that declared by the manufacturer, or presence of another substance giving a diffraction pattern close to that of magnesium citrate.

In **Figure 5**, diffraction patterns for multicomponent dietary supplements intended for people engaging in sports are shown. The magnesium-supplementing compound is magnesium citrate. Diffraction lines characteristic for magnesium citrate are present in the diffraction patterns of *Mex Muscle Excellence* and *Thermo Pump*. Comparison of intensities of lines characteristic for magnesium citrate shows a significant decrease in the intensity of the *Thermo Pump* line, despite the relatively high content of this compound (**Table 1**). It indicates a lower amount of magnesium citrate in *Thermo Pump* than that declared by the manufacturer. Comparing the experimental values of 2θ angles and the calculated values of interplanary distances d_{hkl} gathered in **Table 4** with the data from the ICDD database, their very good accordance may be confirmed. The shifts of the reflections for the individual 2θ diffraction angles are smaller than 0.2°, proving that magnesium citrate is present in the tested preparations.

In the case of *7 Nutrition Bomb Pre-workout* dietary supplement for sportspersons, no lines originating from—$Mg_3(C_6H_5O_7)_2$–were found (**Figure 5**). All visible lines originated from alanine—one of the components of the analyzed product according to its manufacturer. The identified alanine constitutes 25% (5,000 mg) of the total product mass. In this case, the problem of identification of magnesium citrate is probably connected with the composition of the analyzed preparation for sportspersons. Taking into account the information placed on the packaging, the preparation's composition includes more than 20 various substances. According to this description, the total amount of the preparation should contain only 0.15% (30 mg) of magnesium citrate, meaning that the magnesium citrate content may be lower than the roentgenographic detection limit.

Phase Analysis of Dietary Supplements Containing Calcium

In **Figure 6**, diffraction patterns of the following dietary supplements are shown: *Calcium plusssz, Calcium in foil, Calcium in foil + vit.C* containing calcium carbonate $CaCO_3$ as a compound introducing calcium ions to the human organism, in the presence of ascorbic acid. Ascorbic acid was identified in *Calcium plusssz* and *Calcium in foil*, despite the fact that the manufacturer did not declare this component. Lines of citric acid, responsible for the taste of these supplements, have high intensities. In the diffraction patterns of the analyzed supplements (**Figure 6**), three of the strongest diffraction lines characteristic for calcium carbonate ($CaCO_3$) are clearly visible. The intensities of these lines are similar, confirming the amount of calcium carbonate declared by the manufacturer.

Table 5 presents a comparison of diffraction tests for the following dietary supplements: *Calcium plusssz, Calcium in foil, Calcium in foil + vit.C*. Comparison of experimental values of 2θ angles with the data from the ICDD database for calcium carbonate showed a very good accordance with the standard. The determined shifts $\Delta 2\theta$ of the peaks are significantly smaller than 0.2°. It proves that the same crystalline form of $CaCO_3$ is present in these supplements, meaning that the tested sample is authentic.

Figure 7 presents diffraction patterns of the next dietary supplements containing $CaCO_3$. In the case of these three preparations, calcium carbonate is basically the sole component. Only diffraction lines from $CaCO_3$ are present in the diffraction patterns (**Figure 7**). No lines from auxiliary substances (excipients) were found, indicating that the amounts of

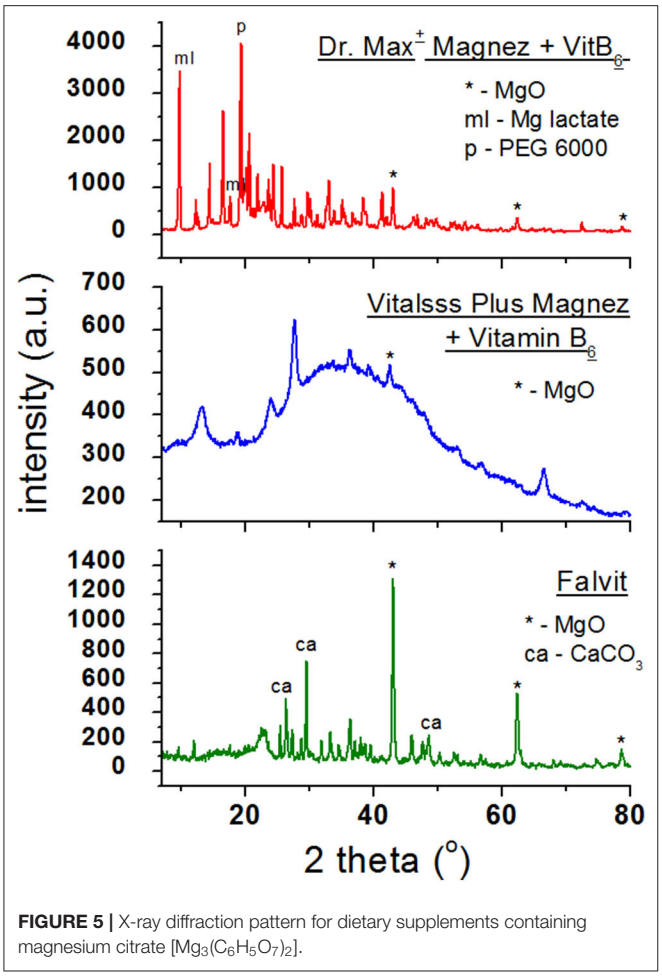

FIGURE 5 | X-ray diffraction pattern for dietary supplements containing magnesium citrate [$Mg_3(C_6H_5O_7)_2$].

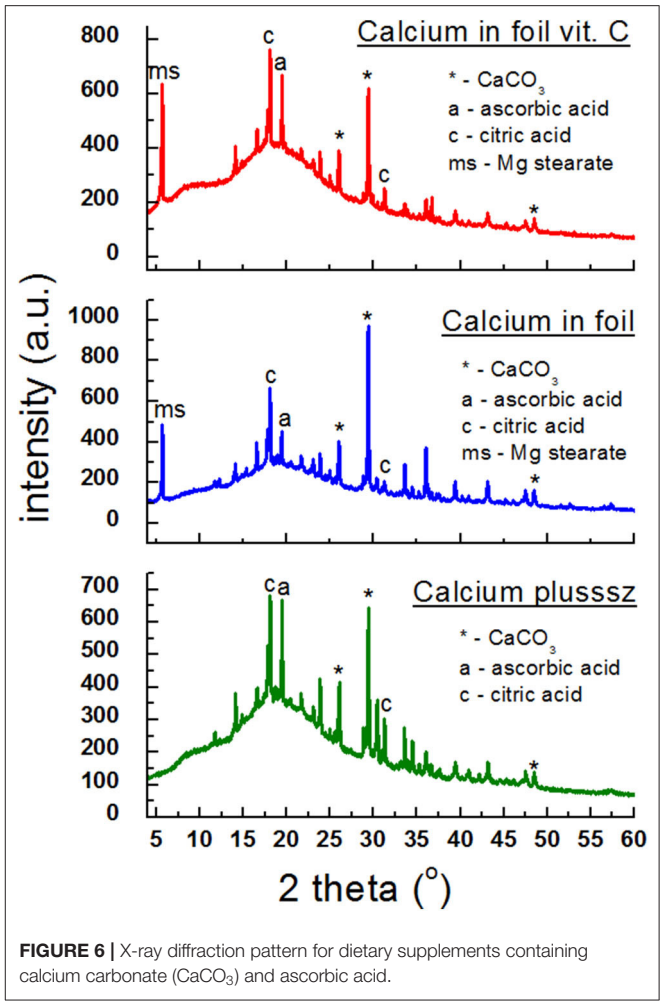

FIGURE 6 | X-ray diffraction pattern for dietary supplements containing calcium carbonate ($CaCO_3$) and ascorbic acid.

these substances are significantly lower than the detection limit or they are not present at all.

Analysis of values of 2θ angles read from the diffraction patterns is in a very good accordance with the data contained in the database, proving that the same crystalline variety of $CaCO_3$ is present in all three products. This good accordance has been confirmed also by the determined $\Delta 2\theta$ difference, which does not exceed 0.2° (**Table 5**).

Figure 8A presents diffraction patterns of *Calcium Alergo Plus* and *Calcium Gluconicum* dietary supplements. According to the manufacturer's information, the active substance of *Calcium Alegro Plus* is constituted by a mixture of an organic and an inorganic calcium salt (calcium lactate and calcium carbonate). $CaCO_3$ is the main component of this preparation; 7 diffraction lines of this compound were identified as having intensities concordant with the ICDD database. For calcium lactate, only one diffraction line with a low intensity was found. The highest intensity in the obtained diffraction pattern is exhibited by the line of SiO_2, being a filler.

Polycrystalline diffraction pattern of *Calcium Gluconicum* consists of many diffraction lines, which are difficult to identify (**Figure 8A**). These lines may originate from auxiliary substances not listed in the composition of this supplement. The active substance of *Calcium Gluconicum* is calcium gluconate. Diffraction lines of this component were identified in the diffraction pattern. On the other hand, the strongest visible diffraction line originates from starch.

For both supplements, *Calcium Alergo Plus* and *Calcium Gluconicum*, a very good accordance of experimental values of 2θ angles and the values of 2θ angles from the ICDD database is evident (**Table 6**). The determined values of $\Delta 2\theta$ are lower than 0.2°, proving the authenticity of the product.

The diffraction pattern of *Molekin* dietary supplement (**Figure 8B**) contains lines of only $CaCO_3$, however, the manufacturer declares also "calcium from seaweed" (in an unknown form). X-ray phase analysis clearly indicates presence of only calcium carbonate ($CaCO_3$), similarly as in the preparations described in **Table 6**.

On the other hand, in *Calcium 500D* (**Figure 8B**) the source of calcium ions according to the manufacturer's claims, was constituted by calcium lactate gluconate, which could not be determined unequivocally in phase analysis. it is probable that a mixture of organic calcium salts: gluconate and lactate, form a broad diffraction peak with a maximum $2\theta = 8.7190°$,

TABLE 5 | Comparison of experimental data with the data from the ICDD database for the following dietary supplements: *Calcium plusssz, Calcium in foil, Calcium in foil + vit.C*, *Kalcikinon, Calcium 400 mg + vit. D3 VITALIS, Vitrum Osteo* ($CaCO_3$ PDF 00–001–0837).

No. of diffraction line	2θ (°) exp.	2θ (°) ICDD	Intensity	Δ2θ	d_{hkl} (Å) exp.	d_{hkl} (Å) ICDD	hkl
Calcium plusssz, Calcium in foil, Calcium in foil + vit.C							
1.	26.0961	26.1884	100	0.0923	3.41	3.40	111
2.	29.3592	29.3554	100	0.0038	3.04	3.04	104
3.	48.4648	48.3749	60	0.0899	1.87	1.88	202
Kalcikinon, Calcium 400 mg + vit. D3 VITALIS, Vitrum Osteo							
1.	22.9932	23.0218	8	0.0286	3.86	3.86	012
2.	29.4363	29.3554	100	0.0809	3.03	3.04	104
3.	35.8795	36.0401	20	0.1606	2.50	2.49	110
4.	39.3147	39.4909	24	0.1762	2.29	2.28	113
5.	43.1593	43.2530	10	0.0937	2.09	2.09	202
6.	47.4802	47.3049	32	0.1753	1.91	1.92	024
7.	48.8083	48.6503	24	0.1580	1.86	1.87	116
8.	57.7010	57.5570	16	0.1440	1.60	1.60	122
9.	62.7736	62.7263	12	0.0473	1.48	1.48	119
10.	64.8629	64.6766	5	0.1863	1.43	1.44	125

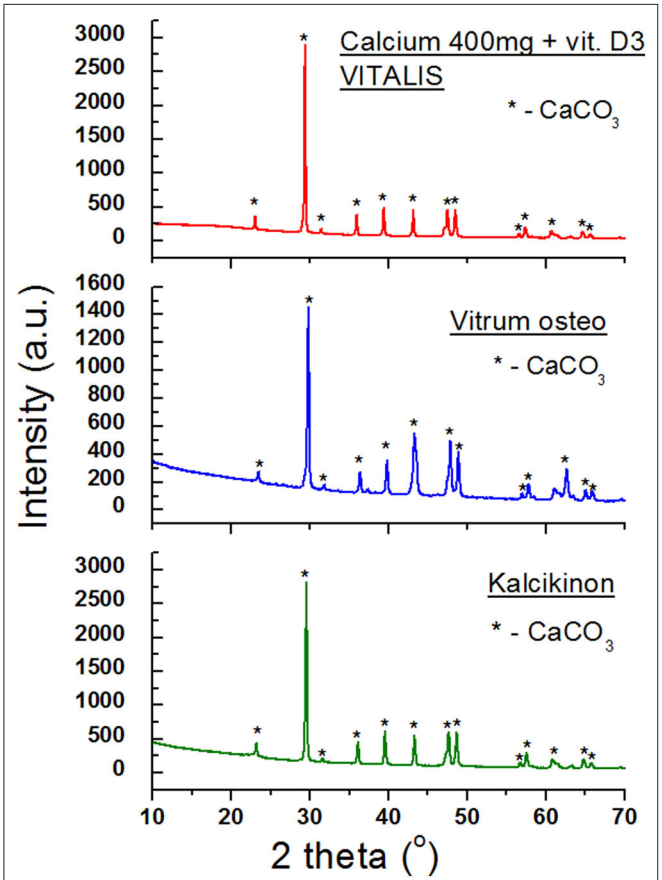

FIGURE 7 | X-ray diffraction patterns for dietary supplements containing calcium carbonate $CaCO_3$.

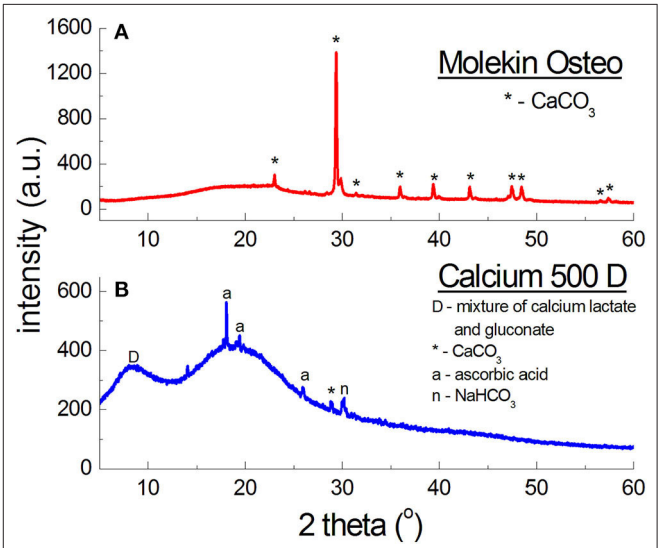

FIGURE 8 | X-ray diffraction pattern for dietary supplements containing organic salts of calcium **(A)** and calcium carbonate $CaCO_3$ and a mixture of organic salts of calcium **(B)**.

because the strongest line for calcium gluconate occurs at the angle of $2\theta = 9.9751°$, and for calcium lactate—at $2\theta = 8.9521°$.

The shape of the line, its width, and maximum value depend on the amounts of lactate and gluconate in this mixture. The manufacturer does not report these values. However, lines originating from calcium carbonate were identified in *Calcium 500D*, this compound likely being the main source of calcium ions in this preparation. Apart from the lines of $CaCO_3$, peaks originating from citric acid, affecting the taste of the supplement, were identified. The manufacturer claims that 1 sachet contains 500 mg of calcium in the form of 3.875 g of calcium lactate gluconate, and 60 mg of ascorbic acid. X-ray analysis shows that the amount of calcium ions is significantly lower. It is proved by intensities of the lines originating from the mixture of calcium

TABLE 6 | Comparison of experimental data with the data from the ICDD database for the following dietary supplements: *Calcium Alergo Plus*, *Calcium Gluconicum, Molekin Osteo,* and *Calcium 500D*.

No. of diffraction line	2θ (°) exp.	2θ (°) ICDD	Intensity	Δ2θ	d_{hkl} (Å) exp.	d_{hkl} (Å) ICDD	hkl
Calcium Alergo Plus – calcium lactate **(PDF 00–029–1526)**							
1.	21.9172	21.9830	50	0.0658	4.05	4.04	–
Calcium Alergo Plus – $CaCO_3$ **(PDF 00–001–0837)**							
1.	23.0303	23.0218	8	0.0850	3.86	3.86	012
2.	29.3939	29.3554	100	0.0385	3.04	3.04	104
3.	35.9557	36.0401	20	0.0844	2.50	2.49	110
4.	39.4638	39.4909	24	0.0271	2.28	2.28	113
5.	43.1303	43.2530	10	0.1227	2.10	2.09	202
6.	47.4825	47.3049	32	0.1776	1.91	1.92	024
7.	48.5081	48.6503	24	0.1422	1.86	1.87	116
Calcium Gluconicum – calcium gluconate **(PDF 00–010–0774)**							
1.	16.1868	16.1607	70	0.0261	5.47	5.48	110
2.	19.4794	19.4072	40	0.0722	4.55	4.57	110
3.	24.4619	24.3661	50	0.0958	3.64	3.65	202
Molekin Osteo – $CaCO_3$ **(PDF 00–001–0837)**							
1.	23.0128	23.0218	8	0.0090	3.86	3.86	012
2.	29.3840	29.3554	100	0.0286	3.04	3.04	104
3.	35.9722	36.0401	20	0.0679	2.49	2.49	110
4.	39.3589	39.4909	24	0.1320	2.29	2.28	113
5.	43.1624	43.2530	10	0.0906	2.09	2.09	202
6.	47.4786	47.3049	32	0.1737	1.91	1.92	024
7.	48.5256	48.6503	24	0.1247	1.87	1.87	116
8.	57.4038	57.5570	16	0.1537	1.60	1.60	122
Calcium 500D – mixture of calcium lactate and gluconate **(PDF: 00-029-1596, 00-010-0774)**							
1.	8.2372	8.9069	100	–	–	–	–
		9.9751	100				

lactate and calcium gluconate, and the lines originating from $CaCO_3$. With such a high amount of calcium ions, the diffraction lines should have higher intensities.

The comparative analysis results for *Molekin Osteo* presented in **Table 6** confirm a very good accordance of the 2θ angle values read from the diffraction pattern with the data from the ICDD database. The determined $\Delta 2\theta$ values are smaller than 0.2°. It proves the authenticity of the *Molekin Osteo* preparation. *Calcium 500D* should be subject to further studies using other methods.

CONCLUSIONS

The X-ray diffractometric studies carried out for 22 commonly available dietary supplements containing calcium and magnesium allowed for ascertaining that the majority of the analyzed products contain appropriate calcium and magnesium compounds declared by the manufacturers in their specifications. Comparison of 2θ angle values at which the diffraction lines originating from calcium and magnesium compounds included into compositions of the tested dietary supplements were recorded, with the data from the ICDD database, showed a very good accordance. It indicates use of substances with the same structural parameters or substances being the same crystalline varieties. In most cases, the difference of 2θ angle values between the experimental data and those from the database is smaller than 0.2°. Abnormalities were found for two dietary supplements containing magnesium ions: *Magnesium KFD Nutrition* and *7 Nutrition Bomb Pre-workout*.

For *Magnesium KFD Nutrition*, the sole visible diffraction line is shifted by more than 0.2° ($\Delta 2\theta = 0.3628$), while for *7 Nutrition Bomb Pre-workout*, no lines of the magnesium compound declared by the manufacturer (magnesium citrate) were identified.

In such a case, when the result of diffractometric analysis is ambiguous or raises some suspicions regarding the authenticity of the product, the tests should be repeated or the analysis expanded with other methods, e.g., IR, UV-Vis, chromatographic methods.

PXRD (Powder X-ray Diffraction) is a fundamental and the most frequently used technique for examination of medical preparations and plays an important role at all stages of pharmaceutical research and development. However, the best practice should consist in an approach in which the XRD studies will be combined with such methods as gas chromatography-mass spectrometry (GC-MS), high performance liquid chromatography (HPLC), Fourier transform infrared spectroscopy (FTIR), or synchrotron radiation (Rendle, 2019).

DATA AVAILABILITY STATEMENT

All datasets generated for this study are included in the article/supplementary material.

AUTHOR CONTRIBUTIONS

IJ was originator of the topic of this manuscript, who prepared all samples to X-ray analysis, who done these measurements and then worked out the results, and wrote the manuscript.

REFERENCES

Bojarski, Z., and Łagiewka, E. (1988). *X-Ray Structural Analysis*. Warszawa: PWN.

Chauhan, A., and Chauhan, P. (2014). Powder XRD technique and its application in science and technology. *J. Analyt. Bioanalyt. Tech.* 5:1000212. doi: 10.4172/2155-9872.1000212

Das, R., Eaqub Ali, M., and Abd Hamid, S. B. (2014). Current application of X-ray powder – a review. *Rev. Adv. Mater. Sci.* 38, 95–109.

DeWitt, K. M. (2015). X-ray powder diffraction method development and validation for the identification of counterfeit pharmaceuticals. *Mater. Sci.* 1–28.

Epp, J. (2016). "X-ray diffraction (XRD) techniques for materials characterization," in *Materials Characterization Using Nondestructive Evaluation (NDE) Methods,* eds G. Huebschen, I. Altpeter, R. Tschuncky, and H. G. Herrmann (Rockville, MD: Woodhead Publishing), 81–124. doi: 10.1016/B978-0-08-100040-3.00004-3

Kugler, W. (2003). X-ray diffraction analysis in the forensic science: the last resort in many criminal cases. *Adv. X-ray Analy.* 46, 1–16.

Maurin, J. K., Pluciński, F., Mazurek, A. P., and Fijałek, Z. (2007). The usefulness of simple X-ray powder diffraction analysis for counterfeit control—the Viagra® example. *J. Pharmac. Biomed. Analy.* 43, 1514–1518. doi: 10.1016/j.jpba.2006.10.033

Rendle, D. F. (2003). X-ray diffraction in forensic science. *Rigaku J.* 19, 11–22.

Rendle, D. F. (2019). "International tables for crystallography," in *Section 7.2.1.3.1. Drugs and Toxicology, Vol. H* (Rockville, MD), 738.

Singh, S., Prasad, B., Savaliya, A. A., Shah, R. P., Gohil, V. M., and Kaur, A. (2009). Strategies for characterizing sildenafil, vardenafil, tadalafil and their analogues in herbal dietary supplements, and detecting counterfeit products containing these drugs. *Trends Analyt. Chem.* 28, 14–28. doi: 10.1016/j.trac.2008.09.004

Stephenson, G. A. (2005). Application of X-ray powder diffraction in the pharmaceutical industry. *Rigaku J.* 22, 2–15.

Stypułkowska, K., Błazewicz, A., Maurin, J., Sarna, K., and Fijałek, Z. (2011). X-ray powder diffractometry and liquid chromatography studies of sibutramine and its analogues content in herbal dietary supplements. *J. Pharmac. Biomed. Analy.* 56, 969–975. doi: 10.1016/j.jpba.2011.08.028

Thatcher, P. J., and Briner, G. P. (1986). The application of X-ray powder diffraction to forensic science. *Powder Diffract.* 1, 320–324. doi: 10.1017/S0885715600011994

USP Pharmacopeial Convention (2011). *General <941> Characterization of Crystalline and Partially Crystalline Solids by X-Ray Powder Diffraction* (Rockville, MD).

Venhuis, B. J., Vredenbregt, M. V., Kaun, N., Maurin, J. K., Fijałek, Z., and de Kaste, D. (2011). The identification of rimonabant polymorphs, sibutramine and analogues of both in counterfeit Acomplia bought on the internet. *J. Pharmac. Biomed. Analy.* 54, 21–26. doi: 10.1016/j.jpba.2010.07.043

World Health Organisation (2006). *Counterfeit Medicines.* Fact Sheet No. 275. Available online at: https://www.gphf.org/images/downloads/library/who_factsheet275.pdf (accessed January 26, 2020).

World Health Organisation (2018). *Substandard and Falsified Medical Products*. Available online at: http://www.who.int/en/news-room/fact-sheets/detail/substandard-and-falsified-medical-products (accessed February 4, 2020).

Conflict of Interest: The author declares that the research was conducted in the absence of any commercial or financial relationships that could be construed as a potential conflict of interest.

APPENDIX

TABLE A1 | List of used ICDD PDF2 (Release 2008) cards.

No.	Chemical formula	Chemical compound	No. PDF card
1.	MgO	Magnesium oxide	00–001– 235
2.	$MgCO_3$	Magnesium carbonate	01–070–8513 01–070–8515
3.	$Mg_3(C_6H_5O_7)_2$	Magnesium citrate	00–001– 0186
4.	$C_6H_{10}MgO_63H_2O$	Magnesium lactate	00–001–0061
5.	$CaCO_3$	Calcium carbonate	00–001–0837 00–001–0628
6.	$C_6H_{10}CaO_6 \times 5H_2O$	Calcium lactate	00–005–0101
7.	$C_{12}H_{22}CaO_{14}$	Calcium gluconate	00–010–0774
8.	$NaHCO_3$	Sodium Carbon Hydrogen Oxide	00–001–0909
9.	$C_6H_8O_6$	Ascorbic acid	00–004–0308
10.	$C_6H_8O_7$	Citric acid	00–001–0251
11.	$(C_6H_{10}O_5)_x$	Starch	00–030–1912
12.	KCl	Potassium chloride	00–004–1476
13.	$C_{36}H_{70}MgO_4$	Magnesium stearate	00–054–1973
14.	$C_3H_7NO_2$	Alanine	00–27–1501

frontiers in Chemistry

ORIGINAL RESEARCH
published: 21 October 2020
doi: 10.3389/fchem.2020.00738

Evaluation of Forensic Data Using Logistic Regression-Based Classification Methods and an R Shiny Implementation

Giulia Biosa[1], *Diana Giurghita*[2]*, *Eugenio Alladio*[3,4], *Marco Vincenti*[4,5] and *Tereza Neocleous*[2]

[1] Forensic Toxicology Laboratory, Department of Health Surveillance and Bioethics, Catholic University of the Sacred Heart, F. Policlinico Gemelli IRCCS, Rome, Italy, [2] School of Mathematics and Statistics, University of Glasgow, Glasgow, United Kingdom, [3] Forensic Biology Unit, Carabinieri Scientific Investigations Department of Rome, Rome, Italy, [4] Department of Chemistry, University of Turin, Turin, Italy, [5] Anti-doping and Toxicology Center "A. Bertinaria" of Orbassano, Turin, Italy

We demonstrate the use of classification methods that are well-suited for forensic toxicology applications. The methods are based on penalized logistic regression, can be employed when separation occurs in a two-class classification setting, and allow for the calculation of likelihood ratios. A case study of this framework is demonstrated on alcohol biomarker data for classifying chronic alcohol drinkers. The approach can be extended to applications in the fields of analytical and forensic chemistry, where it is a common feature to have a large number of biomarkers, and allows for flexibility in model assumptions such as multivariate normality. While some penalized regression methods have been introduced previously in forensic applications, our study is meant to encourage practitioners to use these powerful methods more widely. As such, based upon our proof-of-concept studies, we also introduce an R Shiny online tool with an intuitive interface able to perform several classification methods. We anticipate that this open-source and free-of-charge application will provide a powerful and dynamic tool to infer the LR value in case of classification tasks.

Keywords: classification, likelihood ratio, logistic regression, separation, forensic science, C_{llr}

OPEN ACCESS

Edited by:
Paolo Oliveri,
University of Genoa, Italy

Reviewed by:
Daniel Ramos,
Autonomous University of Madrid, Spain
Roberta Risoluti,
Sapienza University of Rome, Italy

***Correspondence:**
Diana Giurghita
d.giurghita.1@research.gla.ac.uk

Specialty section:
This article was submitted to Analytical Chemistry, a section of the journal Frontiers in Chemistry

Received: *06 April 2020*
Accepted: *17 July 2020*
Published: *21 October 2020*

Citation:
Biosa G, Giurghita D, Alladio E, Vincenti M and Neocleous T (2020) Evaluation of Forensic Data Using Logistic Regression-Based Classification Methods and an R Shiny Implementation. Front. Chem. 8:738. doi: 10.3389/fchem.2020.00738

1. INTRODUCTION

A fundamental task for the forensic experts is that the results of the analyses, which have been performed on the collected pieces of evidence, have to be expressed in a very clear and straightforward way that can be easily shown in courtrooms and that can be immediately, where possible, understood even by non-specialists. However, at the same time, the applied statistical methodologies for data evaluation have to be rigorous and should not compromise the role that the forensic expert plays in the administration of justice (Zadora, 2010).

The main aim of the forensic analysts is to evaluate the physicochemical data from the collected evidence (E) in the framework of two independent, alternative, and mutually exclusive hypotheses (or propositions), H_1 and H_2, in order to estimate the conditional probabilities (P) related to the mentioned hypotheses [i.e., $P(E|H_1)$ and $P(E|H_1)$, which stand for the probability to observe the results from E when H_1 (or H_2) is true]. The comparison between the described conditional

probabilities is performed by their ratio, and it is known as likelihood ratio (LR):

$$LR = \frac{P(E|H_1)}{P(E|H_2)} \quad (1)$$

The LR has been largely adopted in forensic sciences (and courtrooms too) in recent years since it expresses the strength of the observed evidence in favor of proposition H_1 compared to proposition H_2 in a very straightforward way. It can be calculated on both discrete and continuous data, and it is not an assignment of a probability but rather a ratio of probabilities (or density functions for continuous data) and takes values from 0 to $+\infty$. The value of LR equal to 1 represents the condition where the probability of observing the collected evidence when H_1 is true is equal to the probability of E when H_2 is true. In this case, the LR is inconclusive since it provides no support to either of the evaluated propositions. Conversely, the higher the value of the LR, the stronger the support for H_1; on the other hand, the lower the value of the LR, the stronger the support for H_2.

Furthermore, one of the most appreciated features of the LR is that it can be immediately converted into a statement by using well-known verbal scales (Evett et al., 2000). Nowadays, one of the most used scales is the one provided by the European Network of Forensic Sciences Institute (ENFSI) (European Network of Forensic Science Institutes, 2016), which is as follows: for $1 < LR \leqslant 10^1$, there is weak support for H_1 rather than the alternative H_2, for $10^1 < LR \leqslant 10^2$ moderate support, for $10^2 < LR \leqslant 10^3$ moderately strong support, for $10^3 < LR \leqslant 10^4$ strong support, for $10^4 < LR \leqslant 10^5$ very strong support, and for $LR > 10^5$ extremely strong support. The same approach is used for LR values lower than 1.

Another relevant feature of applying the LR in the field of forensics is that it overcomes the so-called "falling off a cliff" problem related to the traditional approach of using cut-off values in classification models (Gill et al., 2006; Pragst et al., 2010; Zadora, 2010; Robertson et al., 2016). In particular, the use of LR avoids the necessity of defining thresholds (such as the largely adopted p-value $= 0.05$ for a significance level of 95%). As a matter of fact, the use of a cut-off such as $p = 0.05$ leads the forensic analyst to completely different (and opposite) conclusions when values close to the defined threshold are observed, such as the cases of $p = 0.049$ or $p = 0.051$. For the first scenario, the proposition H_1 can be rejected, while, for the second scenario, H_1 cannot be rejected. Furthermore, no conclusion can be made about the alternative proposition H_2 because H_2 is not taken into account for the calculation of the p-value. Moreover, a very small difference in the calculated p-value produces a completely different interpretation of the obtained results, thus leading to possible severe consequences for the subjects under investigation (Wasserstein and Lazar, 2016). This approach is particularly inadvisable when dealing with multivariate data since small differences in the calculated probability values (such as, for instance, p-values) could be ascribed to really small differences in the performed analytical measurements. This problem does not occur when the likelihood ratio approach is adopted since the LR does not require the definition of a threshold. Moreover, the degree of support to be delivered to a certain proposition rather than its alternative can be easily related to the magnitude of the LR through the expressions of the cited verbal equivalents.

For these reasons, LR approaches have been largely used in many applications of forensic sciences (Aitken and Taroni, 2004) starting from DNA profiling (Evett and Weir, 1998; Gill et al., 2006) to other forensic fields such as the evaluation of fire debris (Zadora et al., 2005), car paints (Martyna et al., 2015; Michalska et al., 2015), glass fragments (Zadora and Ramos, 2010; Zadora et al., 2014), speaker recognition (Ramos, 2007), and forensic voice comparison with Gonzalez-Rodriguez et al. (2007) being one of the earliest works to introduce LRs derived from logistic regression in the latter field. Another investigated field for the application of LR is the discrimination between chronic and non-chronic alcohol drinkers (Alladio et al., 2017a,b, 2018).

According to the World Health Organization, excessive alcohol consumption is a causal factor in more than 200 disease and injury conditions. Furthermore, the abuse of alcohol severely influences the consumers' lives, leading to different legal, physical, and psychological consequences, especially when dealing with behaviors that might cause road and work accidents.

In recent decades, great interest has been dedicated to the identification of biomarkers capable of recognizing individuals with alcohol-related problems, for both prevention and monitoring purposes. The current approach, from a toxicological point-of-view, aims to identify a person who falls into the category of excessive alcohol consumer through the analysis of indirect biomarkers of alcohol consumption (in blood/serum samples) and, mainly, direct biomarkers (in hair samples, with a length of 0–6 cm) (Kintz et al., 2015).

The most frequently analyzed indirect biomarkers, whose concentration levels in blood are not directly related to the alcohol consumption since they are not formed by alcohol metabolic processes, are aspartate transferase (AST), alanine transferase (ALT), gamma-glutamyl transferase (GGT), mean corpuscular volume of the erythrocytes (MCV), and carbohydrate-deficient-transferrin (CDT) (Pirro et al., 2013). These biomarkers are less frequently evaluated nowadays since they significantly disclose the harmful effects of alcohol on target organs but provide unsatisfactory results in terms of sensitivity and specificity. On the other hand, ethyl glucuronide (EtG) and fatty acid ethyl esters (FAEEs) are the most widely evaluated direct biomarkers of alcohol consumption in hair samples. In particular, EtG is used as reference biomarker since it shows admirable diagnostic sensitivity and specificity results, being capable of assessing both chronic alcohol drinkers (with a cut-off of 30 pg/mg) and teetotaller individuals (with a cut-off of 5 pg/mg). These values have been defined by the Society of Hair Testings (SoHT) and accepted by the forensic community (Society of Hair Testing, 2019).

On the other hand, the determination of FAEEs in hair samples is performed to assist the decision process on chronic alcohol abuse by adding a second biomarker that can be exploited in case of doubtful circumstances (e.g., in case of EtG values close to the 30 pg/mg cut-off). In particular, FAEEs are a family of more than twenty compounds that are synthesized by non-oxidative metabolic esterification processes of fatty acids following the drinking of alcohol. Traditionally, four most present FAEEs were quantified [i.e., ethyl myristate (E14:0), ethyl palmitate (E16:0),

ethyl oleate (E18:0), and ethyl stearate (E18:1)] and their sum was calculated. Moreover, recently, ethyl palmitate (E16:0) has been proposed for alternative interpretation, instead of the sum of the four FAEEs, and possible cut-off values for E16:0 have been updated by the Society of Hair Testing (SoHT), i.e., 0.35 ng/mg for 0–3 cm proximal hair segment and 0.45 ng/mg for 0–6 cm proximal hair segment (Society of Hair Testing, 2019).

The dataset featured in this paper (described in section 2.8) includes samples of both direct and indirect biomarkers of ethanol consumption, collected from two types of alcohol drinkers: chronic and non-chronic. Given the multivariate nature of the data, several multivariate data analysis methods have been proposed to analyze this dataset: Linear Discriminant Analysis (LDA) (Mai, 2013), Quadratic Discriminant Analysis (QDA) (Qin, 2018), binary logistic regression (Murphy, 2012, Chapter 8), as well as penalized versions of logistic regression. The last class of methods, comprising of Firth generalized linear model (Firth GLM) (Firth, 1993), Bayes generalized linear model (Bayes GLM) (Gelman et al., 2008), and GLM-NET (Friedman et al., 2001), have been included to deal with data separation, which occurs when the class variable is perfectly separated by one or more measurement variables. A description of these methods is presented in section 2, while in section 3, we demonstrate how to identify separation in a dataset and discuss the results of a comparison study with the aforementioned methods.

Lastly, in section 3.2, we introduce an R Shiny app, which has been originally developed to provide forensic experts and physicians with a straightforward tool capable of discriminating chronic alcohol drinkers from non-chronic alcohol drinkers through the combination of multivariate data analysis techniques and LR models (involving both uni- and multivariate approaches) following the approaches and the results reported in Alladio et al. (2017b). The R Shiny app can be used with any classification datasets, from any area of forensic science, and for clinical and toxicological purposes. All the methods discussed in this paper are implemented and can be used for obtaining LRs and class prediction. The app has been tested on several well-known datasets that are commonly used in machine learning for classification, such as iris (Dua and Graff, 2019), glass (Dua and Graff, 2019), Pima diabetes (Dua and Graff, 2019), and diamonds (Wickham, 2016), and these are also available to users as part of the R Shiny app to demonstrate its capabilities.

Although the ideas of using penalized (or regularized) logistic regression and kernel density estimation have been previously explored in the context of score-based forensic analysis in applications such as glass (Morrison and Poh, 2018) and voice comparison (Morrison, 2011a), to our knowledge, the particular methods explored in this paper and the R Shiny tool we provide are relatively novel to the forensic sciences.

2. MATERIALS AND METHODS

In this section, we describe logistic regression-based classification methods and we introduce the ideas behind various penalized logistic regression approaches, indicating how they can extend existing methodology commonly used with forensic data. Furthermore, we provide an overview of classification performance measures used to assess the goodness of fit for classification models, and we provide some ideas for how to design a comparison study between several candidate models using cross-validation. Lastly, we provide a description of the alcohol biomarkers dataset (Alladio et al., 2017a) used to illustrate these methods.

In statistics, classification methods tackle the problem of determining the category, or class membership, of an object based on a set of explanatory variables, or features, describing it. The methods covered in this paper are referred to as "supervised learning," meaning a set of observations is typically available whose class membership is *known*. These observations form a training set which is used by a statistical algorithm, or classifier, to map the features of the object to its class through mathematical functions. Ultimately, the purpose of the classifier is to apply the mathematical functions obtained using the training set to determine the class of new objects, based on the same features recorded in the training set. An obvious example of classification is medical diagnostics, where a doctor has to assign a diagnostic to a patient based on different variables: sex, age, blood pressure, etc. In the context of monitoring chronic alcohol abuse, it is of interest to perform classification into one of two categories: chronic or non-chronic alcohol drinker.

2.1. Linear and Quadratic Discriminant Analysis

Linear Discriminant Analysis (LDA) and Quadratic Discriminant Analysis (QDA) are two widely used methods for classification, which, as suggested by their names, produce a linear or quadratic decision boundary between classes. These algorithms can be easily computed and have simple mathematical formulations, are suitable for binary and multi-class classification problems and have no additional parameters that need to be tuned.

A discriminant function is a mathematical function that maps each observation's features directly to a specific class. In the case of LDA, the algorithm estimates weights for each of the features such that the estimated classification is a linear combination of an observation's features and the separation between class means is maximized, while the spread within each class is minimized (Bishop, 2006, Chapter 4).

It should be mentioned that LDA assumes normally distributed (Gaussian) data, features that are statistically independent, and identical covariance matrices for every class. QDA is a more general algorithm for which the assumption of identical covariance matrices is not necessary, and the result is, in essence, a more flexible decision boundary. However, if the distribution of the data is significantly non-Gaussian, then it is very likely that neither LDA nor QDA will perform very well.

2.2. Logistic Regression

A logistic regression model is typically used to identify the relationship between independent variables X_i and a response or dependent variable Y that is binary, meaning it can take two values: e.g., True or False, 1 or 0, chronic or non-chronic drinker,

etc. For illustrative purposes and without loss of generality, we assume the Y variable is labeled as positive (Category 1) or negative (Category 2) for a dataset with N observations. The mathematical form of a logistic regression model is described in Equation (2):

$$\text{logit}(p) = \log\left(\frac{p}{1-p}\right) = \beta_0 + \beta_1 X_1 + \ldots + \beta_k X_k \quad (2)$$

where $\beta_1, \ldots, \beta_k$ are models parameters that need to be estimated, k is the number of independent variables, and p is the probability of success: $P(Y = \text{positive}) = p$. Once the parameters have been estimated, the logistic regression model equation allows us to calculate probabilities for each class of the response variable (Equation 3), as well as the odds (Equation 4), which denotes the ratio of the probability of success to the probability of failure.

The probability is expressed as a function of the predictors in terms of the logistic equation:

$$p = \frac{\exp(\beta_0 + \beta_1 X_1 + \ldots + \beta_k X_k)}{1 + \exp(\beta_0 + \beta_1 X_1 + \ldots + \beta_k X_k)} \quad (3)$$

and the odds as

$$\frac{p}{1-p} = \exp(\beta_0 + \beta_1 X_1 + \ldots + \beta_k X_k). \quad (4)$$

The odds is a ratio of probabilities, and if it is greater than 1 (if $p > 0.5$, then $p/(1-p) > 1$) we classify it as Category 1 (positive), while if it is smaller than 1 (if $p < 0.5$, then $p/(1-p) < 1$) we classify it as Category 2 (negative). This can be compared with the use of the LR for classification.

In the case of a classification problem with two mutually exclusive and exhaustive categories, there is a parallel between p and $P(H_1|E)$ and between $1-p$ and $P(H_2|E)$ where H_1, H_2, and E were defined in section 1. Writing the posterior odds as prior odds times the likelihood ratio gives

$$\frac{P(H_1|E)}{P(H_2|E)} = \frac{P(H_1)}{P(H_2)} \cdot \frac{P(E|H_1)}{P(E|H_2)} \quad (5)$$

providing a relationship between the likelihood ratio, $\frac{P(E|H_1)}{P(E|H_2)}$, and the probability p in Equation (2). For training the logistic regression models used in the remainder of this paper, the prior odds $\frac{P(H_1)}{P(H_2)}$ was assumed to take the value 1, in which case the LR equals $\frac{p}{1-p}$. For different values of the prior odds, $\log\frac{P(H_1|E)}{P(H_2|E)}$ can be obtained from the model described in Equation (2) assuming a fixed value of the prior log-odds $\log\frac{P(H_1)}{P(H_2)}$. The value of the log(LR) can then be calculated as $\log\frac{P(H_1|E)}{P(H_2|E)} - \log\frac{P(H_1)}{P(H_2)}$.

For logistic regression, estimation problems can arise when dealing with a large number of variables relative to the number of observations (N close to "k" scenario) or when perfect or quasi-separation occurs (Heinze and Schemper, 2002; Gelman et al., 2008). The latter scenario refers to situations when one explanatory variable or a combination of explanatory variables completely separate the classes in the dataset. Separation will normally be flagged up by the algorithm implementation, but this can also be observed by inspecting the estimated coefficients and standard errors, which will typically be very large, or by looking at the estimated LRs, which will typically be infinite or zero and is obviously unrealistic. In a logistic regression model, the standard errors associated with each coefficient give a measure of the uncertainty about the coefficient estimate and can be used to test whether the coefficients are significantly different from 0 or to construct confidence intervals for each predictor added in the model. One indication of separation in a logistic regression model is when the estimated standard errors are orders of magnitude larger than the value of the coefficients.

One way to address this problem is to fit a penalized or Bayesian logistic regression model, for example, GLM-NET, Firth GLM, or Bayes GLM, all of which are briefly described in rest of this section.

2.3. GLM-NET

GLM-NET described in Friedman et al. (2010) and implemented in R package `glmnet` (Hastie and Qian, 2014), comprises of fast algorithms that estimate generalized linear models with convex penalties, such as ℓ_1 (the lasso), ℓ_2 (ridge regression) and mixtures of these two, generally known as elastic net penalties.

Ridge regression is a method commonly used when dealing with a large number of explanatory variables, which will inevitably be correlated. The ridge penalty allows many predictors to be included in a model by shrinking the corresponding coefficients of correlated variables toward each other or shrinking less important variable coefficients toward 0. It is important to note that all resulting regression coefficients will be non-zero. On the other hand, lasso will pick one of the correlated variables and ignore the rest, while the elastic-net penalty mixes these two behaviors (regularizes but also excludes variables) (Friedman et al., 2010).

`Glmnet` is a package that fits a generalized linear model via penalized maximum likelihood. The algorithm is very fast, using cyclical coordinate descent—it successively optimizes the objective function for each parameter in turn while the others are kept fixed until convergence is achieved. It can be used with a variety of models: linear, logistic, and multinomial, Poisson, and Cox regression models and can also accommodate multi-class scenarios.

GLM-NET performs regularized logistic regression by maximizing the following penalized log likelihood:

$$\max_{(\beta_0,\beta)\in\mathbb{R}^{k+1}} \left[\frac{1}{N}\sum_{i=1}^{N}\left[Y_i(\beta_0 + X_i^T\beta) - \log\left(1 + e^{(\beta_0 + X_i^T\beta)}\right)\right] - \lambda P_\alpha(\beta)\right] \quad (6)$$

where

$$P_\alpha(\beta) = (1-\alpha)\frac{1}{2}||\beta||^2_{\ell_2} + \alpha||\beta||_{\ell_1} \quad (7)$$

$$= \sum_{j=1}^{k}\left[\frac{1}{2}(1-\alpha)\beta_j^2 + \alpha|\beta_j|\right] \quad (8)$$

P_α is the elastic-net penalty containing the ridge and lasso penalties as special cases when $\alpha = 0$ and $\alpha = 1$, respectively. λ represents a tuning parameter that controls the overall strength of the penalty and can be chosen using cross-validation within the `glmnet` package.

2.4. Firth GLM

Firth GLM described in Heinze and Schemper (2002) and Firth (1993), implemented in R package `brglm2` (Kosmidis, 2020), proposes a solution to the separation problem that involves maximizing a log likelihood penalized by Jeffreys prior (Firth, 1993):

$$\max_{\beta\in\mathbb{R}^{k+1}} \sum_{i=1}^{N}\left[Y_i\log(p_i) + (1-Y_i)\log(1-p_i)\right] + \frac{1}{2}I(\beta) \quad (9)$$

where $I(\beta)$ denotes the Fisher information matrix evaluated at β.

This penalty effectively removes bias from parameter estimates which can be quite serious in sparse or small datasets. In the case of separated data, the profile penalized likelihood is used to construct confidence intervals, see Heinze and Schemper (2002) and Kosmidis et al. (2020) for a more in-depth discussion.

2.5. Bayes GLM

Bayes-GLM described in Gelman et al. (2008) and Chapter 16 of Gelman et al. (2013), implemented in R package `arm` (Gelman et al., 2018), provides a fully Bayesian formulation of a logistic regression model, using weakly informative priors such as Student-t or Cauchy prior distributions for the regression coefficients.

Point estimates and standard errors for the regression coefficients are obtained using a pseudo-data approach, which computes estimates by a modified iteratively weighted least squares algorithm, using a prior-augmented design matrix, X, vector of observations, and weights vector. Section 16.3 in Gelman et al. (2013) provides an extensive illustration of the Bayes-GLM approach.

According to the authors, the choice of weakly informative priors provides regularization and stabilization to the algorithm which are superior to other similar methods such as Firth logistic regression, where the choice of prior (Jeffreys) does not ensure a stable enough estimation.

2.6. Combining LRs

In addition to its use as a classification tool for a two-category problem, as described in section 2.2, logistic regression can be used to produce a weighted average of LRs (called "scores") obtained using different pieces of evidence (or variables). This approach, sometimes referred to as logistic regression fusion, is routinely used in forensic voice comparison and is described in detail in Morrison (2013). This method is especially useful for multivariate data when the number of variables is relatively large compared to the number of observations.

In general, the fusion model can be written as follows:

$$\text{logit}(p) = \log\left(\frac{p}{1-p}\right) = \beta_0^* + \beta_1^* s_1 + \ldots + \beta_k^* s_k \quad (10)$$

where $\beta_0^*, \beta_1^*, \ldots, \beta_k^*$, are the logistic regression coefficients that have to be estimated, and $\frac{p}{1-p}$ is the LR of interest for the practitioner (assuming prior odds of 1, as in section 2.2). In this model $s_1, s_2, \ldots, s_k$ are scores, typically obtained from different data variables or measurements available in the dataset. These scores can be derived as follows: first, we estimate the distribution of both classes for each of the variables of interest, and then we calculate the LR (ratio of the probabilities) for a specific measurement x under each class distribution:

$$s_i = \log(LR) = \log\frac{f(x|H_1)}{f(x|H_2)} \quad (11)$$

In Equation (11), the function f represents the density estimates of each class, which is estimated from a training dataset, where the class membership for each observation is known. Most commonly, these two distributions are assumed to be Gaussian, meaning $f(x) = \frac{1}{\sigma\sqrt{2\pi}}\exp\frac{(x-\mu)^2}{-2\sigma^2}$, however, this is not always suitable. In such situations, kernel density estimation (KDE) can be used specifically to deal with issues such as estimating a multimodal distributions or an unusual behavior in the tails, which the Gaussian distribution can often struggle with. In **Figure 1**, we illustrate these two methods of density estimation and how different the resulting log(LR) can be based on the chosen method.

Intuitively, KDE estimates the underlying density function of some samples $x_1, \ldots, x_n$ by placing a Gaussian distribution over each data point, adding the contributions from each point, and dividing by n to ensure the resulting function is normalized. The Gaussian can be replaced by other non-negative functions, or kernels, denoted K, in which case the resulting density estimate, $\hat{f}$ can be written as follows:

$$f(x) \approx \hat{f}(x) = \frac{1}{nh}\sum_{i=1}^{n} K\left(\frac{x-x_i}{h}\right) \quad (12)$$

In Equation (12), h represents the bandwidth, a parameter which determines how smooth or spiky the resulting density estimation curve should be. In this paper, we use a Gaussian kernel with a bandwidth parameter set according to Silverman's rule (Silverman, 1986, p. 48):

$$h = 0.9\cdot\min\left(\hat{\sigma}, \frac{IQR}{1.34}\right)\cdot n^{-0.2} \quad (13)$$

where $\hat{\sigma}$ and IQR are the standard deviation and interquartile range of the x_i's. The bandwidth parameter

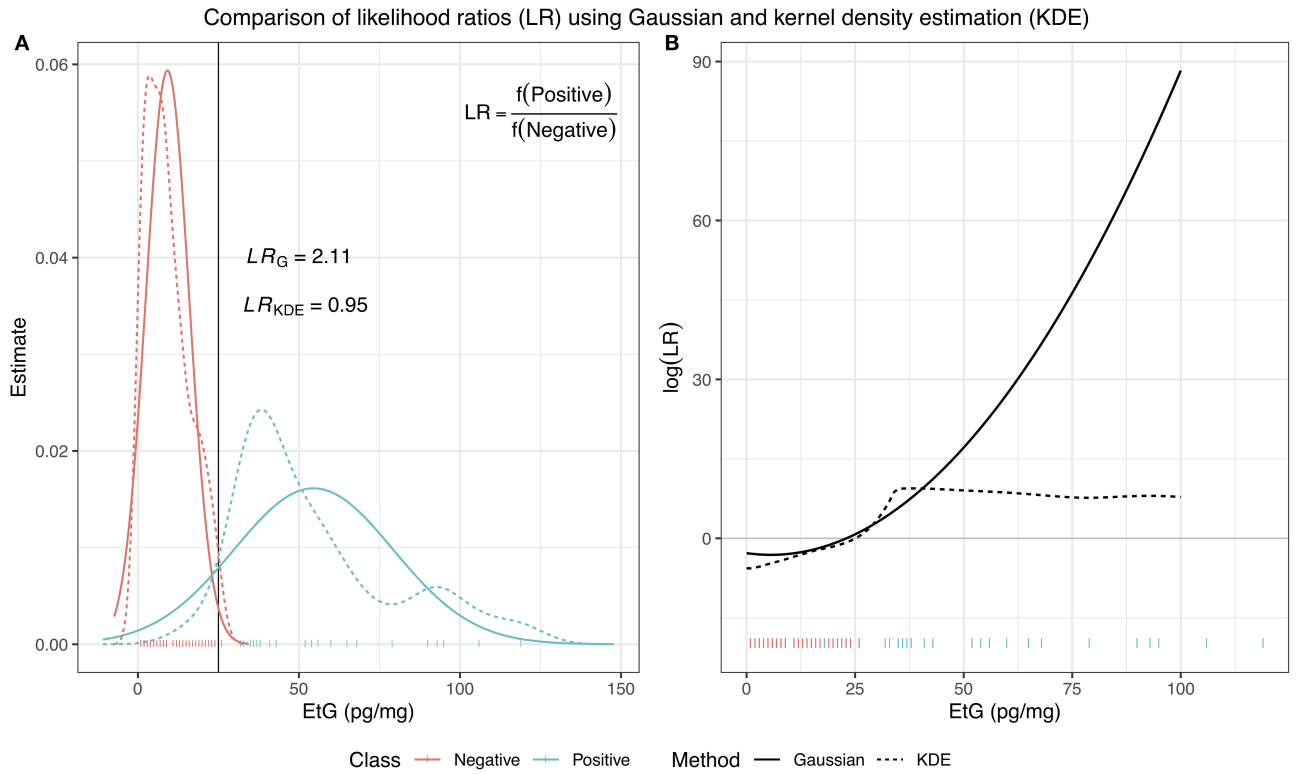

FIGURE 1 | A comparison of LRs using two different methods of density estimation: a Gaussian distribution and kernel density estimator. In **(A)**, for an EtG value of 25, the Gaussian LR has a value of 2.11, indicating the class of an observation with this EtG value should be positive, while the KDE LR has a value of 0.95, indicating that the observation provides similar support for membership of either class. **(B)** Shows the resulting log(LR) evaluated for observations with EtG values between 0 and 100 and illustrates how different the results can be depending on the choice of estimation for the underlying distribution of the data.

can also be chosen using other methods, such as cross-validation, however this comes at an increased computational cost. More discussion on kernel density estimators and the choice of bandwidth can be found in Bishop (2006, Chapter 2.5).

Once the scores are obtained from the variables of interest, the next stage is to use the logistic regression fusion model in Equation (10) to combine all the available pieces of evidence to obtain a calibrated LR. Here, the estimated logistic regression coefficients, $\beta_1^*, \ldots, \beta_k^*$ can be regarded as weights for each score or variable included in the model, providing an extra bonus of ease of interpretation. Since the fusion approach involves a two-stage estimation procedure, to avoid overfitting (obtaining overly optimistic estimates), we use two different datasets at each of these stages, a training dataset to estimate the class distribution for each explanatory variable, and a validation dataset to estimate the logistic regression fusion model coefficients.

In this paper, the fusion method is applied using each of the penalized logistic regression models introduced previously: GLM-NET, Firth GLM, and Bayes GLM, as these methods are equipped to deal with correlated variables and separation issues, both of which can happen the more variables are added to a model.

TABLE 1 | An example of a confusion matrix. N_+ is the number of true positives, $\hat{N}_+$ is the number of estimated positives, N_- is the number of true negatives, and $\hat{N}_-$ is the number of estimated negatives.

		Truth		
		1	**0**	$\sum$
Estimate	1	*TP*	*FP*	$\hat{N}_+ = TP + FP$
	0	*FN*	*TN*	$\hat{N}_- = FN + TN$
	$\sum$	$N_+ = TP + FN$	$N_- = FP + TN$	$N = TP + FP + FN + TN$

2.7. Classification Performance Measures

This section presents the classification measures used to assess the performance of the methods presented in this paper.

The first type of measures rely on the initial calculation of the confusion matrix—a table that allows the visualization of an algorithm's performance based on the numbers of observations correctly and incorrectly classified for each class. An example confusion matrix is provided in **Table 1**, based on the correctly and incorrectly classified observations, denoted as follows:

- true positives (TP): outcomes where the model correctly predicts a positive class.

- true negatives (TN): outcomes where the model correctly predicts a negative class.
- false positives (FP): outcomes where the model incorrectly predicts a positive class.
- false negatives (FN): outcomes where the model incorrectly predicts a negative class.

The classification for each observation is based on the choice of a threshold for the probability estimated by a model. Changing this threshold will change the values of TP, TN, FP, and FN and, consequently, all the measures calculated based on these. Throughout this paper, we use a threshold of 0.5 for the estimated probabilities (corresponding to a threshold of 1 in terms of the LR), meaning an observation with an estimated probability above 0.5 gets classified as a positive and an observation below 0.5 gets classified as a negative.

Table 2 shows a list and definitions of the following classification performance measures including those based on the confusion matrix: precision, recall, specificity, accuracy, error, and F1. Precision and recall are widely used to assess the number of false positives and false negatives, respectively. However, depending of the application, other measures might be of interest, such as the proportion of observations correctly classified (accuracy), the proportion of observations misclassified (error), or the proportion of negatives that are correctly identified (specificity). Often, it is difficult to compare two models with low precision and high recall or vice versa. To make them comparable, the F1 score, which is the harmonic mean of the two, is often used in practice. Murphy (2012, p. 181) presents a more in-depth discussion of classification measures.

Morrison (2011b) explains the downside of using measures such as classification accuracy and error by pointing to the fact that thresholding probabilities to assign class membership to an object lose important information regarding the strength of the evidence in favor of each class. By working directly with the LRs corresponding to each class, one can preserve the strength of evidence in favor of each proposition. As such, we include another classification performance indicator based on the log likelihood ratio cost, which was proposed in the forensic sciences—the C_{llr} (Morrison, 2011b; Ramos et al., 2018). This metric is implemented in the R package `comparison` (Lucy, 2013).

The formula for C_{llr} is as follows:

$$C_{llr} = \frac{1}{2}\left(\frac{1}{N_1}\sum_{i=1}^{N_1}\log\left(1+\frac{1}{LR_{1i}}\right)+\frac{1}{N_2}\sum_{j=1}^{N_2}\log\left(1+LR_{2j}\right)\right) \tag{14}$$

where N_1 and N_2 represent the number of positive (Category 1) and negative (Category 2) sample comparisons, respectively, and LR_1 and LR_2 are the likelihood ratios derived from test pairs known to be of positive and negative origin, respectively.

TABLE 2 | Classification performance measures and corresponding formulae and descriptions for metrics based on the confusion matrix and the C_{llr}, a log likelihood ratio cost metric defined in Equation (14).

Measure	Formula	Description
Precision	$\frac{TP}{\hat{N}_+}$	Measures what proportion of the detected values are actually positive. A model that produces no false positives has a precision of 1.
Recall	$\frac{TP}{N_+}$	Also called *true positive rate* or *sensitivity*. It measures what proportion of the positives were actually detected. A model that produces no false negatives has a recall of 1.
Specificity	$\frac{TN}{N_-}$	Also called *true negative rate*. Measures the proportion of negatives that are correctly identified by the model.
Accuracy	$\frac{TN+TP}{N}$	Rate of correctly classified observations—how many observations were detected correctly out of both classes combined. Best value is 1, worst value is 0.
Error	$\frac{FP+FN}{N}$	Rate of incorrectly classified observations (*classification error*)—how many observations (either positive or negative) were incorrectly classified. Best value is 0, worst value is 1.
F1	$\frac{2\cdot Recall\cdot Precision}{Recall+Precision}$	The harmonic mean of the precision and recall measures, and it is often used in cases with low prevalence by penalizing extreme values. Best value is 1, worst value is 0.
C_{llr}	see Equation (14)	Log likelihood ratio cost. Lower values indicate better performance.

2.7.1. Cross-Validation

While in the previous section we described various classifiers and presented some measures of tracking how good a classifier is, in this section we describe how to design a comparison study between multiple algorithms using cross-validation. Cross-validation can be employed to avoid biased estimates and overfitting issues due to training and testing a classifier on the same dataset. In practice, the most common problems are either the lack of future data (for which the label has to be predicted) or small sample size datasets, which one would ideally use to their fullest capacity to train a classifier (Murphy, 2012).

Cross-validation provides an answer to this problem by partitioning data into a *training set*, which is used for fitting the models, and a *test set*, which is used for predicting the class labels and obtaining the performance measures (or prediction error, or any sort of indicator of goodness-of-fit for the models). The partitioning of the dataset is repeated in all possible ways, making sure that the same observation is not included for testing and training at the same time. Ultimately, the cross-validation goal is to obtain an out-of-sample prediction error for each algorithm, and this is done by averaging the classification error or measures considered over all repetitions. More details and discussion about cross-validation can be found in Venables and Ripley (2013), Murphy (2012), and Gelman et al. (2013).

One of the downsides of cross-validation is that it can get computationally expensive depending on the size of the dataset and the number of models included in the comparison, and a few variations of this procedure have been proposed to address this. Commonly used cross-validation procedures include exhaustive and non-exhaustive methods, based on whether they use all possible ways to split the dataset into training and testing sets or

not. It should be noted that, in the latter case, the average score produced is an *approximate* cross-validation score.

Examples of commonly used cross-validation procedures include:

- *leave-p-out cross-validation*: p observations are used as a testing set and the remaining as the training set. This procedure is repeated in all possible ways of choosing p observations out of the total sample size, and, as expected, becomes unfeasible for even moderately large datasets (there are C_p^n ways to choose p observations from a dataset of size n).
- *k-fold cross-validation*: the dataset is partitioned into k subsets of equal size, one of them being used for testing the algorithms, while the other $k - 1$ being used for training. This is repeated such that each fold, and thus each observation, is used once for testing the models.

In this paper, we use a slightly different cross-validation procedure, due to the fact that some methods investigated (combining LRs using logistic regression fusion) involve multi-step estimation procedure and require the estimation of additional parameters. These parameters should ideally be estimated using data that is neither part of the training, nor testing sets—a further split, forming a *validation* set can be used in this scenario.

2.8. Data

The alcohol biomarker dataset published in Alladio et al. (2017a) presents concentration values of a series of direct and indirect biomarkers of ethanol consumption from 125 individuals classified as either chronic (positive) of non-chronic (negative) alcohol drinkers.

Indirect biomarkers, collected from blood, are as follows: aspartate transferase (AST), alanine transferase (ALT), gamma-glutamyl transferase (GGT), mean corpuscular volume of the erythrocytes (MCV), and carbohydrate-deficient-transferrin (CDT).

Direct biomarkers, collected from hair samples, are the following: ethyl glucuronide (EtG; pg/mg) and the sum of the concentrations of four Fatty Acid Ethyl Esters (FAEEs), mainly ethyl myristate (E14:0), ethyl palmitate (E16:0), ethyl stearate (E18:1), and ethyl oleate (E18:0). Body mass index (BMI) was also collected as a potential factor.

This dataset is displayed in **Figure 2** in the form of bivariate scatterplots of these eight variables, where the points are colored according to the alcohol drinking chronic status. Not in particular how in the scatterplot of FAEEs and EtG perfect separation of the positive and negative classes is achieved. While this kind of pattern is often what is needed to achieve a good classification model, this also indicates that a logistic regression model will most likely experience estimation problems and will be unable to provide reliable LR estimates, as discussed in section 2.2.

3. RESULTS

In this section we present a comparison of the methods introduced in section 2, using the alcohol biomarkers dataset presented in section 2.8.

Our goal is to demonstrate how separation can be identified and to present alternatives that can be used in practice. These alternatives are penalized logistic regression models, presented in section 2, and can be used both in a classification scenario, using the variables directly, or in a fusion scenario, using the scores of the variables. Lastly, we demonstrate how to run a comparison study when various classification or LR-based methods are available.

3.1. Case Study: Alcohol Biomarkers Dataset

In section 2.8, we observe that separation is occurring in the alcohol biomarkers dataset just through visual inspection of plots. However, it is important to know that separation can be more difficult to identify visually when the dataset has a large number of variables and a linear combination of some variables perfectly separates the categories in the data. In this scenario, separation can be detected by inspecting the model estimates for infinite values or any unusual numbers.

For example, a first attempt at fitting a logistic regression model for the alcohol biomarkers dataset fails when using the `glm` function in `R`. This is due to the unusually large standard errors, which can be seen in **Table 3**.

In contrast, the results from penalized logistic regression models shown in **Table 4** indicate that more sensible coefficient estimates and standard errors can be obtained using these methods.

The three logistic regression methods discussed in this paper—Firth GLM, Bayes GLM, and GLM-NET—can be used both as classification methods, by using the explanatory variables directly, or within a fusion model (as discussed in section 2.6), where the goal is to combine LRs or scores from different sources.

The rest of this section contains results of a comparison study between the different LR based and classification methods presented in section 2.

As discussed in section 2.7.1, cross-validation should be employed when carrying out a comparison study or when assessing the prediction performance of a model, as this can lead to overly optimistic performance estimates.

For the alcohol biomarkers dataset, which comprises of 125 observations, the dataset is randomly split such that 50% of observations are assigned to the training set, 40% to the validation set and 10% to the testing set. For classification methods, which do not require a multi-step estimation procedure (which happens for LR fusion methods), both the training and validation sets are used to train the classifier, thus ensuring that all the data *not* in the testing set is used in the fitting procedure to train the model. The split and data allocation is repeated $n_{cv} = 50$ times, and then averages of the performance measures listed in **Table 2** are computed for each algorithm. It should be noted that the results provided using this method are approximate cross-validation scores (since we do not calculate all possible ways to allocate the data), and, due to the Monte Carlo nature of the procedure, the results will be different when the analysis is repeated (unless the random seed generator is saved in advance).

The results in **Table 5** present cross-validation averages of the various classification performance metrics introduced in section 2.7. On average, all the methods have an accuracy of

FIGURE 2 | Alcohol biomarkers dataset, with the color indicating the drinking status of the individuals: red is *Negative* (not chronic) and blue is *Positive* (chronic). The upper diagonal panels display the correlation of variables for the whole data but also separately for each class. Diagonal panels show densities of the data by class, while lower diagonal panels show bivariate scatterplots with points colored according to drinking status.

TABLE 3 | Logistic regression model coefficients and standard errors, estimated for the alcohol biomarkers dataset, using a logistic regression model implemented in the `glm` function in `R`.

	Intercept	FAEEs	EtG	AST	ALT	GGT	MCV	CDT	BMI
Coefficient	−80.353	30.792	2.654	−0.127	−0.197	0.210	0.055	0.246	−0.605
Std. error	2052282.3	75446.6	1899.5	3436.1	2338	1322	30217.2	62386.2	30617.7

Notice the extremely large standard errors which make it impossible to make further inferences using this model in practice. This model output is to be expected in the presence of separation.

over 85%, indicating a high probability that individuals will be correctly classified as chronic or non-chronic alcohol drinkers, when the decision-making is based on a threshold of 0.5 for the predicted probability. **Figure 3** shows boxplots of all the classification metrics, which gives us an idea of how much variability in the estimates was observed in over the 50 cross-validation datasets. These results indicate that fusion methods based on the Firth GLM model implementation have a larger variability compared to the rest, indicating this method is not as reliable in practice. We experienced some problems with the convergence of the algorithm as implemented in the `brglm2` package (Kosmidis, 2020) in four out of the total of 50 dataset in the cross-validation scheme; however, the other implementation of Firth GLM in the `R` package `logistf` (Heinze and Ploner, 2018) performed even worse, with more than half of the models returning convergence warnings.

The best classification performance, based on the average C_{llr}, accuracy, and precision is achieved by the fusion GLM-NET model using kernel density estimation for the scores (see **Table 5**). **Figure 3** shows boxplots of all the classification metrics, which gives us an idea of how much variability in the estimates was observed over the 50 cross-validation datasets. These results indicate that fusion methods based on the Firth GLM model implementation have a larger variability

TABLE 4 | Coefficients and standard errors, estimated for the alcohol biomarkers dataset, using penalized/Bayesian logistic regression models: Firth GLM ran using the `glm` function in the `R` package `brglm2`, Bayes GLM ran using the `bayesglm` function in the `R` package `arm` and GLM-NET ran using the `glmnet` function in the `R` package `glmnet` (standard errors are not provided by default in the `glmnet` package; however, they can be estimated using bootstrapping; the dots indicate variables that have been dropped from the model).

	Intercept	FAEEs	EtG	AST	ALT	GGT	MCV	CDT	BMI
					Firth				
Coefficient	0.171	3.053	0.185	0.118	0.014	−0.020	−0.057	−1.087	−0.162
Std. error	9.015	1.365	0.063	0.087	0.028	0.021	0.076	0.844	0.240
					Bayes GLM				
Coefficient	−10.581	3.129	0.279	0.010	−0.003	0.004	0.004	0.434	−0.032
Std. error	12.200	1.441	0.101	0.115	0.045	0.027	0.114	1.605	0.22
					GLM-NET				
Coefficient	−11.191	4.25	0.298	.	.	.	.	.	.

These methods provide sensible model coefficients and standard errors making them the preferred option for further inferences such as obtaining LRs or prediction for new data.

TABLE 5 | Classification performance measures for the alcohol biomarkers dataset using penalized Gaussian LR methods, penalized kernel density estimate LR methods and classification methods.

	Gaussian LR			Kernel density estimate LR			Classification		
	Firth	GLM-NET	Bayes GLM	Firth	GLM-NET	Bayes GLM	LDA	QDA	Firth
Precision	0.712	0.980	1	0.838	**1**	0.990	1	0.914	0.990
Recall	0.595	0.897	0.934	0.839	**0.948**	0.934	0.852	0.978	0.920
Specificity	0.934	0.996	1	0.936	**1**	0.999	1	0.967	0.998
Accuracy	0.857	0.975	0.987	0.917	**0.993**	0.989	0.966	0.970	0.981
F1	0.763	0.972	0.984	0.839	**0.993**	0.977	0.943	0.934	0.959
Error	0.143	0.025	0.013	0.083	**0.007**	0.011	0.034	0.030	0.019
C_{llr}	1.790	0.293	0.271	0.382	**0.080**	0.098	0.300	0.580	0.244

Results consist of averages obtained from cross-validation using $n_{cv} = 50$ datasets and a classification threshold value of 0.5 for the probability (corresponding to 1 for the LR) for obtaining the confusion matrix. Based on the best values across all performance measures (shown as bold values), the best performing method is GLM-NET using KDE estimation.

compared to the rest, indicating this method is not as reliable in practice.

GLM-NET with KDE LR estimation has an average precision and specificity rate of 100% meaning no non-chronic individuals get labeled as chronic, when the decision-making is based on a threshold of 0.5 for the predicted probability. Furthermore, the average recall rate is 94.8% which means a chronic individual has, on average, around 5.2% probability to get misclassified as a non-chronic alcohol drinker, when that same probability threshold of 0.5 (equivalent to an LR threshold of 1) is used.

The results for Bayes GLM are very similar to those obtained by GLM-NET, for both Gaussian and KDE LR estimation, while Firth seems to be less reliable—the average C_{llr} is an order of magnitude higher for both of these categories. However, using Firth GLM as a classification algorithm is more stable, with comparable results for precision, recall, accuracy, etc. Interestingly, although the classification methods have a similar performance in terms of metrics based on the confusion matrix, their corresponding C_{llr} values are considerably higher than the best LR methods (GLM-NET and Bayes-GLM using KDE). This suggests that when an observation is misclassified, the LR from these methods gives strong support to the wrong proposition. The C_{llr} thus highlights something that would not be obvious by looking at misclassification error rates alone.

3.2. Shiny App

Shiny (Chang et al., 2019) is a package from R software environment (R Core Team, 2019) that allows us to create specific and dynamic interactive web apps. The idea to use R Shiny for developing an open-source tool to perform data analysis came from the necessity to allow analysts, physicians, forensic experts, but also practitioners and laymen in the forensic sciences fields to test, on their own data, several models and statistical approaches aimed to perform robust and comprehensive data evaluations.

We developed an R Shiny app to help practitioners explore the various classification methods discussed in this paper and hopefully apply these well-known algorithms in the statistics and machine learning community to their own datasets.

The app includes functionality for data exploration, classification, and LR-based methods using penalized logistic regression models discussed in this paper.

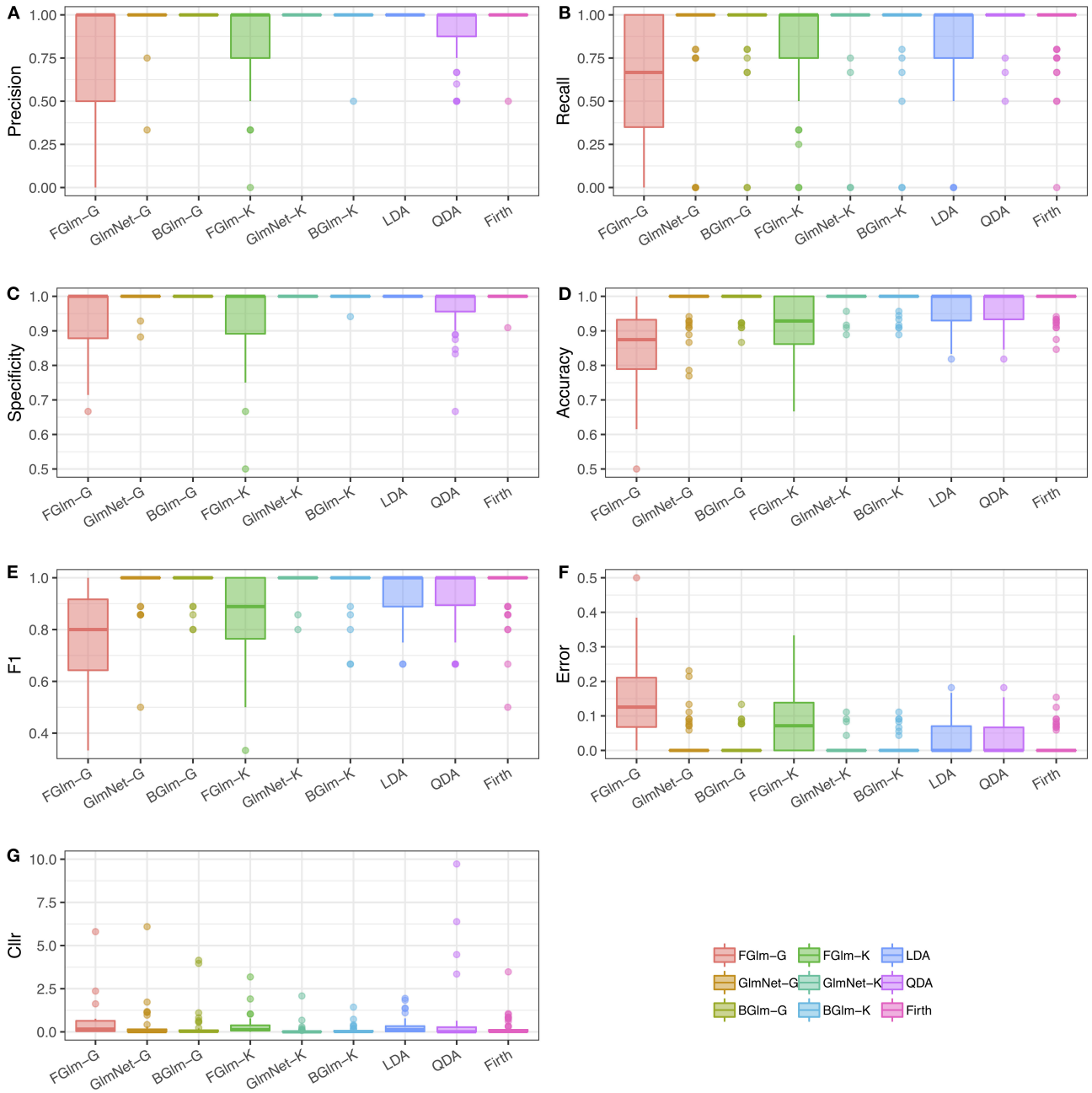

FIGURE 3 | Results of the comparison study between different LR-based and multivariate classification methods. Each figure shows boxplots of different comparison metrics obtained using cross-validation from $n_{cv} = 50$ datasets: precision **(A)**, recall **(B)**, specificity **(C)**, accuracy **(D)**, F1 **(E)**, classification error **(F)**, and C_{llr} **(G)** (as defined in **Table 2**). LR methods using a Gaussian density estimation are indicated with suffix "-G," while LR methods using KDE are indicated with suffix "-K." LDA, QDA, and Firth GLM have been included for comparison as classification methods.

Here are some of the R Shiny app capabilities in more detail:

- data exploration through numerical and visual summaries, see **Figure 4**.
- fitting classification methods for bivariate and multiclass datasets, such as LDA, QDA, logistic regression, Firth GLM, and multinomial logistic regression, model summaries, classification performance measures and visualization plots, see **Figure 5**.
- fitting LR combination methods using penalized logistic regression models, such as GLM-NET, Firth or Bayes GLM, and LR estimation based on a Gaussian distribution or KDE, see **Figure 6** (top).
- method comparison using cross-validation based on metrics discussed in this paper, see **Figure 6** (middle).
- the user can explore and gain an understanding of these methods using in-built datasets which are routinely used in the machine learning community for classification and prediction.

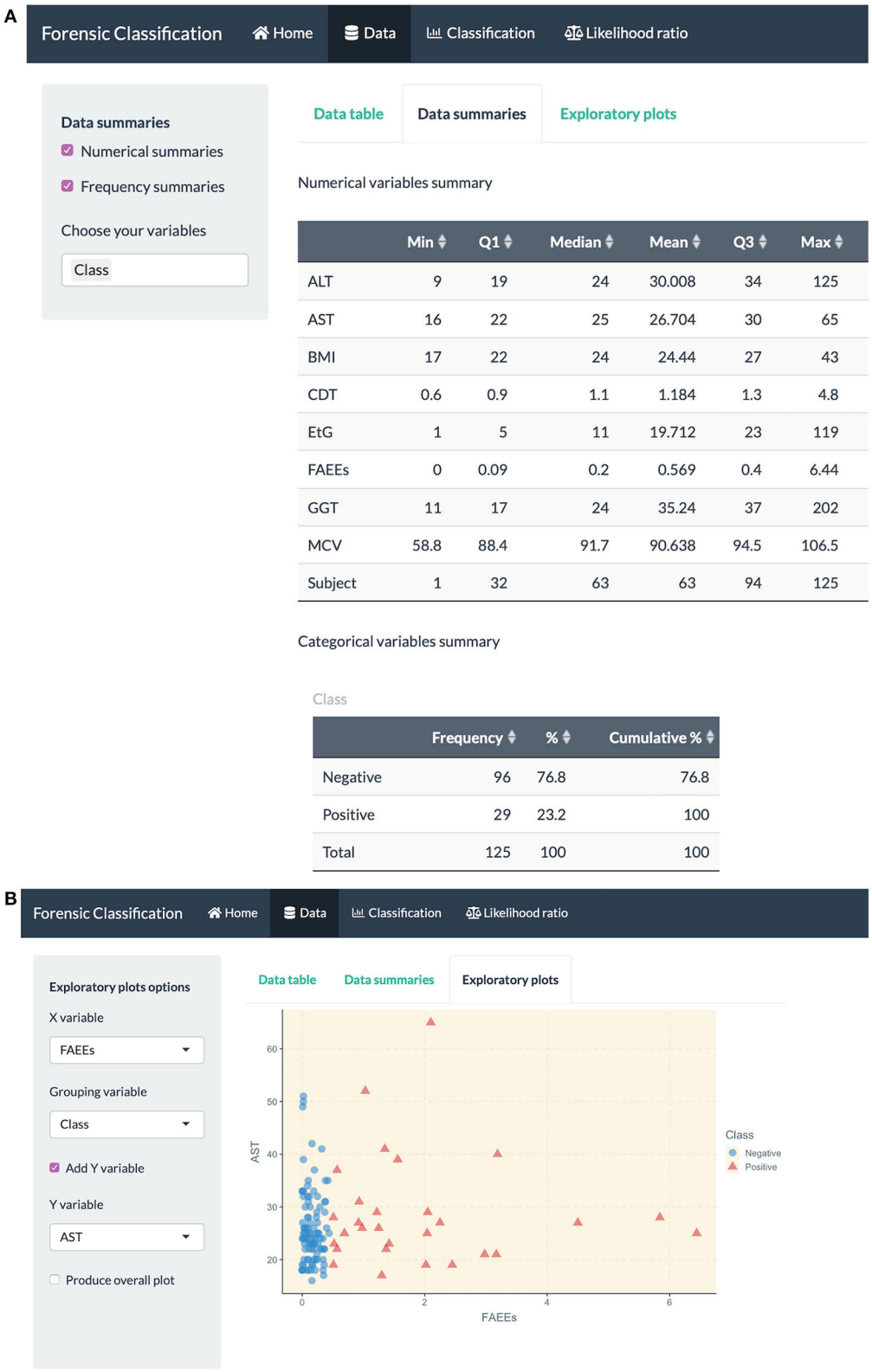

FIGURE 4 | R Shiny app: "Data" tab screenshots, showing **(A)** numerical summaries for variables in the alcohol biomarkers dataset **(B)** exploratory plots.

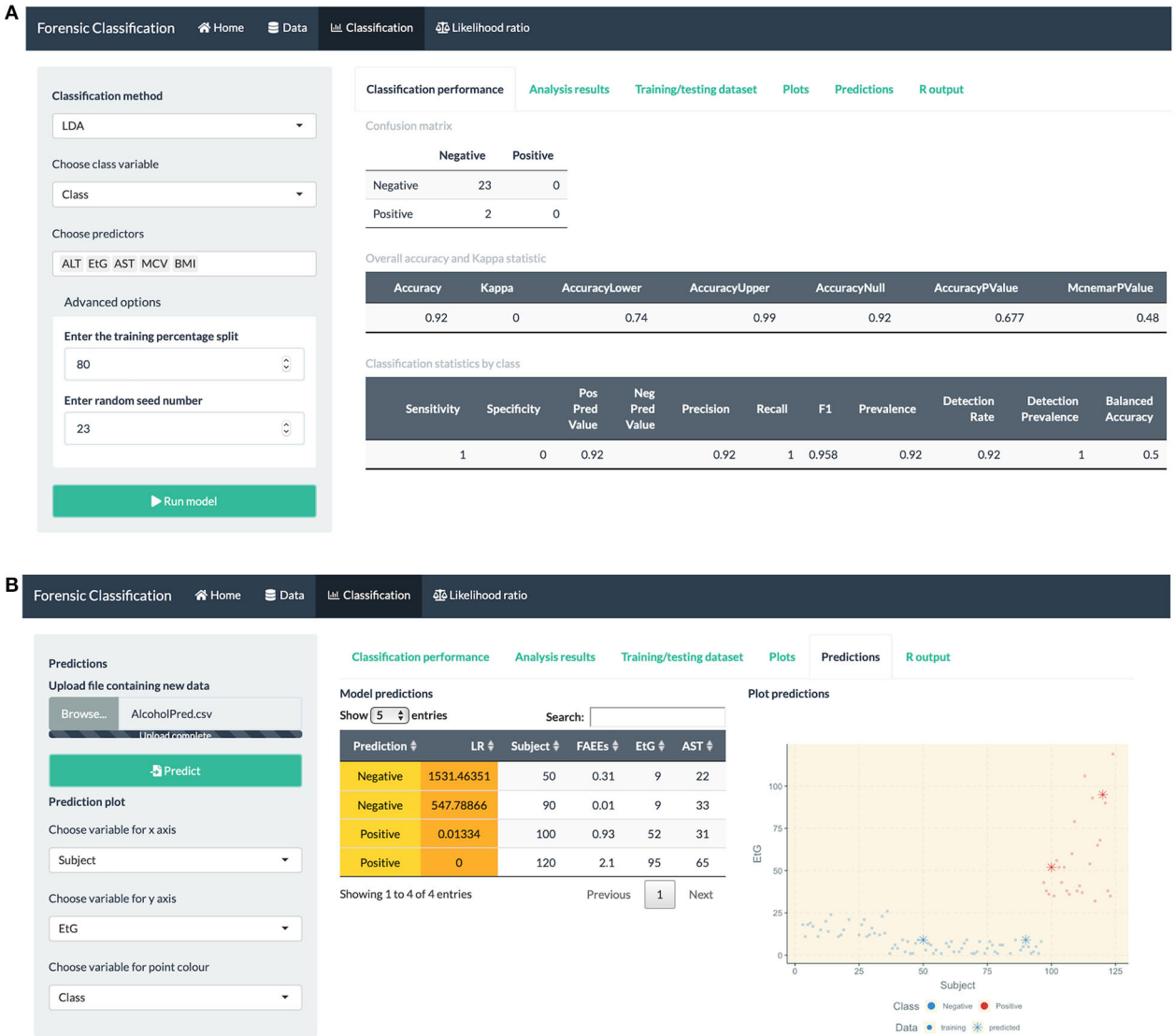

FIGURE 5 | R Shiny app: "Classification" tab screenshots, showing **(A)** confusion matrix and model performance measures: sensitivity, precision, recall, etc. for the alcohol biomarkers dataset **(B)** prediction table, including the predicted class and LR for each observation, and plot showing the training and predicted data.

- uploading an external dataset to run the classification or LR combination methods, see **Figure 6** (bottom).
- prediction capabilities for external data that can be uploaded into the app, see **Figure 5** (bottom).

Additional datasets available within the app are:

Iris (Dua and Graff, 2019) Contains data from three species of iris: setosa, versicolor, and virginica. There are four measurements collected that have been included in this dataset: the sepal length, sepal width, petal length, and petal width in cm. The number of observations in each class is balanced (50 observations per class, 150 in total). It is a multi-class dataset with 150 observations, four explanatory variables, and one output variable.

Glass (Dua and Graff, 2019) It contains data representing seven types of glass: building windows (float processed), building windows (non-float processed), vehicle windows (float processed), vehicle windows (non-float processed), containers, tableware, and headlamps. There are nine explanatory variables: refractive index, along with the chemical composition measured as weight percent in corresponding oxide, Sodium, Magnesium, Aluminum, Silicon, Potassium, Calcium, Barium, and Iron. The dataset is imbalanced, meaning that the 214 total observations are not distributed equally across the seven classes.

Diabetes (Dua and Graff, 2019) This dataset contains measurements of 768 females over 21 years old of Pima Indian heritage, collected with the goal of predicting whether a patient has diabetes (this represents the class variable). The variables collected are: the number of times pregnant, plasma glucose concentration a 2 h in an oral glucose tolerance test, diastolic blood pressure, triceps skin fold thickness, 2-h

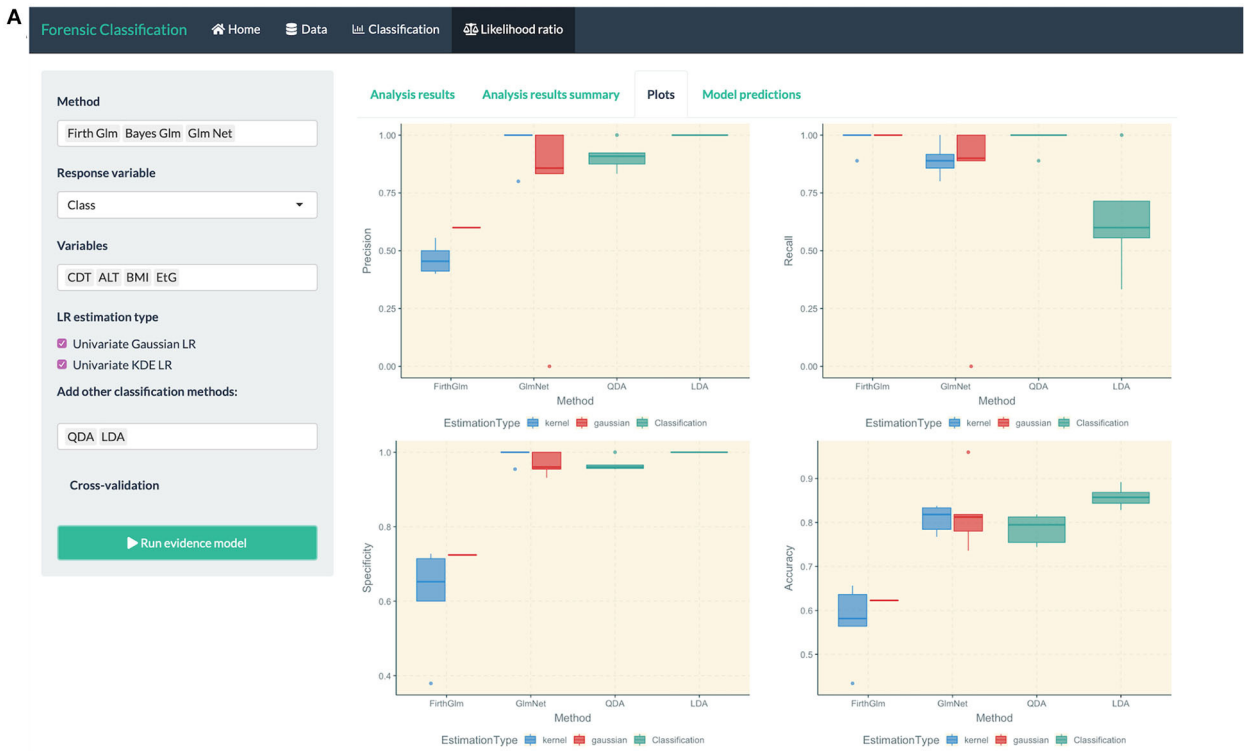

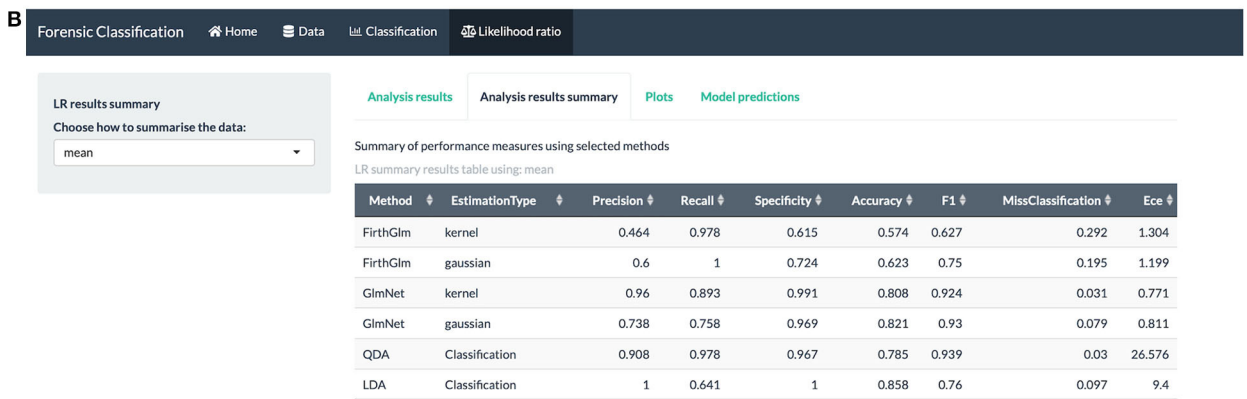

Method	EstimationType	Precision	Recall	Specificity	Accuracy	F1	MissClassification	Ece
FirthGlm	kernel	0.464	0.978	0.615	0.574	0.627	0.292	1.304
FirthGlm	gaussian	0.6	1	0.724	0.623	0.75	0.195	1.199
GlmNet	kernel	0.96	0.893	0.991	0.808	0.924	0.031	0.771
GlmNet	gaussian	0.738	0.758	0.969	0.821	0.93	0.079	0.811
QDA	Classification	0.908	0.978	0.967	0.785	0.939	0.03	26.576
LDA	Classification	1	0.641	1	0.858	0.76	0.097	9.4

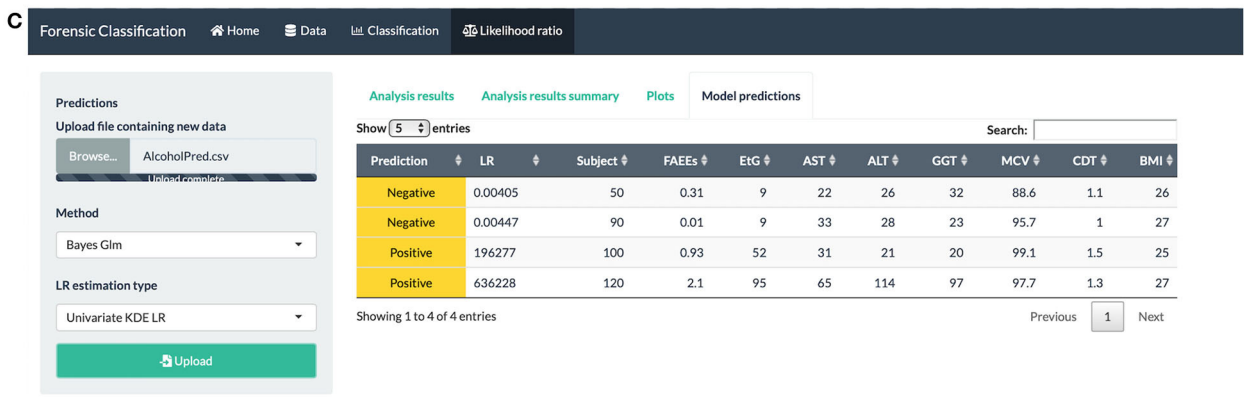

Prediction	LR	Subject	FAEEs	EtG	AST	ALT	GGT	MCV	CDT	BMI
Negative	0.00405	50	0.31	9	22	26	32	88.6	1.1	26
Negative	0.00447	90	0.01	9	33	28	23	95.7	1	27
Positive	196277	100	0.93	52	31	21	20	99.1	1.5	25
Positive	636228	120	2.1	95	65	114	97	97.7	1.3	27

FIGURE 6 | R Shiny app: "Likelihood ratio" tab screenshots, showing in **(A)** model comparison based on LR combination methods (Firth and GLM-NET) and regular classification methods such as LDA and QDA, in **(B)** summary of performance measures for method comparison, in **(C)** prediction table based on the Bayes GLM method with scores estimated using KDE, including the predicted class and LR for each observation in the uploaded dataset.

serum insulin, body mass index, age, and the diabetes pedigree function.

Diamonds (Wickham, 2016) Contains 10 variables recorded for different types of diamonds: price, carat, length, width, depth, total depth percentage, and the width of the top of the diamond relative to the widest point. There are three categorical variables in this dataset describing the quality of the cut (Fair, Good, Very Good, Premium, and Ideal), the diamond color (from J–worst to D–best), and the clarity (I1–worst, SI2, SI1, VS2, VS1, VVS2, VVS1, and IF–best). There are 53,940 observations in this dataset.

The Shiny app is free to use and can be found at the following link: https://dianagiurghita.shinyapps.io/ForensicClassification/

4. DISCUSSION

LR-based methods, such as logistic regression fusion (Morrison, 2011b, 2013) and classification methods such as LDA and QDA are attractive to forensic experts because they allow them to carry out a rigorous, sound statistical analysis. Furthermore, these methods allow experts to present to the courtroom a likelihood ratio, which can easily be put into a statement to convey the strength of the evidence obtained from their analysis for various hypotheses of interest in a case.

In this paper, we present a framework for classification based on penalized logistic regression methods: Firth GLM, Bayes GLM, and GLM-NET. These algorithms are widely known and used in the statistics and machine learning communities as algorithms that can accommodate a large number of explanatory variables, sparse datasets, and correlated variables and can deal with separation or quasi-separation in the data; however, they seem to be less known outside these circles. These methods should be regarded as an extension to logistic regression and logistic regression fusion since they accomplish the same role—they perform classification, prediction, and return LRs—but they have built-in mechanisms to deal with some common estimation problems.

Another extension we provide in this paper is in the context of fusion of LRs: to this end, we present kernel density estimation as an alternative to the widely used Gaussian distribution approximation. This is suitable in situations when the underlying data is multi-modal or not particularly symmetric or bell-shaped.

We demonstrate the use of these penalized logistic regression algorithms on an alcohol biomarkers dataset which includes direct and indirect biomarkers for the identification of chronic alcohol drinkers. These two categories of alcohol drinkers (chronic and non-chronic) can be perfectly separated by two variables in the dataset, and we indicate how to recognize that estimation fails in such scenarios using a logistic regression model. Furthermore, we present a comparison study using the penalized logistic regression model framework proposed in section 2. The best model based on C_{llr}, accuracy and precision is GLM-NET using KDE estimation for LRs, with Bayes-GLM providing similar performance. We find that models based on Firth GLM are less reliable and this can be due to a mixture of factors, including the software implementation being unstable and the choice of penalty involving a prior that is too weak (as pointed out in Gelman et al., 2008).

Lastly, we hope to encourage practitioners to learn more about these methods and apply them when necessary and, to this end, we have built a user-friendly R Shiny app that is freely available and very comprehensive. The app includes all the methods presented in this paper and has in-built datasets that allow users to explore and get a better understanding of penalized logistic regression models.

DATA AVAILABILITY STATEMENT

The alcohol biomarkers dataset used in this paper is published in Alladio et al. (2017a). The R Shiny app can be downloaded at: https://github.com/DianaGiurghita/Forensic-Classification or used online at: https://dianagiurghita.shinyapps.io/ForensicClassification/.

AUTHOR CONTRIBUTIONS

EA, GB, and TN devised the project and the main conceptual ideas. GB, EA, and MV designed and implemented the study that produced the alcohol biomarkers dataset. DG and TN designed the R Shiny app, researched the appropriate statistical methodology, and carried out the data analysis. EA and GB provided feedback and tested the R Shiny app. DG, GB, and EA wrote the manuscript. All authors read and approved the submitted version.

REFERENCES

Aitken, C., and Taroni, F. (2004). *Statistics and the Evaluation of Evidence for Forensic Scientists*. Chichester: John Wiley & Sons. doi: 10.1002/0470011238

Alladio, E., Giacomelli, L., Biosa, G., Di Corcia, D., Gerace, E., Salomone, A., et al. (2018). Development and validation of a Partial Least Squares-Discriminant Analysis (PLS-DA) model based on the determination of ethyl glucuronide (EtG) and fatty acid ethyl esters (FAEEs) in hair for the diagnosis of chronic alcohol abuse. *Forens. Sci. Int.* 282, 221–230. doi: 10.1016/j.forsciint.2017.11.010

Alladio, E., Martyna, A., Salomone, A., Pirro, V., Vincenti, M., and Zadora, G. (2017a). Direct and indirect alcohol biomarkers data collected in hair samples-multivariate data analysis and likelihood ratio interpretation perspectives. 12, 1–8. doi: 10.1016/j.dib.2017.03.026

Alladio, E., Martyna, A., Salomone, A., Pirro, V., Vincenti, M., and Zadora, G. (2017b). Evaluation of direct and indirect ethanol biomarkers using a likelihood ratio approach to identify chronic alcohol abusers for forensic purposes. *Forens. Sci. Int.* 70, 13–22. doi: 10.1016/j.forsciint.2016.12.019

Bishop, C. M. (2006). *Pattern Recognition and Machine Learning*. New York, NY: Springer.

Chang, W., Cheng, J., Allaire, J., Xie, Y., and McPherson, J. (2019). *shiny: Web Application Framework for R. R Package Version 1.4.0*.

Dua, D., and Graff, C. (2019). *UCI Machine Learning Repository*. Irvine, CA: University of California, School of Information and Computer Sciences. Available online at: http://archive.ics.uci.edu/ml (accessed October 15, 2019).

European Network of Forensic Science Institutes (2016). *ENFSI Guideline for Evaluative Reporting in Forensic Science*. Dua, D., and Graff, C. (2017). UCI Machine Learning Repository. Irvine, CA: University of California, Irvine,

School of Information and Computer Sciences. Available online at: http://archive.ics.uci.edu/ml (accessed October 15, 2019).

Evett, I., Jackson, G., Lambert, J., and McCrossan, S. (2000). The impact of the principles of evidence interpretation on the structure and content of statements. *Sci. Justice* 40, 233–239. doi: 10.1016/S1355-0306(00)71993-9

Evett, I. W., and Weir, B. S. (1998). *Interpreting DNA Evidence: Statistical Genetics for Forensic Scientists, Vol. 244*. Sunderland, MA: Sinauer Associates.

Firth, D. (1993). Bias reduction of maximum likelihood estimates. *Biometrika* 80, 27–38. doi: 10.1093/biomet/80.1.27

Friedman, J., Hastie, T., and Tibshirani, R. (2001). *The Elements of Statistical Learning, Vol. 1*. New York, NY: Springer. doi: 10.1007/978-0-387-21606-5_1

Friedman, J., Hastie, T., and Tibshirani, R. (2010). Regularization paths for generalized linear models via coordinate descent. *J. Stat. Softw*. 33, 1–22. doi: 10.18637/jss.v033.i01

Gelman, A., Carlin, J. B., Stern, H. S., Dunson, D. B., Vehtari, A., and Rubin, D. B. (2013). *Bayesian Data Analysis*. Boca Raton, FL: CRC Press. doi: 10.1201/b16018

Gelman, A., Jakulin, A., Pittau, M. G., and Su, Y. (2008). A default prior distribution for logistic and other regression models. *Ann. Appl. Stat*. 2, 1360–1383. doi: 10.1214/08-AOAS191

Gelman, A., Su, Y.-S., Yajima, M., Hill, J., Pittau, M. G., Kerman, J., et al. (2018). *Package Arm. R Package Version 1.10-1*.

Gill, P., Brenner, C., Buckleton, J., Carracedo, A., Krawczak, M., Mayr, W., et al. (2006). DNA commission of the international society of forensic genetics: recommendations on the interpretation of mixtures. *Forens. Sci. Int*. 160, 90–101. doi: 10.1016/j.forsciint.2006.04.009

Gonzalez-Rodriguez, J., Rose, P., Ramos, D., Toledano, D. T., and Ortega-Garcia, J. (2007). Emulating DNA: Rigorous quantification of evidential weight in transparent and testable forensic speaker recognition. *IEEE Trans. Audio Speech Lang. Process*. 15, 2104–2115. doi: 10.1109/TASL.2007.902747

Hastie, T., and Qian, J. (2014). *Glmnet Vignette*. Available online at: http://www. web. stanford. edu/ hastie/Papers/Glmnet_Vignette. pdf (accessed September 20, 2016).

Heinze, G., and Ploner, M. (2018). *logistf: Firth's Bias-Reduced Logistic Regression. R Package Version 1.23*.

Heinze, G., and Schemper, M. (2002). A solution to the problem of separation in logistic regression. *Stat. Med*. 21, 2409–2419. doi: 10.1002/sim.1047

Kintz, P., Salomone, A., and Vincenti, M. (2015). *Hair Analysis in Clinical and Forensic Toxicology*. Amsterdam: Academic Press.

Kosmidis, I. (2020). *brglm2: Bias Reduction in Generalized Linear Models. R Package Version 0.6.2*.

Kosmidis, I., Pagui, E. C. K., and Sartori, N. (2020). Mean and median bias reduction in generalized linear models. *Stat. Comput*. 30, 43–59. doi: 10.1007/s11222-019-09860-6

Lucy, D. (2013). *Comparison: Multivariate Likelihood Ratio Calculation and Evaluation. R Package Version 1.0-4*.

Mai, Q. (2013). A review of discriminant analysis in high dimensions. *Wiley Interdisc. Rev*. 5, 190–197. doi: 10.1002/wics.1257

Martyna, A., Michalska, A., and Zadora, G. (2015). Interpretation of FTIR spectra of polymers and Raman spectra of car paints by means of likelihood ratio approach supported by wavelet transform for reducing data dimensionality. *Analyt. Bioanalyt. Chem*. 407, 3357–3376. doi: 10.1007/s00216-015-8558-9

Michalska, A., Martyna, A., Zieba-Palus, J., and Zadora, G. (2015). Application of a likelihood ratio approach in solving a comparison problem of Raman spectra recorded for blue automotive paints. *J. Raman Spectrosc*. 46, 772–783. doi: 10.1002/jrs.4719

Morrison, G. S. (2011a). A comparison of procedures for the calculation of forensic likelihood ratios from acoustic-phonetic data: multivariate kernel density (MVKD) versus Gaussian mixture model-universal background model (GMM-UBM). *Speech Commun*. 53, 242–256. doi: 10.1016/j.specom.2010.09.005

Morrison, G. S. (2011b). Measuring the validity and reliability of forensic likelihood-ratio systems. *Sci. Just*. 51, 91–98. doi: 10.1016/j.scijus.2011.03.002

Morrison, G. S. (2013). Tutorial on logistic-regression calibration and fusion: converting a score to a likelihood ratio. *Austr. J. Forens. Sci*. 45, 173–197. doi: 10.1080/00450618.2012.733025

Morrison, G. S., and Poh, N. (2018). Avoiding overstating the strength of forensic evidence: shrunk likelihood ratios/Bayes factors. *Sci. Just*. 58, 200–218. doi: 10.1016/j.scijus.2017.12.005

Murphy, K. P. (2012). *Machine Learning: A Probabilistic Perspective*. Cambridge, MA: MIT Press.

Pirro, V., Oliveri, P., Sciutteri, B., Salvo, R., Salomone, A., Lanteri, S., et al. (2013). Multivariate strategies for screening evaluation of harmful drinking. *Bioanalysis* 5, 687–699. doi: 10.4155/bio.13.12

Pragst, F., Rothe, M., Moench, B., Hastedt, M., Herre, and Simmert, D. (2010). Combined use of fatty acid ethyl esters and ethyl glucuronide in hair for diagnosis of alcohol abuse: interpretation and advantages. *Forens. Sci. Int*. 196, 101–110. doi: 10.1016/j.forsciint.2009.12.028

Qin, Y. (2018). A review of quadratic discriminant analysis for high-dimensional data. *Wiley Interdisc. Rev*. 10:e1434. doi: 10.1002/wics.1434

R Core Team (2019). *R: A Language and Environment for Statistical Computing*. Vienna: R Foundation for Statistical Computing.

Ramos, D. (2007). *Forensic evaluation of the evidence using automatic speaker recognition systems* (Ph.D. thesis). Universidad autónoma de Madrid, Madrid, Spain.

Ramos, D., Franco-Pedroso, J., Lozano-Diez, A., and Gonzalez-Rodriguez, J. (2018). Deconstructing cross-entropy for probabilistic binary classifiers. *Entropy* 20:208. doi: 10.3390/e20030208

Robertson, B., Vignaux, G. A., and Berger, C. E. (2016). *Interpreting Evidence: Evaluating Forensic Science in the Courtroom*. Chichester: John Wiley & Sons. doi: 10.1002/9781118492475

Silverman, B. (1986). *Density Estimation for Statistics and Data Analysis*. London: Chapman and Hall. doi: 10.1007/978-1-4899-3324-9

Society of Hair Testing (2019). *2019 Consensus for the Use of Alcohol Markers in Hair for Supporting the Assessment of Abstinence and Chronic Alcohol Consumption*.

Venables, W. N., and Ripley, B. D. (2013). *Modern Applied Statistics With S-PLUS*. New York, NY: Springer Science & Business Media.

Wasserstein, R. L., and Lazar, N. A. (2016). The ASA statement on p-values: context, process, and purpose. *Am. Stat*. 70, 129–133. doi: 10.1080/00031305.2016.1154108

Wickham, H. (2016). *ggplot2: Elegant Graphics for Data Analysis*. New York, NY: Springer-Verlag. Available online at: https://ggplot2.tidyverse.org (accessed October 15, 2019).

Zadora, G. (2010). Evaluation of evidential value of physicochemical data by a Basyesian network approach. *J. Chemometr*. 24, 346–366. doi: 10.1002/cem.1307

Zadora, G., Borusiewicz, R., and Zieba-Palus, J. (2005). Differentiation between weathered kerosene and diesel fuel using automatic thermal desorption-GC-MS analysis and the likelihood ratio approach. *J. Separ. Sci*. 28, 1467–1475. doi: 10.1002/jssc.200400085

Zadora, G., Martyna, A., Ramos, D., and Aitken, C. (2014). *Statistical Analysis in Forensic Science - Evidential Value of Multivariate Physicochemical Data, 1st Edn*. Chicester: John Wiley & Sons, Ltd. doi: 10.1002/9781118763155

Zadora, G., and Ramos, D. (2010). Evaluation of glass samples for forensic purposes - an application of likelihood ratios and an information theoretical approach. *Chemometr. Intell. Lab. Syst*. 8.2, 63–83. doi: 10.1016/j.chemolab.2010.03.007

Conflict of Interest: The authors declare that the research was conducted in the absence of any commercial or financial relationships that could be construed as a potential conflict of interest.

frontiers in Chemistry

ORIGINAL RESEARCH
published: 17 November 2020
doi: 10.3389/fchem.2020.586067

Puparial Cases as Toxicological Indicators: Bioaccumulation of Cadmium and Thallium in the Forensically Important Blowfly *Lucilia sericata*

Julita Malejko[1], *Krzysztof Deoniziak*[2]*, *Marlena Tomczuk*[1], *Joanna Długokencka*[1] and *Beata Godlewska-Żyłkiewicz*[1]*

[1] Department of Analytical Chemistry, Faculty of Chemistry, University of Bialystok, Białystok, Poland, [2] Laboratory of Insect Evolutionary Biology and Ecology, Faculty of Biology, University of Bialystok, Białystok, Poland

OPEN ACCESS

Edited by:
Grzegorz Zadora,
University of Silesia of Katowice, Poland

Reviewed by:
Przemyslaw Niedzielski,
Adam Mickiewicz University, Poland
Roberta Risoluti,
Sapienza University of Rome, Italy

***Correspondence:**
Krzysztof Deoniziak
krzysztofdeo@gmail.com
Beata Godlewska-Żyłkiewicz
bgodlew@uwb.edu.pl

Specialty section:
This article was submitted to Analytical Chemistry, a section of the journal Frontiers in Chemistry

Received: 22 July 2020
Accepted: 16 October 2020
Published: 17 November 2020

Citation:
Malejko J, Deoniziak K, Tomczuk M, Długokencka J and Godlewska-Żyłkiewicz B (2020) Puparial Cases as Toxicological Indicators: Bioaccumulation of Cadmium and Thallium in the Forensically Important Blowfly Lucilia sericata. Front. Chem. 8:586067. doi: 10.3389/fchem.2020.586067

In this study, we present entomotoxicological data on the accumulation of cadmium and thallium in a forensically important blowfly, *Lucilia sericata*, and evaluate the reliability and utility of such information as toxicological evidence for poisoning as a cause of death. We observed that Cd and Tl content in different growing stages of *L. sericata* (larvae, puparial cases, and adults) was increasing with increasing metal concentration in the feeding substrate, namely metal-enriched liver. However, patterns of accumulation differed between the two metals investigated, showing a linear relationship for Cd and a saturable pattern for Tl. For cadmium, the highest bioaccumulation factor (BAF) was found in the larval stage (in the range of 0.20–0.25), while for thallium, puparial cases accumulated more metal than the other stages tested (BAF in the range of 0.24–0.42). Thallium was also observed to have a negative effect on larval growth, resulting in lower weight and smaller puparial size. With this study, we update the information on the bioaccumulation of cadmium in forensically important blowflies and provide the first report on the bioaccumulation of thallium as well as its developmental impact in blowflies. Specifically, our results suggest that analysis of puparial cases could yield useful information for entomotoxicological investigations. The content of Cd and Tl in larvae, puparial cases, and adults of *L. sericata* was determined by inductively coupled plasma mass spectrometry (ICP-MS). The validation parameters of the method such as sensitivity, detection limits, quantification limits, precision, and accuracy were evaluated. The method detection limit (MDL) for all types of samples was in the range of 1.6–3.4 ng g^{-1} for Cd and 0.034–0.15 ng g^{-1} for Tl, and the accuracy of the method was confirmed by a high recovery of metals from certified reference materials (91.3% for Cd and 94.3% for Tl).

Keywords: entomotoxicology, *Lucilia sericata*, cadmium, thallium, bioaccumulation factor, ICP-MS

INTRODUCTION

Forensic entomology is commonly associated with death investigations, in which its main application is in determination of the minimum postmortem interval ($_{min}$PMI). This is accomplished by estimating the time of insect colonization, based on knowledge of the rate of development of pioneer colonizers and on the succession of different insect species during the decomposition of animal/human remains (Greenberg, 1991; Campobasso et al., 2004; Bugelli et al., 2017a). Entomological evidence can also be used to support investigators in determining the presence of drugs or toxins in the body at the time of death, even if decomposition is at an advanced stage.

The use of insects as a source of toxicological evidence, known as entomotoxicology, relies on the fact that many insects can accumulate pollutants from their feeding substrates in their tissues (Pounder, 1991). Of the many species that may be present on or in a dead body, blowflies (Diptera: Calliphoridae) are usually the first to appear on the crime scene, and they may provide crucial information—such as the cause of death—months or even years after body decomposition (Wang et al., 2008; Byrd and Castner, 2010; Braga et al., 2013). This approach was first used in 1980, when phenobarbital was detected in fly larvae collected from a skeletonized body. This finding fundamentally altered the determination of the cause of death, and gave rise to a new application for entomology in forensic science (Beyer et al., 1980). Since then, blowflies have been used as bioindicators of toxins present in bodies that are in an advanced stage of decomposition and thus lack direct forensic matrices (e.g., blood, organs) (Greenberg, 1991; Campobasso et al., 2004; Bugelli et al., 2017a). In a similar way, fly larvae may be also used as indicators of environmental pollution (Owings et al., 2019). To date, various drugs and toxic substances have been detected in different developmental stages of blowflies, in both experimental studies on animal carcasses and human bodies as well as in bodies analyzed in criminal investigations (reviewed in Silva et al., 2017). Entomotoxicological studies focus not only on the qualitative and quantitative analysis of toxicants, but also on their impact on insect growth, development, and survival, which enable an accurate determination of PMI. Although there have been some critiques of the use of entomotoxicology in forensic science (Gaudry et al., 2001; Tracqui et al., 2004), many studies have shown that insects can provide reliable evidence in toxicological analysis during criminal investigations (Silva et al., 2017; Chophi et al., 2019).

Cadmium (Cd) and thallium (Tl) are toxic metals that are responsible for many accidental and intentional poisonings (Cavanagh, 1991; Desenclos et al., 1992; Meggs et al., 1994; Hoffman and Hoffman, 2000; Chang et al., 2012; Nishijo et al., 2017; Rafati Rahimzadeh et al., 2017). Of the two, thallium is more toxic to humans, with a lethal dose between 6 and 40 mg kg^{-1}, compared to a lethal dose of more than 70 mg kg^{-1} for cadmium (Agency for Toxic Substances Disease Registry, 1992, 1999). Cadmium accumulates in almost all human tissues and induces production of metallothionein, a cysteine-rich metal-binding protein. Its toxic effect is observed in the liver, kidneys, skeletal system, and cardiovascular system, and it has also been classified as a human carcinogen. The biological half-life of Cd in the human body has been estimated to be 10–30 years (Sigel et al., 2013; Powers and Dean, 2015; Lech and Sadlik, 2017). Monovalent thallium is similar to potassium in ionic radius and electrical charge, which contributes to its toxic nature. It interferes with many enzymes and has a strong affinity to –SH groups. In the past, thallium salts were widely used as rodenticides, but these were withdrawn from the market due to its high toxicity and the large number of human poisonings, accidental or intentional. Gastroenteritis, polyneuropathy, and alopecia are considered the classic syndromes of thallium poisoning (Reith, 2009; Karbowska, 2016).

With this in mind, we decided to perform a quantitative analysis of Cd and Tl accumulation in a forensically important blowfly in order to determine if such information could be useful as toxicological evidence for poisoning as a cause of death. To date, the effect of cadmium on forensically important blowflies (Diptera: Calliphoridae) has been investigated mainly in the context of life history traits (e.g., survival or development rate) in the species *Chrysomya albiceps* (Al-Misned, 2001, 2003), *Chrysomya megacephala* (Singh and Bhupinderjit, 2017), and *Lucilia sericata* (Simkiss et al., 1993; Moe et al., 2001); of these studies, only the latter two conducted experiments to assess the content of cadmium in insects. Instead, the only published study on the effects of thallium in insects characterized the tolerance of *Chironomus riparius* (Diptera: Chironomidae) to waterborne exposure (Belowitz et al., 2014). To the best of our knowledge, thallium accumulation in blowflies, and the potential value of such data for the field of entomotoxicology, has not yet been studied.

As the model species in our study we used the cosmopolitan and necrophagous fly *L. sericata* (Meigen, 1826) (Diptera: Calliphoridae), which occurs in a broad range of ecosystems throughout the world. *L. sericata* is a common model organism in forensic studies (Byrd and Castner, 2010). As mentioned above, adult flies of this species are often the first insects to arrive at a corpse, and larvae are used in estimation of PMI (Reibe et al., 2010). *L. sericata* has been widely used in experimental studies of entomotoxicology (reviewed in Silva et al., 2017), variation in life history traits (Gallagher et al., 2010), or alterations in arthropod communities and succession patterns on cadavers (Prado e Castro et al., 2012). Here, we characterized the accumulation of cadmium and thallium in different developmental stages of *L. sericata* and assessed the impact this exposure had on insect growth (weight of third-instar larvae, length and width of puparia). In addition to the larval and adult stages, which are typically used in entomotoxicological studies (Chophi et al., 2019), we also chose to analyze empty puparial cases. Puparial cases are shed by emerging adults, and may be present near cadavers up to several years after death (Braga et al., 2013). Cases are formed during pupariation from the cuticle of third-instar larvae and can serve as an alternative material for toxicological analysis when living insects and suitable tissues are missing. Puparial cases have been shown to be useful in determination of PMI (Zhu et al., 2017) and in the identification of species present on a cadaver (Braga et al., 2013). They can also provide important evidence during toxicological analysis, as drugs such as

cocaine (Nolte et al., 1992), amitriptyline (Miller et al., 1994), and metabolites of methylenedioxyamphetamine (Goff et al., 1997) have been detected in puparial cases. However, there have only been a few analyses of toxic metals in puparial cases (Silva et al., 2017; Chophi et al., 2019). Interestingly, an earlier study on *L. sericata* suggested a mechanism for detoxification via puparial cases (Simkiss et al., 1993), a hypothesis that we test further in the current work.

Cadmium and thallium content was determined in various developmental stages of *L. sericata* using inductively coupled plasma mass spectrometry (ICP-MS). ICP-MS is one of the most widely used analytical techniques in inorganic testing laboratories, due to its wide dynamic range, high sensitivity, low limits of detection, and fast multi-elemental analysis (Sakai, 2015). Data quality can be improved significantly through the use of an octopole-based collision/reaction cell operating in helium collision mode, which is very effective in eliminating a wide range of matrix-based interference. In this work, we also describe a methodological protocol to help other researchers to achieve comparable results.

MATERIALS AND METHODS

Instrumentation

An Agilent 8800 Triple Quadrupole ICP-MS (ICP-QQQ, Agilent Technologies, Singapore) was used to determine the Cd and Tl content of biological samples. The apparatus was equipped with a MicroMist glass concentric nebulizer, a Peltier-cooled quartz double-pass Scott-type spray chamber, a quartz torch with a 2.5-mm i.d., Ni interface cones, an x-lens, and an octopole reaction system (ORS3). Samples were introduced directly into the ICP-MS using a SPS 4 autosampler with a standard peristaltic pump and tubing (i.d. 1.02 mm).

A Solaar M6 (Thermo Electron Corporation, Gloucester, UK) atomic absorption spectrometer, equipped with an electrothermal atomizer and a Zeeman background correction system, was used to determine the Cd concentration of liver samples.

A Milestone ETHOS Plus Microwave Labstation (Italy) was used for microwave-assisted digestion of samples. Samples were homogenized using a blender with a glass jar (Łucznik, Poland), a mechanical micro-stirrer (MPW-321; Mechanika Precyzyjna, Poland), and a SONOREX DIGIPLUS ultrasonic bath (DL 255H; ultrasonic nominal power: 160 W, power settings: 20–100%, ultrasonic frequency: 35 kHz) from Bandelin (Germany). A Memmert UE 400 oven (Germany) was used to dry biological samples. A DSX110 inverted microscope (Olympus Corporation, Japan) was used for measurements of puparial length and width.

Reagents and Materials

All solutions were prepared in Milli-Q water, which was obtained from a Millipore Direct-Q 3 UV water purification system (France). Concentrated HNO_3 (≥69%, TraceSelect, Fluka, France) and H_2O_2 (≥30%, for trace analysis, Sigma-Aldrich, France) were used for sample digestion. Indium (1,000 mg L^{-1}, $In(NO_3)_3$ in 2% HNO_3), supplied by Merck (Germany), was used as an internal standard for ICP-MS measurements. The ICP-MS stock tuning solution contained 10 mg L^{-1} each of Li, Y, Ce, Tl, and Co in a matrix of 2% HNO_3, and was supplied by Agilent Technologies (USA). The cadmium standard solution (1,000 mg L^{-1} Cd in 0.5 mol L^{-1} HNO_3, traceable to SRM from NIST, Certipur®) and thallium ICP standard (1,000 mg L^{-1} Tl in 2–3% HNO_3, traceable to SRM from NIST, Certipur®) were obtained from Merck (Germany).

Two certified reference materials (CRMs) were used to check the accuracy of the method: MODAS-4 Cormorant Tissue (MODAS, Poland), with a certified Cd concentration of 17.2 ± 2.1 ng g^{-1}, and Seronorm? Trace Elements Urine L-2 (SERO, Norway), with a certified Tl concentration of 9.70 ± 0.67 μg L^{-1} (acceptable range: 8.36–11.04 μg L^{-1}).

Substrate Preparation

Fresh homogenized pig liver was enriched with Cd or Tl and used as a substrate for larvae of *L. sericata*. The pig liver used in both cases was acquired from a single individual. Each portion of liver (100 g) was placed in glass container, to which was added 20 mL standard solution of either Cd (C_1: 0.3254 mg; C_2: 0.6538 mg; C_3: 1.2832 mg) or Tl (T_1: 0.0755 mg; T_2: 0.3268 mg; T_3: 0.6542 mg), prepared with Milli-Q ultrapure water. Control samples (C_0 and T_0) were prepared by mixing 10 mL of Milli-Q water with 100 g of fresh homogenized pig liver. Each sample was sonicated in an ultrasonic bath for 30 min at 60% power. The vessels were cooled with ice to avoid heating during the sonication process. Next, from each of the prepared substrates (C_{0-3} and T_{0-3}), three portions (20 g each) were taken and transferred to 250 mL plastic containers. Summarizing, three individual samples of each liver substrate (control or with one of the three concentrations of metal) were prepared. After preparation, 5 g of each substrate was used to determine its thallium or cadmium concentration. These samples were stored at −20°C until analysis.

Rigorous precautions were taken to avoid contamination throughout the procedure. Prior to use, all plastic materials and glassware were thoroughly rinsed with Milli-Q water, soaked for 48 h in 2 mol L^{-1} nitric acid, and finally rinsed several times with Milli-Q water.

Breeding and Sampling

First-instar larvae of *L. sericata* were provided by Biomantis Ltd., Kraków, Poland. Newly hatched larvae were packed in 100-mL plastic containers with an addition of saline, and shipped as a medical consignment to the Faculty of Biology, University of Bialystok, Poland. The consignment was protected by thermo-insulating packaging with the addition of a cooling insert. The package was delivered within 24 h of shipment. After delivery, the plastic container was removed from the packaging in order to acclimatize the larvae to room temperature (21.5°C). After 1 h, larvae were deposited on the substrate in random order.

In general, 47 larvae were placed in each 250-mL plastic container (with either control substrate or substrate enriched with different concentrations of cadmium or thallium), which was then covered with sterile gauze. There were three replicates for each treatment. All containers were then placed in one clear plastic box (58.3 × 39.2 × 18.3 cm), together with two 250-mL plastic containers half-filled with distilled water (to

maintain humidity) and a digital weather station for measuring temperature and humidity during the experiment. The container was covered with a clear plastic lid in a way that allowed air exchange. Larvae were reared in an air-conditioned room at 21.5°C and 80–90% humidity, with 10 h daylight and 14 h darkness. Larvae were checked twice a day.

Third-instar larvae (hereafter "larvae") were moved to a new 250-mL plastic container after about 96 h, when they entered their wandering stage and started to move intensively on the sides of the container and the sterile gauze. Before being placed in their new container, all larvae were rinsed with Milli-Q water and dried on blotting paper. In line with the rules for the collection of insects from the scene (Brundage and Byrd, 2016), a sample of 15 larvae was collected from each of the cadmium (C_{0-3}) and thallium (T_{0-3}) substrates; each sample was then divided into three subsamples, which were weighed and stored at −20°C until further analysis. To avoid including any changes in larval weight that occurred during storage, weights were recorded immediately after collection (Bugelli et al., 2017b). The remaining larvae in their plastic containers were then placed back in the clear plastic box for pupation. After all larvae entered the pupal stage, the puparia from the Tl-treated groups were measured with a DSX110 inverted microscope. Adults started to emerge 17 days after entering the wandering stage. After emergence, samples of puparial cases and adults were collected and stored at −20°C for further analysis. In total, for each substrate (control or different Cd/Tl concentration), nine sub-samples of larvae, puparial cases, and adults were collected. The experiments were conducted in accordance with Polish law (e.g., Animal Protection Law, Animal Husbandry Act) and all provisions and regulations stipulated therein.

Pre-treatment of Samples and CRMs

Biological samples were dried in an oven for 12 h until they reached a constant weight (liver samples at 105°C; samples of larvae, puparial cases, and adults of *L. sericata* at 40°C). Dry samples of liver (0.2–0.3 g), larvae (0.06–0.2 g), puparial cases (0.01–0.02 g), and adults (0.05–0.1 g), as well as samples of the CRM MODAS-4 Cormorant Tissue (0.2 g) were placed in Teflon vessels for microwave-assisted acid digestion. Concentrated HNO_3 (2 mL) and H_2O_2 (1 mL) were added, and the vessels were left for 1 h for sample pre-digestion. Next, the vessels were sealed and heated in the microwave system. The digestion conditions were: 1 min at 150°C, 1 min at 160°C, 5 min at 200°C, 5 min at 210°C, and 5 min at 210°C. For the Seronorm? Trace Elements Urine L-2 CRM, a sample of freeze-dried material was reconstituted in 5 mL of Milli-Q water, then 1 mL of this solution was placed in a quartz crucible and digested in hot concentrated HNO_3 (0.5 mL) and H_2O_2 (0.5 mL). After cooling, all digests were transferred to polyethylene vessels and stored in a refrigerator. Samples were diluted with Milli-Q water or 2% HNO_3 prior to analysis.

Conditions for the Measurement of Cd and Tl

The optimized ICP-MS operating conditions for the determination of Cd and Tl in mineralized samples are given in **Supplementary Table 1**. The monitored isotopes were ^{111}Cd, ^{114}Cd, and ^{205}Tl. These were monitored both in standard mode (no gas) and in He mode (using helium as a collision gas with a flow rate of 5 mL min^{-1}). All calibration standards were prepared in 2% HNO_3. Indium (^{115}In) was used as an internal standard. Electrothermal atomic absorption spectrometry (ETAAS) was used to determine Cd concentrations in liver samples during optimisation of substrate preparation. The cadmium hollow cathode lamp (Thermo Scientific, UK) was operated at 5 mA current. All measurements were performed using standard pyrolytically coated graphite furnaces. Absorbance signals were measured with 0.5 nm spectral bandpass at 228.8 nm. The time/temperature program was: drying at 100°C for 30 s, 800°C for 20 s, ashing at 1,000°C for 3 s, and atomization at 2,500°C for 3 s. Magnesium nitrate (20 μg) was used as a chemical modifier for the determination of Cd concentration. The concentration of each analyte was measured from the calibration graph.

Calculation of Bioaccumulation Factor

The bioaccumulation factor (BAF) was calculated as the ratio of the metal content in tested samples of *L. sericata* to the metal content in the feeding substrate, as follows:

$$BAF = \frac{\text{metal content in tested organism } \left(\mu g\, g^{-1}\ \text{d.w.}\right)}{\text{metal content in feeding substrate } \left(\mu g\, g^{-1}\ \text{d.w.}\right)}$$

Statistical Analysis

The Mann–Whitney *U*-test was used to evaluate differences in Cd and Tl concentration and in the bioaccumulation factors of the three tested developmental stages of *L. sericata*. Monte Carlo permutations, with 10,000 randomizations and a 99% confidence interval, were used to test for statistical significance. The weight of larvae and the length and width of puparia were compared among groups using one-way ANOVA and Tukey HSD *post-hoc* tests. The distribution of the data was analyzed with a Shapiro–Wilk test. All of the statistical analyses were two-tailed and were performed using SPSS Statistics v. 26 (IBM Corporation, USA).

RESULTS

Optimization of the Method of Substrate Preparation

We first conducted preliminary studies to optimize the method of preparation of the metal-enriched liver substrate and to ensure that the metal was distributed homogenously throughout the entire matrix. The liver (600 g) was rinsed with distilled water, quartered, and blended for 10 min. Liver samples (100 g) were then homogenized with different volumes of cadmium solution (10 or 20 mL, each containing 0.325 mg Cd). Half of the samples were subjected to mechanical stirring (for 5 min) and the other half to sonication in an ultrasonic bath (for 30 min, at 60% power). During sonication, the vessels were cooled with ice to avoid heating. After homogenization, four randomly selected sub-samples (∼1 g each) were dried in an oven for 12 h at 105°C, then digested in a microwave digestion system according to the

procedure described in Section Pre-treatment of samples and CRMs. The Cd content of liver samples was determined by ETAAS under the conditions described in Section Conditions for the measurement of Cd and Tl. The instrumental detection limit (IDL), calculated as three times the standard deviation of the response for a blank sample (2% HNO_3) divided by the slope of the calibration curve, was 0.15 ng mL^{-1}. The concentration of Cd in control liver tissue was 0.066 ± 0.010 μg g^{-1} (d.w.).

In total, there were four groups of enriched liver samples, which differed in the volume of Cd solution added during preparation (10 or 20 mL, both containing 0.325 mg Cd) and method of homogenization (mechanical stirring or ultrasound); four samples were analyzed from each group. The average concentration of Cd in tissue homogenized by mechanical stirring was 13.99 ± 0.56 μg g^{-1} in the 10-mL group and 13.04 ± 0.56 μg g^{-1} in the 20-mL group. When tissues were homogenized by ultrasound, the average Cd concentration was 12.41 ± 0.97 μg g^{-1} in the 10-mL group and 12.91 ± 0.35 μg g^{-1} in the 20-mL group. The best repeatability of measurement (relative standard deviation, or RSD, of 2.7%), and thus better homogeneity of the liver sample, was therefore achieved using ultrasonic homogenization after the addition of 20 mL of cadmium solution. These conditions were used to prepare liver substrate for all further experiments. Moreover, this homogenization method enabled the simultaneous preparation of multiple samples and avoided loss or contamination via laboratory tools during substrate preparation.

Determination of Cd and Tl by ICP-MS: Validation of the Method

Calibration graphs were recorded for two cadmium isotopes (^{111}Cd and ^{114}Cd) and one thallium isotope (^{205}Tl) with and without the use of collision cell technology. The signal of the internal standard was more stable in He mode. However, the results were comparable in both modes, indicating selectivity of the method and a lack of interference in the tested samples. For the calculation of results, the signals registered in both measurement modes were used. Intermediate precision, expressed as the RSD of the slopes of calibration graphs recorded on different days, was in the range of 0.8–4.1% ($n = 3$) for cadmium and 3.2–6.7% ($n = 4$) for thallium. The instrumental detection limit (IDL) calculated as three times the standard deviation (SD) of the signal of blank sample (SD_{blank}) (2% HNO_3) divided by the slope of the calibration graph (a), was 0.049 ng g^{-1} for Cd and 0.015 ng g^{-1} for Tl, while the instrumental quantification limit (IQL) calculated as (10 × SD_{blank})/a was 0.16 ng g^{-1} for Cd and 0.051 ng g^{-1} for Tl. The method detection limit (MDL), calculated as 3 × $SD_{control}$ of the response of control samples (mineralized samples of liver and different developmental stages of *L. sericata*) divided by the slope of the calibration graph (a), and the method quantification limit (MQL), calculated as (10 × $SD_{control}$)/a, are presented in **Table 1**. These values are inherent to the chemical measurement process and represent both instrumental and procedural components, i.e., dilution and mineralization. These low MDL and MQL thus enabled the detection of cadmium and thallium in as little as 0.01 g of sample for puparial cases. The repeatability of results (as RSD in %) was calculated for three sub-samples of liver enriched with each concentration of metal. It was in the range of 0.24–2.3% for Cd and 1.1–6.8% for Tl. The reproducibility of the results (RSD) was evaluated using the three sub-samples taken from each treated group of larvae, puparial cases, and adults, and was found to be in the range of 1.4–26.8% for cadmium and 2.5–25.1% for thallium. Only in two cases the RSD was found to be higher than 30% (34.1% for Cd and 31.4% for Tl). These higher RSD values may have resulted from the fact that, as the amount of material to be tested was sometimes very small, the samples were not homogenized before sampling (individual flies were mineralized).

TABLE 1 | Method detection limit (MDL) and method quantification limit (MQL) of the ICP-MS method of Cd and Tl determination in biological samples.

	Cadmium		Thallium	
	MDL (ng g^{-1})	MQL (ng g^{-1})	MDL (ng g^{-1})	MQL (ng g^{-1})
Liver	1.6	5.2	0.036	0.12
Larvae	1.6	5.5	0.094	0.31
Puparial cases	2.2	7.3	0.15	0.51
Adults	3.4	11.4	0.034	0.11

The determined concentrations of metals in CRMs (15.7 ± 1.5 ng g^{-1} Cd in MODAS-4 Cormorant Tissue, 9.15 ± 0.23 μg L^{-1} Tl in Seronorm? Trace Elements Urine L-2) were consistent with the reference values, which verified the accuracy of the method. The average recoveries of analytes from the CRMs, with the estimated expanded uncertainties for $k = 2$, were 91.3 ± 12.6% for Cd and 94.3 ± 6.9% for Tl. The uncertainties were estimated using the single laboratory validation concept (Barwick and Ellison, 2000).

Cadmium Accumulation in Larvae, Puparial Cases, and Adults of *L. sericata*

First, we used ICP-MS to determine the Cd content in control (unenriched) liver samples and liver tissues enriched with different concentrations of metal, which were all used as substrates for larvae. In control liver tissues (C_0), the Cd content (as d.w.) was 94.1 ± 5.9 ng g^{-1}, while in treated liver samples, Cd concentrations were much higher: 11.566 ± 0.028 μg g^{-1} in C_1, 23.83 ± 0.54 μg g^{-1} in C_2, and 46.98 ± 0.56 μg g^{-1} in C_3. Substrate C_3 contained a concentration of Cd that was equal to the median lethal dose (LD_{50}: 50 μg g^{-1}) for rats and mice (Agency for Toxic Substances Disease Registry, 1999).

Cadmium was detected in all developmental stages (larvae, adults, and puparial cases) of *L. sericata* collected from control and enriched substrates, with the mean cadmium concentration in each stage given in **Supplementary Table 2**. Concentrations in studied samples ranged from 15.4 ng g^{-1} to 9.5 μg g^{-1}. Cadmium concentrations increased significantly in larvae, puparial cases, and adults with an increase in the Cd concentration in the food substrate (**Figure 1**, **Table 2**), and demonstrated a linear relationship in the studied concentration range (**Supplementary Figure 1**). The concentration of cadmium

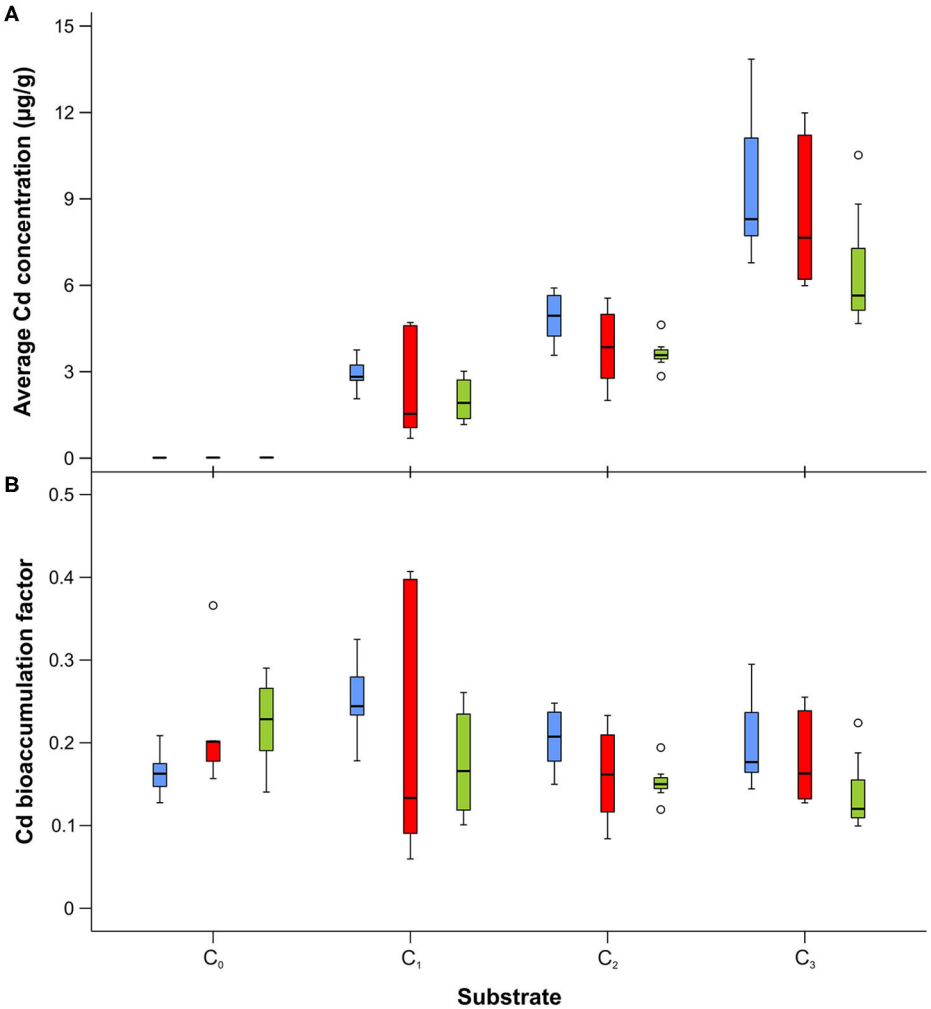

FIGURE 1 | Box and whisker plots showing differences in average cadmium concentration **(A)** and bioaccumulation factor **(B)** in larvae (blue), puparial cases (red), and adults (green) of *Lucilia sericata* exposed to different Cd concentration (C_0-C_3). Boxes indicate median and first and third quartiles. Whiskers represent the minimal and maximal values within 1.5 times the interquartile range. Open circles are outliers with values more than 1.5 times the interquartile range.

TABLE 2 | Difference of Cd concentration determined in *Lucilia sericata* larvae, puparial cases, and adults from control and Cd treated groups (C_0-C_3).

Sample	**Larvae**			**Puparial cases**			**Adults**		
Substrate	**C_0**	**C_1**	**C_2**	**C_0**	**C_1**	**C_2**	**C_0**	**C_1**	**C_2**
C_1	$N = 15$	–	–	$N = 14$	–	–	$N = 14$	–	–
	$Z = -3.182$			$Z = -3.130$			$Z = -3.130$		
	$p < 0.001$			**$p = 0.001$**			**$p = 0.001$**		
C_2	$N = 15$	$N = 18$	–	$N = 14$	$N = 14$	–	$N = 15$	$N = 15$	–
	$Z = -3.182$	$Z = -3.400$		$Z = -3.130$	$Z = -1.214$		$Z = -3.240$	$Z = -3.125$	
	$p < 0.001$	**$p < 0.001$**		**$p = 0.001$**	$p = 0.263$		**$p < 0.001$**	**$p = 0.001$**	
C_3	$N = 15$	$N = 15$	$N = 15$	$N = 15$	$N = 15$	$N = 15$	$N = 15$	$N = 15$	$N = 16$
	$Z = -3.182$	$Z = -3.576$	$Z = -3.576$	$Z = -3.240$	$Z = -3.240$	$Z = -3.240$	$Z = -3.240$	$Z = -3.240$	$Z = -3.361$
	$p < 0.001$	**$p < 0.001$**	**$p < 0.001$**	**$p < 0.001$**	**$p = 0.001$**	**$p < 0.001$**	**$p = 0.001$**	**$p = 0.001$**	**$p = 0.001$**

Bold values denote statistical significance at the $p < 0.05$.

TABLE 3 | Difference of Cd concentration in *Lucilia sericata* larvae, puparial cases, and adults from groups treated with the same Cd concentration.

Substrate	C_1		C_2		C_3	
Sample	**Larvae**	**Puparial cases**	**Larvae**	**Puparial cases**	**Larvae**	**Puparial cases**
Puparial cases	$N = 16$	–	$N = 16$	–	$N = 17$	–
	$Z = -0.476$		$Z = -1.641$		$Z = -0.962$	
	$p = 0.678$		$p = 0.114$		$p = 0.376$	
Adults	$N = 16$	$N = 14$	$N = 17$	$N = 15$	$N = 17$	$N = 16$
	$Z = -2.276$	$Z = -0.064$	$Z = -2.694$	$Z = -0.347$	$Z = -2.983$	$Z = -2.836$
	$\mathbf{p = 0.023}$	$p = 1.000$	$\mathbf{p = 0.006}$	$p = 0.778$	$\mathbf{p = 0.002}$	$\mathbf{p = 0.004}$

Bold values denote statistical significance at the $p < 0.05$.

TABLE 4 | Difference of Cd bioaccumulation factor in *Lucilia sericata* larvae, puparial cases and adults from control and Cd treated groups (C_0-C_3).

Sample	Larvae			Puparial cases			Adults		
Substrate	C_0	C_1	C_2	C_0	C_1	C_2	C_0	C_1	C_2
C_1	$N = 15$	–	–	$N = 14$	–	–	$N = 14$	–	–
	$Z = -2.946$			$Z = -0.447$			$Z = -1.469$		
	$\mathbf{p = 0.001}$			$p = 0.703$			$p = 0.165$		
C_2	$N = 15$	$N = 18$	–	$N = 15$	$N = 15$	–	$N = 15$	$N = 15$	–
	$Z = -2.239$	$Z = -1.987$		$Z = -0.579$	$Z = -0.231$		$Z = -2.430$	$Z = -0.347$	
	$\mathbf{p = 0.027}$	$p = 0.051$		$p = 0.606$	$p = 0.871$		$\mathbf{p = 0.015}$	$p = 0.775$	
C_3	$N = 15$	$N = 18$	$N = 18$	$N = 16$	$N = 16$	$N = 17$	$N = 16$	$N = 16$	$N = 17$
	$Z = -1.414$	$Z = -2.075$	$Z = -0.662$	$Z = -0.265$	$Z = -0.265$	$Z = -0.289$	$Z = -2.805$	$Z = -1.323$	$Z = -1.732$
	$p = 0.183$	$\mathbf{p = 0.041}$	$p = 0.546$	$p = 0.839$	$p = 0.848$	$p = 0.816$	$\mathbf{p = 0.004}$	$p = 0.213$	$p = 0.094$

Bold values denote statistical significance at the $p < 0.05$.

was significantly higher in larvae than in adult flies for all three Cd-treated groups (C_1-C_3), while it was higher in puparial cases than in adult flies for group C_3 (highest substrate concentration) only (**Figure 1**, **Table 3**).

The mean bioaccumulation factor for Cd in larvae reached a value of about 0.20–0.25, and was slightly higher for samples reared on the C_1 substrate (**Figure 1**, **Supplementary Table 3**). However, differences in bioaccumulation were found to be significant only between larvae reared on the C_1 and C_3 substrates (**Table 4**). For puparial cases, the mean bioaccumulation factor was lower, reaching values of 0.16–0.23, and the lowest values were obtained for adult flies (between 0.12 and 0.18) with no significant differences among substrates (**Table 4**, **Supplementary Table 3**).

Thallium Accumulation in Larvae, Puparial Cases, and Adults of *L. sericata*

ICP-MS was used to determine the thallium content (as d.w.) in control (unenriched) liver tissues and liver samples enriched with different concentrations of metal. In control tissues (T_0), the Tl concentration was 1.00 ± 0.75 ng g^{-1}, while enriched liver samples had concentrations of 2.943 ± 0.071 μg g^{-1} in T_1, 13.95 ± 0.15 μg g^{-1} in T_2, and 29.1 ± 2.0 μg g^{-1} in T_3. All substrates contained Tl concentrations that were below the lethal dose (LD_{50}), which for different thallium salts has been reported to be in the range of 6–40 μg g^{-1} for humans and 29–39 μg g^{-1} for rats (Agency for Toxic Substances Disease Registry, 1999). The mean thallium concentrations in the developmental stages of *L. sericata* studied here are presented in **Supplementary Table 2**. The Tl content in larvae and adults ranged from 0.3 to 2.1 μg g^{-1}, and in puparial cases from 1.2 to 7.0 μg g^{-1}. Thallium concentrations generally increased in all stages—larvae, puparial cases, and adults—with an increase in the metal concentration in the food substrate (**Figure 2**, **Table 5**). Non-significant differences were only observed in larvae as well as puparial cases between T_2 and T_3 substrates (**Table 5**). The correlation between concentrations of Tl in the substrate and Tl levels in all developmental stages was not linear, and instead demonstrated a saturable relationship (**Supplementary Figure 1**). Thallium concentrations were significantly higher in puparial cases than in larvae and adult flies for all Tl-treated groups (**Figure 2**, **Table 6**). Tl concentrations also tended to be lower in adult flies compared to larvae, but this difference was only significant for the group reared on the substrate with the highest metal concentration, T_3 (**Table 6**).

The mean bioaccumulation factor for Tl was significantly higher in puparial cases (BAF in the range of 0.24–0.42) than in larvae (0.07–0.12) or adults (0.04–0.10) (**Supplementary Table 3**). BAF generally decreased with an increase in the metal concentration of the food substrate, and the biggest differences were observed for higher thallium concentrations (**Figure 2**, **Table 7**).

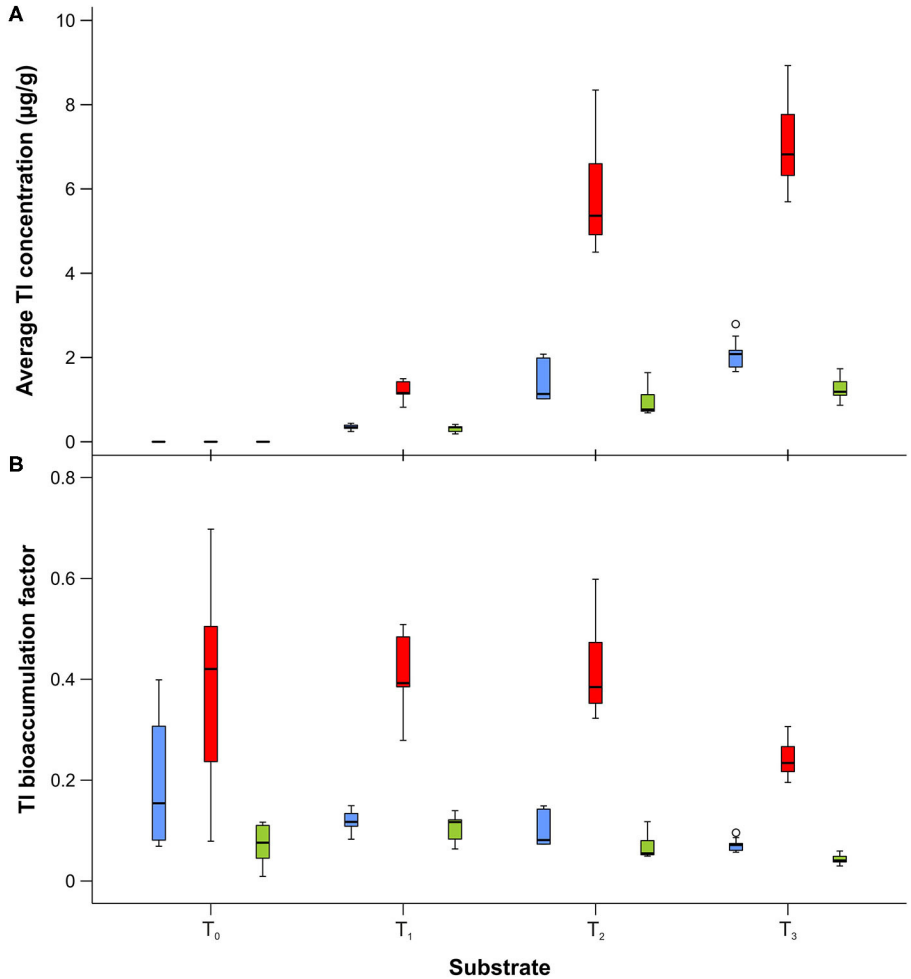

FIGURE 2 | Box and whisker plots showing differences in average thallium concentration **(A)** and bioaccumulation factor **(B)** in larvae (blue), puparial cases (red), and adults (green) of *Lucilia sericata* exposed to different Tl concentration (T_0-T_3). Boxes indicate median and first and third quartiles. Whiskers represent the minimal and maximal values within 1.5 times the interquartile range. Open circles are outliers with values more than 1.5 times the interquartile range.

Larval Weight and Puparial Size

The mean weight of third-instar larvae was generally lower for samples reared on substrates that contained cadmium or thallium (**Figure 3**). However, significant differences among groups were observed only for larvae reared with thallium [ANOVA: $F_{(3,22)} = 4.125$, $p < 0.018$], not with cadmium [ANOVA: $F_{(3,29)} = 0.476$, $p = 0.701$]. *Post-hoc* comparisons using the Tukey HSD test revealed that the mean weight of third-instar larvae was significantly lower when raised on the T_3 substrate compared to the T_0 substrate ($M = 0.007$, SD $= 0.002$, $p = 0.010$).

Significant differences were observed in the length [ANOVA: $F_{(3,116)} = 7.818$, $p < 0.001$] and width [ANOVA: $F_{(3,116)} = 6.721$, $p < 0.001$] of puparia acquired from larvae reared with different thallium concentrations (**Figure 3**). *Post-hoc* comparisons using the Tukey HSD test indicated that puparia from the T_0 substrate were significantly longer than those from the T_1 ($M = 0.275$, SD $= 0.092$, $p = 0.017$), T_2 ($M = 0.311$, SD $= 0.092$, $p = 0.006$), and T_3 ($M = 0.431$, SD $= 0.092$, $p < 0.001$) groups. Instead, puparia length did not differ significantly among the metal-enriched substrates (T_1, T_2, and T_3). Similarly, a Tukey HSD test revealed that the mean width of puparia from the T_0 substrate was significantly larger than values obtained from T_2 ($M = 0.108$, SD $= 0.038$, $p = 0.030$) and T_3 ($M = 0.170$, SD $= 0.038$, $p < 0.001$). The width of puparia did not differ significantly between samples from T_0 and T_1 or among samples from T_1, T_2, and T_3 ($p > 0.05$).

DISCUSSION

Accumulation of Cadmium and Thallium

To the best of our knowledge, this report presents the first examination of the relationship between Tl exposure and bioaccumulation in different developmental stages of the forensically important blowfly *L. sericata*. The effect of cadmium on the development and survival of blowfly

TABLE 5 | Difference of Tl concentration determined in *Lucilia sericata* larvae, puparial cases and adults from control and Tl treated groups (T_0-T_3).

Sample	Larvae			Puparial cases			Adults		
Substrate	**T_0**	**T_1**	**T_2**	**T_0**	**T_1**	**T_2**	**T_0**	**T_1**	**T_2**
T_1	$N = 10$	–	–	$N = 17$	–	–	$N = 17$	–	–
	$Z = -2.558$			$Z = -3.464$			$Z = -3.464$		
	$p = 0.008$			**$p < 0.001$**			**$p < 0.001$**		
T_2	$N = 9$	$N = 11$	–	$N = 15$	$N = 16$	–	$N = 16$	$N = 17$	–
	$Z = -2.449$	$Z = -2.739$		$Z = -3.240$	$Z = -3.334$		$Z = -3.361$	$Z = -3.464$	
	$p = 0.015$	**$P = 0.005$**		**$p < 0.001$**	**$p < 0.001$**		**$p < 0.001$**	**$p < 0.001$**	
T_3	$N = 13$	$N = 15$	$N = 14$	$N = 17$	$N = 18$	$N = 16$	$N = 17$	$N = 18$	$N = 17$
	$Z = -2.777$	$Z = -3.182$	$Z = -1.933$	$Z = -3.464$	$Z = -3.576$	$Z = -1.958$	$Z = -3.464$	$Z = -3.576$	$Z = -2.213$
	$p = 0.003$	**$p < 0.001$**	$P = 0.058$	**$p < 0.001$**	**$p < 0.001$**	$P = 0.055$	**$p < 0.001$**	**$p < 0.001$**	**$P = 0.026$**

Bold values denote statistical significance at the $p < 0.05$.

TABLE 6 | Difference of Tl concentration in *Lucilia sericata* larvae, puparial cases, and adults from groups treated with the same Tl concentration.

Substrate	T_1		T_2		T_3	
Sample	**Larvae**	**Puparial cases**	**Larvae**	**Puparial cases**	**Larvae**	**Puparial cases**
Puparial cases	$N = 15$	–	$N = 12$	–	$N = 18$	–
	$Z = -3.182$		$Z = -2.842$		$Z = -3.576$	
	$p = 0.001$		**$p = 0.003$**		**$p < 0.001$**	
Adults	$N = 15$	$N = 18$	$N = 13$	$N = 15$	$N = 18$	$N = 18$
	$Z = -0.943$	$Z = -3.576$	$Z = -1.757$	$Z = -3.240$	$Z = -3.400$	$Z = -3.576$
	$p = 0.394$	**$p < 0.001$**	$p = 0.096$	**$p < 0.001$**	**$p < 0.001$**	**$p < 0.001$**

Bold values denote statistical significance at the $p < 0.05$.

TABLE 7 | Difference of Tl bioaccumulation factor in *Lucilia sericata* larvae, puparial cases, and adults from control and Tl treated groups (T_0-T_3).

Sample	Larvae			Puparial cases			Adults		
Substrate	**T_0**	**T_1**	**T_2**	**T_0**	**T_1**	**T_2**	**T_0**	**T_1**	**T_2**
T_1	$N = 10$	–	–	$N = 17$	–	–	$N = 17$	–	–
	$Z = -0.213$			$Z = 0.000$			$Z = -1.925$		
	$p = 0.912$			$p = 1.000$			$p = 0.060$		
T_2	$N = 9$	$N = 11$	–	$N = 15$	$N = 16$	–	$N = 16$	$N = 17$	–
	$Z = -0.735$	$Z = -0.913$		$Z = 0.000$	$Z = -0.053$		$Z = 0.000$	$Z = -2.502$	
	$p = 0.559$	$p = 0.425$		$p = 1.000$	$p = 1.000$		$p = 1.000$	**$p = 0.009$**	
T_3	$N = 13$	$N = 15$	$N = 14$	$N = 17$	$N = 18$	$N = 16$	$N = 17$	$N = 18$	$N = 17$
	$Z = -1.852$	$Z = -2.946$	$Z = -1.933$	$Z = -1.732$	$Z = -3.311$	$Z = -3.334$	$Z = -1.828$	$Z = -3.576$	$Z = -2.983$
	$p = 0.075$	**$p = 0.001$**	$p = 0.060$	$p = 0.094$	**$p < 0.001$**	**$p < 0.001$**	$p = 0.070$	**$p < 0.001$**	**$p = 0.001$**

Bold values denote statistical significance at the $p < 0.05$.

populations has been studied for *C. albiceps* (Al-Misned, 2001, 2003), *C. megacephala* (Singh and Bhupinderjit, 2017), and *L. sericata* (Simkiss et al., 1993; Moe et al., 2001), but only in a few studies bioaccumulation factors for Cd have been calculated.

When we reared larvae of *L. sericata* on a metal-enriched substrate, we observed different accumulation patterns for cadmium and thallium. For Cd, there was clearly a linear relationship between the Cd content of the liver substrate and that found in different developmental stages of *L. sericata*, with correlation coefficients (R) in the range of 0.994–0.997. Instead, the relationship for Tl was obviously nonlinear, indicating that Tl accumulation is saturable at higher metal concentrations in all developmental stages (R between 0.998 and 1.000). In this, our results are similar to those of Belowitz et al. (2014), who reported saturable accumulation of Tl by larvae of *C. riparius*, with a maximum accumulation (B_{max}) of ∼4,600 μmol kg^{-1} wet mass. Those authors hypothesized that this phenomenon was the

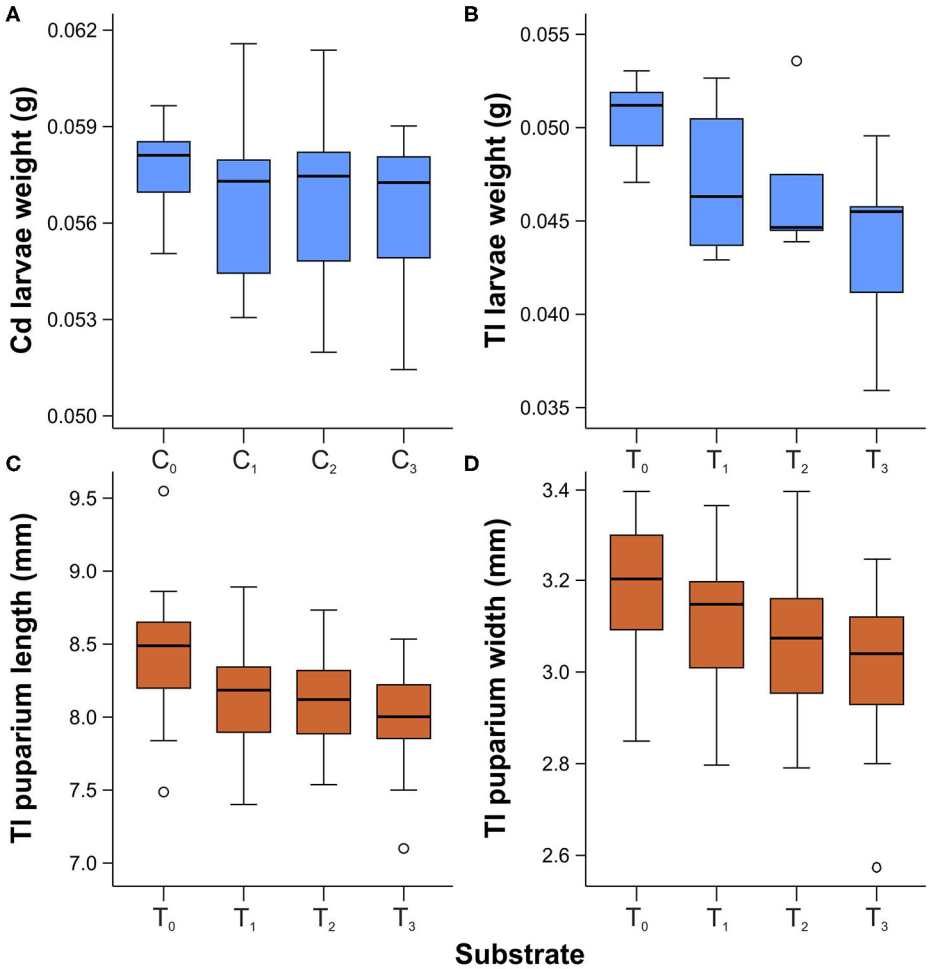

FIGURE 3 | Box and whisker plots showing differences in weight of third instar larvae reared on substrates enriched with cadmium **(A)** and thallium **(B)**, and length **(C)** and width **(D)** of puparia acquired from larvae reared on substrate enriched with thallium. Boxes indicate median and first and third quartiles. Whiskers represent the minimal and maximal values within 1.5 times the interquartile range. Open circles are outliers with values more than 1.5 times the interquartile range.

result of the limited availability of metal-binding proteins, such as metallothioneins (cysteine-rich proteins), that could decrease the metabolically available fraction. However, this hypothesis is not consistent with our results, as both Cd and Tl have the ability to bind sulfhydryl groups (–SH), and the responses of *L. sericata* to high doses of Cd and Tl were clearly different. Here, the bioaccumulation pattern for Cd was similar to that described for different developmental stages of the Asian Corn Borer, *Ostrinia furnacalis*, a type of grass moth (Luo et al., 2020). Our observation that the content of both Cd and Tl in adult flies was lower than in larvae was also consistent with previous reports (Kraus et al., 2014; Luo et al., 2020).

In this study, we noted clear differences between Cd and Tl with respect to accumulation in puparial cases (**Figures 1**, **2**): mean Cd content was lower in puparial cases than in larvae, while the opposite was true for Tl. Our results thus provide evidence that, in this species, thallium is accumulated in the puparial cases (**Figure 2**). Previous studies have reported that one mechanism of detoxification among insects involves the exuviae, the coverings shed by the final larval stage or newly emerged adults. In the dragonfly species *Gomphus flavipes*, Simon et al. (2019) found that, for certain metals—Al, Fe, and Mn—and under certain living conditions, exuviae contained higher metal concentrations than either larvae or adults, demonstrating that molting plays a role in detoxification. Similarly, Kraus et al. (2014) reported that some trace elements, such as Zn, Cd, and Cu, were lost during metamorphosis, leading to 2- to 125-fold higher concentrations in larvae compared to adults, and a higher exposure risk for predators of larvae compared to predators of adults. Moreover, Muscatello and Liber (2009) found that between 22% and 58% of the U accumulated in *Chironomus tentans* was lost via the pupal skin during metamorphosis, which confirmed an important role of the pupal case in detoxification. Our finding that the Tl content in adults was lower than in larvae, and considerably lower than in puparial cases, suggests that this mechanism probably dominates in *L. sericata*'s detoxification of Tl. However, it should be considered that metals can be also excreted in the meconium of last-instar larvae or newly emerged adults. Indeed,

Simon et al. (2019) reported that <10% of the metal burden lost during metamorphosis could be attributed to the exuviae whereas more than 50% was typically lost through meconium. This latter mechanism is more likely to play a role for Cd, as the concentration of Cd in adults was lower than in larvae, while concentrations in larvae and puparial cases were not statistically different. Furthermore, differences in metal concentration among different developmental stages of *L. sericata* were most visible in the groups reared on the substrate with the highest Cd concentration (**Figure 1**, **Supplementary Table 2**). These results are consistent with the work of Luo et al. (2020), who studied the routes of Cd excretion in *O. furnacalis* and found high levels of Cd in feces (95.49 $\mu g\ g^{-1}$), silk (82.98 $\mu g\ g^{-1}$), and pupal cases (76.87 $\mu g\ g^{-1}$). Simkiss et al. (1993) observed an almost constant concentration of Cd in emerging adults of *L. sericata*, but the Cd concentration in puparial cases varied, from levels that were similar to those of adults to ones that were significantly higher.

To compare the transfer of toxins from the surrounding environment to a living organisms, the bioaccumulation factor is often used. Although cadmium is very readily assimilated, and its concentration in organisms is often higher than in their food (Moe et al., 2001), we observed that the mean BAF of Cd in larvae was about 0.20–0.25 (**Figure 1**; **Supplementary Table 3**), and was even lower for adult flies, reaching values between 0.12 and 0.18, with no significant differences among substrates. These data are comparable to the results obtained by Diener et al. (2015), who studied the bioaccumulation of Cd in different life stages of *Hermetia illucens* that were reared on chicken feed spiked with heavy metals. In that study, BAF values decreased from 0.21 to 0.13 with an increase in the concentration of Cd in feed from 2 to 50 $\mu g\ g^{-1}$. For puparial cases, higher values were obtained (in the range of 0.86–1.41) than those found in our study. Instead, a species of ground beetle, *Poecilus cupreus*, that was fed Cd-contaminated larvae of *Musca domestica* demonstrated much lower BAF values, in the range of 0.001 to 0.046, depending on the accumulation period (Kramarz, 1999). Contradictory results were obtained by Moe et al. (2001), who observed that concentrations of Cd in adult flies of *L. sericata* (up to 400 $\mu g\ g^{-1}$ dry mass) were up to eight times the wet-mass concentration in the diet. However, that study used a different compound of Cd (cadmium(II) acetate) and type of nutrient substrate (agar, yeast, and horse blood) than the present work. To date, the only report in the literature for thallium described the uptake of waterborne Tl by larvae of *C. riparius* (Belowitz et al., 2014). Concentration factors (CFs) that indicated how much more Tl was in insect tissue relative to the aqueous concentration were calculated. In that study, CFs of Tl in whole animals were 18- and 5-fold at the two lowest Tl exposures (0.7 and 5.5 $\mu g\ mL^{-1}$), and ∼4-fold over the range of the higher exposure concentrations (5.5–150 $\mu g\ mL^{-1}$). In our study, the BAF values for Tl were always below 1, with the highest values observed for puparial cases.

To date, no information has been published regarding the potential use of puparial cases of *L. sericata* as toxicological evidence of metal poisoning. Moreover, the Guidelines for Collection of Biological Samples for Clinical and Forensic Toxicological Analysis (Dinis-Oliveira et al., 2016) only mention the use of fly larvae, and only for qualitative analysis. Here we demonstrate that empty puparial cases may also provide useful forensic information. For Tl, an increased content in insect remains could be an indicator of the high content of this metal in larval feed. However, as the bioaccumulation pattern is not linear, the results should only be considered qualitatively. For Cd, the concentration in puparial cases was proportional to the Cd content of the substrate, but the application of this relationship to quantitative analyses should be further studied for different Cd compounds over a wider range of concentrations. Because empty puparial cases can be found in the proximity of human remains even after many years, this type of information has the potential to be highly useful in interpreting the analytical results of legal and medical investigations of accidental and intentional poisonings.

Effect of Cadmium and Thallium on Life History Traits of *L. sericata*

For the population of *L. sericata* tested here, the weight of larvae and size of puparia were affected by the presence of metal in the food substrate. In particular, we found that thallium had a negative effect on larval growth, with higher Tl concentrations resulting in lower weight and smaller puparial size. This is a novel finding in the forensic entomotoxicology literature, since to our knowledge thallium determination and its effect on fly development has not been previously assessed. Earlier investigations of Cd in *L. sericata* reported that the mean weight of both larvae and puparia decreased with increasing cadmium concentration in the food substrate (Simkiss et al., 1993; Singh and Bhupinderjit, 2017). Although our results did not reveal any statistically significant differences in larval weight between control and cadmium treatments, mean weight was slightly lower for larvae reared on cadmium compared to the control population. Various studies have reported a general reduction in insect growth as a result of exposure to cadmium (Schmidt et al., 1992; Ortel, 1996; Cervera et al., 2004; Sildanchandra and Crane, 2009) and other toxic metals (Purschke et al., 2017). However, Płachetka-Bozek et al. (2018) found that certain cadmium concentration in food had a variable effect on the growth of *Spodoptera exigua* (Lepidoptera: Noctuidae) larvae. These inconsistencies may arise from differences in the cadmium source used, the concentration in the food substrate, the type of feeding substrate, rearing conditions, or fly population tested (Simkiss et al., 1993; Silva et al., 2017; Płachetka-Bozek et al., 2018).

Methodological Commentary

A common weakness of numerous experimental studies is lack of standardization in the methods used, which makes it difficult to replicate results (Chophi et al., 2019). In this work, we describe our methodology in detail with the goal of facilitating comparisons among the results of entomotoxicological studies.

We chose as a model organism the commonly available insect species *L. sericata*, belonging to the family of true flies (Diptera). To simulate the process of decay of the feeding substrate, as

well as the ingestion and accumulation of toxins, a homogenized meat substrate spiked with cadmium or thallium was used to feed larvae. The use of liver matrix has been criticized in the past because certain toxicants (e.g., drugs) may undergo chemical reactions in liver tissues (Silva et al., 2017). However, in our view these shortcomings did not apply to enrichment with metals. In a pilot experiment, we optimized the method of homogenization of the metal-enriched substrate and confirmed the homogeneity of the solid substrate. In addition to generating a more homogenous substrate, the use of ultrasound for homogenization reduced the risk of sample loss or contamination from laboratory tools during substrate preparation. As recommended by the rules for collection of insects from the scene (Brundage and Byrd, 2016), we collected a fixed number of individuals ($\geq$15) from each substrate; before being frozen for storage, larvae were rinsed with Milli-Q water to avoid external contamination from the metal-enriched substrate. We chose to not use an acidic solution for rinsing samples in order to avoid causing additional stress for the organisms. Moreover, Timmermans et al. (1992) reported no significant difference in Cd concentration for larvae of *C. riparius* that were rinsed in distilled water vs. those rinsed in diluted nitric acid.

The determination of Cd and Tl in forensic samples is a challenging task due to the generally limited amounts of sample available for analysis. Here, this problem was solved by using ICP-MS, as the calculated method detection limit allowed to obtain reliable results even for samples smaller than 0.01 g. The method limit of detection, that includes both the instrumental and procedural constituents, i.e., dilution and mineralization steps, should be preferably reported. The reproducibility of results of Cd and Tl determination in samples between parallel experiments was acceptable (below 25%), only in single cases slightly exceeded 30%. It must be mentioned that individual organisms were used for mineralization, without any initial grinding or homogenization of dried biomass. We expect that the homogenization of samples would further improve the reproducibility of results. Finally, the accuracy of our method was verified by analysis of certified reference materials.

CONCLUSIONS

In this study, we demonstrate that larvae, adults, and empty puparial cases of *L. sericata* found on decomposing human remains, can be used as an alternative material for the detection of Cd and Tl present in the body at the time of death. Our experiment revealed that these metals accumulated in larvae feeding on contaminated liver substrates, and the ingested metals were retained through the puparial stage and were detected in the adult insects. The accumulation of Cd and Tl was studied for different metal concentration in the food substrate. It was observed that the metal content in larvae, puparial cases and adults exposed to contaminated liver substrate was significantly higher than those exposed to control substrate and increased with increasing metal concentration in the liver. Of the three developmental stages analyzed, the highest average content of Cd was found in larvae, whereas for Tl, the highest bioaccumulation factor was observed for puparial cases. The accumulation of thallium in these chitinized remnants could be of great importance in forensic examinations, as puparial cases can be found near human remains for an extremely long period of time. To the best of our knowledge, this is the first report on thallium accumulation in different developmental stages of a forensically important blowfly, and demonstrates the potential usefulness of this kind of evidence in entomotoxicological investigations. Our experiments also revealed that exposure to thallium had an adverse effect on larval growth, resulting in lower mean weight and smaller puparial size. Small quantity of samples, especially puparial cases, required the use of sensitive analytical method of Cd and Tl determination. This study confirmed that the ICP-MS method described here is characterized by low limits of detection and quantification, very good precision, acceptable reproducibility, and good accuracy, and was thus suitable for the determination of Cd and Tl in different developmental stages of blowfly.

DATA AVAILABILITY STATEMENT

The raw data supporting the conclusions of this article will be made available by the authors, without undue reservation.

AUTHOR CONTRIBUTIONS

JM investigation, data calculation, and writing original document. KD investigation, statistical analysis, and writing original manuscript. MT and JD investigation. BG-Ż conceptualization, writing, and supervision. All authors contributed to the article and approved the submitted version.

FUNDING

This publication has received financial support from the Polish Ministry of Science and Higher Education under subsidy for maintaining the research potential of the Faculty of Biology and the Faculty of Chemistry, University of Bialystok.

ACKNOWLEDGMENTS

We would like to thank Marcin Sielezniew for support during the study. The ICP-MS instrument was financed by EU funds via the project with contract numbers: POPW.01.03.00-20-034/09-00.

SUPPLEMENTARY MATERIAL

The Supplementary Material for this article can be found online at: https://www.frontiersin.org/articles/10.3389/fchem.2020.586067/full#supplementary-material

REFERENCES

Agency for Toxic Substances and Disease Registry. (1992). *Toxicological Profile for Thallium*. U.S. Public Health Service.

Agency for Toxic Substances and Disease Registry. (1999). *Toxicological Profile for Cadmium*. Atlanta, GA: U.S. Department of Health and Human Services, Public Health Service.

Al-Misned, F. A. M. (2001). Biological effects of cadmium on life cycle parameters of *Chrysomya albiceps* (Wiedemann) (Diptera: Calliphoridae). *Kuwait J. Sci. Eng*. 28, 179–188.

Al-Misned, F. A. M. (2003). Effect of cadmium on the longevity and fecundity of the blowfly *Chrysomya albiceps* (Wiedemann) (Diptera: Calliphoridae). *Kuwait J. Sci. Eng*. 30, 81–94.

Barwick, V. J., and Ellison, S. L. R. (2000). *VAM Project 3.2.1 Development and Harmonisation of Measurement Uncertainty Principles, Part (d): Protocol for Uncertainty Evaluation from Validation Data*. LGC (Teddington) Limited.

Belowitz, R., Leonard, E. M., and O'Donnell, M. J. (2014). Effects of exposure to high concentrations of waterborne Tl on K and Tl concentrations in *Chironomus riparius* larvae. *Comp. Biochem. Phys. C*. 166, 59–64. doi: 10.1016/j.cbpc.2014.07.003

Beyer, J., Enos, W., and Stalic, M. (1980). Drug identification through analysis of maggots. *J. Forensic Sci*. 25, 411–412. doi: 10.1520/JFS12147J

Braga, M. V., Pinto, Z. T., Carvalho Queiroz, M. M., Matsumoto, N., and Blomquist, G. J. (2013). Cuticular hydrocarbons as a tool for the identification of insect species: puparial cases from Sarcophagidae. *Acta Trop*. 128, 479–485. doi: 10.1016/j.actatropica.2013.07.014

Brundage, A., and Byrd, J. H. (2016). Forensic entomology in animal cruelty cases. *Vet. Path*., 53, 898–909. doi: 10.1177/0300985816651683

Bugelli, V., Campobasso, C. P., Verhoff, M. A., and Amendt, J. (2017b). Effects of different storage and measuring methods on larval length values for the blow flies (Diptera: Calliphoridae) *Lucilia sericata* and *Calliphora vicina*. *Sci. Justice* 57, 159–164. doi: 10.1016/j.scijus.2016.10.008

Bugelli, V., Papi, L., Fornaro, S., Stefanelli, F., Chericoni, S., Giusiani, M., et al. (2017a). Entomotoxicology in burnt bodies: a case of maternal filicide-suicide by fire. *Int. J. Legal Med*. 133, 1299–1306. doi: 10.1007/s00414-017-1628-0

Byrd, J. H., and Castner, J. L. (2010). "Insects of forensic importance," in *Forensic Entomology: the Utility of Arthropods in Legal Investigations*, eds. J. H. Byrd, J. L. Castner (Boca Raton, FL: CRC Press), 39–126.

Campobasso, C. P., Gherardi, M., Caligara, M., Sironi, L., and Introna, F. (2004). Drug analysis in blowfly larvae and in human tissues: acomparative study. *Int. J. Legal Med*. 118, 210–214. doi: 10.1007/s00414-004-0448-1

Cavanagh, J. B. (1991). What have we learnt from Graham Frederick Young? Reflections on the mechanism of thallium neurotoxicity. *Neuropath. Appl. Neuro*. 17, 3–9. doi: 10.1111/j.1365-2990.1991.tb00687.x

Cervera, A., Maymó, A. C., Sendra, M., Martínez-Pardo, R., and Garcerá, M. D. (2004). Cadmium effects on development and reproduction of *Oncopeltus fasciatus* (Heteroptera: Lygaeidae). *J. Insect Physiol*. 50, 737–749. doi: 10.1016/j.jinsphys.2004.06.001

Chang, Y., Wen, J., Cai, J., Xiao-Ying, W., Yang, L., and Yd, G. (2012). An investigation and pathological analysis of two fatal cases of cadmium poisoning. *Forensic Sci. Int*. 220, 1–3. doi: 10.1016/j.forsciint.2012.01.032

Chophi, R., Sharma, S., Sharma, S., and Singh, R. (2019). Forensic entomotoxicology: current concepts, trends and challenges. *J. Forensic Legal. Med*. 67, 28–36. doi: 10.1016/j.jflm.2019.07.010

Desenclos, J. C., Wilder, M. H., Coppenger, G. W., Sherin, K., Tiller, R., and VanHook, R. M. (1992). Thallium poisoning: an outbreak in Florida, 1988. *South. Med. J*. 85, 1203–1206. doi: 10.1097/00007611-199212000-00012

Diener, S., Zurbrügg, C., and Tockner, K. (2015). Bioaccumulation of heavy metals in the black soldier fly, *Hermetia illucens* and effects on its life cycle. *J. Insects as Food Feed*. 1, 261–270. doi: 10.3920/JIFF2015.0030

Dinis-Oliveira, R. J., Vieira, D. N., and Magalhães, T. (2016). Guidelines for collection of biological samples for clinical and forensic toxicological analysis. *Forensic Sci. Res*. 1, 42–51. doi: 10.1080/20961790.2016.1271098

Gallagher, M. B., Sandhu, S., and Kimsey, R. (2010). Variation in developmental time for geographically distinct populations of the common green bottle fly, *Lucilia sericata* (Meigen). *J. Forensic Sci*. 55, 438–443. doi: 10.1111/j.1556-4029.2009.01285.x

Gaudry, E., Myskowiak, J.-B., Chauvet, B., Pasquerault, T., Lefebvre, F., and Malgorn, Y. (2001). Activity of the forensic entomology department of the French Gendarmerie. *Forensic Sci. Int*. 120, 68–71. doi: 10.1016/S0379-0738(01)00427-3

Goff, M. L., Miller, M. L., Paulson, J. D., Lord, W. D., Richards, E., and Omori, A. I. (1997). Effects of 3,4-methylenedioxymethamphetamine in decomposing tissues on the development of *Parasarcophaga ruficornis* (Diptera:Sarcophagidae) and detection of the drug in postmortem blood, liver tissue, larvae, and puparia. *J. Forensic Sci*. 42, 276–280. doi: 10.1520/JFS14110J

Greenberg, B. (1991). Flies as forensic indicators. *J. Med. Entomol*. 28, 565–577. doi: 10.1093/jmedent/28.5.565

Hoffman, R. S., and Hoffman, R. (2000). Thallium poisoning during pregnancy: a case report and comprehensive literature review. *J. Toxicol. Clin. Toxicol*. 38, 767–775. doi: 10.1081/CLT-100102390

Karbowska, B. (2016). Presence of thallium in the environment: sources of contaminations, distribution and monitoring methods. *Environ. Monit. Assess*. 188, 640. doi: 10.1007/s10661-016-5647-y

Kramarz, P. (1999). Dynamics of accumulation and decontamination of cadmium and zinc in carnivorous invertebrates. 1. The ground beetle, *Poecilus cupreus* L. B. *Environ. Contam. Toxiocol*. 63, 531–537. doi: 10.1007/s001289901013

Kraus, J. M., Walters, D. M., Wesner, J. S., Stricker, C. A., Schmidt, T. S., and Zuelling, R. E. (2014). Metamorphosis alters contaminants and chemical tracers in insects: Implications for food webs. *Environ. Sci. Technol*. 48, 10957–10965. doi: 10.1021/es502970b

Lech, T., and Sadlik, J. K. (2017). Cadmium concentration in human autopsy tissues. *Biol. Trace Elem. Res*. 179, 172–177. doi: 10.1007/s12011-017-0959-5

Luo, M., Cao, H.-M., Fan, Y.-Y., Zhou, X.-C., Chen, J.-X., Chung, H., et al. (2020). Bioaccumulation of cadmium affects development, mating behavior, and fecundity in the Asian Corn Borer, Ostrinia furnacalis. *Insects*. 11:7. doi: 10.3390/insects11010007

Meggs, W. J., Hoffman, R. S., Shih, R. D., Weismann, R. S., and Goldfrank, L. R. (1994). Thallium poisoning from maliciously contaminated food. *J. Toxicol. Clin. Toxicol*. 32, 723–730. doi: 10.3109/15563659409017979

Miller, M., Lord, W., Goff, M., Donnelly, B., McDonough, E., and Alexis, J. (1994). Isolation of Amitriptyline and Nortriptyline from fly puparia (Phoridae) and beetle exuviae (Dermestidae) associated with mummified human remains. *J. Forensic Sci*. 39, 1305–1313. doi: 10.1520/JFS13717J

Moe, S. J., Stenseth, N. C., and Smith, R. H. (2001). Effects of a toxicant on population growth rates: sublethal and delayed responses in blowfly populations. *Funct. Ecol*. 15, 712–721. doi: 10.1046/j.0269-8463.2001.00575.x

Muscatello, J. R., and Liber, K. (2009). Accumulation and chronic toxicity of uranium over different life stages of the aquatic invertebrate *Chironomus tentans*. *Arch. Environ. Contam. Toxicol*. 57, 531–539. doi: 10.1007/s00244-009-9283-1

Nishijo, M., Nakagawa, H., Suwazono, Y., Nogawa, K., and Kido, T. (2017). Causes of death in patients with Itaiitai disease suffering from severe chronic cadmium poisoning: a nested case-control analysis of a follow-up study in Japan. *BMJ Open* 7:e015694. doi: 10.1136/bmjopen-2016-015694

Nolte, K. B., Pinder, R. D., and Lord, W. D. (1992). Insect larvae used to detect cocaine poisoning in a decomposed body. *J. Forensic Sci*. 37, 1179–1185. doi: 10.1520/JFS13304J

Ortel, J. (1996). Metal-supplemented diets alter carbohydrate levels in tissue and hemolymph of gypsy moth larvae (Lymantria dispar, Lymantriidae, Lepidoptera). *Environ. Toxicol. Chem*. 15, 1171–1176. doi: 10.1002/etc.5620150723

Owings, C. G., Banerjee, A., Asher, T. M. D., Gilhooly, W. P. III., Tuceryan, A., Huffine, M., et al. (2019). Female blow flies as vertebrate resource indicators. *Sci. Rep*. 9:10594. doi: 10.1038/s41598-019-46758-9

Płachetka-Bozek, A., Kafel, A., and Augustyniak, M. (2018). Reproduction and development of Spodoptera exigua from cadmium and control strains under differentiated cadmium stress. *Ecotoxicol. Environ. Saf*. 166, 138–145. doi: 10.1016/j.ecoenv.2018.09.016

Pounder, D. J. (1991). Forensic entomo-toxicology. *J. Forensic Sci. Soc*. 31, 469–472. doi: 10.1016/S0015-7368(91)73189-7

Powers, R. H., and Dean, D. E. (2015). *Forensic Toxicology: Mechanisms and Pathology*. Boca Raton, FL: CRC Press.

Prado e Castro, C., Serrano, A., Martins da Silva, P., and Garcia, M. D. (2012). Carrion flies of forensic interest: a study of seasonal community composition and succession in Lisbon, Portugal. *Med. Vet. Entomol*. 26, 417–431. doi: 10.1111/j.1365-2915.2012.01031.x

Purschke, B., Scheibelberger, R., Axmann, S., Adler, A., and Jäger, H. (2017). Impact of substrate contamination with mycotoxins, heavy metals and pesticides on the growth performance and composition of black soldier fly larvae (*Hermetia illucens*) for use in the feed and food value chain. *Food Addit. Contam. Part A*. 34, 1410–1420. doi: 10.1080/19440049.2017.1299946

Rafati Rahimzadeh, M., Rafati Rahimzadeh, M., Kazemi, S., and Moghadamnia, A. A. (2017). Cadmium toxicity and treatment: an update. *Caspian J. Intern. Med*. 8, 135–145. doi: 10.22088/cjim.8.3.135

Reibe, S., Doetinchem, P., and Madea, B. (2010). A new simulation-based model for calculating post-mortem intervals using developmental data for *Lucilia sericata* (Dipt.: Calliphoridae). *Parasitol. Res*. 107, 9–16. doi: 10.1007/s00436-010-1879-x

Reith, S. (2009). *Toxicological Review of Thallium and Compounds*. Washington, DC: U.S. Environmental Protection Agency.

Sakai, K. (2015). *Routine Soil Analysis Using an Agilent 8800 ICP-QQQ*. Application note. Agilent Technologies.

Schmidt, G. H., Ibrahim, N. M. M., and Abdallah, M. D. (1992). Long-term effects of heavy metals in food on developmental stages of *Aiolopus thalassinus* (Saltatoria: Acrididae). *Arch. Environ. Con. Tox*. 23, 375–382. doi: 10.1007/BF00216248

Sigel, A., Sigel, H., and Sigel, R. K. O. (2013). *Cadmium: From Toxicity to Essentiality*. New York, NY: Springer.

Sildanchandra, W., and Crane, M. (2009). Influence of sexual dimorphism in *Chironomus riparius* Meigen on toxic effects of cadmium. *Environ. Toxicol. Chem*. 19, 2309–2313. doi: 10.1002/etc.5620190921

Silva, E. I. T., Wilhelmi, B., and Villet, M. H. (2017). Forensic entomotoxicology revisited - towards professional standardisation of study designs. *Int. J. Leg. Med*. 131, 1399–1412. doi: 10.1007/s00414-017-1603-9

Simkiss, K., Daniels, S., and Smith, R. H. (1993). Effects of population density and cadmium toxicity on growth and survival of blowflies. *Environ. Pollut*. 81, 41–45. doi: 10.1016/0269-7491(93)90026-K

Simon, E., Tóthmérész, B., Kis, O., Jakab, T., Szalay, P. E., Vincze, A., et al. (2019). Environmental-friendly contamination assessment of habitats based on the trace element content of dragonfly exuviae. *Water* 11, 2200. doi: 10.3390/w11112200

Singh, D., and Bhupinderjit, K. H. (2017). Effect of cadmium chloride on the development of *Chrysomya megacephala* (Diptera:Calliphoridae) and its importance to postmortem interval estimate. *J. Forensic Sci. Criminal Invest*. 3, 555622. doi: 10.19080/JFSCI.2017.03.555622

Timmermans, K. R., Peeters, W., and Tonkes, M. (1992). Cadmium, zinc, lead and copper in *Chironomus riparius* (Meigen) larvae (Diptera, Chironomidae): uptake and effects. *Hydrobiologia*. 241, 119–134. doi: 10.1007/BF00008264

Tracqui, A., Keyser-Tracqui, C., Kintz, P., and Ludes, B. (2004). Entomotoxicology for the forensic toxicologist: much ado about nothing? *Int. J. Legal Med*. 118, 194–196. doi: 10.1007/s00414-004-0442-7

Wang, J., Li, Z., Chen, Y., Chen, Q., and Yin, X. (2008). The succession and development of insects on pig carcasses and their significances in estimating PMI in south China. *Forensic Sci. Int*. 179, 11–18. doi: 10.1016/j.forsciint.2008.04.014

Zhu, G.-H., Jia, Z.-J., Yu, X.-J., Wu, K.-S., Chen, L.-S., Lv, J.-Y., et al. (2017). Predictable weathering of puparial hydrocarbons of necrophagous flies for determining the postmortem interval: a field experiment using Chrysomya rufifacies. *Int. J. Legal Med*. 131, 885–894. doi: 10.1007/s00414-016-1507-0

Conflict of Interest: The authors declare that the research was conducted in the absence of any commercial or financial relationships that could be construed as a potential conflict of interest.

frontiers in Chemistry

ORIGINAL RESEARCH
published: 25 November 2020
doi: 10.3389/fchem.2020.572952

Molecular Networking: A Useful Tool for the Identification of New Psychoactive Substances in Seizures by LC–HRMS

Flaminia Vincenti[1,2], *Camilla Montesano*[1]*, *Francesca Di Ottavio*[3], *Adolfo Gregori*[4], *Dario Compagnone*[3], *Manuel Sergi*[3]* *and Pieter Dorrestein*[5]

[1] Department of Chemistry, Sapienza University of Rome, Rome, Italy, [2] Department of Public Health and Infectious Disease, Sapienza University of Rome, Rome, Italy, [3] Faculty of Bioscience and Technology for Food, Agriculture and Environment, University of Teramo, Teramo, Italy, [4] Department of Scientific Investigation (RIS), Carabinieri, Rome, Italy, [5] Collaborative Mass Spectrometry Innovation Center, Skaggs School of Pharmacy and Pharmaceutical Sciences, University of California, San Diego, San Diego, CA, United States

OPEN ACCESS

Edited by:
Paolo Oliveri,
University of Genoa, Italy

Reviewed by:
Giuseppe Egidio De Benedetto,
University of Salento, Italy
Eugenio Alladio,
University of Turin, Italy

***Correspondence:**
Camilla Montesano
camilla.montesano@uniroma1.it
Manuel Sergi
msergi@unite.it

Specialty section:
This article was submitted to Analytical Chemistry, a section of the journal Frontiers in Chemistry

Received: 15 June 2020
Accepted: 09 October 2020
Published: 25 November 2020

Citation:
Vincenti F, Montesano C, Di Ottavio F, Gregori A, Compagnone D, Sergi M and Dorrestein P (2020) Molecular Networking: A Useful Tool for the Identification of New Psychoactive Substances in Seizures by LC–HRMS. Front. Chem. 8:572952. doi: 10.3389/fchem.2020.572952

New Psychoactive Substances (NPS) are a global concern since they are spreading at an unprecedented rate. Despite their commerce still being limited compared to traditional illicit drugs, the identification of NPS in seizures may represent a challenge because of the variety of possible structures. In this study we report the successful application of molecular networking (MN) to identify unexpected fentanyl analogs in two seizures. The samples were extracted with 1 mL of methanol and analyzed with an untargeted data-dependent acquisition approach by LC–HRMS. The obtained data were examined using the MN workflow within the Global Natural Product Search (GNPS). A job was submitted to GNPS by including both seizures and standard mixtures containing synthetic cannabinoids and fentanyls raw files; spectra obtained from standards were used to establish representative networks for both molecular classes. All synthetic cannabinoids in the mixture were linked together resulting in a molecular network despite their different fragmentation spectra. Looking at fentanyls, all the molecules with the typical 188.143 and 105.070 fragments were combined in a representative network. By exploiting the standard networks two unexpected fentanyls were found in the analyzed seizures and were putatively annotated as para-fluorofuranylfentanyl and (iso)butyrylfentanyl. The identity of these two fentanyl analogs was confirmed by NMR analysis. Other m/z ratios in the seizures were compatible with fentanyl derivatives; however, they appeared to be minor constituents, probably impurities or synthetic byproducts. The latter might be of interest for investigations of common fingerprints among different seizures.

Keywords: new psychoactive substances, LC-HRMS, molecular networking, untarget analysis, seizure analysis

INTRODUCTION

The most common approach used in forensic laboratories to identify and quantify illicit drugs in seized samples is targeted mass spectrometry (MS), usually coupled with Gas (GC) or Liquid Chromatography (LC). Targeted MS approaches are able to detect hundreds of illegal drugs at a trace level in a single analysis, in complex matrices such as biological samples or plant extracts (Archer et al., 2011; Smith et al., 2015). Identification and quantitation are carried out comparing retention times, fragmentation spectra and, for quantitative purposes, peak areas with analytical standards. Standards are generally very expensive and, sometimes, particularly for newly synthesized drugs and unknown metabolites, not commercially available (Laks et al., 2004).

These limitations of targeted analysis are exploited by drug producers to circumvent controls. This issue resulted in the New Psychoactive Substances (NPS) phenomenon. Several new drugs synthetized from known molecules by means of simple structural modifications such as alkylation, dealkylation, oxidation, reduction etc. were introduced in the market, becoming undetectable by traditional targeted screening. These new drugs are proliferating at an unprecedented rate, posing a significant risk to public health since they have unpredictable toxicological effects (Tai and Fantegrossi, 2014; Rivera et al., 2017; Weinstein et al., 2017).

The use of untargeted approaches is essential to solve this problem by exploiting suitable analytical tools; high resolution mass spectrometry (HRMS) is, at the moment, the most appropriate approach. From a theoretical point of view, having the accurate mass of a molecule and the isotopic pattern, the chemical formula of a compound can be confirmed or even ascertained, with a low rate of false positives. The study of the fragments may be an additional tool for the identification of unknown substances. Thus, HRMS, coupled with LC or GC for complex matrices, has been used to identify unexpected substances such as NPS in seized materials and metabolites in biofluids (Wille et al., 2017; Dei Cas et al., 2019). In seizures, HRMS can also represent an important tool to detect impurities and synthetic by-products to obtain a fingerprint of the samples. These signatures may be used to assess correlations among samples including their origin (Münster-Müller et al., 2019). HRMS has, then, become essential in forensic toxicology for the detection of unknown substances; however, the complexity of the data generated from the analysis of a sample is high and annotation is still a bottleneck, often limiting the use of the collected data. A number of proprietary or open software and platforms exist for the analysis of complex raw data from untargeted LC–HRMS analysis; they only allow the annotation of known compounds, through library searches (Hohrenk et al., 2020).

Molecular Networking (MN) is a computational strategy that may help visualization and interpretation of the complex data arising from MS analysis. MN is able to identify potential similarities among all MS/MS spectra within the dataset and to propagate annotation to unknown but related molecules (Wang et al., 2016). This approach exploits the assumption that structurally related molecules produce similar fragmentation patterns, and therefore they should be related within a network (Quinn et al., 2017). In MN, MS/MS data are represented in a graphical form, where each node represents an ion with an associated fragmentation spectrum; the links among the nodes indicate similarities of the spectra. By propagation of the structural information within the network, unknown but structurally related molecules can be highlighted and successful dereplication can be obtained (Yang et al., 2013); this may be particularly useful for metabolite and NPS identification.

MN has been implemented in different fields, particularly metabolomics and drug discovery (Quinn et al., 2017); MN in forensic toxicology was previously used by Allard et al. (2019) for the retrospective analysis of routine cases involving biological sample analysis. Yu et al. (2019) also used MN analysis for the detection of designer drugs such as NBOMe derivatives and they showed that unknown compounds could be recognized as NBOMe-related substances by MN.

In the present work the Global Natural Products Social platform (GNPS) was exploited to analyze HRMS/MS data obtained from the analysis of seizures collected by the Italian Department of Scientific Investigation of Carabinieri (RIS). The potential of MN to highlight and support the identification of unknown NPS belonging to chemical classes such as fentanyls and synthetic cannabinoids has been demonstrated.

MATERIALS AND METHODS

Chemicals and Working Solutions

16 fentanyl derivatives and 16 synthetic cannabinoids were purchased from Cayman Chemical (Ann Arbor, Michigan, USA) and were used as reference compounds. The list is provided in **Tables 1**, **2**. Methanol, ultrapure water, and acetonitrile were of HPLC grade and were purchased from Fisher Scientific Italia (Rodano, MI, Italy), while formic acid was from Sigma Aldrich (Milan, Italy). Two separate working solutions with a final concentration of 100 ng/mL in methanol were prepared from the stock solutions of the drugs and then stored at -20°C.

Seizure Samples

Two seized samples (A and B) collected during investigative operations by RIS between September 2017 and December 2018 were analyzed by LC–HRMS. Since these samples are connected to criminal activity, it is not possible to provide further information such as location and exact data collection.

Seized samples were stored at room temperature until extraction, then 1 mg of seizure was extracted with 1 mL of methanol, vortexed for 1 min, sonicated at 25°C for 10 min and finally filtered through a 0.22 μm nylon filter from Agilent (Santa Clara, CA, USA). The obtained extracts are diluted 1: 10000 and subsequently 5 μL are injected into the UHPLC system.

UHPLC–HRMS Analysis

Both the standard solutions and the seizures extracts were analyzed by UHPLC–HRMS. Ten μL of sample were injected into a UHPLC Dionex^{TM} UltiMate^{TM} 3000 Rapid Separation Liquid Chromatography (RSLC) system (Thermo Fisher

TABLE 1 | List of synthetic cannabinoids included in the standard mixture.

Analyte	Molecular formula	Exact Mass (m/z)	Fragment 1 (m/z)	Fragment 2 (m/z)
UR-144	$C_{21}H_{29}NO$	312,2321	125,0960	214,1219
JWH-073	$C_{23}H_{21}NO$	328,1695	155,0488	200,1065
UR-144 N(4-hydroxypentyl)	$C_{21}H_{29}NO_2$	328,2271	125,0959	230,1165
XLR-11	$C_{21}H_{28}FNO$	330,2227	125,0959	232,1128
JWH-018	$C_{24}H_{23}NO$	342,1852	155,0488	214,1221
AB-005	$C_{23}H_{32}N_2O$	353,2587	112,1121	98,0966
JWH-122	$C_{25}H_{25}NO$	356,2008	169,0644	214,1221
N5-OH-JWH018	$C_{24}H_{23}NO_2$	358,1801	155,0488	230,1178
N-COOH-JWH018	$C_{24}H_{21}NO_3$	372,1594	155,0488	244,0959
JWH-081	$C_{25}H_{25}NO_2$	372,1958	185,0593	214,1221
MAM2201	$C_{25}H_{24}FNO$	374,1914	169,0644	232,1126
AM-1220	$C_{26}H_{26}N_2O$	383,2117	98,0966	112,1120
JWH-200	$C_{25}H_{24}N_2O_2$	385,1910	155,0488	114,0913
N-COOH-MAM2201	$C_{25}H_{23}NO_3$	386,1750	169,06440	244,09620
N5-OH-JWH-081	$C_{25}H_{25}NO_3$	388,1907	185,05930	230,11690
WIN-55	$C_{27}H_{26}N_2O_3$	427,2016	155,04880	100,07580

TABLE 2 | Fentanyl derivatives included in the standard mixtures.

Fentanyl derivative standard	m/z	Molecular formula
4-Anpp	**281,2012**	**$C_{19}H_{24}N_2$**
Despropionyl Para-Fluorofentanyl	**299,1918**	**$C_{19}H_{23}FN_2$**
Acetyl Fentanyl	**323,2118**	**$C_{21}H_{26}N_2O$**
Acrylfentanyl	**335,2118**	**$C_{22}H_{26}N_2O$**
Fentanyl	**337,2274**	**$C_{22}H_{28}N_2O$**
α-Methylfentanyl	**351,2431**	**$C_{23}H_{30}N_2O$**
Ortho-Fluorofentanyl	**355,2180**	**$C_{22}H_{27}FN_2O$**
Cis-3-methylthiofentanyl	357,1995	$C_{21}H_{28}N_2OS$
Ocfentanyl	**371,2129**	**$C_{22}H_{27}FN_2O_2$**
Furanylfentanyl	**375,2067**	**$C_{24}H_{26}N_2O_2$**
Remifentanyl	377,2071	$C_{20}H_{28}N_2O_5$
Butyryl-fentanyl-carboxy Metabolite	**381,2173**	**$C_{23}H_{28}N_2O_3$**
Sufentanyl	387,2101	$C_{22}H_{30}N_2O_2S$
Alfentanyl	417,2609	$C_{21}H_{32}N_6O_3$

Analytes in bold correspond to nodes in the fentanyl network.

Scientific, San Jose, CA, USA). Compounds separation was performed with a C18 Accucore™ column (30 x 2.1 mm) from Thermo Fisher packed with 2.6 μm spherical solid core ultrapure particles. Mobile phases were 10 mM ammonium formate + 0.1% formic acid in water (mobile phase A) and 0.1% formic acid in acetonitrile (mobile phase B) using a flow rate of 0.5 mL min^{-1}. A linear gradient was applied in order to elute the compounds; from 0 to 1 min B was maintained at 5%, from 1 to 9 min B was increased to 100%, maintained at 100% for 2 min and afterwards 2.5 min re-equilibration at 5% B was performed. The C18 column was held at 40°C.

Analyses were performed with a Q Exactive Orbitrap MS from Thermo Fisher Scientific (Bremen, Germany) equipped with a Heated Electrospray Ionization (H-ESI) in positive mode. H-ESI conditions were set as follows: source temperature 340°C, capillary temperature 380°C, spray voltage 3.50 kV, S-lens RF level 60.0. Nitrogen was used for both sheath and auxiliary gas and was set at 60 and 20, respectively.

Untargeted analysis was conducted in Full MS/dd-MS2 acquisition mode, which combines a full scan with a set of data dependent MS2 scans. Full scan was carried out at a resolution of 35,000 (FWHM) in a scan range of 50–850 m/z. Automatic Gain Control (AGC) was 1e6 and Maximum Injection Time was 100 ms. MS/MS analyses were carried out with a resolution of 17,500 (FWHM), AGC and Maximum IT were set, respectively at 5e5 and 100 ms. Fragmentation was performed in HCD cell at three different values of normalized collision energy (NCE) 20, 30 and 40 with a dynamic exclusion of 30s, with nitrogen as collision gas.

Data Processing

Raw data files obtained from the untargeted analysis of the selected samples and the standard mixtures were converted to .mzXML using MSConvert (http://proteowizard.sourceforge.net) in order to transform spectra from profile to centroid mode. The .mzXML files were uploaded on Global Natural Product Social Molecular Networking (GNPS) through WinSCP (version 5.17.3) and analyzed with the GNPS platform (http://gnps.ucsd.edu). For the MS-Cluster and spectral library search, parent ion mass and MS/MS fragment ion tolerance were set at 0.02 Da in order to create consensus spectra. Links between nodes were created when the cosine score was <0.7 and a minimum number of 6 common fragment ions were shared by at least one MS/MS spectrum. An exhaustive guide for MN building by means of GNPS was recently provided (Aron et al., 2020). Two separate jobs were carried out for synthetic cannabinoids and fentanyls, respectively, molecular networks are available at:

https://gnps.ucsd.edu/ProteoSAFe/status.jsp?task=3b4d5e5b455140ceb842d2aa13e51c1c

https://gnps.ucsd.edu/ProteoSAFe/status.jsp?task=193e9ab161554741a119940e2c52a2b0.

For each job, samples were separated into different groups, spectrum files of standard solutions were loaded as group 1 (G1), seizure A was labeled as G2 while seizure B as G3. For each group triplicate files were loaded. Library annotations were obtained from the comparison between the MS/MS spectra with several spectral libraries, including GNPS, NIST17, HMDB, and Massbank; at least 6 fragment ions should match the MS/MS spectra contained in those libraries with a cosine score of 0.7. The selected parameters allow a false discovery rate (FDR) of 1%, data obtained using Passatutto (Scheubert et al., 2017).

Finally, the resulting spectral network was uploaded in Cytoscape 3.8 to obtain better visualization, the nodes were labeled with ID and precursor masses; the edges with the mass differences between the connected nodes, and the edges thickness is proportional to cosine score. Nodes were colored in different colors according to the group where the precursor was detected.

All the software programs used in these steps are open source and can be accessed freely online.

NMR Analysis

NMR experiments were recorded at 298 K on a AVANCE III spectrometer (Bruker BioSpin, GmbH, Germany), equipped with a multinuclear z-gradient inverse probe-head operating at the proton frequency of 400.13 MHz.

Assignments were made via ^{1}H NMR as well as bidimensional ^{1}H/^{1}H correlation spectroscopy (^{1}H/^{1}H–COZY) and ^{1}H/^{13}C–heteronuclear single-quantum correlation spectroscopy (^{1}H/^{13}C–HSQC). Spectra were analyzed with ACD NMR manager software ver. 12 (ACD/Labs, Toronto, Canada).

RESULTS AND DISCUSSION

The aim of this study was to exploit MN to process the data obtained from the analysis of seizures using HRMS/MS in untargeted acquisition mode. The GNPS platform is helpful for investigation purposes related to drug seizures because of the ability to annotate illicit drugs even in the absence of standards. This is achieved by exploiting the available libraries and propagating, at the same time, the annotation to structurally related substances by MN, which is very promising for NPS identification.

Initially LC-HRMS chromatographic parameters were adjusted in order to obtain an optimal separation and peak shape for the analytes included in the standard mixtures. Being the method aimed to the detection of molecules not included in the target list, further adjustments to the method were necessary in order to allow retention of compounds in a wider polarity range with respect to the standards. The Full MS/dd-MS2 acquisition mode, which combines a full scan with a set of data dependent MS2 scans, provides a unique tool for untargeted analysis. Then a fine tuning was made on the HRMS parameters in order to obtain the best sensitivity together with a suitable resolution and accuracy: full scan and MS/MS resolution, AGC, injection time and fragmentation conditions were adjusted.

The LC–MS/MS raw files arising from the analysis of the standard mixtures and the seizure samples were separated in three groups as described in §2.4 and submitted to GNPS. The obtained networks allowed the visual exploration of compound families, within the different samples. Each node had a distinctive color based on the group to which they belonged. When a query MS/MS spectrum matched a GNPS library entry, the node was highlighted.

Synthetic Cannabinoids Network

GNPS spectral libraries were able to identify 5 of the 16 drugs included in the standard mixture; no relevant matches were identified in the seizures (G2 and G3). Annotation was carried out based on the exact mass and the match between the fragmentation spectrum and the GNPS spectral databases.

Attention was then paid to the spectral families. A large network of 31 nodes was identified as the synthetic cannabinoids network; it was remarkable that all 16 cannabinoids included in the sample were recognized as one integrated network with cosine score $>$ 0.7 (**Figure 1**). The network also contained additional nodes that did not correspond to the added standards. It was observed that most of these "unknowns" had a lower intensity; then after applying a filter on precursor intensity (1E7), only 9 of them were kept. Examining the data, it was observed that all the nodes were correlated to precursors with a mean R_t within 1% of the standards suggesting that they were adducts and fragments of the standards. Notably, the precursor charge of most unknown was 0 and their precursor mass corresponded to [M-1]. All these nodes were excluded from the network, the final network is shown in **Figure 1**.

Interestingly, analytes not sharing common fragments were connected within the network, nicely showing the potential of MN to reveal new synthetic cannabinoids that cannot be identified using conventional approaches such as precursor ion or neutral loss scanning. In fact, MN not only groups fragmentation spectra (MS2) with ions at identical m/z, but also MS2 that are offset by the same m/z difference as the precursor ion. MS/MS structural similarity is expressed by the cosine scores for the vectors generated from an m/z value and the respective intensity of the product ions. In the present study the aim was to construct a "training network" with standards and to exploit it to possibly annotate unknown seizure samples. In fact, considering that related molecules are connected into the same subnetwork, even unknown but structurally related compounds will be included in this cluster, offering an interesting perspective to annotate new synthetic cannabinoids.

Raw files were then separated in different groups; group 1 included the standards while group 2 and 3 the seizures. The two seizures were previously analyzed by a target LC-HRMS method including nearly 50 NPS but no positivities were found. No synthetic cannabinoids were found in the seizures using the MN-based screening method.

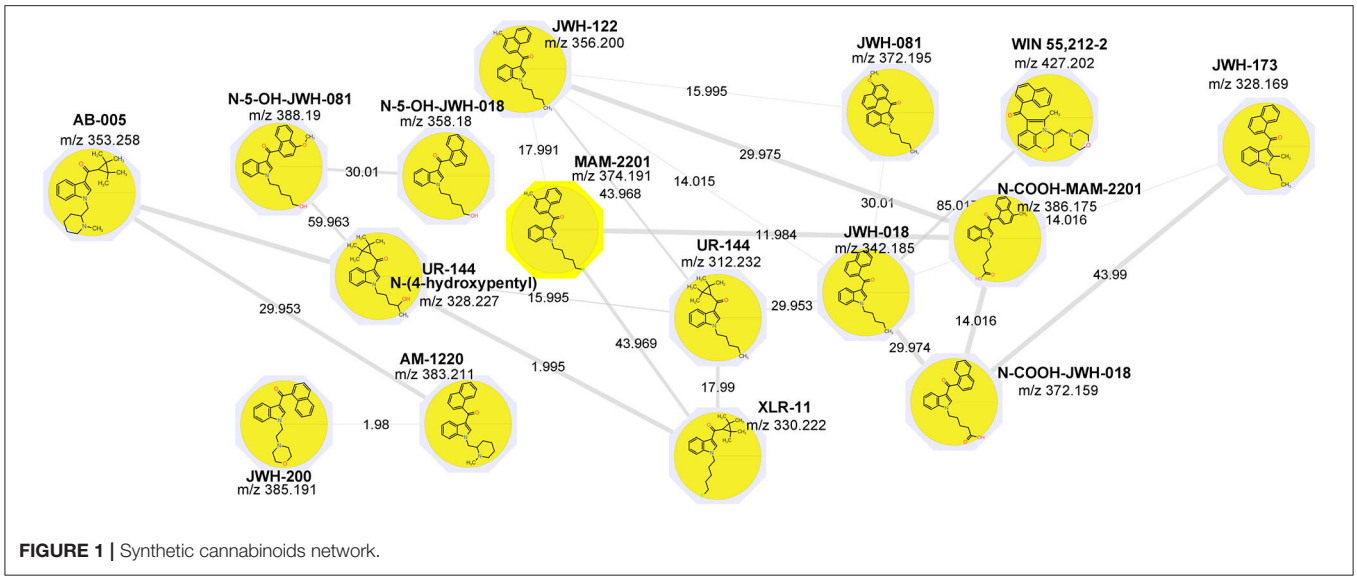

FIGURE 1 | Synthetic cannabinoids network.

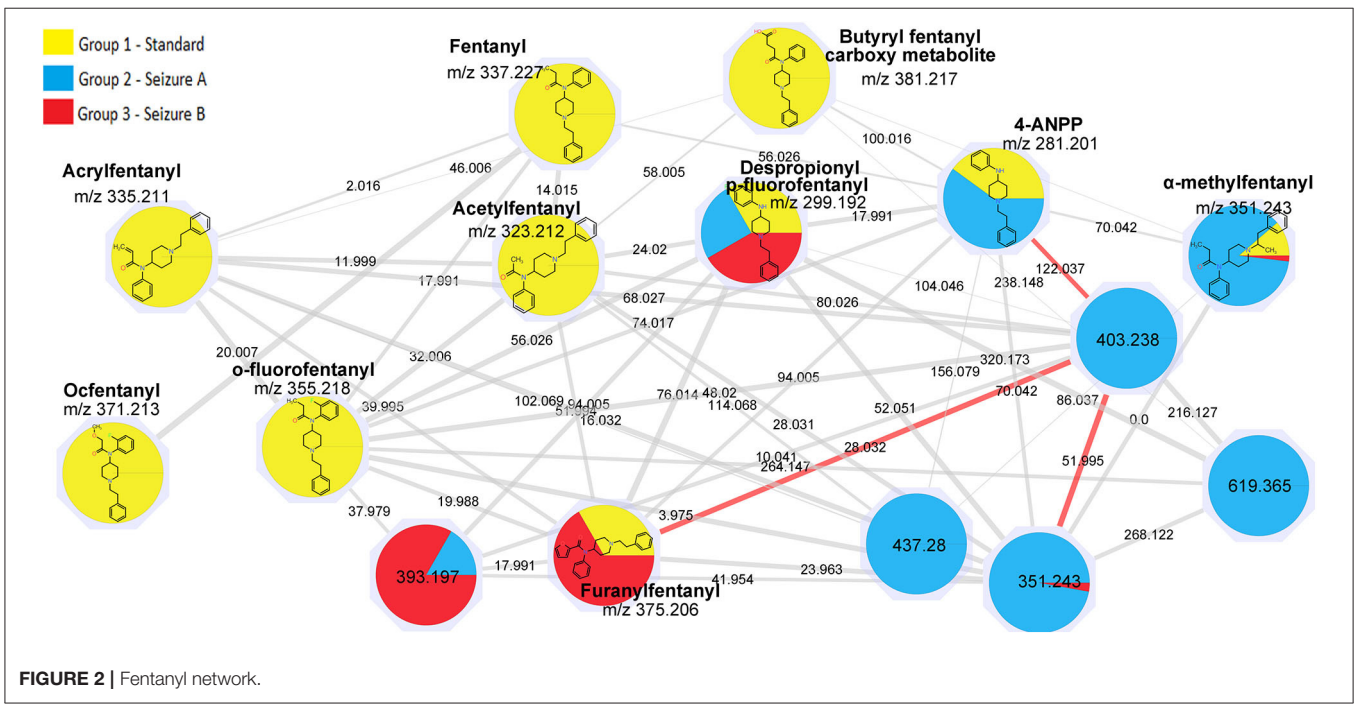

FIGURE 2 | Fentanyl network.

Fentanyl Network

For fentanyls, 4 out of 16 compounds of the mixture were correctly identified by library matching, namely fentanyl (identified as "Innovar" which is a trade name of a drug containing fentanyl) remifentanyl, sufentanyl, and alfentanyl while no hits were found for the remaining drugs. Among the drugs identified by the library matching, only fentanyl (m/z 337.227) was included in a network (**Figure 2**). The original network contained 25 nodes, however, as reported above for synthetic cannabinoids, nodes with lower intensity and nodes that were likely to belong to adducts and in-source fragments were deleted; the cleaned network included 16 nodes.

Ten of the standards included in the mixture were found in this network as reported in **Table 2**. These drugs correspond to the yellow colored nodes, while nodes from group 2 are colored in blue and group 3 in red. From a visual analysis it can be noticed that nodes belonging to this network are from the three groups, suggesting that seizures A (group 2) and B

(group 3) contained fentanyl derivatives. In the case of fentanyls, differently from synthetic cannabinoids not all the standards of the mixture were included in the network. This can be explained observing the molecular structures of the identified fentanyls (**Figure 3**) which lead to completely different fragmentation spectra. Fentanyls not included in the network were those not having the typical phenylethyl piperidine moiety which gives rise to MS2 spectra with the characteristic m/z 188.143 and 105.070 fragments.

This results in showed a limitation of MN for the identification of fentanyl derivatives with a different base structure. Future algorithms may be able to find additional connections, even when the overall fragmentation behavior is altered, as long as some overlap in fragmentation is present.

However, good data were obtained for the seizures; some unknown hits were connected to the standard fentanyl network suggesting that they were structurally related to the standards, with a cosine score >0.9. A number of nodes were exclusively found in the seizures while some nodes were common to seizures and standard mixture as listed in **Table 3**.

In addition to the identification of unexpected drugs, an important feature of MN analysis is that the structures of the unknowns may be hypothesized, based on the precursor mass difference between nodes. The node with mass 299.192 corresponded to despropionyl para-fluorofentanyl, which is known to be a metabolite of 4-fluoroisobutyryl fentanyl, but also a precursor in the synthesis of para-fluorofentanyl; the presence of this compound in both seizures suggested that they contained a para-fluorofentanyl derivative. From the analysis of the network, it can be noticed that despropionyl para-fluorofentanyl is connected to the node with m/z 393.197 (cos 0.95) which was found in both seizures and was among the most intense peaks in seizure B. The delta mass between these two nodes was 94.005, which correspond to a $C_5H_2O_2$ moiety; the node with m/z 393.197 was also connected to furanylfentanyl node with a cosine score of 0.93 and, in this case the delta mass between these two nodes was 17.991 which possibly arose from the addition of a fluorine and the loss of a proton. This observation suggested that peak with m/z 393.197 is a fluoro-furanylfentanyl; the presence of despropionyl para-fluorofentanyl in the seizures

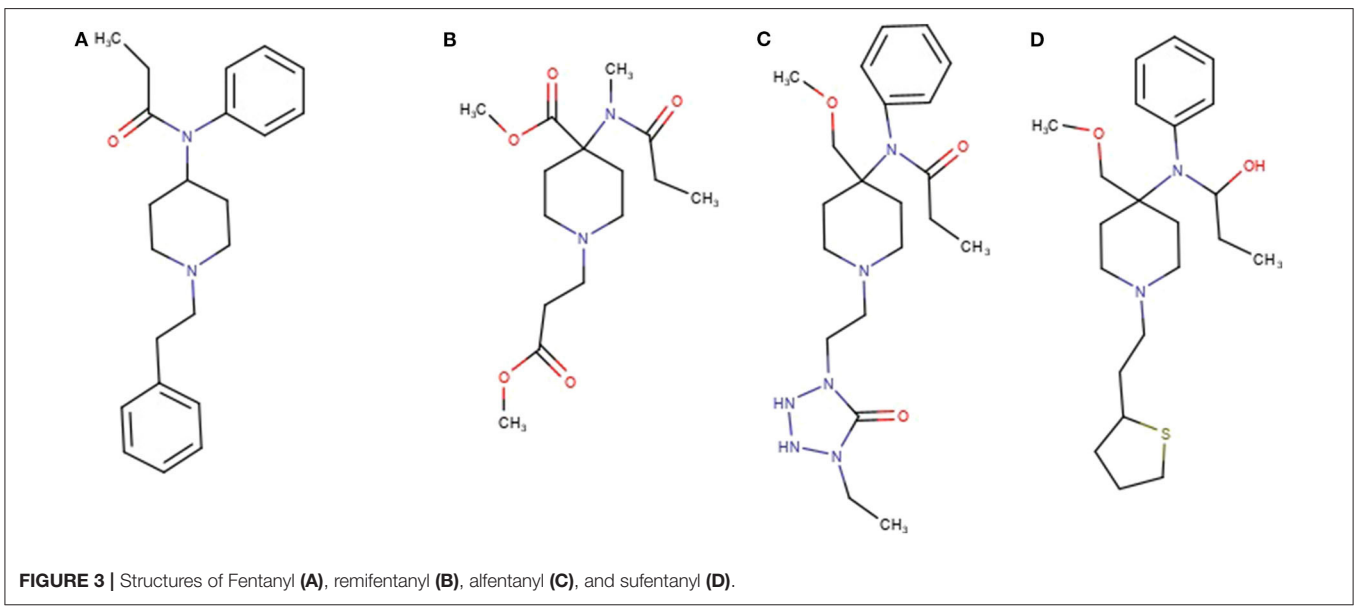

FIGURE 3 | Structures of Fentanyl **(A)**, remifentanyl **(B)**, alfentanyl **(C)**, and sufentanyl **(D)**.

TABLE 3 | Nodes exclusively found in the seizures and nodes common to seizures and standard mixture.

Node Precursor m/z	Node Rt (s)	Group	ID
403.238	230.90	Seizure A	*dimethylfuranyl-fentanyl*
619.365	317.06	Seizure A	unknown
437.280	242.78	Seizure A	unknown
351.243	409.30	Seizure A and standard mix	α-methylfentanyl
281.201	180.26	Seizure A and standard mix	4-ANPP
351.243	212.88	Seizure A and B	*(iso)butyrylfentanyl*
393.197	188.91	Seizure B and A	*Para-fluorofuranylfentanyl*
299.192	143.84	Seizure A and B + standard mix	despropionyl para-fluorofentanyl
375.206	142.75	Seizure A and B + standard mix	furanylfentanyl

indicate that it could be para-fluorofuranylfentanyl, arising from the addition of a furanyl moiety ($C_5H_3O_2$) to the precursor despropionyl para-fluorofentanyl.

Another interesting observation was that two different nodes had m/z 351.243. One of these corresponded to α-methylfentanyl which was among the selected standards. In fact, it was found in group 1, the corresponding spectrum showed the characteristic fragment 202.159 (**Figure 4**) which arose from the loss of the methylated phenylethyl piperidine moiety. The spectrum of the node which shared the same mass of α-methylfentanyl is different and only the typical m/z 188 and 105 fragments are present, suggesting that the phenylethyl piperidine moiety was unmodified; this compound, which was found in both seizures and mainly in seizure A, can be putatively annotated as butyrylfentanyl or isobutyrylfentanyl.

Seizure A also contained 4-ANPP which is a well-known fentanyl precursor (Drug Enforcement Administration, 2010) and 3 unknown compounds, namely m/z 437.280, 619.365, and 403.238 whose spectra are shown in **Figure 5**. All three spectra are compatible with fentanyl derivatives on the basis of the presence of the characteristic m/z 105 and 188 fragments, but the precursor masses do not match with any known fentanyl. Compared with the peaks putatively annotated as butyrylfentanyl and 4-Fluoro-furanylfentanyl, their intensity is 2–3 order of magnitude lower. Interestingly the node with mass 403.238 is central in the fentanyl network, supporting the thesis that it may

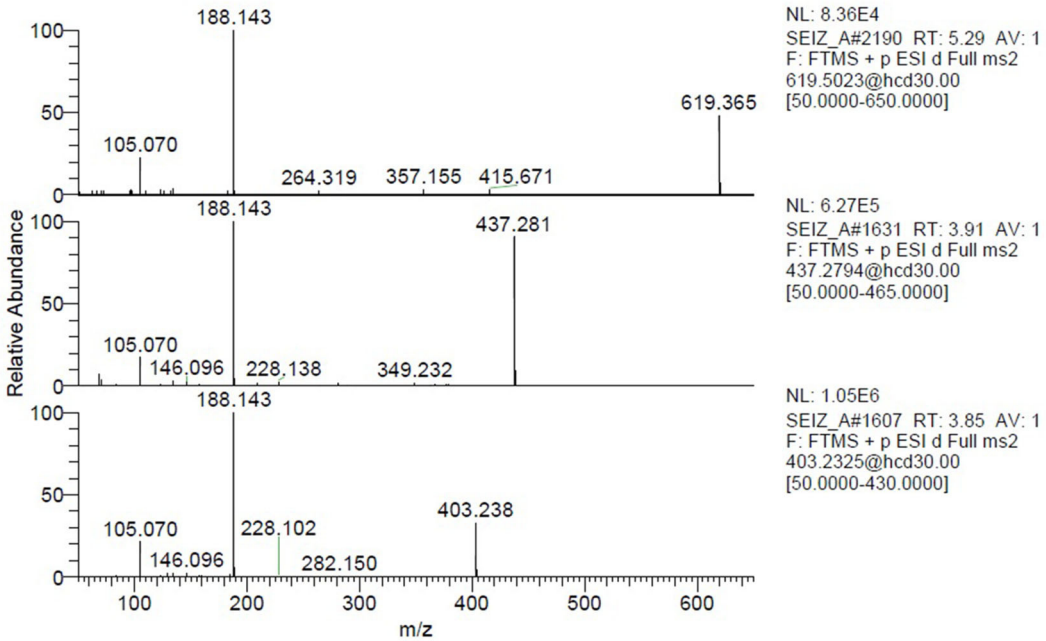

FIGURE 4 | MS/MS spectra of the two nodes with precursor m/z = 351.243.

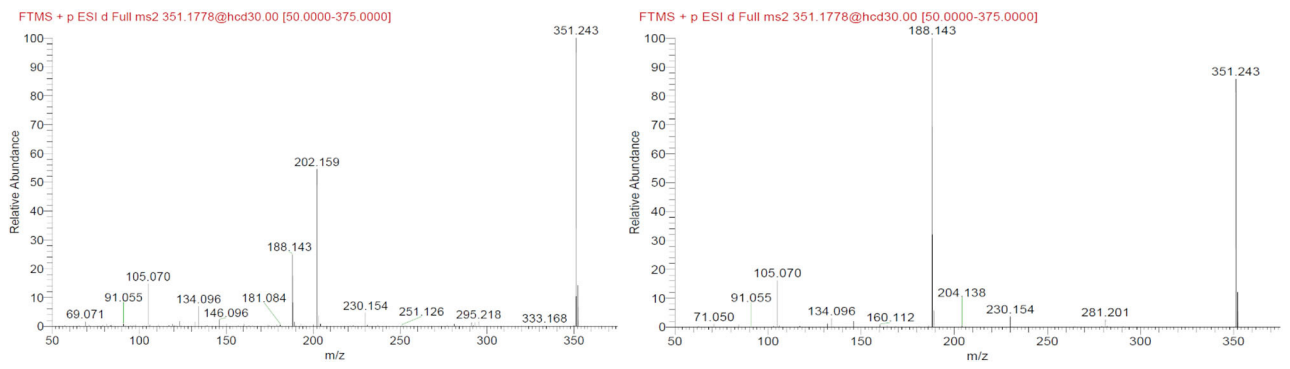

FIGURE 5 | Spectra of the unknown nodes with precursor m/z = 619.365, 437.281, and 403.238.

be a fentanyl derivative. The node is linked to 4-ANPP (Δmass 122.037, $C_7H_6O_2$), furanylfentanyl (Δmass 28.032, C_2H_4) and butyrylfentanyl (Δmass 51.995, C_3O) among others, with cosine score >0.9. By taking into account the delta masses between nodes (**Figure 2**) and the fragmentation spectrum a possible assignation could be dimethylfuranyl-fentanyl.

A hypothesis is that the three unknown compounds in seizure A are synthetic byproducts and even if it was not possible to assign a possible structure for all these compounds at this stage, the detection of possible impurities is a tool for investigations since they might be an important marker for its source and are likely to be specific for a particular synthesis site or wholesaler.

NMR Analysis of Seizures

The fentanyls in the seized samples were finally identified by ^1H and ^{13}C NMR spectroscopy (including 2D experiments).

4-Fluorofuranyl Fentanyl

Monodimensional and homonuclear ^1H-^1H TOCSY experiments allowed for the identification of the spin systems which include aromatic protons and three protons of the furan moiety at 7.36, 6.22, and 5.61 ppm, respectively. Moreover, it was possible to observe the presence of another seven non-magnetically equivalent CH groups in the aromatic region on the basis of heteronuclear ^1H-^{13}C HSQC. Due to the molecule symmetry, 3 of these resonances belong to the protons 2'-6', 3'-5', and 4' of the benzene ring in the phenylethylpiperidin moiety. Instead, the fluorophenyl moiety is bonded to a tetrahedric nitrogen atom, implying the loss of molecular symmetry in this group; given the similarity in the chemical shifts observed in the spectrum, the fluoride must be in position 4 to reach the total number of non-equivalent carbons.

Isobutyrylfentanyl

The presence of iBF was also confirmed by NMR, the spectra showed the typical signals of fentanyl analogs while the existence of the iso-butyl moiety was confirmed by the presence of a doublet at 0.91 ppm in the proton spectrum (data not shown). This multiplicity was not possible for a CH_3 belonging to a linear chain, but only to an iso-butyl one.

CONCLUSIONS

The data reported demonstrated the potential of GNPS in the forensic field particularly for NPS analysis. In fact, library matching with crowdsourced databases may allow the annotation of unexpected compounds, on the other hand MN allows to connect unknown compounds to "standard networks," simplifying the annotation of new drugs. In the reported cases, putative assignment of modifications was possible on the basis of the precursor mass difference. Two previously unidentified fentanyls were found in the analyzed seizures. They were putatively identified as para-fluorofuranylfentanyl and (iso)butyrylfentanyl by connections to fentanyl standard network nodes. To confirm these annotations the samples were analyzed by NMR. It was also shown that structurally related compounds that do not share common fragments, such as some synthetic cannabinoids, formed an integrated network.

This study demonstrates that GNPS is a very useful tool in forensic investigations particularly for identification of new drugs and metabolites. In future, MN could represent an important tool in the forensic field, but to reach its full potential the public sharing of data is needed.

DATA AVAILABILITY STATEMENT

The datasets presented in this study can be found in online repositories. The names of the repository/repositories and accession number(s) can be found below: https://gnps.ucsd.edu/ProteoSAFe/status.jsp?task=3b4d5e5b455140ceb842d2aa13e51c1c; https://gnps.ucsd.edu/ProteoSAFe/status.jsp?task=193e9ab161554741a119940e2c52a2b0.

AUTHOR CONTRIBUTIONS

FV: investigation and data acquisition. CM: writing—original draft, data analysis, and conceptualization. FD: data analysis. AG: project administration and supervision. DC: supervision and writing-reviewing and editing. MS: conceptualization, methodology, and writing–original draft and editing. PD: conceptualization and editing. All authors contributed to the article and approved the submitted version.

REFERENCES

Allard, S., Allard, P.-M., Morel, I., and Gicquel, T. (2019). Application of a molecular networking approach for clinical and forensic toxicology exemplified in three cases involving 3-MeO-PCP, doxylamine, and chlormequat. *Drug Test. Anal.* 11, 669–677. doi: 10.1002/dta.2550

Archer, R. P., Treble, R., and Williams, K. (2011). Reference materials for new psychoactive substances. *Drug Test. Anal.* 3, 505–514. doi: 10.1002/dta.317

Aron, A. T., Gentry, E. C., McPhail, K. L., Nothias, L. F., Nothias-Esposito, M., and Bouslimani, A., et al. (2020). Reproducible molecular networking of untargeted mass spectrometry data using GNPS. *Nat. Protoc.* 15, 1954–1991. doi: 10.1038/s41596-020-0317-5

Dei Cas, M., Casagni, E., Arnoldi, S., Gambaro, V., and Roda, G. (2019). Screening of new psychoactive substances (NPS) by gas-chromatography/time of flight mass spectrometry (GC/MS-TOF) and application to 63 cases of judicial seizure. *Forensic Sci. Int. Synerg.* 1, 71–78. doi: 10.1016/j.fsisyn.2019.04.003

Drug Enforcement Administration, Department of Justice (2010). *Control of Immediate Precursor Used in the Illicit Manufacture of Fentanyl as a Schedule II Controlled Substance*. Final rule. Fed. Regist.

Hohrenk, L. L., Itzel, F., Baetz, N., Tuerk, J., Vosough, M., and Schmidt, T. C. (2020). Comparison of software tools for liquid chromatography–high-resolution mass spectrometry data processing in nontarget screening of environmental samples. *Anal. Chem.* 92, 1898–1907. doi: 10.1021/acs.analchem.9b04095

Laks, S., Pelander, A., Vuori, E., Ali-Tolppa, E., Sippola, E., and Ojanpera, I. (2004). Analysis of street drugs in seized material without primary reference standards. *Anal. Chem.* 76, 7375–7379. doi: 10.1021/ac048913p

Münster-Müller, S., Hansen, S., Opatz, T., Zimmermann, R., and Pütz, M. (2019). Chemical profiling of the synthetic cannabinoid MDMB-CHMICA: Identification, assessment, and stability study of synthesis-related impurities in seized and synthesized samples. *Drug Test. Anal.* 11, 1192–1206. doi: 10.1002/dta.2652

Quinn, R. A., Nothias, L. F., Vining, O., Meehan, M., Esquenazi, E., and Dorrestein, P. C. (2017). Molecular networking as a drug discovery, drug metabolism, and precision medicine strategy. *Trends Pharmacol. Sci.* 38, 143–154. doi: 10.1016/j.tips.2016.10.011

Rivera, J. V., Vance, E. G., Rushton, W. F., and Arnold, J. K. (2017). Novel psychoactive substances and trends of abuse. *Crit. Care Nurs. Q.* 40, 374–382. doi: 10.1097/CNQ.0000000000000174

Scheubert, K., Hufsky, F., Petras, D., Wang, M., Nothias, L. F., Dührkop, K., et al. (2017). Significance estimation for large scale metabolomics annotations by spectral matching. *Nat. Commun.* 8:1494. doi: 10.1038/s41467-017-01318-5

Smith, J. P., Sutcliffe, O. B., and Banks, C. E. (2015). An overview of recent developments in the analytical detection of new psychoactive substances (NPSs). *Analyst.* 140, 4932–4948. doi: 10.1039/c5an00797f

Tai, S., and Fantegrossi, W. E. (2014). Synthetic cannabinoids: pharmacology, behavioral effects, and abuse potential. *Curr. Addict. Rep.* 1, 129–136. doi: 10.1007/s40429-014-0014-y

Wang, M., Carver, J. J., Phelan, V. V., Sanchez, L. M., Garg, N., Peng, Y., et al. (2016). Sharing and community curation of mass spectrometry data with Global Natural Products Social Molecular Networking. *Nat. Biotechnol.* 34, 828–837. doi: 10.1038/nbt.3597

Weinstein, A. M., Rosca, P., Fattore, L., and London, E. D. (2017). Synthetic cathinone and cannabinoid designer drugs pose a major risk for public health. *Front. Psychiatry* 8:156. doi: 10.3389/fpsyt.2017.00156

Wille, S. M. R., Eliaerts, J., Di Fazio, V., and Samyn, N. (2017). Challenges concerning new psychoactive substance detection in oral fluid. *Toxicol. Anal. Clin.* 29, 11–17. doi: 10.1016/j.toxac.2016.12.004

Yang, J. Y., Sanchez, L. M., Rath, C. M., Liu, X., Boudreau P. D., Bruns, N., et al. (2013). Molecular networking as a dereplication strategy. *J. Nat. Prod.* 76, 1686–1699. doi: 10.1021/np400413s

Yu, J. S., Seo, H., Kim, G. B., Hong, J., and Yoo, H. H. (2019). MS-based molecular networking of designer drugs as an approach for the detection of unknown derivatives for forensic and doping applications: a case of NBOMe derivatives. *Anal. Chem.* 91, 5483–5488. doi: 10.1021/acs.analchem.9b00294

Conflict of Interest: The authors declare that the research was conducted in the absence of any commercial or financial relationships that could be construed as a potential conflict of interest.

Advantages of publishing in Frontiers

OPEN ACCESS
Articles are free to read for greatest visibility and readership

FAST PUBLICATION
Around 90 days from submission to decision

HIGH QUALITY PEER-REVIEW
Rigorous, collaborative, and constructive peer-review

TRANSPARENT PEER-REVIEW
Editors and reviewers acknowledged by name on published articles

Frontiers
Avenue du Tribunal-Fédéral 34
1005 Lausanne | Switzerland

Visit us: www.frontiersin.org
Contact us: frontiersin.org/about/contact

REPRODUCIBILITY OF RESEARCH
Support open data and methods to enhance research reproducibility

DIGITAL PUBLISHING
Articles designed for optimal readership across devices

FOLLOW US
@frontiersin

IMPACT METRICS
Advanced article metrics track visibility across digital media

EXTENSIVE PROMOTION
Marketing and promotion of impactful research

LOOP RESEARCH NETWORK
Our network increases your article's readership